Multicomponent Encapsulation into Protein Nanocarriers for Co-Delivery of Therapeutics

Dissertation

zur Erlangung des Grades

„Doktorin der Naturwissenschaften“

im Promotionsfach Chemie

am Fachbereich Chemie, Pharmazie, Geographie und Geowissenschaften

der Johannes Gutenberg-Universität Mainz

vorgelegt von

Natkritta Hüppe

geboren in Nakhon Ratchasima, Thailand

Mainz, 2022

Die vorliegende Arbeit wurde im Zeitraum von Mai 2018 bis Dezember 2021 am Max-Planck-Institut für Polymerforschung in Mainz angefertigt. Ich versichere, die vorliegende Arbeit selbstständig angefertigt zu haben. Alle verwendeten Hilfsmittel und Quellen habe ich eindeutig als solche kenntlich gemacht. Weder die vorliegende Arbeit noch Teile davon wurden bei einer anderen Fakultät bzw. einem anderen Fachbereich als Dissertation eingereicht.

Mainz, den 27.07.2022 _____

Natkritta Hüppe

Dekanin:

Erste Gutachterin:

Zweiter Gutachter:

Tag der mündlichen Prüfung:

Abstract

Successful tumor vaccination relies on a strong and durable immune response. Common soluble vaccine formulations lack the efficiency for sufficient stimulation of immune cells against tumor cells. This thesis presents the development of a multifunctional nanocarrier to enhance immune cell stimulation and tumor vaccination.

In **chapter A**, biodegradable protein nanocarriers (PNCs) were prepared by an interfacial crosslinking in inverse miniemulsion *via* a metal-free azide-alkyne click reaction of azide-modified human serum albumin (HSA-N_3) with hexanediol dipropiolate (HDDP). The bioorthogonal azide-alkyne click chemistry used for the crosslinking did not interfere with the cargo molecules, preserving their bioactivity. The density and degradability of PNCs was controlled by the type and amount of crosslinker. When a disulfide bond was integrated into HDDP, obtained PNCs-HDDP-SS demonstrated additive degradation by enzyme (proteinase K) and reducing agent (DTT). Multiple adjuvants were successfully encapsulated into PNCs with high efficiency. When delivered simultaneously in one carrier, the adjuvants achieved stronger stimulation of dendritic cells compared to not encapsulated adjuvants.

In **chapter B**, the developed procedure for the bioorthogonal multicomponent encapsulation into protein nanocarriers was transferred to model-antigen ovalbumin (OVA), creating adjuvant-loaded OVA-NCs as an all-in-one nanovaccine. The co-delivery of antigen and adjuvants in one system lead to successful antigen presentation on dendritic MHC-receptors, expression of costimulatory marker molecules CD80 and CD86 and secretion of pro-inflammatory cytokines (TNFα, IL-6 and IL-12). Developed dual adjuvant (R848+MDP)-loaded OVA-NCs demonstrated strong DC-mediated T cell stimulation, resulting in efficient tumor treatment of mouse models bearing a melanoma tumor. Combining multiple vaccine components into one drug delivery system proved synergistic effects for tumor vaccination.

Formation of nanocarriers by bioorthogonal crosslinking often requires modification of the nanocarrier material and use of a chemical crosslinker. In **chapter C**, interfacial denaturation of proteins by heating in inverse miniemulsion obtained stable PNCs without the use of modifications and crosslinkers. Changing the single-emulsion to a double W/O/W emulsion improved the dispersion of prepared protein nanocarriers in water and a model dye could be encapsulated with high efficiency. Moreover, PNCs *via* interfacial denaturation demonstrated higher enzymatic degradability and faster release of cargo molecules than PNCs crosslinked with unselective 1,4-toluene diisocyanate (TDI) crosslinker. PNCs crosslinked with

chemoselective crosslinker HDDP obtained fast dye release similar to PNCs without crosslinker, indicating low effect of HDDP on the degradability of PNCs.

In **chapter D**, modification of protein nanocarriers with magnetic (Fe_3O_4 nanoparticles), stealth (polyethylene glycol) and targeting (DC-specific CD11c-antibody) properties enabled the investigation of carrier-protein and carrier-cell interactions. Magnetic PNCs was used to study intracellular uptake, trafficking and protein corona formation by microscopic methods and proteomics. Surface modification of PNCs with stealth polymer PEG decreased unspecific uptake of PNCs into macrophages. Attachment of DC-targeting antibodies to PNCs mediated higher uptake into DCs compared to unmodified PNCs. The knowledge gained from studying the effect of nanocarrier modification on their biological fate facilitates the development of an optimal nanovaccine.

Multifunctional protein nanocarriers loaded with multiple adjuvants and modified with stealth and targeting properties are promising delivery systems to promote a strong and durable anti-tumor immune response through DC-mediated T cell stimulation.

Zusammenfassung

Eine erfolgreiche Tumorimpfung hängt von einer starken und dauerhaften Immunreaktion ab. Herkömmlichen löslichen Impfstoffformulierungen mangelt es an Effizienz, um eine ausreichende Stimulation der Immunzellen gegen Tumorzellen zu erreichen. Diese Dissertation stellt die Entwicklung eines multifunktionalen nanodimensionalen Wirkstoffträgers vor, welches die Immunstimulation und die Tumorimpfung verbessern soll.

In **Kapitel A** wurden biologisch abbaubare Nanoträger aus Proteinen (PNCs) für die Verkapselung von therapeutischen Wirkstoffen entwickelt. Die Protein-Nanoträger wurden durch eine Grenzflächenvernetzung in einer inversen Miniemulsion mittels einer metallfreien Azid-Alkin-Click-Reaktion von Azid-modifiziertem humanem Serumalbumin (HSA) mit Hexandioldipropiolat (HDDP) hergestellt. Die verwendete bioorthogonale Azid-Alkin-Click-Chemie beeinträchtigte die Wirkstoffe nicht, sodass ihre Bioaktivität erhalten blieb. Die Art und Menge des Vernetzers steuerte die Dichte und Abbaubarkeit der PNCs. Wenn eine Disulfidbindung in das HDDP integriert wurde, konnten die resultierenden PNCs-HDDP-SS additiv sowohl durch Enzyme (Proteinase K) als auch mit einem Reduktionsmittel (Dithiothreitol) abgebaut werden. Mehrere Adjuvantien wurden erfolgreich mit hoher Effizienz in PNCs eingekapselt. Wenn die Adjuvantien gemeinsam verkapselt in einem Nanoträger verabreicht wurden, erreichten sie eine stärkere Stimulation dendritischer Zellen verglichen mit unverkapselten Adjuvantien.

In **Kapitel B** wurde das entwickelte Verfahren für die bioorthogonale Multikomponenten-Verkapselung in Protein-Nanoträger auf das Modellantigen Ovalbumin übertragen und somit Adjuvanz-beladene OVA-Nanoträger (OVA-NCs) als nanodimensionales Vakzin hergestellt. Die simultane Verabreichung von Antigen und Adjuvanz in OVA-NCs führte zu einer erfolgreichen Antigenpräsentation auf dendritischen MHC-Rezeptoren, zur Expression der kostimulatorischen Markermoleküle CD80 und CD86 sowie zur Sekretion von proinflammatorischen Zytokinen (TNFα, IL-6 und IL-12). Die mit R848 und MDP-beladenen OVA-NCs zeigten eine starke DC-vermittelte T-Zell-Stimulation, welche zu einer effizienten Tumorbehandlung von Melanomen an Mausmodellen führte. Die Kombination mehrerer Impfstoffkomponenten in einem Wirkstoffträgersystem demonstrierte eine synergistische Wirkung bei der Tumorbehandlung.

Die Herstellung von Nanoträgern durch bioorthogonale Vernetzung erfordert häufig eine Modifizierung des Nanoträgermaterials und die Verwendung eines chemischen Vernetzers. In

Kapitel C konnten stabile PNCs über Grenzflächendenaturierung von Proteinen durch Erhitzen in einer inversen Miniemulsion erzeugt werden, ohne dass Modifikationen und/oder Vernetzer eingesetzt werden mussten. Der Einsatz einer doppelten W/O/W-Emulsion anstatt der einfachen W/O-Emulsion verbesserte die Dispergierung der hergestellten Protein-Nanoträger in Wasser und ein Modellfarbstoff konnte mit hoher Effizienz eingekapselt werden. Darüber hinaus zeigten PNCs, hergestellt durch Grenzflächendenaturierung, eine höhere enzymatische Abbaubarkeit und eine schnellere Freisetzung von Farbstoff als PNCs, die mit unselektivem 1,4-Toluoldiisocyanat (TDI)-Vernetzer vernetzt waren. PNCs, die mit dem chemoselektiven Vernetzer HDDP vernetzt wurden, setzten den Farbstoff ähnlich schnell frei wie PNCs ohne Vernetzer, was auf einen geringen Einfluss von HDDP auf die Abbaubarkeit von PNCs hinweist.

In **Kapitel D** ermöglichte die Modifizierung von Protein-Nanoträgern mit magnetischen (Fe_3O_4-Nanopartikel), „Stealth“ (Polyethylenglykol) und zielgerichteten (DC-spezifischer CD11c-Antikörper) Eigenschaften die Untersuchung von Träger-Protein- und Träger-Zell-Interaktionen. Magnetische PNCs wurden zur Untersuchung des zellulären Aufnahmeprozesses mit mikroskopischen Methoden und zur Untersuchung der Adsorption von intrazellulären Proteinen verwendet. Die Oberflächenmodifizierung von PNCs mit dem Stealth-Polymer PEG verringerte die unspezifische Aufnahme von PNCs in Makrophagen. Die Modifizierung von DC-gerichteten Antikörpern an PNCs führte zu einer höheren Aufnahme in DCs im Vergleich zu unmodifizierten PNCs. Die gewonnenen Erkenntnisse über das biologische Schicksal der Nanoträger, beeinflusst durch die Modifizierungen, unterstützen die Entwicklung eines optimalen nanodimensionalen Impfstoffs.

Multifunktionale Protein-Nanoträger, die mit mehreren Adjuvantien beladen und mit Stealth- und Targeting-Eigenschaften modifiziert werden können, sind vielversprechende Trägersysteme, um eine starke und dauerhafte Anti-Tumor-Immunantwort durch DC-vermittelte T-Zell-Stimulation zu erreichen.

Graphical Abstract

Chapter A – Multicomponent Encapsulation into Fully Degradable Protein Nanocarriers *via* Azide-Alkyne Click Reaction

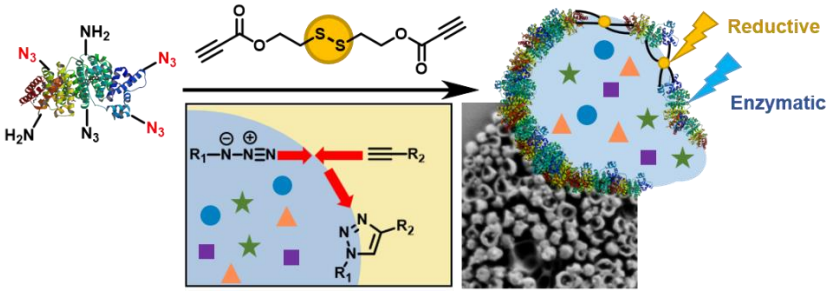

Chapter B – Dendritic Cell-Mediated T Cell Stimulation by Adjuvant-Loaded Ovalbumin Nanocarriers for Anti-Tumor Vaccination

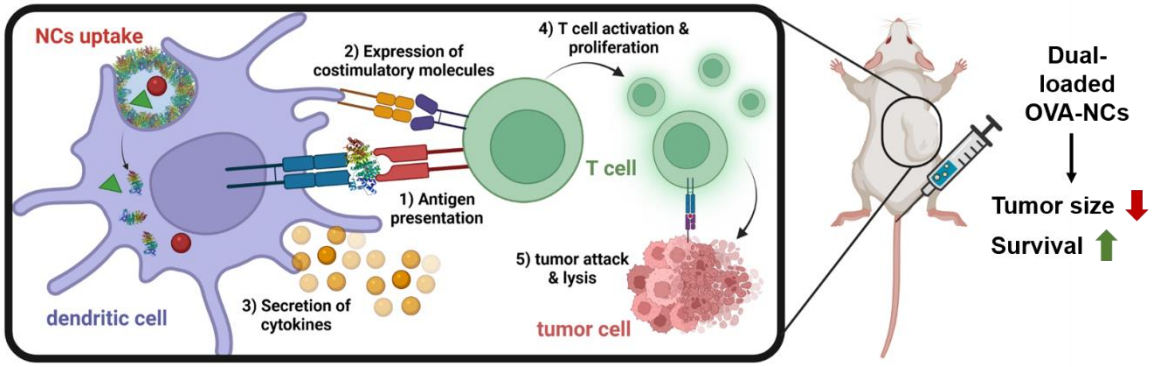

Chapter C – Protein Nanocarriers *via* Interfacial Denaturation

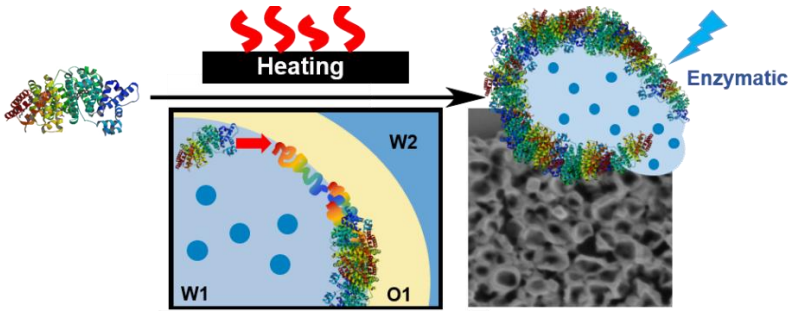

Chapter D – Modification of Protein Nanocarriers for Cell Trafficking, Stealth and Targeting

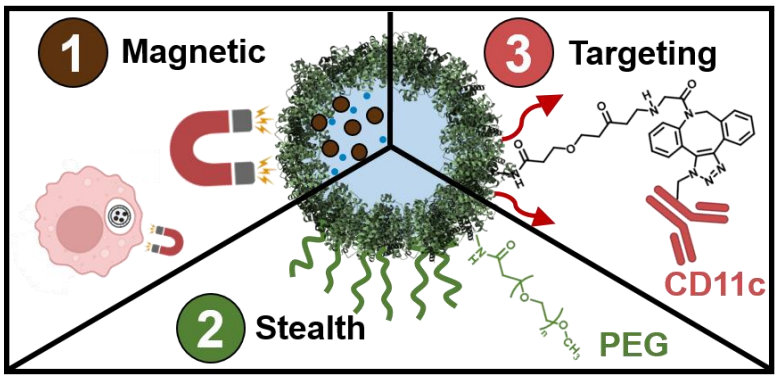

Table of Contents

I. Motivation

Cancer is still the major cause of death worldwide with one in five deaths linked to cancer. Established therapies with anti-cancer drugs have increased the survival rate of patients if the cancer is detected in early stages. However, often cancer is diagnosed in late stages, because cancer cells have properties to hide from our immune system or deactivate it. In our fight against cancer, monotherapy such as chemotherapy proved to lack the efficacy for successful cancer treatment. Edward Jenner first studied the use of antigens to induce an immunity, a so-called vaccination, in the 18th century. Since then, various vaccines have been developed to treat diseases to extinction of some, such as small pox. Immunotherapy aims to treat cancer by prophylactic or therapeutic vaccination. To achieve this, the immune cells have to be sufficiently stimulated to overcome the hiding and deactivating mechanisms of cancer cells. To the motto "The more the merrier", multifunctional systems facilitate a more complex strategy to tackle the complex concept of cancer vaccination. Using multiple therapeutics in combination might create a synergistic system to achieve strong and enduring immune responses. The challenge of multicomponent formulations is achieving high local concentration of the therapeutics at the target site. Common soluble formulations cannot offer that due to systemic distribution and fast excretion. Encapsulation of the therapeutic agents into nanocarriers offers an effective strategy for co-delivery to target cells. The challenge for nanocarrier-mediated vaccination is the development of an all-in-one nanocarrier. Multifunctional nanocarriers require 1) a strategy for a bioorthogonal co-encapsulation of therapeutics into biodegradable nanocarriers, 2) an optimal combination of antigen and multiple adjuvants for synergistic stimulation of dendritic cells (DCs) and 3) stealth polymers to decrease unspecific uptake and prolong circulation time and 4) targeting functionalities to enhance delivery efficacy to dendritic cells (Figure 1).

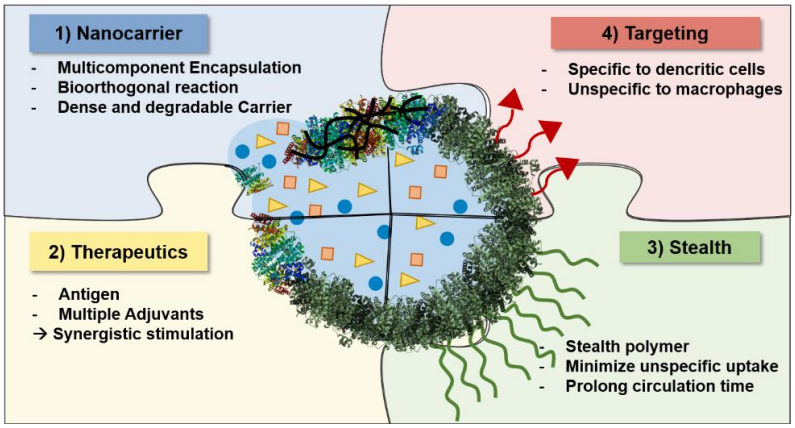

Figure 1. Requirements for multifunctional nanocarriers as anti-tumor nanovaccines. Figure created by Natkritta Hüppe.

Therefore, this thesis aims to develop a multifunctional nanocarrier as a nanovaccine that combines all the requirements for an optimal drug delivery to immune cells and induce a strong anti-tumor response. In chapter A and B, a nanocarrier is designed for a multicomponent encapsulation into degradable protein nanocarriers *via* bioorthogonal azide-alkyne click reaction (A) or interfacial denaturation (B) in inverse miniemulsion. For the cargo-encapsulation, an inverse miniemulsion approach allows a simultaneous encapsulation of multiple cargo molecules with high control and efficiency. The chemoselective click reaction or chemistry-free approach for the preparation of the nanocarrier prevents including the cargo molecules in the reaction and preserves their bioactivity. In chapter B, ovalbumin acts as a biodegradable nanocarrier material and model-antigen in one. Various combinations of adjuvants are co-encapsulated into ovalbumin nanocarriers to study their synergistic properties. In chapter D, the nanocarriers are modified at the surface with stealth polymers and DC-targeting antibodies to increase the specific uptake into DCs and therapeutic efficiency due to high local concentration of therapeutics. Combining all these approaches in one drug delivery system could create a multifunctional nanovaccine and enhance anti-tumor vaccination.

II. State of the Art

Chapter II is presented in the manuscript “Nanocarriers with Multiple Cargo Load – A Comprehensive Synthesis Guideline Using Orthogonal Strategies”; published in Macromolecular rapid communications, 2022, [2200611]. https://doi.org/10.1002/marc.202200611.

Abstract

Multifunctional nanocarriers enhance the treatment efficacy for modern therapeutics and have gained increasing importance in biomedical research. Co-delivery of multiple bioactive molecules enables synergistic therapies. Co-encapsulation of cargo molecules into one nanocarrier system is challenging due to different physicochemical properties of the cargo molecules. Additionally, co-encapsulation of multiple molecules simultaneously should proceed with high control and efficiency. Orthogonal approaches for the preparation of nanocarriers are essential to encapsulate sensitive bioactive molecules while preserving their bioactivity. Preparation of nanocarriers by physical processes (i.e. self-assembly or coacervation) and chemical reactions (i.e. click reactions, polymerizations, etc.) are considered as orthogonal methods to most cargo molecules. This review shall act as a guideline to allow the reader to select a suitable preparation protocol for a desired nanocarrier system. This article helps to select for combinations of cargo molecules (hydrophilic-hydrophobic, small-macro, organic-inorganic) with nanocarrier material and synthesis protocols. The focus of this article lies on the co-encapsulation of multiple cargo molecules into biocompatible and biodegradable nanocarriers prepared by orthogonal strategies. With this toolbox, the selection of a preparation method for a known set of cargo molecules to prepare the desired biodegradable and loaded nanocarrier shall be provided.

II. 1. Introduction

Therapies with a single drug often lack the efficiency to treat complex diseases. A combination of multiple active agents can create multifunctional and/or synergistic systems and enhance the treatment efficiency. This review article will act as a guideline on how to prepare biodegradable nanocarrier systems by so-called "orthogonal" encapsulation strategies loaded with multiple cargo molecules. "Orthogonal" means in this case that the preparation of the nanocarrier structure does not hamper the activity of the cargo, e.g. does not react chemically or destroy them physically.

The co-delivery of complex drug molecules is, for example, important in modern immunotherapy, as successful tumor vaccination needs a strong and durable immune response. Combinations of several adjuvants demonstrated a synergistic stimulation of immune cells with enhanced anti-tumor vaccination effect.[1] Co-delivery of cargo molecules with high local concentrations at the target site is challenging with common soluble formulations due to systemic distribution and fast excretion of the cargo molecules. Encapsulation of the cargo molecules into nanocarriers pose the only way to enable multicomponent systems and achieve effective simultaneous co-delivery. Furthermore, early-tumor diagnostic is also an important step to successful tumor treatment. The next level in nanomedicine is the combination of therapy and diagnosis, so-called theranostics, in one multifunctional delivery system to enhance treatment efficacy. Especially the heterogenicity of tumors make image-guided therapies necessary and multifunctional nanocarriers could be applied for imaging, diagnosis, and therapy simultaneously, enabling early-stage treatment.[2, 3] Co-encapsulation of cargo molecules with different physicochemical properties is challenging in terms of control, efficacy, and orthogonality of the encapsulation process. Facing the importance of bioactive compounds for medical therapy, orthogonal encapsulation strategies ensure preservation of the cargo's bioactivity and increase the efficacy of drug delivery systems. "Orthogonal" means for one using chemoselective reactions, which do not involve the cargo in the reaction during the preparation of nanocarriers. In the same sense, nanocarriers formed by physical approaches such as self-assembly or coacervation can also be considered orthogonal to the cargo, but also here the cargo should not be altered, e.g. by denaturation.[4] Since orthogonality is an important criterion in encapsulation of medical agents, we will focus on orthogonal pathways to encapsulate multiple cargo molecules into nanocarriers. Furthermore, the physicochemical properties of the cargo molecules such as solubility and molecular weight influence the choice of encapsulation strategies. This becomes challenging for co-encapsulation, when cargo

molecules with different physicochemical properties like e.g. hydrophobicity, solubility, or molecular weight need to be encapsulated simultaneously. Besides encapsulation, the release of the cargo molecules afterwards at the target site is also essential for the design of an efficient drug delivery system. Therefore, nanocarriers with tailored degradability or release mechanisms are required to ensure successful release of the cargo molecules.

The challenges faced are to provide high encapsulation efficiency, multicomponent encapsulation and orthogonality as well as biocompatible and degradable nanocarrier materials in one nanocarrier system. This review shall act as a guideline to allow the reader to select a suitable preparation protocol for a desired nanocarrier system. This article helps to select for combinations of cargo molecules (hydrophilic-hydrophobic molecules, low molar mass compounds-macromolecules and organic-inorganic cargo molecules) with nanocarrier material and synthesis protocols. This article summarizes strategies for the co-encapsulation of multiple cargo molecules into biocompatible and biodegradable nanocarriers for drug delivery prepared by orthogonal strategies (Figure 2). With this toolbox, the selection of a preparation method for a known set of cargo molecules to prepare the desired biodegradable and loaded nanocarrier shall be provided. We focus on biomedical applications, but the principle of co-encapsulation by orthogonal approaches applies also for other fields, such as food or energy applications when multiple cargo molecules need to be protected or delivered simultaneously.

Low molar mass drugs (MW < 1 kDa) can interact and diffuse rapidly through many biological barriers and membranes, theoretically reaching the target site with high effectivity. Their rapid diffusion through the vascular system enables fast systemic distribution, but also causes fast excretion.[5, 6] Concerning cancer treatment, high local concentrations of drugs leads to high anti-tumor effects and is more desired than systemic distribution. Furthermore, the high cytotoxicity of chemotherapeutics causes severe side effects for patients, when applied systemically. In order to protect the body from the toxic drugs and protect the drugs from fast excretion, encapsulation into nanocarriers is an efficient method to enhance pharmacokinetics of drugs.[7] Biomacromolecules such as antigens,[8] proteins[9] or nucleic acids (RNA,[10] DNA[11]) have emerged as therapeutics for biomedical application. The challenge with biobased macromolecular therapeutic agents (BTAs) is their low stability in many biological environments, in which they can degrade quickly. Therefore, nanocarriers as a platform to protect the BTAs during delivery are in major focus to develop novel treatments.[12] The challenge for delivery of macromolecules is their high molar mass, which requires a high degradation degree of the nanocarriers to ensure efficient release.[13] Additionally, to prevent

involvement of sensible BTAs in the nanocarrier preparation and to preserve their bioactivity, bio-orthogonal chemistries have to be chosen.

The solubility characteristics of the cargo molecules is one of the most important factors to be considered, when designing an optimal encapsulation strategy.[14] Hydrophilicity and hydrophobicity of the cargo mediate its solubility in the different phases, i.e. during the nanocarrier preparation, within the nanocarrier and afterwards in the surrounding environment. Therefore, choosing the suitable method with the right solvents influences the encapsulation efficiency during the nanocarrier preparation and entrapment efficiency during the delivery.

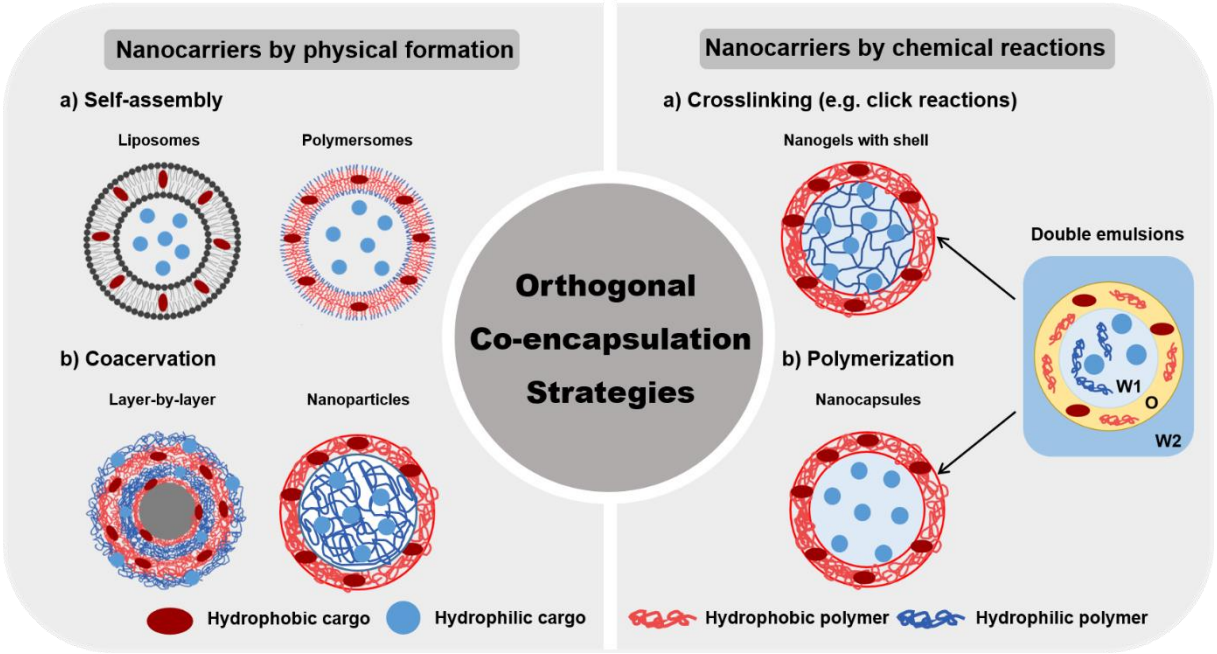

Figure 2. Orthogonal strategies for co-encapsulation of hydrophobic and hydrophilic cargo molecules into nanocarriers. Figure created with Biorender.com by Natkritta Hüppe.

II. 2. Co-Encapsulation of Hydrophobic and Hydrophilic Cargo Molecules

II. 2.1. Encapsulation of Hydrophobic Cargo Molecules

Hydrophobic cargo molecules have a low water solubility (mostly below 1 mg/mL) and require organic solvents.[15] Many biocompatible and degradable synthetic polymers, such as polylactic acid (PLA), are soluble in organic solvents and thus optimal for the encapsulation of hydrophobic molecules into polymeric nanocarriers. The nanocarriers can be prepared either by physical formation, e.g. precipitation or self-assembly, or by chemical reactions, e.g.

polymerization or crosslinking (Table 1 gives an overview on different techniques to encapsulate hydrophobic cargo).

Table 1. Orthogonal strategies to encapsulate hydrophobic cargo molecules into degradable nanocarriers.

<table>
<tr><th>Physical formation</th><th>Materials</th><th>Ref.</th><th>Chemical reactions</th><th>Materials</th><th>Ref.</th></tr>
<tr><td colspan="6">Nanoparticles</td></tr>
<tr><td>Desolvation</td><td rowspan="4">Natural Polymers: Albumin, dextran, gelatin, chitosan, alginate
Synthetic Polymers: PLA, PCL, PLGA, PBCA</td><td>16-22</td><td rowspan="3">Emulsion polymerization: radical, anionic, cationic, ROMP, polyaddition, polycondensation</td><td rowspan="3">PS, PMMA, PBCA, PLA, PCL, PLGA, PI</td><td rowspan="3">48-53</td></tr>
<tr><td>Self-assembly</td><td>23-27</td></tr>
<tr><td>Solvent Evaporation</td><td>28,29</td></tr>
<tr><td>Salting-Out</td><td>30</td><td>Crosslinking in or at interface of O/W emulsion</td><td>Albumin, dextran, gelatin, chitosan, alginate</td><td>55,60,61</td></tr>
<tr><td colspan="6">Polymeric Micelles</td></tr>
<tr><td rowspan="3">Self-assembly of amphiphilic polymers</td><td>Hydrophobic block: PLA, PCL, PLGA, PACA</td><td rowspan="3">38,39</td><td>Core-Crosslinked</td><td rowspan="3">Click crosslinking reactions: CuAAC, SPAAC, IEDDA, Thiol-ene</td><td rowspan="3">47, 62</td></tr>
<tr><td>Hydrophilic block: PEG, POx, Dextran, chitosan, PVP</td><td>Shell-Crosslinked</td></tr>
<tr><td></td><td>Interlayer-Crosslinked</td></tr>
</table>

a) Nanocarriers by Physical Formation

Nanoparticles are a common class of nanocarriers for the delivery of cargo molecules. Hydrophobic molecules are encapsulated into nanoparticle's matrix during the physical formation of the nanocarriers by precipitation or self-assembly.[16-18] For example, in the desolvation method, water-soluble polymers are used as nanocarrier materials and the nanocarriers are formed by coacervation of the water-soluble polymers upon addition of a desolvating agent, i.e. an organic solvent (Figure 3). The hydrophobic drug can be dissolved in

the desolvating agent, e.g. ethanol or acetone. Upon addition of the drug-containing desolvating agent to an aqueous solution of the nanocarrier material, precipitation of the polymer is induced to form nanoparticles. The drug is entrapped during the precipitation of the polymer.[16, 19] The desolvation method is easy and cheap, but often lack high control over size and loading efficiency.[20] Crosslinking of the nanocarriers can improve their stability and encapsulation efficiency. For example, in albumin nanoparticles, glutaraldehyde[21] or carbodiimides[22] react with the primary amines to crosslink the proteins.[17] However, depending on the cargo, targeting amines as crosslinkable groups may not be orthogonal to the cargo (especially when biomolecules are loaded) and other encapsulation strategies need to be considered. A similar method that uses solubility change to form nanoparticles is the self-assembly method.[23, 24] Human serum albumin (HSA) nanoparticles were loaded with hydrophobic paclitaxel due to the interaction of the drug with the hydrophobic domains of HSA.[25, 26] Using β-mercaptoethanol to break the disulfide bonds in the protein exposes the hydrophobic domains of the protein, which self-assemble upon addition of hydrophobic drugs in aqueous media.[27] Induction of protein self-assembly was also achieved by modifying the primary amine groups with octane aldehyde, increasing the hydrophobicity of the protein.[24] The self-assembly method demonstrated higher drug-loading compared to most desolvation methods.[19]

Precipitation in emulsions offers the encapsulation of hydrophobic cargo molecules into polymeric nanoparticles with higher control over size and loading efficiency. The hydrophobic cargo molecule and the polymer (mostly synthetic) are dissolved in the oil phase. The oil-phase is dispersed in an aqueous continuous phase to form an oil-in-water (O/W) emulsion. The nanoparticles are formed by precipitating the polymer inside of the oil droplet through solvent evaporation.[28, 29] The hydrophobic cargo molecule, dissolved in the oil droplet, is entrapped in the polymer matrix during the precipitation leading to high encapsulation efficiencies.

In the salting-out approach, the polymer and hydrophobic cargo molecules are dissolved in a water-miscible organic solvent (e.g. acetone). The addition of salts (e.g. MgCl, CaCl) to the aqueous solution first impedes the miscibility of the solvents, forming an O/W emulsion. Dilution of the emulsion reverses the salting-out effect, leading to diffusion of the organic solvent to the aqueous phase. The polymer precipitates and entraps the cargo molecules within its matrix. Compared to the conventional emulsion diffusion method, the initial formation of an emulsion by salts enables higher control over the preparation of nanocarriers with smaller size, narrow size distributions, and high encapsulation efficiencies.[30]

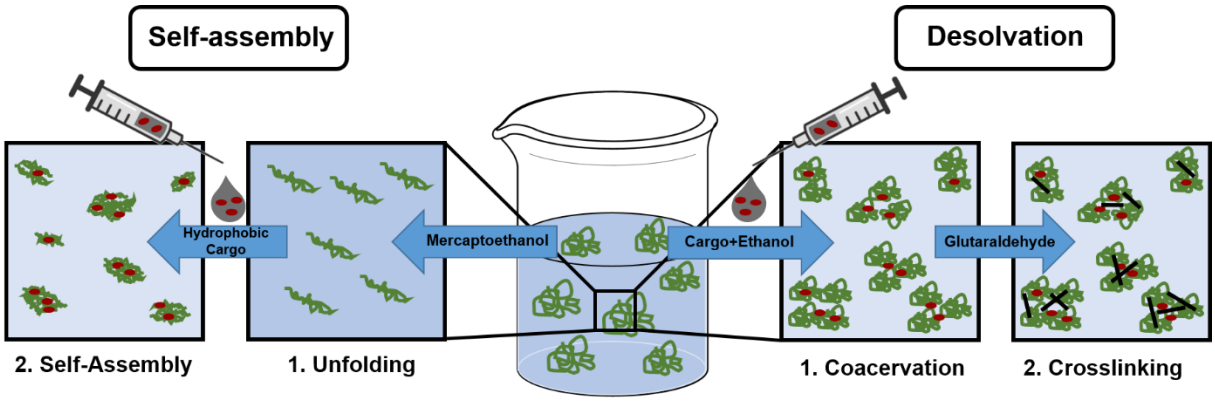

Figure 3. Encapsulation of hydrophobic cargo molecules during the preparation of nanocarriers by self-assembly or desolvation method. Figure created with ChemDraw 2.0 by Natkritta Hüppe.

Synthetic polymers are convenient nanocarrier materials, as they can be synthesized in high purity, controlled sequence and can be tailored to desired properties. Polylactic acid (PLA),[31, 32] poly-ε-caprolactone (PCL), and poly-D,L-lactide-*co*-glycolide (PLGA)[33] are the most common biodegradable synthetic polymers used for nanoparticles by emulsion techniques.[28, 30] Besides these polyesters, also several natural polymers have been applied as matrix for nanocarriers due to their biocompatibility and biodegradability. Since typically hydrophilic polysaccharides (e.g. chitosan,[34] alginate,[35] and gelatin[36,28]) or proteins (e.g. albumins) are used in biomedical applications, the formation of nanocarriers proceed through desolvation or self-assembly. Owing to their natural role in binding hydrophobic molecules, such as steroid hormones or fatty acids, albumins have been widely utilized as non-immunogenic and non-toxic nanocarrier materials.[19, 37]

Self-assembled micelles of amphiphilic block copolymers have also been used to encapsulate hydrophobic drugs in their hydrophobic core.[38, 39] The driving force of the self-assembly process is the noncovalent interaction between the hydrophobic blocks in aqueous solution, forming a hydrophobic core and hydrophilic shell. The hydrophilic shell allows dispersion of polymeric micelles in water, often poly(ethylene glycol) (PEG) or PEG-alternatives, such as poly(2-oxazoline)s (POx) have been used as the hydrophilic block. Both polymers are highly water-soluble, biocompatible and prolong blood circulation times by the so-called stealth effect.[40, 41] Bio-based chitosan,[42] dextran,[43] or poly(vinylpyrrolidone) (PVP)[44] have also been applied as materials for polymeric micelles. Regarding the hydrophobic block, there are various synthetic polymers available, but in context of biodegradability and biocompatibility, PLA, PCL,[44] PLGA,[45] and polyalkylcyanoacrylates (PACA),[46] have received considerable attention.

b) Nanocarriers by Chemical Reactions

Polymeric micelles can also be crosslinked at the core, shell or interlayer depending on the site of the crosslinkable group to increase their stability.[47] For example, chemical groups allowing click chemistry (Figure 4A) are attached to the amphiphilic polymers, mostly at the hydrophobic core-forming block, resulting in core-crosslinked micelles. Instead of using an external reagent to crosslink the polymeric nanocarriers, the cargo itself can act as a crosslinker. For example, Liu *et al.* designed core-crosslinked polymer micelles by phenol-yne click chemistry (Figure 4B).[48] The amphiphilic block copolymer poly(ethylene glycol)-*b*-poly(2-hydroxyethyl methacrylate (mPEG-PHEMA) was modified with alkyne groups by esterification with 5-hexynoic acid (HA). Since the cargo curcumin naturally possesses phenolic groups, the core was crosslinked by a phenol-yne click reaction upon self-assembly and curcumin entrapment. Resulting pH-responsive curcumin-loaded micelles proved higher stability during dilution in water, higher encapsulation efficiency, and thus a more efficient drug delivery compared to non-crosslinked micelles. Owing to the formed vinyl ether bond, the micelles were pH-responsive and rapidly hydrolyzed in intracellular acidic conditions (pH = 5), releasing curcumin in its natural form with preserved bioactivity.

Emulsion polymerization is a common strategy to prepare polymeric nanocarriers and entrap cargo molecules during a chemical transformation.[49] While conventional emulsion polymerization is limited with regards to encapsulation due to diffusion processes, in contrast the microemulsion and miniemulsion techniques allow high encapsulation and offer a versatile chemistry.[50, 51] Polymeric nanocarriers prepared by polymerization in emulsions mostly include non-degradable latexes such as polystyrene (PS) and polyacrylates (e.g. poly(methyl methacrylate), PMMA) but also degradable polymers such as PBCA, PLA and PCL or crosslinked biopolymers.

A miniemulsion is formed from dispersing two immisible solvents by high shear forces, e.g. ultrasonication or a microfluidizer, forming nanosized droplets in a size range of 50-500 nm. Polymeric nanocarriers can be prepared in miniemulsion by a variety of reactions such as anionic/cationic polymerizations, ring-opening metathesis, polyaddition and polycondensation.[50] For encapsulation of hydrophobic cargo, a direct oil-in-water miniemulsion is applied. The cargo is dissolved in the oil droplets and is entrapped in the polymer matrix upon polymerization. Huang *et al.* developed the synthesis of poly(*n*-butyl cyanoacrylate) nanoparticles *via* anionic miniemulsion polymerization.[52] They demonstrated

that the miniemulsion polymerization achieved high loading of hydrophobic paclitaxel compared to conventional emulsion polymerization.

In contrast to miniemulsions, microemulsions form spontaneously and are thermodynamically stable. Their characteristic small sizes (< 50 nm) enable unique possibilities due to a large interfacial area, small space domain and optical transparancy. Various polymerizations similar to the miniemulsion techniques have been realized in either W/O, O/W or bicontinous microemulsions. However, high amounts of surfactant (and costabilizer) are needed to stabilize the droplets, limiting the use of microemulsion polymerization in spite of their easy preparation.With the development of polymerizable surfactants, the drawback of high amounts of free surfactant was optimized.[53]

Besides polymerizations, nanocarriers have also been prepared by crosslinking either after self-assembly whithin the dispersed phase or at the interface of the droplets.[54] Click chemistry is the most common orthogonal crosslinking reaction that enables chemoselective crosslinking of the polymer matrix, which needs chemical modification, without reaction with the desired cargo molecules.[55] The most applied click reactions in the biomedical field include azide-alkyne (copper-catalyzed (CuAAC)[56, 57] or strain-promoted (SPAAC)),[58] thiol-ene and inverse-electron-demand diels-alder (IEDDA)[59] and more (Figure 4A).[60, 61] Several nanocarrier morphologies were developed with crosslinking chemistry, for example nanoparticles, hollow nanocapsules, nanogels, or micelles.[47] For example, Zou *et al.* encapsulated the hydrophobic drug paclitaxel into degradable PLGA nanocarriers by CuAAC in miniemulsion. The alkyne-functionalized polymer was crosslinked by a diazide-modified paclitaxel, which served as both the drug and crosslinker, leading to higher encapsulation efficiencies compared to physically encapsulated drug.[62]

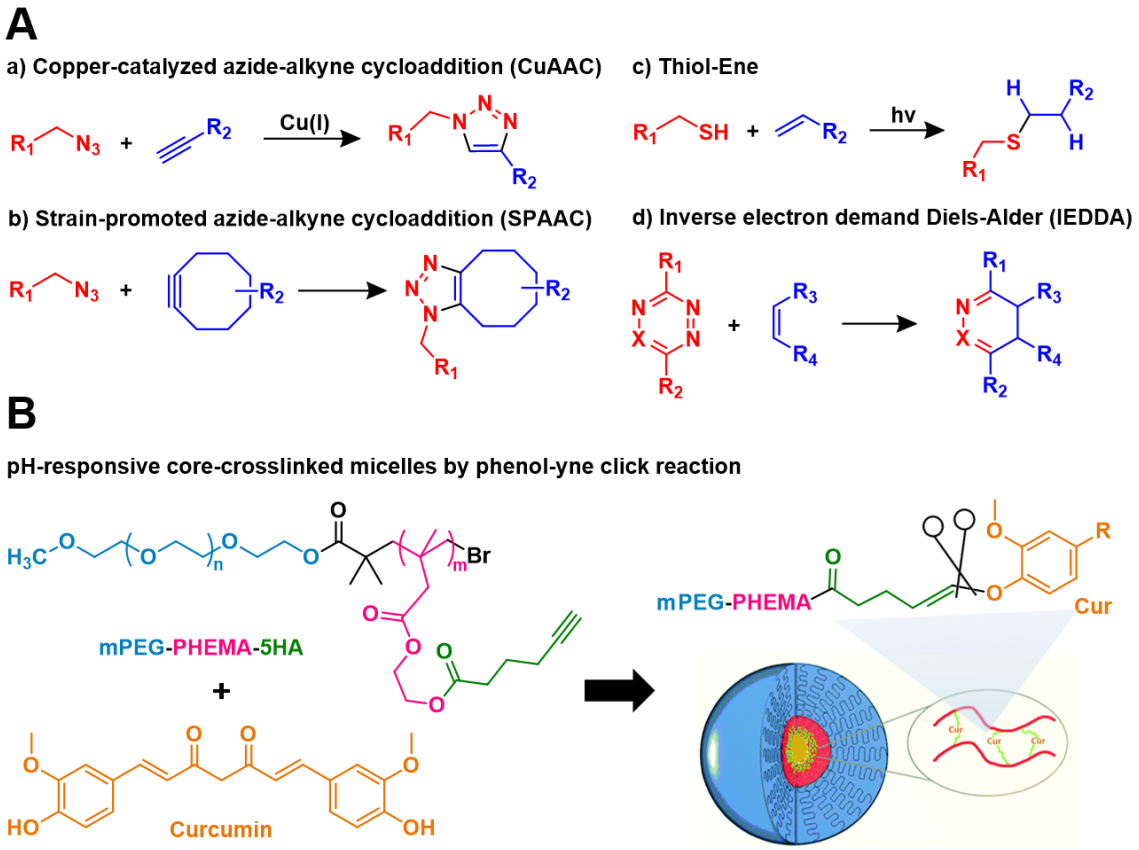

Figure 4. A) Examples of click reactions for orthogonal preparation of nanocarriers *via* crosslinking. B) pH-responsive reversibly core-crosslinked micelles by phenol-yne click reaction with curcumin. Image adapted from reference[48]. Published by Royal Society of Chemistry. Copyright © 2019. All rights reserved.

II. 2.2. Encapsulation of Hydrophilic Cargo Molecules

With increasing interest in biological therapeutics, such as peptides, proteins or nucleic acids, as well as the extensive development of small, hydrophilic drugs, encapsulation strategies for the delivery of hydrophilic components emerged rapidly.[63] Owing to their high water-solubility, hydrophilic molecules exhibit a rapid clearance, leading to low biodistribution and intracellular absorption.[64] Encapsulation of hydrophilic drugs into nanocarriers improves their pharmacokinetics and delivery efficacy. Orthogonal encapsulation approaches for hydrophilic molecules -similar to hydrophobic cargo- include self-assembly systems or chemical reactions at the interface of - in this case - inverse emulsions (Table 2).

Table 2. Orthogonal strategies to encapsulate hydrophilic cargo molecules into degradable nanocarriers.

Physical formation	Materials	Ref.	Chemical reactions	Materials	Ref.
Nanoparticles/Nanocapsules					
Solid lipid nanoparticles: Solvent evaporation in emulsion	Lipids, e.g. fatty acids, fatty alcohols, esters	66-70	Inverse Emulsions: Crosslinking (TDI, TET, TAD, copper-free AAC)	Proteins (Albumins), Carbohydrates (dextran, hyaluronic acid)	71,72, 77-84
Spray-drying,	Synthetic Polymers: PLA, PCL, PLGA, PBCA	16	Inverse Emulsions: polymerization (RAFT, anionic, polyaddition, polycondensation)	PBCA, PLA, PCL, PLA-co-PCL, PLGA,	85,86
Desolvation		68,74 ,75			
Nanogels					
Gelation (temperature, pH, ionic strength)	Natural Polymers: albumin, dextran, gelatin, chitosan, alginate	19, 65	Click crosslinking reactions: CuAAC, SPAAC, IEDDA, Thiol-ene	Natural polymers, e.g. hyaluronic acid, dextran	55,56, 87-90

a) Nanocarriers by Physical Formation

Similar to hydrophobic cargo molecules, hydrophilic compounds can be encapsulated into nanocarriers by physical processes such as precipitation and self-assembly.[63] In the desolvation method, the hydrophilic cargo molecule is dissolved in the aqueous media alongside the hydrophilic polymer. The cargo is entrapped into the nanocarriers upon addition of the desolvating agent and precipitation of the polymers. Biopolymers such as proteins,[17] gelatin,[36] alginate,[35] and other (poly)saccharides[18] but also synthetic polymers such as PLA, PLGA, and PCL have been used to encapsulate hydrophilic molecules by desolvation or salting out.[30]

A spray drying process can be used to prepare nanocarriers as a dry powder.[16] Spray droplets are generated from a solution of the nanocarrier material and the cargo. The spray droplets are air-dried to form cargo-loaded nanocarriers, which are separated from the drying air as a dry powder. The spray drying method is a convenient process to form nanocarriers in a continuous and scalable single-step approach.

Nano-sized hydrogels are convenient to encapsulate hydrophilic molecules by an inverse emulsion technique. When using proteins or carbohydrates, nanogels can be formed by gelation upon change in temperature, pH value, or ionic strength.[65] For example when hydrophilic cargo is dissolved together with proteins, the heat-induced denaturation results in the formation of nanogels, held together by hydrogen bonds, electrostatic or hydrophobic interactions.[19]

Lipids are an optimal nanocarrier material due to their high biocompatibility, biodegradability and broad availability with the majority of nanocarriers in clinical use are based on lipidic formulations.[66, 67] Similar to polymeric micelles, lipidic nanocarriers self-assemble from amphiphilic lipids. Solid lipid nanoparticles are prepared similar to polymeric nanoparticles *via* precipitation or emulsion techniques, such as solvent evaporation or solvent diffusion.[68] Commonly, lipids such as fatty acids, fatty alcohols, or glycerol esters are used for preparing lipid nanocarriers.[69] Charged lipids such as cationic lipids, which have permanently charged heads (e.g. 1,2-di-O-octadecenyl-3-trimethylammonium-propane (DOTMA)), or ionizable lipids, which are protonated at low pH values (e.g. DC-cholesterol), as well form solid lipid nanocarriers. Solid lipid nanoparticles have proven to be excellent nanocarriers for encapsulating and delivering small molecular drugs[69] as well as hydrophilic macromolecules such as mRNA[70] due to ionic interactions of the gene with the charged lipid material.

b) Nanocarriers by Chemical Reactions

Hydrophilic molecules can be encapsulated *via* chemical reactions in inverse W/O emulsions. As nanocarrier material, water-soluble biopolymers can be used, for example proteins[71] or carbohydrates,[18, 72] but also degradable polymers, such as PLA, PCL, PLA-*co*-PCL, PLGA, and others have been used.[22, 30] In an inverse emulsion, the cargo is dissolved in an aqueous aqueous solution and dispersed in an organic solvent to prepare a W/O emulsion.[49, 73] The cargo is entrapped in the nanocarriers either upon polymerization or crosslinking of polymers,[74] allowing the encapsulation of BTAs such as dsDNA, siRNA, oligonucleotides, or proteins with high efficiency.[12, 75] While designing nanocarriers for hydrophilic drugs, the density of the nanocarriers'matrix is extremly important to prevent premature leakage of the hydrophilic

cargo from the inside into the surrounding by osmotic pressure difference. Crosslinking of the polymer matrix decreases permeability for small cargo molecules: a crosslinking reagent is added to the inverse emulsion to crosslink the nanocarrier material either i) in the dispersed phase (a hydrophilic crosslinker) or ii) in the continuous phase (a hydrophobic crosslinker that reacts at the interface). In the first case, solid nanocarriers are formed, while in the latter, nanocapsules with a solid shell and liquid core are generated.[76] Interfacial crosslinking requires less nanocarrier material and offers high encapsulation efficiency and concentrations of cargo molecules.[54, 76] Furthermore, when a chemoselective reaction is applied, the hydrophilic cargo can be encapsulated without their involvement, preserving their activity. Various orthogonal crosslinking types were developed for the interfacial reaction in the inverse miniemulsion to prevent the involvement of the cargo, preserving the bioactivity.[54] If the cargo does not possess nucleophilic groups, such as amines or alcohols, polyaddition with 1,4-toluene diisocyanate (TDI) has been used for various matrix polymers, such as hydroxyethyl starch,[77, 78] proteins (e.g. ovalbumin,[71] horse radish peroxidase,[79] or hepatitis c virus protein[80]). However, a major side reaction of TDI-crosslinking is the hydrolysis of the isocyanate groups, which leads first to the formation of amines and eventually urea linkages, which can hamper the biodegradation of the nanocarriers. In spite of this side reaction and possible reaction with cargo molecules, also the straightforward isocyanate chemistry was used to encapsulate and release hydrophilic cargo molecules (e.g. dyes,[71] adjuvants,[81] or dsDNA[77]). However, the content of covalent modification of the cargo molecules remained unclear in these cases. With the development of orthogonal crosslinking reactions, Piradashvili *et al*. demonstrated the preparation of fully degradable protein nanocarriers using the metal-free tetrazole-ene cycloaddition (TET-click) in inverse miniemulsion (Figure 5A).[82] The crosslinking reaction between a TET-modified protein with a difunctional strained norbornene was induced by irradiation with UV-light (254 nm). The resulting protein nanocarriers demonstrated a prominent core-shell morphology and self-fluorescence due to the formed pyrazoline cycloadduct by TET-click. A therapeutic cargo, Resiquimod (R848), could successfully be encapsulated into protein nanocarriers with high efficiency. Due to the high enzymatic degradability of the protein nanocarriers, the delivery of R848 to dendritic cells followed by intracellular release of the cargo lead to an efficient immune response. In comparison to protein nanocarriers prepared by crosslinking with TDI, nanocarriers by TET-click reaction demonstrated higher immune response, underlining the importance of an orthogonal crosslinking reaction to preserve the cargo's activity. The disadvantage of a TET-click reaction is the need of UV-light to induce the crosslinking process. UV-light or other harsh initiators, such as metal catalysts, can affect sensitive cargo molecules

and decrease their bioactivity. Hüppe *et al.* developed the preparation of protein nanocarriers without the addition of initiators by using a metal-free azide-alkyne click reaction (Figure 5B).[83] Azide-modified human serum albumin was crosslinked with hexanediol dipropiolate (HDDP) at the interface of an inverse miniemulsion. A crosslinker such as HDDP with an activated dialkyne reacts under mild conditions without the need of an initiator. With inserting a disulfide bond into the crosslinker, the protein nanocarriers are degradable by enzymatic as well as reductive degradation. By this approach, a triple combination of adjuvants, i.e. Resiquimod (R848), muramyl dipeptide (MDP) and polyinosinic-polycytidylic acid (Poly(I:C)) and dye Cy5-Oligo, could be encapsulated into fully-degradable protein nanocarriers with high control over the encapsulation efficiency. The multi-loaded nanocarriers demonstrated an additive immune activation of dendritic cells, exceeding the single-loaded nanocarriers.

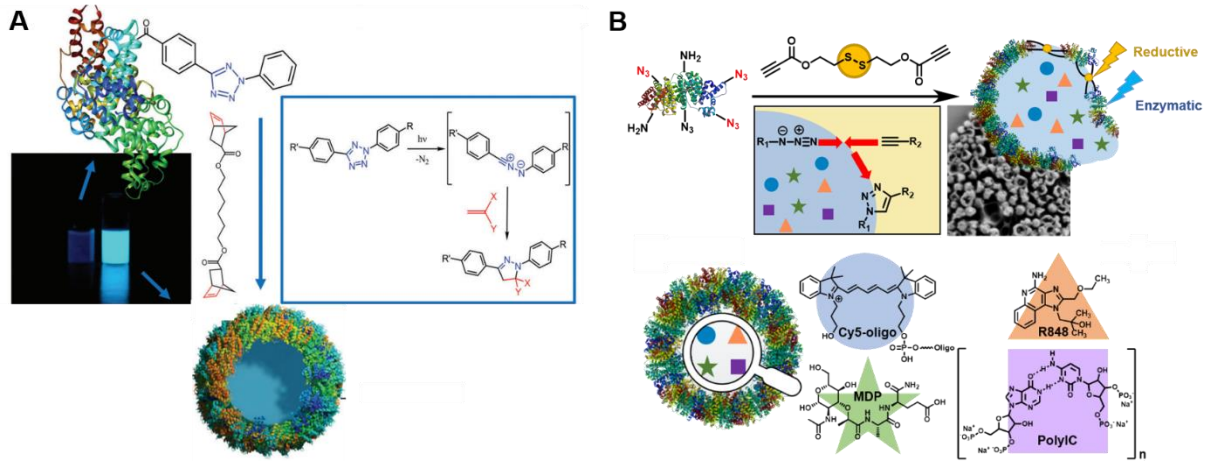

Figure 5. Preparation of protein nanocarriers (PNCs). A) Non-fluorescent protein–TET conjugates were cross-linked by dinorbornene in inverse miniemulsion to obtain self-fluorescent protein nanocarriers; reaction mechanism of the bioorthogonal UV-light induced 1,3 dipolar tetrazole– ene cycloaddition. Image adapted from reference [82] with permission from the Royal Society of Chemistry. Copyright © 2017. This open access article is licensed under CC-BY-3.0. B) Multicomponent encapsulation into protein nanocarriers through interfacial azide-alkyne crosslinking with hexane-diol-dipropiolate in inverse miniemulsion. Chemical structures of Cy5-oligo dye and adjuvants R848, MDP and Poly(I:C) encapsulated into human serum albumin nanocarriers. Image adapted from reference [83] with permission from the Royal Society of Chemistry. Copyright © 2022**.** This open access article is licensed under CC-BY-3.0.

In a similar approach, protein nanocarriers were formed *via* a Diels-Alder reaction of the tryptophane moieties of proteins with triazolinedione (TAD) in an inverse miniemulsion.[84] In this paper, the authors found that different crosslinking chemistries affected the protein conformation and hence carrier-protein and carrier-cell interaction. Other encapsulation strategies *via* inverse miniemulsion includes carbohydrates as carrier materials, where for example azide-modified hyaluronic acid[72] was crosslinked through a copper-free azide-alkyne click chemistry with hexanediol dipropiolate and dextran-based polyaldehydes through polycondensation with polyhydrazides to pH-responsive hydrazones.[85]

Sun *et al.* designed a novel interfacial reversible addition fragmentation transfer (RAFT) polymerization in inverse miniemulsion to encapsulate methyl orange and bovine serum albumin) with high efficiency (~ 90%).[86] An amphiphilic RAFT agent was synthesized with the desired hydrophilic-lipophilic balance (HLB), acting as the emulsifier as well as RAFT chain transfer agent. The disperse phase contained of the zwitterionic monomer, poly(ethylenegylcol) diacrylate as the crosslinker and the initiator 2,2′-azobis(2-methylpropionitrile) (AIBN), resulting in nanocapsules with a well-defined core-shell structure. The zwitterionic nanocapsules (ZNCs) demonstrated dual-responsive swelling dynamics triggered by salt or temperature and cargo was released rapidly.

W/O microemulsions can as well be applied for the preparation of nanocarriers with similar strategies as introduced for miniemulsion. Compared to miniemulsion, microemulsion droplets have a size below 50 nm, presenting excellent templates for preparation of super small nanocarriers. A broad of biodegradable water-soluble polymers were used for the preparation of nanocarriers in reverse microemulsions, including several proteins and polysaccharides.[53] The polymer, dissolved in the water droplet, can be crosslinked *ex situ* (addition of crosslinker to the aqueous phase before emulsification) or *in situ* (addition of crosslinker after emulsification). Craparo *et al.* prepared biodegradable polyaspartamid-nanocarriers by photo-initiated crosslinking in inverse microemulsion.[87] Functionalization of α,β-poly(N-2-hydroxyethyl)-D,L-aspartamide (PHEA) with glycidyl methacrylate (GMA) introduced reactive vinyl and ester groups into the polymer. The double bonds enabled UV-induced crosslinking of the polymers and the ester groups enable hydrolytic degradability of the polymeric nanocarrier. Water-soluble cytarabine could successfully be encapsulated into PHEA-GMA nanocarriers and released upon enzymatic or chemical hydrolysis.

Nanogels are versatile drug delivery systems as they are biocompatible, degradable and tunable in permeability.[88, 89] As emerging nanocarriers for delivery of hydrophilic molecules, especially BTAs, orthogonal approaches were developed, such as metal-free strain-promoted azide-alkyne cycloaddition, thiol-ene, tetrazol-ene or Diels-Alder reactions.[55, 56, 88] Chen *et al.* reported bioorthogonal encapsulation of intracellular protein drugs, cytochrome c (CC) and granzyme B (GrB), respectively, into hyaluronic acid (HA)-nanogels *via* catalyst-free tetrazol-alkene photo-click reaction (Figure 6).[90] Biocompatible and biodegradable HA-nanogels were prepared from a redox-responsive cystamine methacrylate and lysine-tetrazole derivatives. The protein-loaded HA-nanogels were successfully taken up by cancer cells and protein could be released by reductive degradation of the disulfide bond inside the cancer cells, exhibiting high redox

potentials. The protein-loaded HA-nanogels demonstrated high anti-tumor effects even at low doses. This proves the preserved bioactivity of the protein due to the bioorthogonal reaction.

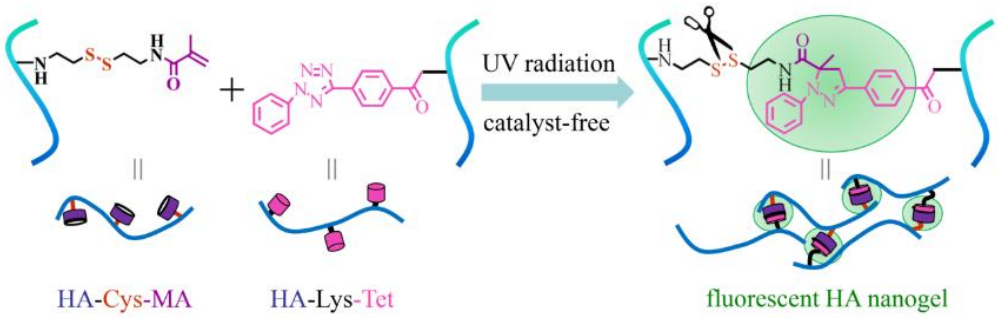

Figure 6. Illustration of nanogel formation from HA-Cys-MA and HA-Lys-Tet *via* catalyst-free and bioorthogonal tetrazol-alkene photo-click reaction. Image reprinted from reference [90] with permission of ACS. Copyright © 2016 American Chemical Society.

A similar HA-based approach was developed by Famili *et al.*, who crosslinked HA-tetrazine with PEG-norbornene to prepare HA-hydrogels.[91] The catalyst-free inverse-demand Diels-Alder reaction allowed a bioorthogonal *in situ* encapsulation of Fab1-antibody fragments without altering the cargo. The intact antibody fragments were completely released from the hydrogel matrix over a period of several weeks *in vitro* and maintained their full antigen binding capacity. Other nanogels based on biopolymers were prepared by tetrazine-norbornene reaction, such as alginate and gelatin.[88]

II. 2.3. Co-Encapsulation of Hydrophilic and Hydrophobic Cargo Molecules

Co-encapsulation of multiple cargo molecules with different physicochemical properties is important to create multifunctional nanocarriers with enhanced therapeutic efficacy due to a synergistic effect of multiple therapeutics.[75] Learning from the developed orthogonal encapsulation strategies of hydrophobic and hydrophilic cargo molecules, respectively, drug delivery systems for co-encapsulation of both molecules were developed with similar approaches by physical entrapment or crosslinked nanocarriers. Moreover, the co-delivery of small molecules and macromolecules requires nanocarriers with, on one hand, low permeability to keep small cargo molecules entrapped, and, on the other hand, an efficient degradability to release large cargo molecules. Depending on the small cargo, hydrophilic or hydrophobic, different approaches have to be taken for co-encapsulation of small molecules with macromolecules.

Table 3. Orthogonal strategies to co-encapsulate hydrophobic and hydrophilic cargo molecules into degradable nanocarriers.

Physical formation	**Material/ Cargo**	**Ref.**	**Chemical reactions**	**Material /Cargo**	**Ref.**
Nanoparticles/Nanocapsules					
Layer-by-layer	Anionic: poly(sodium)styrene sulfonate, Cationic: Poly(allylamine)*HCl; degradable: PCL-PAA, PArg-PLGA, chitosan, proteins	110-118	Double Emulsions: solvent evaporation+ crosslinking	DOX-erlonitib, verteprofin-cisplatin	20, 119-122,126-131
Liposomes					
Thin-layer hydration Freeze-thaw cycles dehydration-rehydration, reverse-phase evaporation	Material: Charged lipids: DOTMS, DC-cholesterol Cargo: Doxorubicin-combretastatin, tariquidar-paclitaxel, cytarabin-daunorubicin	66,91,95-102			
Polymersomes					
Electroformation, microfluidics, DED	Rhodamine B-camptothecin	103-109			

a) Nanocarriers by Physical Formation

Important for a successful co-encapsulation is the presence of two different compartments in the nanocarriers: either a hydrophobic core with a hydrophilic shell or a hydrophobic shell with a hydrophilic core, both of which are able to encapsulate hydrophilic and hydrophobic compounds separately. Combining the encapsulation strategies for hydrophobic and hydrophilic molecules, both can be encapsulated simultaneously into liposomes,[92] polymersomes, or layered polymeric nanoparticles (Figure 7).[93-95]

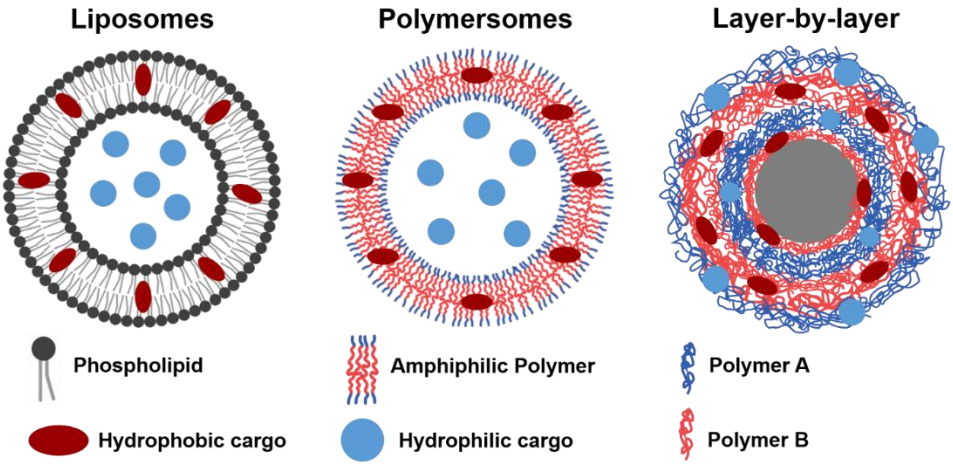

Figure 7. Co-encapsulation of hydrophilic and hydrophobic cargo molecules into liposomes, polymersomes and layer-by-layer nanocarriers. Created in Biorender.com by Natkritta Hüppe.

A double-layered liposomes are formed by a self-assembly process of amphiphilic phospholipids in aqueous media, creating a lipid bilayer with a hydrophobic inner layer and a hydrophilic core.[66] Phosphatidylcholine, originated from soybean or egg yolk, and its hydrogenated derivatives are usually applied as the lipidic nanocarrier material for liposomes.[96] The thin-layer hydration method is a common method for preparation of liposomes.[66] The lipid solution is reduced and upon addition of an aqueous solution, the lipid film is hydrated to assemble into a lipid bilayer, forming liposomes. The encapsulation of drugs proceeds with dissolving the hydrophilic drug in the external aqueous phase and the drug is encapsulated with assembly of the liposomes. Although this method is a convenient approach for the encapsulation into liposomes, it lacks high encapsulation efficiency due to the large volume of aqueous phase compared to the entrapped volume. If expensive cargo molecules like therapeutic drugs should be encapsulated, a low encapsulation efficiency is cost-intensive for recycling the drug and scale-up the process in clinical developments.[66] Therefore, other strategies were developed for efficient loading of hydrophilic cargo molecules into liposomes. The liposomes are loaded with hydrophilic drugs either by passive loading, where the drug is encapsulated during the self-

assembly, or active loading, where first the liposome is formed and the drug loaded afterwards by a transmembrane diffusion due to a pH value or ionic gradient.[97] In case of the freeze-thaw cycle method, the first step is identical to the thin-layer hydration, except as a next step the liposome dispersion undergoes several freeze-thaw cycles to increase the drug loading with each re-assembly of the liposomes (Figure 8A).

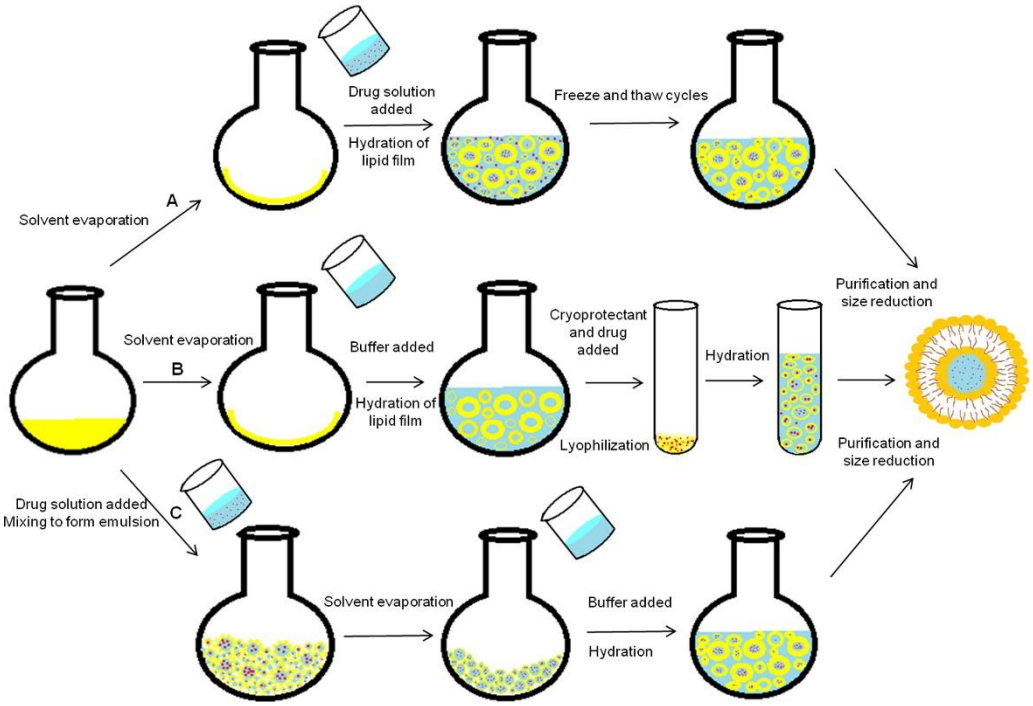

Figure 8. Preparation of liposomes as nanocarriers for encapsulation of hydrophilic cargo molecules by A) freeze-thaw cycles, B) dehydration-rehydration of preformed empty vesicles and C) reverse-phase evaporation methods. Image reprinted with permission from reference[97]. Published by Elsevier B.V. Copyright © 2014. All rights reserved.

Another strategy with high payload is the dehydration-rehydration approach, where first the liposomes are formed with the thin-layer method using only buffer as hydration solution (Figure 8B). Then the drug is added to the liposome dispersion and lyophilized. With rehydration of the lyophilized liposomes the drug is encapsulated with high efficiency. A third method, the reverse-phase evaporation, uses an emulsion approach, where an aqueous drug solution is dispersed in the lipid-containing oil (Figure 8C). The liposomes form first with solvent evaporation followed by hydration and the lipid bilayer assembles around the aqueous drug droplets, resulting in high encapsulation efficiency. Besides high loading, the permeability of the lipid bilayer plays a crucial role to prevent leakage of drugs. In general, the liquid crystalline phase of the bilayer is more permeable to hydrophilic cargo molecules compared to the gel state.[97] Therefore, the addition of cholesterol mediates the membrane organization and increases the stability of the membrane and entrapment efficiency of the cargo molecules.[98, 99] Other factors influencing the drug loading and entrapment are the lipid concentration, the length

of the overall lipid chain as well as the hydrophobic carbon tail length of the phospholipid and (electrostatic) interaction of the drug with the lipid bilayer.[100] Besides efficient drug loading and entrapment into the nanocarriers, the drug release plays a significant role for efficient drug delivery. Owing to the high availability and tailored synthetic approaches for lipidic materials, liposomes can be designed with a variety of release mechanisms with stimuli ranging from pH value, magnetic field, hyperthermia, light and ultrasound.[101, 102]

Upon liposome formation, hydrophobic drugs can be entrapped in the hydrophobic layer and the hydrophilic drug in the aqueous core. For example hydrophilic doxorubicine (Dox) hydrochloride and hydrophobic debydrochlorinatoin Dox,[92] Dox and combretastatin,[103] tariquidar and paclitaxel, cytarabin and daunorubicin and more combinations, were encapsulated into liposomes.[93] The encapsulation efficiency of hydrophobic drugs into the lipid bilayer depends on the solubility of the drug in the lipid bilayer, influenced as well by the membrane composition.[98] Regarding hydrophilic compounds, the membrane properties such as thickness, permeability and polarity affects the encapsulation of hydrophilic cargo molecules as well.[97] Although liposomes have been widely used to encapsulate BTAs and small molecular drugs, such as DOX-siRNA or PTX-pDNA, loading of BTAs was difficult to control with such methods and ratios of e.g. siRNAs in the carrier was rather low (~3500 siRNA per liposome).[93]

Polymersomes present a similar strategy for orthogonal co-encapsulation by owning hydrophilic and hydrophobic compartments.[104, 105] Similar to liposomes, polymersomes are prepared through self-assembly of amphiphilic block copolymers. Polymersomes are obtained by solvent-free methods (film hydration, electroformation or gel-assisted hydration) and solvent-displacement methods (solvent injection, emulsion phase transfer, or microfluidics).[106] Often, preparation methods for polymersomes (e.g. electroformation or microfluidics) require special equipment and are time consuming. Houbrechts *et al.* developed a strategy to form giant polymersomes by a simple double emulsification approach, which allowed efficient encapsulation of large components, such as proteins.[107] Single double emulsion droplets (DED) were used as templates to form the polymersomes by self-assembly upon solvent displacement. Instead of using microfluidics to form the DEDs, a simple double emulsification approach is used with one low molecular weight block copolymer acting as the surfactant for both emulsions and the polymersome material itself. This allowed an easy and fast strategy to form polymersomes with basic laboratory equipment, suitable for clinical scale-up. Cargo molecules are encapsulated into polymersomes by passive entrapment in either the membrane or inner space. In comparison to liposomes, polymersomes have a lower lateral fluidity and

transmembrane permeability, retaining cargo molecules with higher efficiency. However, low permeability can be problematic in terms of release. Fortunately, polymers can be synthesized with a variety of chemistry and tuned to desired permeability and responsivity.[108] Besides synthetic amphiphilic block copolymers (e.g. PCL-*b*-PEO), also amphiphilic biopolymers can be applied as nanocarrier material to encapsulate both hydrophilic and hydrophobic compounds into vesicles.[109] For example, Pramod *et al*. developed vesicles based on amphiphilic polysaccharides for dual-encapsulation of hydrophilic and hydrophobic compounds.[110] The amphiphilic polysaccharide was obtained from naturally available dextran as the hydrophilic backbone, modified with aliphatic chains from the cashew nut as hydrophobic tails. The amphiphilic dextran-based polymer self-assembled into vesicles of d_h ~120 nm, in which hydrophilic cargo molecules, such as rhodamine B, were encapsulated into the core and hydrophobic molecules, such as anticancer drug camptothecin, in the shell. By encapsulation, the stability of the hydrophobic drug against hydrolysis could be increased almost 10-fold compared to its isolated form. The developed dextran-based vesicles were degradable at the aliphatic ester linkage connected to the dextran-backbone by esterase and thus releasing both cargo molecules. The encapsulated anticancer drug formulation demonstrated a 1.5-fold higher activity in neutralizing fibroblasts than the free drug, underlining the importance of drug delivery systems to enhance therapeutic efficacy. This drug co-delivery system is an elegant example for an orthogonal co-encapsulation approach into biocompatible and biodegradable polymer vesicles.

In case of polymeric nanoparticles, when combining hydrophilic and hydrophobic polymers by layering them to a nanoparticle, hydrophilic and hydrophobic cargo molecules can be co-encapsulated into the respective layer. Polymeric nanocarriers *via* layer-by-layer (LbL) assembly utilize electrostatic complexation of polyelectrolytes, forming multilayer assemblies of polymers.[111] This method is based on the alternating assembly of oppositely charged polymers around a preformed charged core particle. The LbL-assembly approach applied in aqueous media without the use of chemical reactions or modifications enables a mild encapsulation strategy of sensitive cargo molecules, such as genes, with preservation of their structure and activity. Solid nanocarriers (e.g. polystyrene, silica or polycarbonate[112]) act as core templates for layering and can be removed by dissolution (e.g. with THF, HF, or HCl, respectively) to obtain hollow nanocarriers. Preformed cargo-loaded nanocarriers (e.g. liposomes, charged nanoparticles, crosslinked nanogels) can as well be applied as core templates to prepare core- and shell-loaded LbL-nanocarriers.[111, 113] Since the properties (e.g. permeability) of the nanocarriers depend on the properties of the polyelectrolyte pairs, the

majority of LbL-nanocarriers are prepared from synthetic polymers, mainly anionic poly(sodium styrene sulfonate) and cationic poly(allylamine) hydrochloride. However, with regard to biomedical applications, more biocompatible and degradable polyelectrolytes (e.g. poly(*N*-vinyl caprolactam)/poly(L-aspartic acid), poly(L-arginine)/poly(L-glutamic acid)) are of higher interest. For example, LbL nanocarriers were prepared from chitosan/alginate NPs and a combination of lapatinib and paclitaxel could be simultaneously encapsulated into respective layers.[114] The cargo itself can act as a polyelectrolyte: proteins and polypeptides are convenient polyelectrolytes for LbL-approaches due to their amphoteric character.[115, 116] Nucleic acids, DNA[117] and RNA,[118] can act as both cargo and polyelectrolyte: for example, siRNA was used as polyelectrolyte for the LbL-assembly of nanocarriers resulted in higher siRNA content compared to passive entrapment processes (e.g. liposomes).[119] Additionally, the layering can proceed onto a nanosized core, in which small molecular drugs have been encapsulated, providing an efficient strategy for co-encapsulation of drugs and BTAs. Deng *et al*. utilized the LbL approach to co-deliver siRNA with the low molar mass drug doxorubicin (DOX) to counteract drug resistance of triple-negative breast cancer (Figure 9).[119] The authors prepared the nanocarriers from a doxorubicin-loaded liposome (core) and alternately deposited poly-L-arginine and siRNA onto the core *via* ionic interactions. The resulting NCs effectively entrapped up to 3500 siRNA chains per layer - similar numbers were obtained in a whole liposome. The dual-loaded NCs demonstrated synergistic effects, with an 8-fold decrease in tumor volume compared to the control treatment. The liposome core could load hydrophilic as well as hydrophobic drugs, allowing a broad application for co-encapsulation of BTAs with low molar mass drugs. The developed NCs composed of a liposome with layered deposition could further be improved by deposition of an outer layer with stealth and targeting moieties, creating a multifunctional drug delivery system.

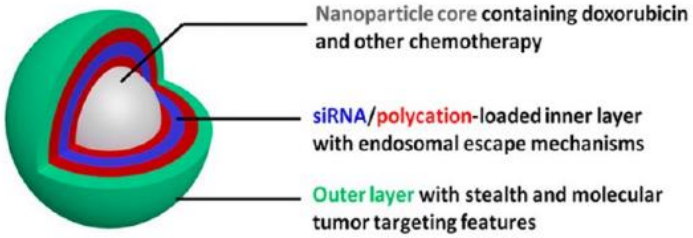

Figure 9. Co-encapsulation of biomacromolecules and small molecular drugs into nanoparticles *via* layer-by-layer method. Image reprinted from reference [119]. Copyright © 2013 American Chemical Society.

b) Nanocarriers by Chemical Reactions

Hydrophilic and hydrophobic cargo molecules can also be encapsulated simultaneously by double emulsion approaches.[120-123] Usually, as a first step the hydrophilic cargo is dissolved in the aqueous phase, either or not with a hydrophilic nanocarrier material, e.g. gelatin, which is then dispersed in an organic phase containing the hydrophobic cargo and a nanocarrier matrix material. Then, this W/O emulsion is dispersed in a second aqueous solution to generate the double W/O/W emulsion. W/O/W emulsions are prone to coalescence of the internal water droplets and W/O emulsion droplets (Figure 10A). Furthermore, as water diffusion from the internal to the outer aqueous phase would dissolve the inner water droplets, several stabilizers have to be added to the double emulsion.[124] Surfactants with low HLB values, such as polyglycerol polyricinoleate (PGPR; HLB = 4), stabilize the first W/O emulsion to prevent coalescence of the internal water droplets.[125] The W/O emulsion is then stabilized towards the outer aqueous phase with another surfactant (high HLB), such as sodium dodecylsulfate (SDS, HLB = 40), or *via* Pickering stabilization.[121, 126] Afterwards, the core-shell nanoparticles are formed through solvent evaporation of the organic layer to encapsulate hydrophobic components in the polymeric shell and the hydrophilic components in the aqueous core (Figure 10B).[123] With the double emulsion method various combination of cargo molecules (e.g. DOX and erlonitib,[127] verteprofin and cisplatin,[128] siRNA,[20, 28, 121] or DNA and thiazoles[123]) were co-encapsulated into degradable polymeric NPs based on PCL, PLA, or PLGA.[121, 129]

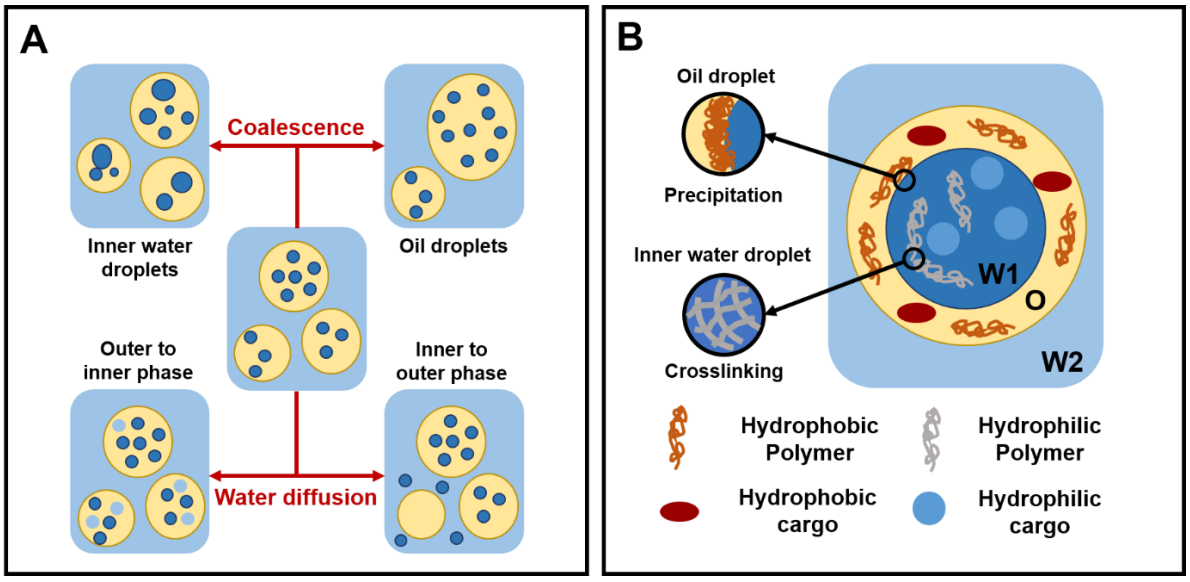

Figure 10. A) Schematic representation of possible instabilities occurring in W/O/W double emulsions. Image adapted from reference [120] with permission from the American Chemical Society. Copyright © 2018. All rights reserved. B) Co-encapsulation of hydrophobic and hydrophilic compounds into nanocarriers by preparation in double emulsions. W1 = inner aqueous phase; O = inner oil phase; W2 = outer aqueous phase.

Various crosslinking chemistries were applied to form core-shell nanocarriers with either a hydrophilic or a hydrophobic core. Lipid-polymer hybrid materials, i.e. "lipogels" were used to encapsulate hydrophilic and hydrophobic components simultaneously.[130] Homyak *et al.* reported lipogels for co-encapsulation in a single-pot method with three formation steps (Figure 11).[131] The inner core contained of the hydrophilic cargo (green-fluorescent protein (GFP) and polymer precursors (2-(2-methoxyethoxy)ethyl methacrylate (DEGM)). The core was coated with a lipid layer by self-assembly of the liposome upon hydration. The core was crosslinked by UV-induced polymerization and crosslinking with (*N,N′*-bis(methacryloyl)-L-cystine (CDM). In a last step, the lipogel was loaded with the second hydrophobic cargo (dye) into the lipid bilayer shell. The technique for lipogel formation could be transferred to various combinations of lipidic and gel-like nanocarriers for co-delivery of hydrophilic and hydrophobic compounds.[130, 132]

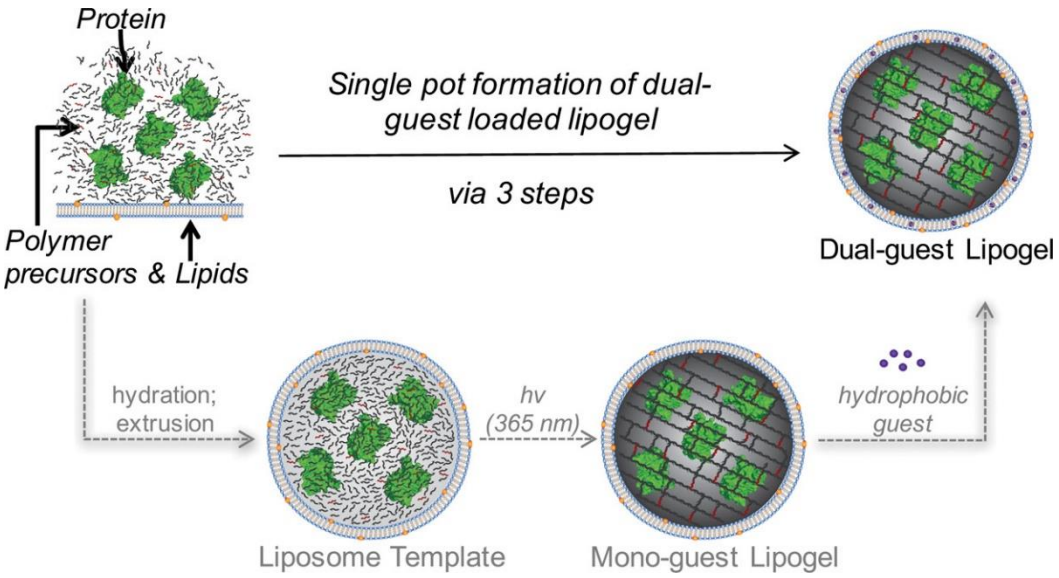

Figure 11. Single-pot method to prepare lipogels *via* liposomal templating and subsequent core cross-linking under UV irradiation for co-encapsulation of hydrophilic compounds (here green-fluorescent protein) into the crosslinked gel-core and hydrophobic compounds (here DiI dye) into lipid-bilayer. Image reprinted with permission from reference [131]. Copyright © 2017 American Chemical Society. All rights reserved.

II. 3. Co-Encapsulation of Organic and Inorganic Cargo Molecules

The combination of organic molecules, such as therapeutic drugs, with inorganic nanoparticles for imaging, creates multifunctional nanocarriers for theranostics.[2, 3] Important imaging materials compose of inorganic nanoparticles (NPs), such as gold NPs, iron oxide NPs or quantum dots (QD), possessing unique optical, plasmonic, electric or magnetic properties.[133] For example, the quantum mechanical effects in gold NPs makes them efficient contrast agents

for photoacoustic imaging or computed tomography (CT).[134] Inorganic nanoparticles (INPs) can be stabilized with either hydrophilic or hydrophobic coatings, such as citrate- or oleic acid-groups, to disperse them into water or organic solvents, respectively.[135] Therefore, co-delivery of INPs with therapeutic agents are based on previous developed co-encapsulation strategies. For example, self-assembled nanocarriers, such as micelles or liposomes, have as well demonstrated efficient co-encapsulation properties of INPs with therapeutics.[136, 137] Wang *et al.* combined anti-cancer drug quercetin with fluorescent polyacrylic acid-terminated silicon quantum dots (PAAc-SiQDs) by co-encapsulation into biodegradable PEG-*b*-PLA nanocarriers (Figure 12).[138] The nanocarriers were prepared by a double emulsion process using an internal emulsion of DMSO in DCM, which was emulsified and stabilized in an aqueous polyvinyl alcohol solution. The amphiphilic polymer (dissolved in DCM) encapsulated the quercetin and PAAc-SiQDs in DMSO during the self-assembly. The resulting dual-loaded nanocarriers exhibited a strong red fluorescence, which enabled monitoring of the drug. Encapsulation of quercetin resulted in higher anti-cancer efficiency compared to the free drug.

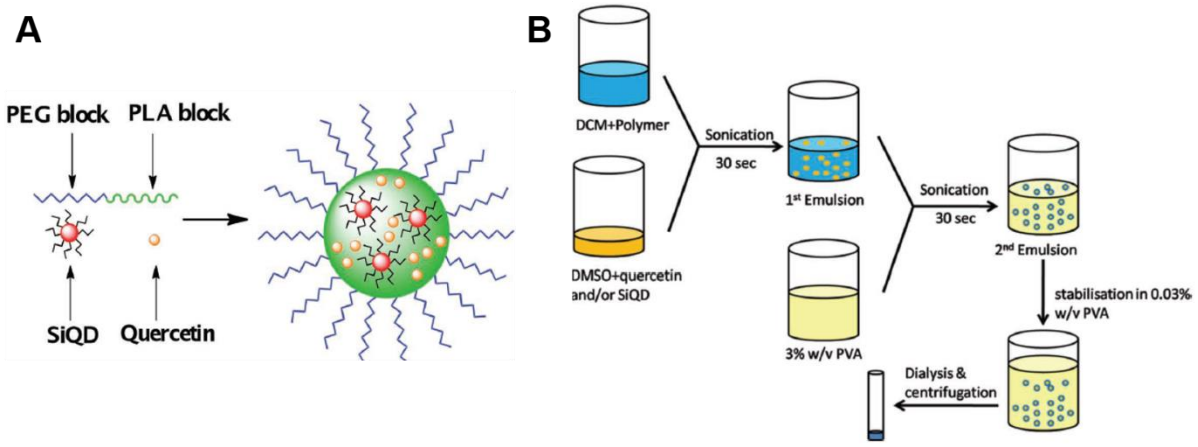

Figure 12. A) Co-Encapsulation of quercetin and polyacrylic acid-terminated silicon quantum dots into poly(ethylene glycol)-poly(lactic acid) nanoparticles. B) Schematic of co-encapsulation into PEG-PLA nanocarriers by double emulsion method. Adapted from reference [138] with permission from John Wiley & Sons, Inc. Copyright © 2013. All rights reserved.

The double emulsion strategy combined with solvent evaporation was also used to co-encapsulate INPs with both hydrophilic and hydrophobic drugs.[139] The hydrophilic drug was dissolved in the inner aqueous phase, entrapped by a polymeric shell, which again entraps Fe_3O_4-NPs and hydrophobic cargo upon solvent evaporation.[140] Several publications reported the co-encapsulation of DOX with iron oxide nanoparticles into degradable PLGA nanocarriers by single emulsion and double emulsion solvent evaporation.[141] Anisotropic Janus particles have raised interested as drug delivery systems due to their unique structural asymmetry.[142] Lim *et al.* demonstrated the co-encapsulation of INPs and small molecular drugs into

biocompatible anisotropic Janus particles by single-step solvent emulsion technique.[143] The hybrid Janus particles based on PLGA or PLA with PMMA could efficiently encapsulate oleic acid coated iron oxide NPs and drugs DOX and PTX by selective encapsulation into the different "faces" of the Janus structure.

II. 4. Conclusion

Nanocarriers with multiple cargo load are promising multifunctional drug delivery systems to improve treatment efficiency. However, the co-encapsulation of multiple molecules, especially with different physicochemical properties, simultaneously into one nanocarrier system is challenging and requires a complex design of the nanocarrier preparation. In an optimal co-encapsulation strategy, multiple cargo molecules can be encapsulated with high loading efficiency and without the cargo involving in the nanocarriers formation process. Orthogonal approaches are essential for the encapsulation of bioactive cargo molecules to keep them active – a chemical reaction might decrease their activity. Orthogonal strategies to prepare nanocarriers can be divided in two groups: 1) Nanocarriers by physical formation such as self-assembly into liposomes or polymeric micelles and 2) Nanocarriers by chemical reactions such as click crosslinking or polymerizations. For co-encapsulation of hydrophobic and hydrophilic molecules, there are nanocarriers such as liposomes or layer-by-layer nanoparticles, which offer both hydrophobic and hydrophilic domains, in which cargo molecules can be loaded. With such multi-domain nanocarriers, a broad range of cargo molecules from hydrophilic to hydrophobic, low molar mass or macromolecules and organic with inorganic can be co-encapsulated and co-delivered simultaneously. To date, co-delivery systems focused on dual-loaded nanocarriers, but creating multifunctional systems with more than two active components could be promising to achieve synergistic properties for efficient multitherapy. Furthermore, drug delivery in nanocarriers especially *in vivo* depend on more effects, where issues of low circulation time, unspecific uptake into cells and fast liver excretion limit the clinical application of nanocarriers. To tackle these issues nanocarriers have to be equipped with not only multiple bioactive compounds inside but also multifunctional properties outside, such as stealth and targeting. Combining all those requirements in one nanocarrier system is of high demand to achieve translation of nanocarriers as drug delivery systems into clinical therapy.

III. Results and Discussion

Chapter A – Multicomponent Encapsulation into Fully Degradable Protein Nanocarriers *via* Azide-Alkyne Click Reaction

Chapter A is mostly presented in the paper "Multicomponent Encapsulation into Fully Degradable Protein Nanocarriers *via* Azide-Alkyne Click Reaction in Miniemulsion Allows the Co-Delivery of Immunotherapeutics"; published in Nanoscale Horiz., 2022, **7**, 908-915. For the thesis, this chapter was extended with additional experiments, optimizations and details.

Contributions:

Natkritta Hüppe is the main author of the paper and this chapter. Natkritta Hüppe synthesized and characterized the modified protein and resulting protein nanocarriers as well as the azide-transfer agent and crosslinker involved as stated in the experimental part. The surfactant poly((ethylene/butylene)-*block*-(ethylene oxide)) was synthesized by [redacted]. ICP spectroscopy was performed by [redacted], MALDI-TOF was performed by [redacted] and horse radish peroxidase activity assay was performed by [redacted]. I performed all degradation and release experiments as well as the analytical and quantification measurements for the degradation and release experiments. [redacted] performed the encapsulation of protein nanocarriers into polymeric vesicles and the degradation experiments. I performed the quantification of Resiquimod and muramyl dipeptide. For quantification of polyinosinic-polycytidylic acid, I performed the degradation and release of Poly(I:C) from the protein nanocarrier and the released amount was measured by [redacted] with HPLC. All electron microscopy measurements were performed by [redacted] (SEM) and [redacted] (TEM). Sample preparation for SEM was performed by me. [redacted] performed *in vitro* experiments with the adjuvant-loaded protein nanocarrier.

Abstract

Encapsulation of multiple adjuvants along with antigens into nanocarriers allows a co-delivery to antigen-presenting cells for the synergistic induction of robust immune responses. However, loading cargos of different molar masses, polarities, and solubilities in high efficiencies remains a challenge. Therefore, we developed a strategy to encapsulate a triple combination of the so-called adjuvants, i.e. with Resiquimod (R848), muramyl dipeptide (MDP) and polyinosinic-polycytidylic acid (Poly(I:C)) into human serum albumin (HSA) nanocarriers. The loading is conducted *in situ* while the nanocarrier is formed by an orthogonal and metal-free click reaction at the interface of an inverse miniemulsion. By this unique approach, high encapsulation efficiency without harming the cargo during the nanocarrier formation process and regardless of their physical properties is achieved, thus keeping their bioactivity. Furthermore, we demonstrated high control over the encapsulation efficiency and varying the amount of each cargo did not influence the efficiency of multicomponent encapsulation. Azide-modified HSA was crosslinked with hexanediol dipropiolate (HDDP) at the interface of a water-in-oil miniemulsion. Varying the crosslinker amount allowed us to tailor the density and degradation rates of the protein shell. Additional installation of disulfide bonds into the crosslinker created redox-responsive nanocarriers, which degraded both by protease and under reducing conditions with dithiothreitol. The prepared HSA nanocarrier were efficiently taken up by dendritic cells and exhibited an additive cell activation and maturation, exceeding the nanocarriers loaded with only a single drug. This general protocol allows the orthogonal and metal-free encapsulation of various drugs or adjuvants at defined concentrations into the protein nanocarriers.

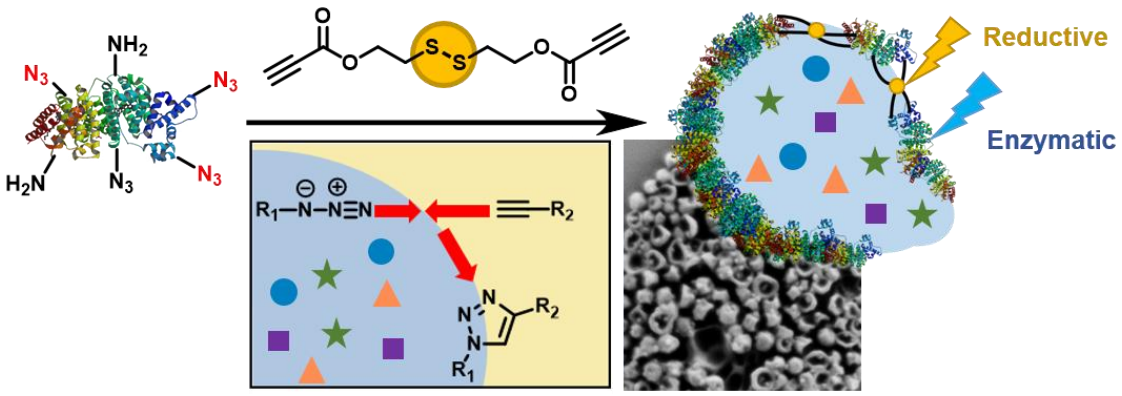

Figure 13. Multicomponent encapsulation into dual-responsive protein nanocarriers by interfacial azide-alkyne click reaction in inverse water-in-oil miniemulsion. Protein structure was obtained from DrugBank online (https://go.drugbank.com/drugs/DB00062, 28.11.2021) and was adapted. Figure created in ChemDraw by Natkritta Hüppe.

III. A1. Introduction

Biochemical Biochemical processes in the body rely on a complex interplay of multiple components. If medical therapy aims to mimic or enhance those processes, multiple therapeutic components have to be integrated into one system. For example, in immunotherapy, the biggest challenge is the exhaustion of immune cells due to the immunosuppressive tumor microenvironment.[144-146] Hence, effective tumor treatment relies on the induction of a strong and durable immune response. Monotherapy proved to be insufficient to overcome these challenges and efforts have to be made to realize a combinatorial treatment with multiple components.[147, 148] True to the motto "The more the merrier", a combination of multiple components enables additive effects for enhanced treatment efficacy. In vaccination approaches, a combination of multiple adjuvants yields a synergistic effect in dendritic cell-directed T cell stimulation, increasing the vaccination effect.[109, 149-151]

The key to success is an efficient process for multicomponent encapsulation of cargo molecules with different physicochemical properties such as molar mass, polarity, and solubility.

Common methods to prepare protein nanocarriers include desolvation, self-assembly or gelation. For example, Abraxane® is a nanoparticle based on albumin-bound paclitaxel, which is commercially used in cancer therapy. Paclitaxel is entrapped into the albumin nanoparticle during the albumin aggregation by a desolvation process. Although efficient entrapment of drugs can be achieved with those methods, there is a lack of control when multiple drugs should be encapsulated simultaneously into one nanocarrier. Especially when the cargo molecules have different physicochemical properties such as solubility, controlled and efficient encapsulation of all components is challenging with methods relying on random entrapment.

To design the optimal nanocarrier, several requirements are necessary: 1. simultaneous encapsulation of multiple cargo molecules, 2. selective reaction for the shell formation without harming the cargo, 3. dense carriers for the transport in the body, and 4. Degradadation of the carriers at the target site. Combining all requirements in one process proved to be challenging. Our developed process combines all four requirements and enables controlled and efficient multicomponent encapsulation into fully degradable protein nanocarriers (PNCs) *via* azide-alkyne click reaction in inverse miniemulsion.

For the first requirement, an inverse miniemulsion allows the simultaneous encapsulation of different water-soluble cargo molecules into nanocarriers with a defined concentration.[49] In an inverse miniemulsion, the shell material is crosslinked at the interface of the water-droplets *via* an oil-soluble crosslinker, forming a nanocarrier with a liquid core. The water-soluble cargo molecules are encapsulated inside the nanocarriers during the interfacial shell formation. For the second requirement, click reactions enable selective linkage between shell material and crosslinker without involving the cargo in the shell formation reaction.[152, 153] Previously, protein nanocarriers were prepared by UV-initiated photoclick tetrazole-ene reaction in inverse miniemulsion.[82] However, UV-light or other harsh initiators, such as metals,[154] can destroy sensitive cargo molecules leading to loss of bioactivity. A crosslinker such as hexanediol dipropiolate (HDDP) with an activated alkyne reacts without a catalyst in an azide-alkyne click reaction.[72, 155] The amount of crosslinker influences the number of links between the shell material and might control the density of the nanocarrier shell for the third requirement. The last requirement is a degradable shell material ensuring the release of the cargo from nanocarriers. Proteins have been widely used as nanocarrier materials, because of their natural biocompatibility and degradability.[81, 82, 156, 157]

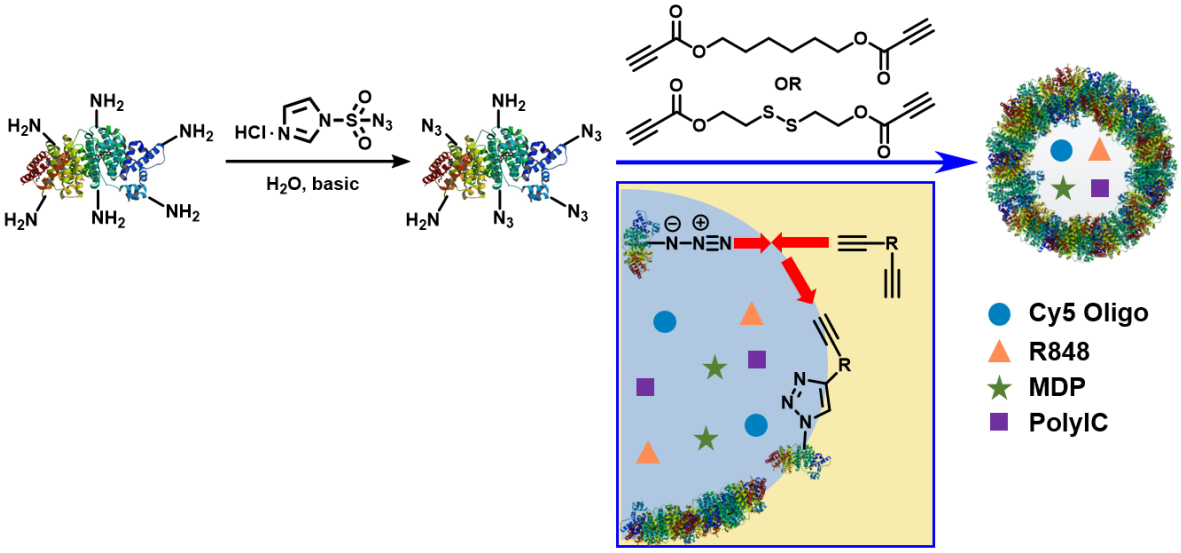

Figure 14. Multicomponent encapsulation into protein nanocarriers through interfacial azide-alkyne crosslinking reaction. Protein structure was obtained from DrugBank online (https://go.drugbank.com/drugs/DB00062, 28.11.2021) and was adapted. Figure created in ChemDraw by Natkritta Hüppe.

III. A2. Preparation of Protein Nanocarriers

III. A2.1 Azide-Functionalization of Proteins

For the preparation of protein nanocarriers through azide-alkyne click reaction, the shell material has to be functionalized with azide moieties. To establish a reliable protocol, different chemistries were investigated and are summarized here: Common reactions with azide compounds, for example with an 1-(2-azidoethyl)-3-(2-(2-(2-isocyanatoethoxy) ethoxy)methyl) urea[18], are performed in organic solvents, such as dimethylsulfoxide (DMSO) (Scheme 1).

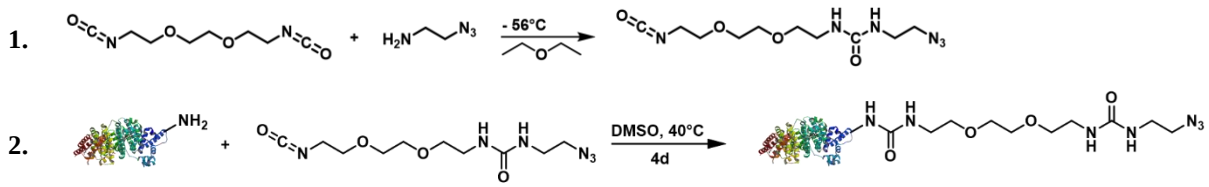

Scheme 1. Azide-functionalization of proteins with 1-(2-azidoethyl)-3-(2-(2-(2-isocyanatoethoxy) ethoxy)methyl) urea in dimethylsulfoxide. Protein structure was obtained from DrugBank online (https://go.drugbank.com/drugs/DB00062, 28.11.2021) and was adapted. Figure created in ChemDraw by Natkritta Hüppe.

Since the protein was not soluble in DMSO, the functionalization was carried out in a suspension. Although, human serum albumin (HSA) could be successfully functionalized with azide groups, proved by the prominent azide-signal in the infrared (IR) spectra (Figure 15), the azide-bearing protein was not soluble in water or even buffer anymore.

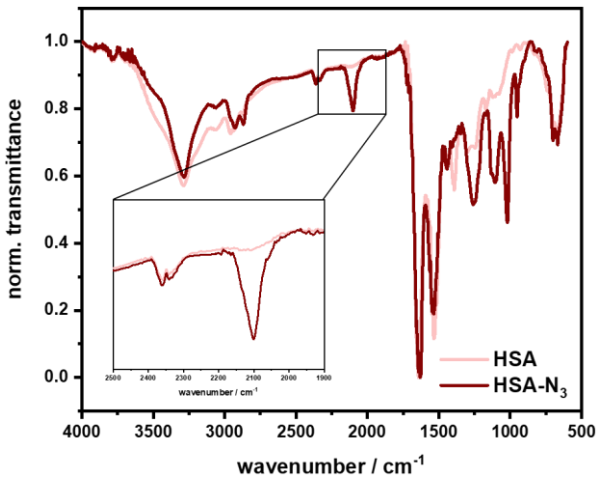

Figure 15. Infrared spectra of native human serum albumin (HSA) and HSA after reaction with azide-PEG-isocyanate in dimethylsulfoxide.

One reason for the loss of solubility is that proteins are prone to denature in organic solvents. The long reaction time of 4 days in DMSO resulted possibly in denaturation of the protein and decrease of water solubility. The rather large azide reagent, if reacting with the numerous amine groups of proteins, influences the protein folding and thus its stability and solubility. This approach was discarded as water-solubility and stability in aqueous media is the key for the formation of protein nanocarrier through interfacial crosslinking in a water-in-oil miniemulsion. Therefore, using a reaction, which is carried out in aqueous media would be a better approach to functionalize proteins with azide groups. Azide transfer agents such as 1-imidazole-sulfonyl azide hydrochloride offers azide functionalization of amines through a direct transfer reaction in aqueous media with minimal change to the protein. The azide transfer agent was synthesized from sulfuryl chloride, sodium azide and imidazole according to literature (Scheme 2).[158]

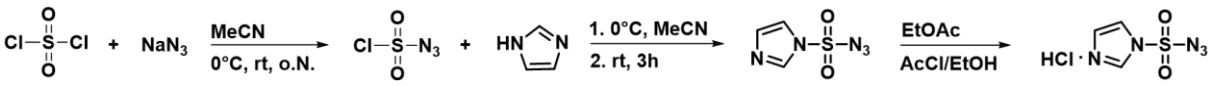

Scheme 2. Synthesis of 1-imidazole-sulfonyl azide hydrochloride according to Goddard-Borger *et al.* [158]

The compound is transformed into a water-soluble compound by forming a hydrochloride salt. 1-imidazole-sulfonyl-azide hydrochloride was obtained as proved in the ^{1}H NMR spectrum in high yield (97%) and a high water-solubility was observed (Figure 16). The salt form of 1-imidazole-sulfonyl azide not only enables water-solubility but also a higher stability for a safer procedure without the formation of toxic or explosive side products compared to other routes.[159]

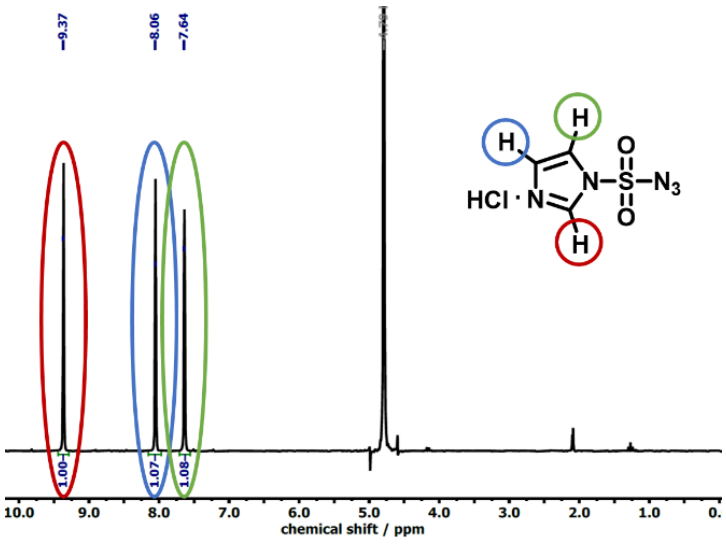

Figure 16. ^{1}H NMR spectrum of 1-imidazole-sulfonyl azide hydrochloride in D_2O.

The quantitative amount of azide groups was determined with the fluorescamine assay in borate buffer at pH 8.2 (Figure 17). Fluorescamine reacts with amine groups to a fluorescent product, measurable by UV/Vis spectroscopy (λ_{ex} = 365 nm, λ_{em} = 480 nm). Glycine was used for the standard calibration curve and lysozyme (six lysine groups) was used as a reference. A decreased amount of amine groups indicated a successful transfer to azide groups.

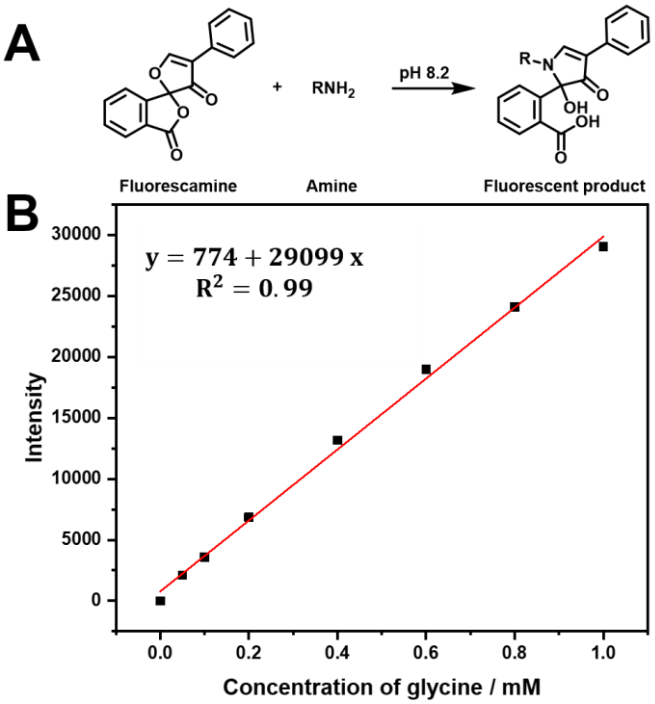

Figure 17. Reaction of fluorescamine with amines to a fluorescent product in borate buffer at pH 8.2. Quantification of amines with glycine as calibration substrate.

The azide transfer with 1-imidazole-sulfonyl azide hydrochloride was performed with copper sulfate as a catalyst.[158] Proteins, especially serum albumins have the purpose form a complex with toxic metal salts such as copper in the blood, which makes purifying the modified protein from the metal by simple dialysis difficult. As expected, a significant amount of copper was still detectable with inductively coupled plasma atomic optical emission spectroscopy (ICP-OES) in HSA after the azide-functionalization reaction catalyzed with copper sulfate (Table 4). Since the following nanocarrier formation is based on a metal-free azide-alkyne click reaction, remaining copper in the protein would ruin the concept of a biocompatible nanocarrier formation. An azide-functionalization should be performed without needing a metal catalyst. Schoffelen *et al*. investigated the metal-free and pH-controlled introduction of azide moieties to proteins.[160] They claim that under higher basic conditions (pH 11), where the nucleophilicity of the amine moiety is increased, an azide transfer can be performed without support of a catalyst (Scheme 3).

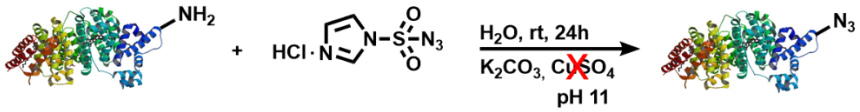

Scheme 3. Copper-free functionalization of proteins with azide groups through reaction of amines with 1-imidazole-sulfuryl azide hydrochloride under basic conditions. Protein structure was obtained from DrugBank online (https://go.drugbank.com/drugs/DB00062, 28.11.2021) and was adapted.

Azide-functionalized HSA (HSA-N_3) synthesized through a copper-free reaction with 1-imidazol-sulfonyl azide hydrochloride at high basic conditions showed a significantly low amount of copper, almost below detection limit as determined by ICP-OES (Table 1). It has to be noted that the commercial serum albumin obtained low amount of copper, whereas the used potassium carbonate contains > 0.1 ppm of copper according to the bottle label. The number of amines decreased after reaction, indicating a successful metal-free azide functionalization. Moreover, under high basic conditions more amines reacted compared to the copper-catalyzed reactions, demonstrating a high reactivity of amine groups in basic media with no need of a catalyst.

Table 4. Azide-functionalization of human serum albumin with and without copper as catalyst. Number of azide groups ($N_{ex}(N_3)$) quantified by the theoretical ($N_{theo}(NH_2)$) and experimental ($N_{ex}(NH_2)$) number of amines, measured with the fluorescamine assay.

Protein	**c(Cu) / mgL^{-1}**	***M* / gmol^{-1}**	**$N_{theo}(NH_2)$**	**$N_{ex}(NH_2)$**	**$N_{ex}(N_3)$**
HSA, nat.	0.017	66700	30-35	30	-
HSA-N_3, +Cu	1.22	67400	-	11	19
HSA-N_3, -Cu	0.05	68300	-	4	26

For the azide-alkyne click reaction, human serum albumin (HSA) was functionalized at the lysine residue by a metal-free transfer reaction using 1-imidazol-sulfuryl azide hydrochloride into azide groups.[158] After functionalization, the fluorescamine assay showed that about 19 amines of the 59 lysine residues per HSA (30-35 accessible lysine groups) were transformed into azide groups. The degree of functionalization changed with pH value as lower pH values led to lower nucleophilicity of the amine and less transfer reactions, whereas pH 9.5 gave an optimal balance between yielding high number of transfer reactions and maintaining the protein structure (Table 5).

Table 5. Azide-functionalization of human serum albumin at different pH values and times. Number of azide groups ($N_{ex}(N_3)$) quantified by the theoretical ($N_{theo}(NH_2)$) and experimental ($N_{ex}(NH_2)$) number of amines before and after the reaction, measured with the fluorescamine assay.

	pH	t/h	$N_{theo}(NH_2)$	$N_{ex}(NH_2)$	$N_{ex}(N_3)$
HSA, nat.	-	-	30-35	35	-
HSA-N_3	8.2	2	-	37	-
HSA-N_3		4	-	33	2
HSA-N_3		8	-	30	5
HSA-N_3		16	-	29	6
HSA-N_3		24	-	29	6
HSA-N_3		48	-	21	14
HSA-N_3	9.5	2	-	28	7
HSA-N_3		4	-	22	13
HSA-N_3		8	-	13	22
HSA-N_3		16	-	6	29
HSA-N_3		24	-	5	30
HSA-N_3		48	-	2	33
HSA-N_3	11	2	-	10	16
HSA-N_3		4	-	3	32
HSA-N_3		8	-	2	33
HSA-N_3		16	-	3	32
HSA-N_3		24	-	3	32
HSA-N_3		48	-	2	33

A comparison of the IR spectra of natural and azide-modified HSA showed successful modification as demonstrated by the presence of the characteristic azide signal at 2100 cm^{-1} (Figure 18A). The advantage of azide-functionalization with 1-imidazol-sulfuryl azide hydrochloride is that only the amine group is transferred to an azide, with minimal changes or attachments compared to other azide-functionalization reactions. Therefore, no significant changes in the secondary structure of the protein were observed by circular dichroism (CD) spectroscopy (Figure 18B). The modified protein remained highly water-soluble (> 100 mg/mL) further highlighting the mildness of the transfer reaction. The change in mass after the azidation also indicates a successful introduction of azide groups to HSA (Figure 18C).

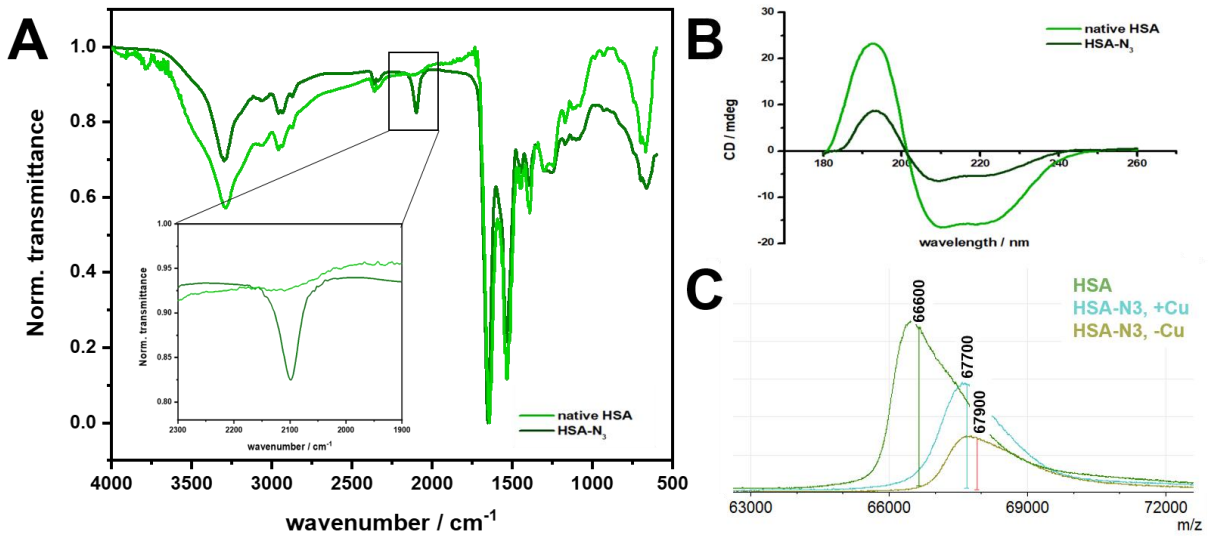

Figure 18. A) Infrared spectra of natural human serum albumin (HSA) compared to copper-free azide-functionalized HSA. B) Circular dichroism spectra of native HSA and azide-functionalized HSA (HSA-N_3). C) MALDI-TOF of human serum albumin (HSA, green), HSA-N_3 *via* copper-catalyzed azide-functionalization (blue) and HSA-N_3 *via* copper-free azide-functionalization.

Human serum albumin was successfully functionalized with azide-groups by a copper-free reaction with 1-imidazole-sulfuryl azide hydrochloride. The milder reaction in aqueous media maintained the integrity of the protein (cf. CD spectrum) and the water-solubility after modification. The amount of azide moieties could be controlled by the pH value of the reaction media, where higher pH enabled higher functionalization degree.

With a water-soluble azide-functionalized protein in hand, protein nanocarriers can be prepared through a metal-free azide-alkyne crosslinking in inverse miniemulsion.

III. A2.2 Azide-Alkyne Crosslinking of Proteins in Inverse Miniemulsion

The challenge of a multicomponent encapsulation is to achieve encapsulation of cargo molecules of different physicochemical characteristics with high efficiency and a defined concentration in one process. The inverse miniemulsion allows simultaneous encapsulation of different water-soluble cargo molecules into nanocapsules with a defined concentration.[49] In an inverse miniemulsion, nano-sized water droplets, containing a shell material, are dispersed with high shear forces in an oil. An oil-soluble reagent, i.e. crosslinker, must be added to the emulsion to link the shell material at the water droplet interface, forming a nanocapsule with a liquid core. The cargo molecules are also dissolved in the water droplets and are encapsulated with high efficiency in the nanocapsules during the interfacial shell formation. The nanocarriers are then transferred into an aqueous phase by a surfactant change, when redispersing the organic nanocarrier dispersion in an aqueous surfactant solution (Figure 19).

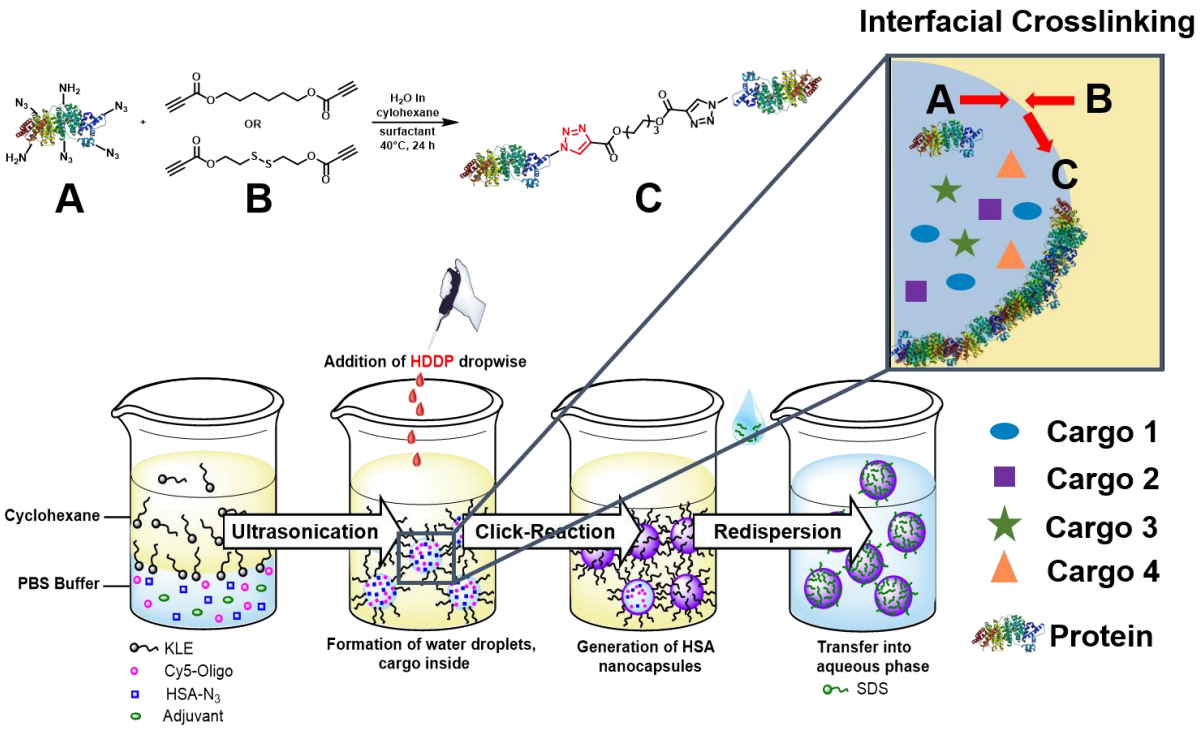

Figure 19. Preparation of protein nanocarriers (PNCs) by interfacial crosslinking of azide-functionalized proteins with hexanediol dipropiolate (HDDP) or HDDP-disulfide (HDDP-SS) in inverse miniemulsion and transfer of PNCs into water by surfactant change. Protein structure was obtained from DrugBank online (https://go.drugbank.com/drugs/DB00062, 28.11.2021) and was adapted. Figure created in ChemDraw by Natkritta Hüppe.

For the formation of protein nanocarriers (PNCs) by azide-alkyne click reaction, we chose the dialkyne hexanediol dipropiolate (HDDP) as a crosslinker of the azide-modified proteins. The carbonyl group located next to the alkyne moiety activates the alkyne by an inductive effect, allowing a click reaction without using a metal catalyst.[155] Moreover, inserting a disulfide bond into the chemical structure of HDDP (i.e. to HDDP-SS) created a crosslinker prone to degradation by a reducing agent.[72] The oil soluble HDDP reacts with the azide-functionalized protein in a metal-free click reaction at the water-droplet interface, forming a protein shell.

The PNCs were prepared in an inverse water-in-oil miniemulsion with cyclohexane as the continuous and an aqueous buffer as the dispersed phase (Figure 19). The aqueous nanodroplets were prepared with high shear forces using ultrasonication and were stabilized by the surfactant poly((ethylene/butylene)-*block*-(ethylene oxide)) (P((E/B)-*b*-EO)).[161] A stable inverse miniemulsion without merging of the droplets enables formation of the shell at the interface without disruption. The stability of the inverse miniemulsion was monitored by dynamic light scattering (DLS) at a 173° backscattering detection angle. The size and polydispersity index (PDI) of the droplets did not change over a period of 12 h (Figure 20), indicating that the formed inverse miniemulsion droplets with P((E/B)-*b*-EO) stayed stable and no merging of the droplets occurred.

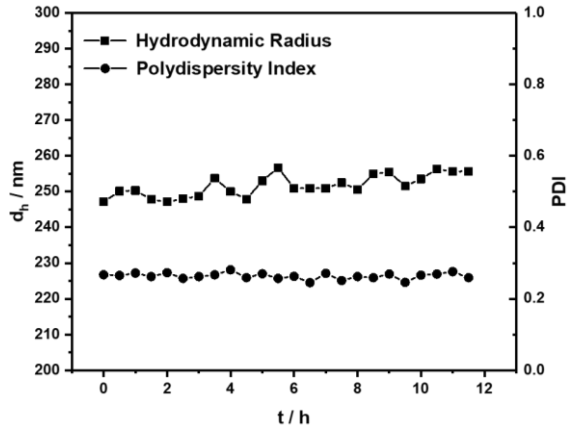

Figure 20. Stability of inverse water-in-cyclohexane miniemulsion droplets with P((E/B)-*b*-EO) as surfactant, measured by dynamic light scattering at 173° detection angle.

The protein shell formed through an interfacial crosslinking at the water droplet interface after addition of HDDP or HDDP-SS to the inverse miniemulsion. In the IR spectra of the HSA-NCs, the azide signal at 2100 cm^{-1} decreased due to the formation of the triazole during the click reaction (Figure 21A). The hydrodynamic diameters (d_h) of the PNCs in cyclohexane were determined to be approx. 300 nm by dynamic light scattering (DLS) (Figure 21B). After redispersion in water using sodium dodecyl sulfate (SDS, 0.02 mM) as the surfactant followed by washing, the diameters decreased to approx. 250 nm with a zeta potential of approx. -30 mV (Figure 21C).

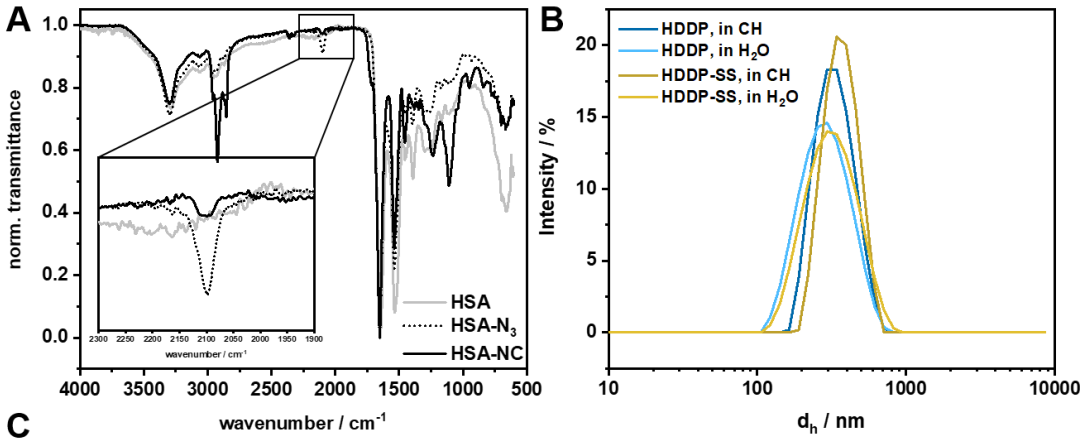

Protein	N_{theo} (NH_2)	N_{ex} (NH_2)	N_{ex} (N_3)	Linker	$d_{h,CH}$ / nm	PDI_{CH}	$d_{h,water}$ / nm	PDI_{water}	ζ /mV
HSA	30-35	11	19-24	HDDP	302	0.13	264	0.23	-30
HSA	30-35	11	19-24	HDDP-SS	327	0.14	254	0.17	-34

Figure 21. A) Infrared spectra of native, HSA-N_3 (…) and HSA-NC (–). B) Dynamic light scattering of HSA-NCs in cyclohexane and H_2O using HDDP or HDDP-SS as crosslinker. C) Analytic data of HSA-NCs using HDDP and HDDP-SS.

Scanning electron microscopy (SEM) and transmission electron microscopy (TEM) micrographs in cyclohexane revealed a core-shell morphology of the PNCs similar to a deflated football (Figures 22). There was no significant difference between PNCs crosslinked with HDDP or HDDP-SS and in both cases, collapsed nanocarriers with a core-shell morphology could be observed.

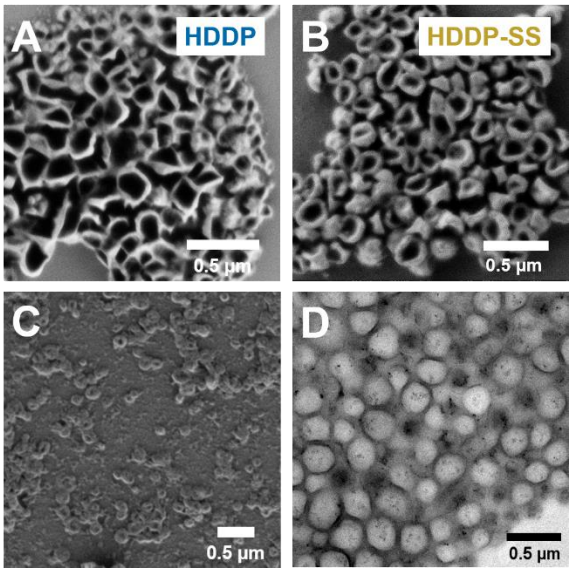

Figure 22. Scanning electron micrographs of A) HSA-HDDP-NCs in cyclohexane, B) HSA-HDDP-SS-NCs in cyclohexane, C) HSA-HDDP-NCs in water. D) Transmission electron micrograph of HSA-HDDP-NCs in cyclohexane.

The purification of the PNCs after redispersion into an aqueous SDS-solution made a precise handling and new protocol necessary. Due to the swelling of the crosslinked protein-matrix a purification of the soft PNCs by centrifugation was not possible. After removing the supernatant, no pellet of PNCs was obtained. With repeated washing of the aqueous dispersion through an ultrafiltration tube (MWCO 100 kDa) no nanocarriers were lost and excess of SDS could be removed. The yield of nanocarriers in water achieved with the standard operating procedure[162] for PNCs by inverse miniemulsion was around 13%. For biological experiments, especially *in vivo* experiments, a high amount of PNCs was needed. Additionally, with application of expensive biomedical cargo molecules a low yield of PNCs would waste a significant amount of material. Therefore, the yield of HSA-NCs should be increased. Following the standard operating procedure, PNCs were purified by centrifugation at 1500*g*. A significant amount of smaller PNCs was lost during the centrifugation step. With higher centrifugation speed, the amount of collected PNCs could be increased. Since higher centrifugation speed could damage the capsule shell and lead to unwanted release of cargo, the encapsulation efficiency (EE) of encapsulated dye was monitored with increasing the centrifucation speed. The centrifugation speed during the purification in cyclohexane was

increased in 500*g* steps up to 3000*g*. The obtained PNCs were analyzed regarding size, PDI and EE. The average size of PNCs decreased with higher centrifugation speed and the size distribution remained about the same (Table 6, Figure 23). The EE decreased slightly compared to the lowest centrifugation speed, indicating that no significant damage was done to the capsule shell and dye was kept entrapped. Overall, the yield was increased to 62% with increasing the centrifugation speed during the purification in cyclohexane.

Table 6. Increasing the yield of human serum albumin nanocarriers by increasing the centrifugation speed during purification in cyclohexane.

Centrifugation Speed	d_h (CH) / nm	PDI (CH)	m (PNCs, CH) / mg	d_h (H_2O) / nm	PDI (H_2O)	m (PNCs, H_2O) / mg	EE / %
1500*g*	276	0.12	14	294	0.22	6.7	71
2000*g*	234	0.13	8.1	243	0.22	4.4	65
2500*g*	189	0.16	4.5	203	0.15	4.8	63
3000*g*	162	0.16	4.2	160	0.17	1.9	67
Combined	252	0.17	30.84	202	0.23	17.83	-

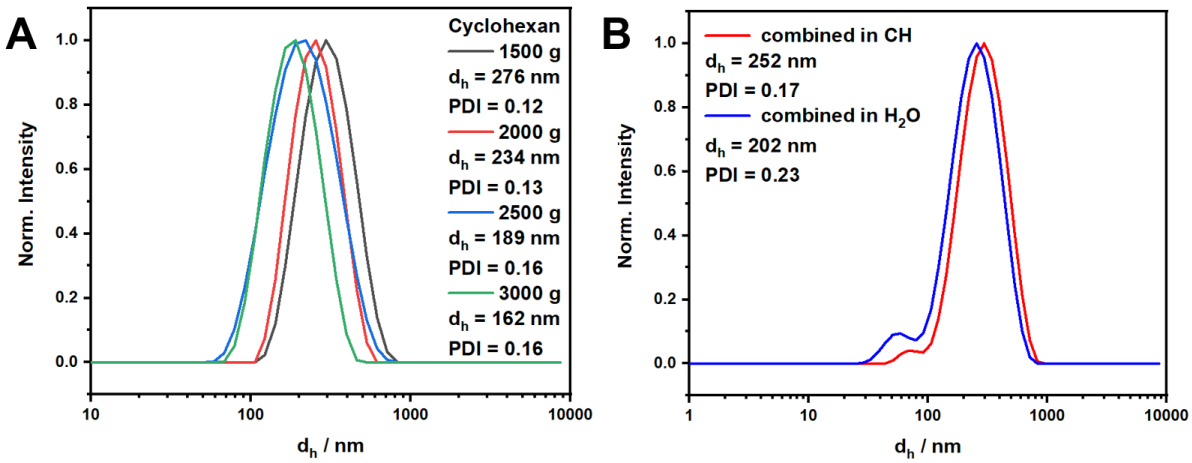

Figure 23. Dynamic light scattering of human serum albumin nanocarriers A) purified in cyclohexane at different centrifugation speed. B) All fractions combined in cyclohexane and after transfer into water.

After redispersion of PNCs into water 36% yield was obtained, doubled the yield as before. Due to the higher centrifugation speed and collection of smaller nanocarriers the size distribution of all collected carriers combined was broader compared to the other protocol. A second distribution with diameters <100 nm appeared in the DLS measurement. A broader distribution was accepted for the following experiments.

Formation of Protein Nanocarriers in an Inverse Miniemulsion Stabilized with Polyglycerol-polyricinoleate (PGPR)

In the group and several previous papers on protein nanocarriers (and others) prepared by an inverse miniemulsion, the typical surfactant was P((E/B)-*b*-EO). The block copolymer P((E/B)-*b*-EO) is synthesized by growing poly(ethylene oxide) (PEO) from the copolymer poly(ethylene-*co*-butylene) (i.e. Kraton liquid). However, the Kraton liquid is not commercially available anymore, making P((E/B)-*b*-EO) as such a "finite" surfactant. Moreover, attempts to synthesize the surfactant with other routes have yet to achieve a product with similar properties. Therefore, it would be an advantage to establish the synthesis of PNCs with commercially available surfactants such as polyglycerol-polyricinoleate (PGPR). PGPR is a cheap and FDA-approved surfactant used for emulsification of chocolate.[163] The inverse miniemulsion was performed with PGPR and the stability of formed water-in-cyclohexane nanodroplets was monitored by DLS at 173° over 18 h and no significant changes in size and PDI could be observed (Figure 24A). However, double concentration of PGPR (10 wt%) had to be used to achieve stable inverse miniemulsion droplets compared to P((E/B)-*b*-EO) (5 wt%). Less PGPR lead to merging of the nanodroplets and phase separation, where stable nanocarrier were unable to form. Nevertheless, with 10 wt% PGPR, stable PNCs could be formed by interfacial crosslinking with HDDP in the inverse miniemulsion. The size and PDI as well as core-shell morphology of PGPR-stabilized PNCs were comparable to the PNCs obtained with P((E/B)-*b*-EO) as shown in the DLS (Figure 24B) and scanning electron micrographs (Figure 24C). The downside with the surfactant was the high amount (min. 75 mg) compared to shell material (50 mg) required to obtain a stable miniemulsion.

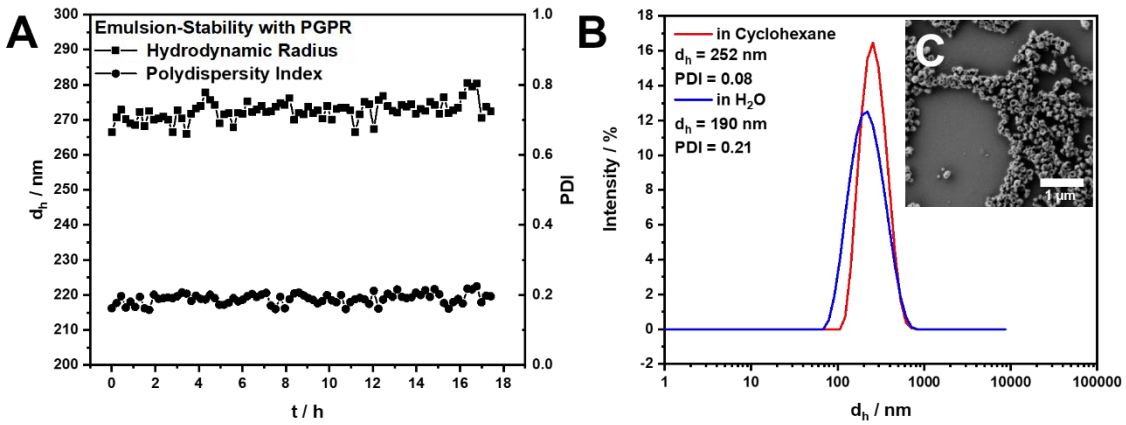

Figure 24. A) Size and size distribution of water-in-cyclohexane nanodroplets in an inverse miniemulsion stabilized with polyglycerol-polyricinoleate (PGPR). B) Dynamic light scattering of protein nanocarrier (PNCs) in cyclohexane (red) and water (blue). C) Scanning electron micrograph of PNCs in cyclohexane.

Protein Nanocarriers from Horse Radish Peroxidase (HRP)

Proteins as materials for nanocarriers are not only naturally biocompatible and degradable, but they offer a high versatility in properties and special functionalities, such as antigens or enzymes.[79] The procedure for forming human serum albumin nanocarriers can be easily transferred to other proteins, such as enzyme horse radish peroxidase (HRP). Using a functional protein is also a great way to investigate the influence of the crosslinking on the structure of the protein, which in enzymes could be expressed by change of enzymatic activity. First, HRP was functionalized with azide groups by 1-imidazol-sulfuryl azide hydrochloride at basic conditions. HRP was successfully functionalized with azide moieties as shown in the IR spectra by the characteristic azide signal at 2100 cm^{-1} (Figure 25A). HRP-N_3 maintained a high water-solubility after purification and lyophilization. After the reaction, the enzymatic activity of HRP-N_3 was reduced by 40%, probably due to the high basic pH of 11 during the transfer reaction (Figure 25C). The nanocarriers formation was performed according to the established procedure for HSA-NCs. The formation of nanodroplets by high shear forces did not significantly influence the enzymatic activity of HRP and only a slight loss in activity was observed. Azide-modified HRP was used as a shell material for the formation of PNCs through interfacial crosslinking with HDDP in inverse miniemulsion. The PNCs based on HRP exhibited similar results in size and morphology compared to HSA-NCs (Figure 25B and D). This demonstrated the excellent reproducibility and transferability for forming PNCs by the developed protocol. Moreover, the HRP-NCs were still enzymatically active, showing approx. 60% of the native enzyme activity (Figure 25C). Moreover, crosslinking had no influence in the enzymatic activity of HRP, since the activity did not change from after the emulsification to after the shell formation, indicating that the structural integrity of the protein was maintained as far as enzymatic activity was maintained.

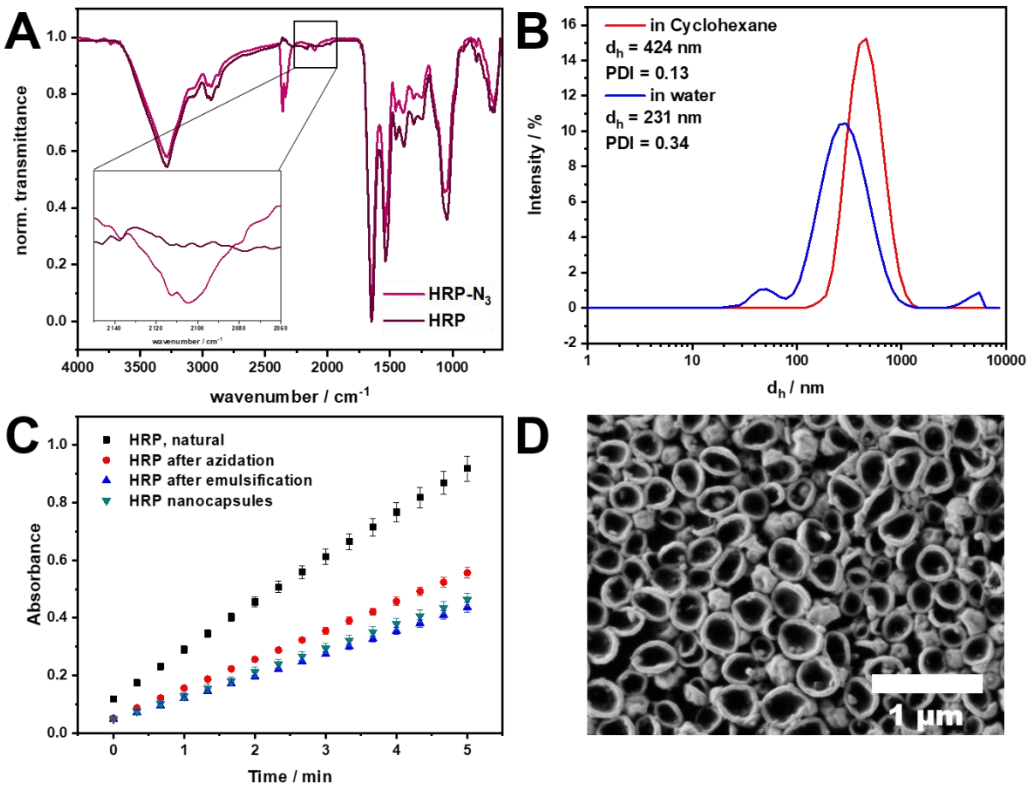

Figure 25. A) Infrared spectroscopy spectra of horseradish peroxidase (HRP) before and after functionalization with azide groups. B) Dynamic light scattering of HRP nanocarriers in cyclohexane (red) and water (blue). C) Enzymatic activity of HRP at different stages of nanocarrier formation procedure quantified with ABTS Assay.

In summary, stable water-in-oil droplets emulsified with P((E/B)-*b*-EO) lead to the successful formation of protein nanocarriers through interfacial crosslinking with hexanediol dipropiolate in inverse miniemulsion. A prominent core-shell morphology could be proved with electron microscopy and a model dye could successfully be encapsulated into PNCs with high efficiency by the inverse miniemulsion process. The yield of PNCs could be increased by increasing the centrifugation speed during the purification process without compromising the high encapsulation efficiency. Stable PNCs were formed in inverse miniemulsion by using commercially available PGPR as surfactant and comparable results in size and morphology were obtained to P((E/B)-*b*-EO)-stabilized inverse miniemulsion. A functional protein, here enzyme horse radish peroxidase, could be used as shell material to form PNCs by interfacial azide-alkyne crosslinking with HDDP in inverse miniemulsion with maintaining 60% of enzymatic activity of HRP-NCs. PNCs could be obtained with the established protocol and water-soluble cargo could be encapsulated with high efficiency during interfacial azide-alkyne crosslinking in inverse miniemulsion. The established protocol would allow encapsulation of more than one water-soluble cargo during the PNCs formation and fulfil the first requirement for multicomponent encapsulation into degradable nanocarriers. The second requirement was a biorthogonal chemistry for the nanocarrier formation without involving the cargo. The

successful modification of proteins with azide groups and following crosslinking by metal-free azide-alkyne click chemistry demonstrated fulfillment of the second requirement by the established protocol. The possibility to use protein, even functional ones, enables degradability and release of cargo from the PNCs, realizing the forth requirement. From the four requirements to design an optimal nanocarrier for co-delivery, only the third requirement of a dense carrier was left. The density of the nanocarrier shell is dependent on the number of crosslinks between the proteins and therefore amount of azide and dialkyne crosslinker. The influence of the crosslinking degree on the shell thickness and density and resulting dependence of encapsulation efficiency and leakage is shown in the next section.

III. A2.3 Influence of Crosslinking Degree on the Shell Thickness and Density

Degradability of nanocarriers ensures efficient release of cargo molecules at the target site. Not only a degradable shell is necessary for an optimal nanocarrier design, but also a dense protein shell preventing leakage of small cargo molecules from the nanocarriers is required. The formation of protein nanocarriers in inverse miniemulsion requires a crosslinker, which reacts with the proteins and links them to a protein shell. The amount of crosslinker influences the number of links between the proteins and thus controls the density of the protein shell. By varying the amount of HDDP crosslinker, shell thickness and size of PNCs could be influenced (Figure 26). When the interfacial crosslinking of azide-modified protein with HDDP was performed with an alkyne:azide ratio of 20:1, PNCs with a d_h = 250 nm and approx. 20 nm shell thickness were obtained (measured from scanning electron micrographs). With a lower alkyne:azide ratio, the shell thickness decreased, while the diameters increased. Lower crosslinking density results in an increased swelling of the looser protein shell, expressed in a higher hydrodynamic size of the PNCs (Figure 26).

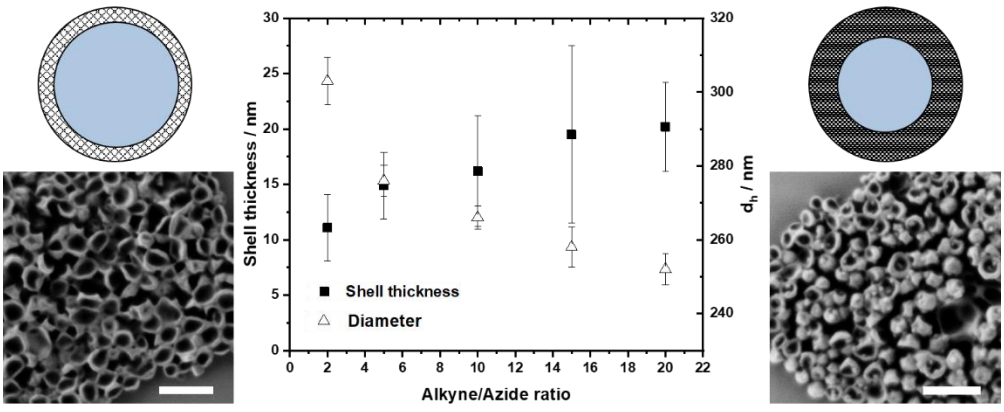

Figure 26. Influence of alkyne:azide ratio on the shell thickness (■) and diameter (Δ) of protein nanocarriers. SEM images of HSA nanocarriers using a 2:1 (left) and 20:1 (right) ratio (Scale bar: 0.5µm).

The amount of crosslinker additionally influenced the encapsulation efficiency after water transfer. The encapsulation efficiency of dextran-sulforhodamine B (*M* = 10 kDa) decreased from 62% to 39% when 20 eq. HDDP or only 2 eq. HDDP were used, respectively (Figure 27A). Additionally, the PNCs were loaded with a small molecule dye sulfurhodamine-101 (*M* = 606.71 g/mol) to record diffusion of the dye through the crosslinked protein shell over a period of five days. The amount of dye was quantified from the fluorescence intensity of the aqueous supernatant after separation from the nanocarriers by centrifugation. Although a lower crosslinking density lead to a faster diffusion through the nanocarrier shell, attributed to the thinner and looser shell walls, the amount of dye in the supernatant was less than 5% after five days. Even less than 2% for 20 eq. of HDDP (Figure 27B). With a higher amount of crosslinker and thus higher crosslinking density, unwanted diffusion of dye from the PNCs could be minimized, resulting in less than 2% diffused dye after five days.

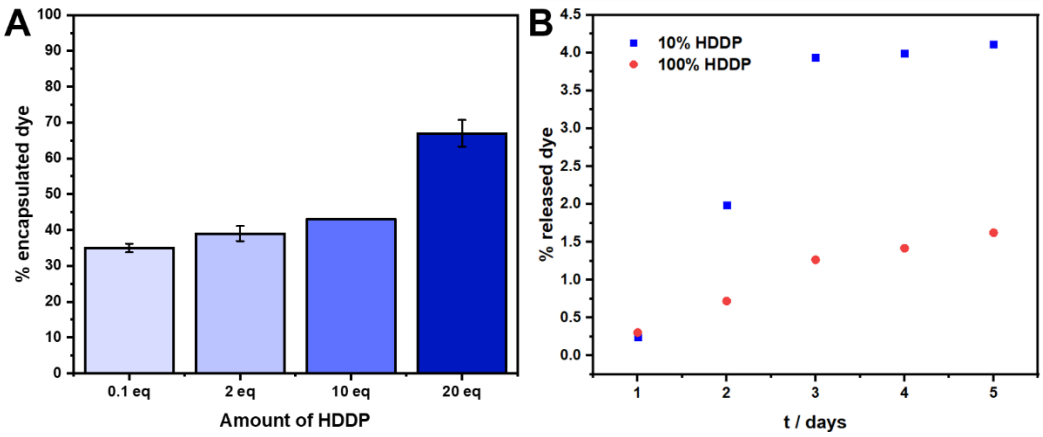

Figure 27. A) Amount of encapsulated dextran-sulforhodamine B (*M* = 10 kDa) encapsulated into protein nanocarriers crosslinked with different amount of HDDP (n = 1). Measured by fluorescence. B) Amount of released sulforhodamine 101 from protein nanocarriers upon storage at room temperature. Measured by fluorescence.

The permeability of the crosslinked protein shell could be influenced by the amount of crosslinker and leakage of small molecule dye from PNCs could be prevented with a higher amount of crosslinker. The crosslinking degree influenced the shell thickness as well with higher crosslinker amount a thicker and denser shell could be obtained. The high crosslinking degree with a thicker and denser protein shell could also have an influence on the degradation kinetics of the protein nanocarrier, especially when the peptide bonds have to be accessible to enzyme degradation. The degradation of protein nanocarriers by enzyme and reducing agent as well as the influence of the crosslinking degree on the degradation and release of dye is investigated in the next section.

III. A3. Degradation of Protein Nanocarriers

The degradability of nanocarriers at the target site ensures the release of the cargo and thus is an important requirement for the design of an optimal nanocarrier. If high molecular weight cargo molecules such as nucleic acids or other proteins are encapsulated, a high degradation rate is needed to enable efficient release of big cargo molecules. Proteins are naturally degradable by enzymes and are optimal shell material for the nanocarrier formation. By using a degradable crosslinker as well, a high degradation degree of nanocarrier could be realized. The dialkyne crosslinker hexanediol dipropiolate with a disulfide bond (HDDP-SS) builds a protein nanocarrier susceptible to reduction. Thus, a protein nanocarrier crosslinked with HDDP-SS obtains a dual-degradability by enzyme and reducing agent. Furthermore, the crosslinking degree and shell thickness could influence the degradation by enzyme as well as reducing agent.

III. A3.1 Enzymatic Degradation of Protein Nanocarriers

For the degradation of protein nanocarriers, PNCs were treated with proteinase K (5 U/mL) for 24 h in PBS buffer. A sample of PNCs treated with PBS buffer served as a control sample. DLS measurements revealed the degradation of PNCs by proteinase K in a decreased size from 254 to 71 nm and broader distribution from 0.16 to 0.42, while the control sample did not change significantly (Figure 25). The derived count rate (DCR) in DLS gives the signal strength of samples or scattering intensity in the absence of the laser attenuation filter. Therefore, a decreased DCR from 4300 to 180, as observed here for PNCs treated with proteinase K, could indicate a degradation of PNCs to smaller fragments with smaller scattering intensity.

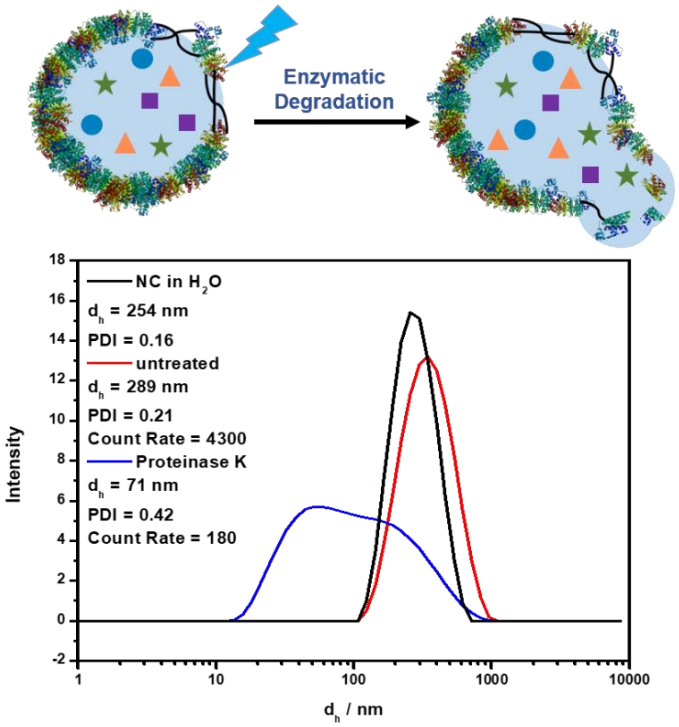

Figure 28. Release of cargo molecules from protein nanocarriers (PNCs) through enzymatic degradation. DLS of PNCs in water (black), untreated (red) and treated with proteinase K (5 U/mL) for 24 h at 37 °C. Protein structure was obtained from DrugBank online (https://go.drugbank.com/drugs/DB00062, 28.11.2021) and was adapted.

The degradation of the PNCs was investigated by monitoring the release of dextran-rhodamine B (M = 10 kDa, λ_{em} = 570 nm). Crosslinking the PNCs with different amounts of HDDP or HDDP-SS enabled investigating the influence of shell density on the degradation kinetics. The PNCs degraded upon the addition of proteinase K (5 U/mL) and the amount of released dye was detected in the aqueous supernatant. Depending on the time of the degradation experiment, the amount of released dye increased and reached a plateau of approx. 90% dye after 96 h in all cases (Figure 29A). However, the crosslinking density, i.e. the amount of HDDP used during the PNCs formation, influenced the degradation rate of the protein shell and thus the release of the dye. Time and crosslinker dependence of dye-release was observed for the enzymatic degradation of PNCs crosslinked with HDDP-SS as well (Figure 29B).

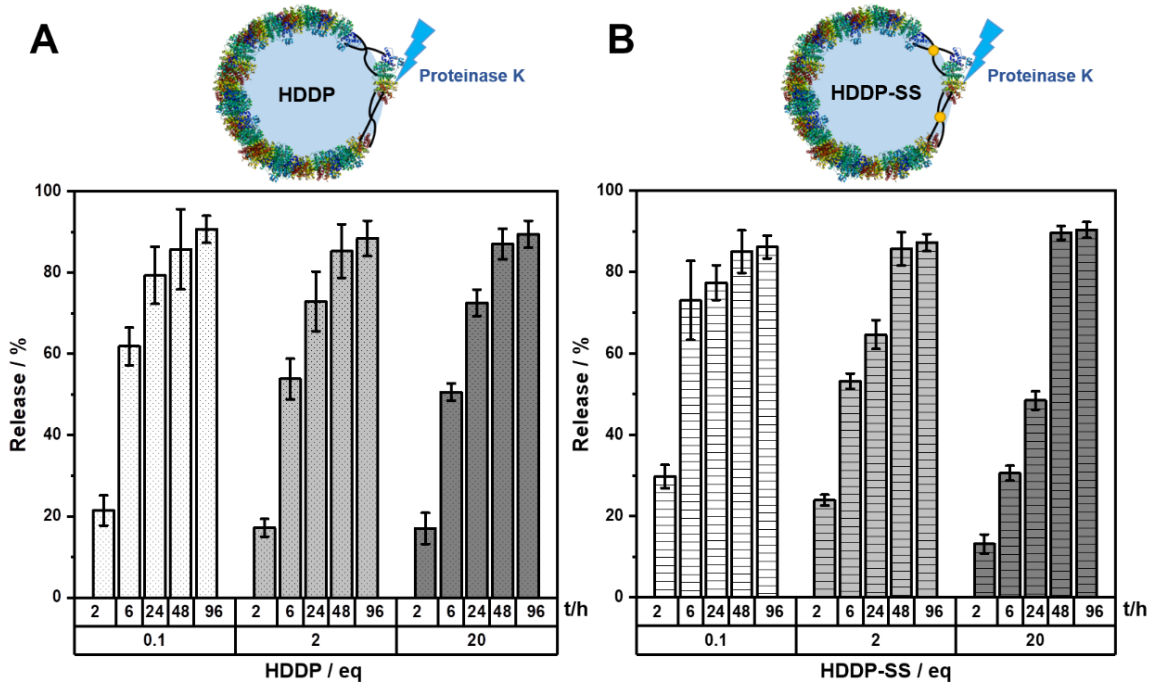

Figure 29. Release kinetics of dextran-rhodamine B (10 kDa) from protein nanocarriers (PNCs) prepared with different crosslinking densities as indicated by the ratio of HDDP or HDDP-SS / eq. and degraded by proteinase K (5 U/mL): A) PNCs crosslinked with HDDP, B) PNCs crosslinked with HDDP-SS. Protein structure was obtained from DrugBank online (https://go.drugbank.com/drugs/DB00062, 28.11.2021) and was adapted.

Protein nanocarriers were successfully degraded by proteinase K and released dye could be measured from the supernatant. The release of cargo depended on the crosslinking degree of the protein shell. In all cases of crosslinking degree, a high release of model dye could be achieved, demonstrating the high degradability even under an artificial setup with a defined and low concentration of proteinase K. Therefore, it can be assumed, that in cellular environment where a high concentration of undefined enzyme cocktail is present, the enzymatic degradation of protein nanocarrier in cells should be much higher. Nevertheless, a degradable crosslinker could still offers an improvement in degradability of protein nanocarrier.

III. A3.2 Reductive Degradation of Protein Nanocarriers

Cells not only exhibit enzymes for degradation, but also reducing agents, such as glutathione, are present that can trigger degradation. Reductive degradability was introduced to PNCs by the crosslinker, for example with a disulfide bond. Disulfide bonds can be inserted into the hexyl backbone of the dialkyne crosslinker HDDP, generating a crosslinker degradable by reductive stimuli. As demonstrated, PNCs crosslinked with HDDP-SS (PNC-HDDP-SS) had similar properties as with HDDP and were also enzymatically degradable (Figure 26B). With reductive degradation of HDDP-SS in PNCs by reducing agent dithiothreitol (DTT), the protein

was not influenced (Scheme 4). Keeping the integrity of the protein shell material could be necessary when using functional proteins such as enzymes or antigens.

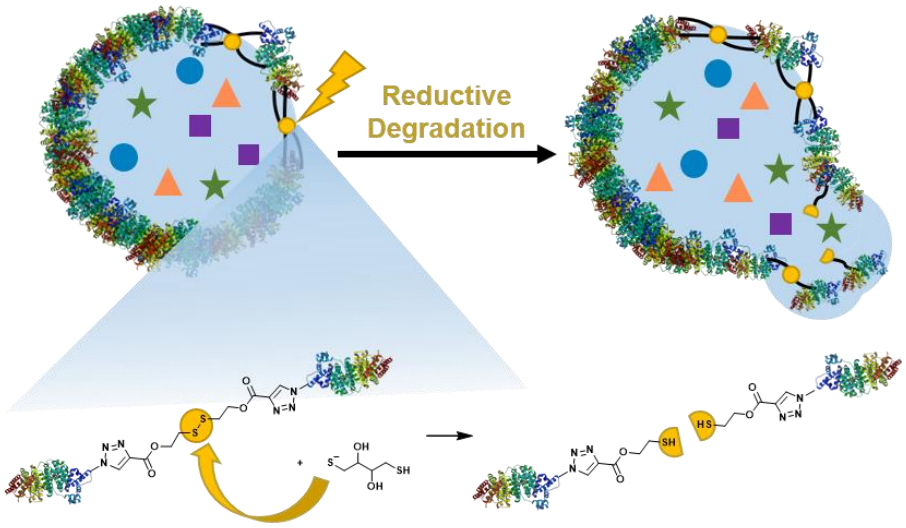

Scheme 4. Reductive degradation of protein nanocarriers crosslinked with HDDP-SS by dithiothreitol. Protein structure was obtained from DrugBank online (https://go.drugbank.com/drugs/DB00062, 28.11.2021) and adapted. Figure was created by Natkritta Hüppe.

For reductive degradation of PNC-HDDP-SS, the NCs were treated with 25 mM DTT. DLS was applied to quantify the degradation rates of PNCs: Following DTT treatment the size of the NCs decreased significantly and a broadening of the polydispersity index could be observed (Figure 30A). After 24 h the nanocarriers were degraded to smaller fractions, while also some aggregated to bigger fractions. After 44 h those aggregates also degraded and the size and size distribution decreased significantly. After addition of DTT, the turbid PNCs dispersion appeared clear, which could indicate a degradation of PNCs (Figure 30B). Additionally, the derived count rate (DCR) was monitored upon DTT treatment and decreased significantly during the degradation experiment, indicating the formation of smaller fragments with lower scattering intensity. More DTT was added after 15 h as DTT tends to decompose over time. Afterwards the DCR of the PNCs dispersion decreased to the lower limit of the DLS apparatus indicating an almost complete degradation of the PNCs after 42 h (Figure 30B).

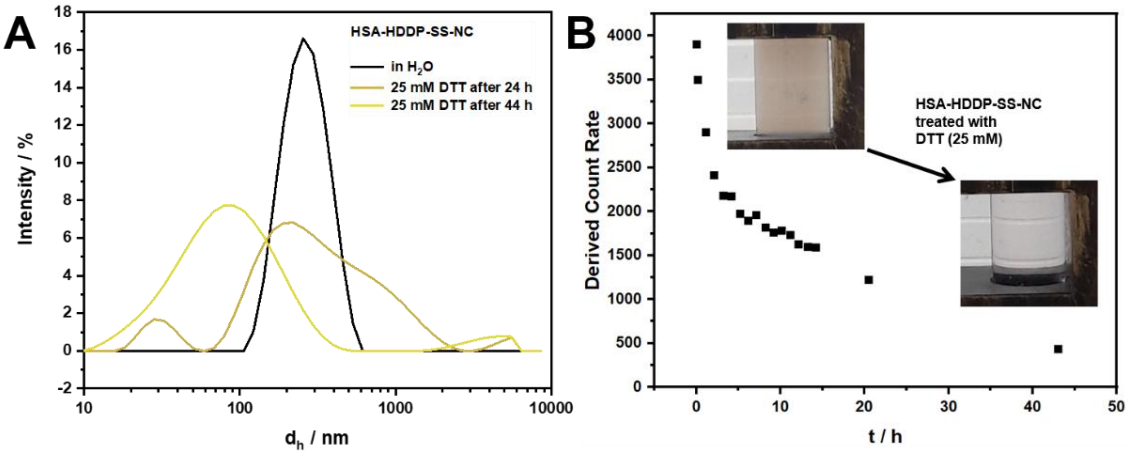

Figure 30. DLS measurements of human serum albumin nanocarriers crosslinked with HDDP-SS (HSA-HDDP-SS-NCs) before and after treatment with 25 mM dithiothreitol (DTT) for 24 h and 44 h. Influence of the derived count rate (DCR) of HSA-HDDP-SS-NCs upon treatment with 25 mM DTT measured by DLS.

The protein nanocarriers crosslinked with reductive-sensitive HDDP-SS demonstrated high degradability upon treatment with dithiothreitol. With the developed protocol for protein formation control over density and degradability could be achieved. The developed degradable protein nanocarriers can be applied to encapsulate therapeutical cargo for biomedical purpose. However, the established protocol allows even more applications, where cargo molecules have to be encapsulated, delivered to the target and released upon degradation.

III. A3.3 Degradation by Enzymatic and Reductive Stimuli

Degradability is an important property nanocarriers have to possess to ensure release of the delivered cargo. The advantage of biological polymers such as proteins over synthetic polymers is their natural degradability in physiological environment. The degree of degradability needed for efficient release is dependent on the molecular weight of the cargo. To achieve a high release rate of high molecular weight cargo molecules such as RNA, DNA or polymers, a high degradability of the nanocarriers at the target site is indispensable. High degradability of PNCs can be realized by installing two orthogonal degradation stimuli. PNCs crosslinked with HDDP-SS can be degraded by both enzymatic and reductive stimuli (Figure 31). The dual-degradation property of PNCs-HDDP-SS could increase high release of macromolecules in cellular environment.

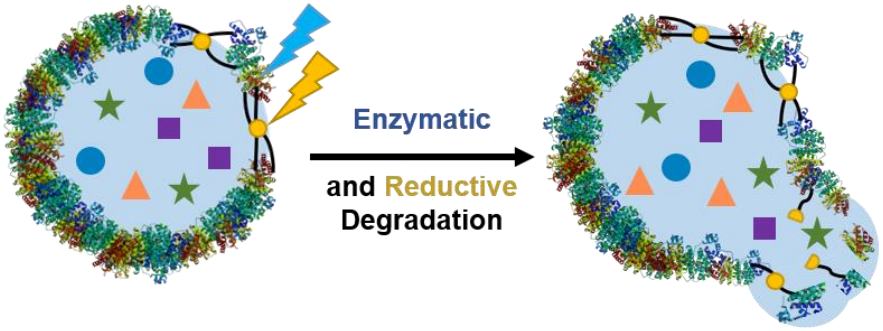

Figure 31. Dual-degradation of protein nanocarrier crosslinked with HDDP-SS through enzymatic and reductive stimuli. Protein structure was obtained from DrugBank online (https://go.drugbank.com/drugs/DB00062, 28.11.2021) and was adapted. Figure created by Natkritta Hüppe.

Before performing the degradation experiments with both proteinase K and DTT, the influence of the reductive reagent DTT on the enzymatic activity of the proteinase K was investigated. Proteinase K possesses five cysteine residues and two disulfide bonds, which could be reduced upon DTT addition, changing the tertiary structure of the protein and thus its enzymatic activity. Proteinase K was treated with different concentrations of DTT over three time points and its enzymatic activity measured by an assay with hemoglobin as substrate. Hemoglobin is degraded by proteinase K into peptides and amino acids, soluble in trichloro acetic acid (TCA). The Folin reagent reacts with the amines to a colored product (Figure 32A). A standard calibration curve with tyrosine was measured to quantify the enzymatic cleavage of peptide bonds by proteinase K (Figure 32B).

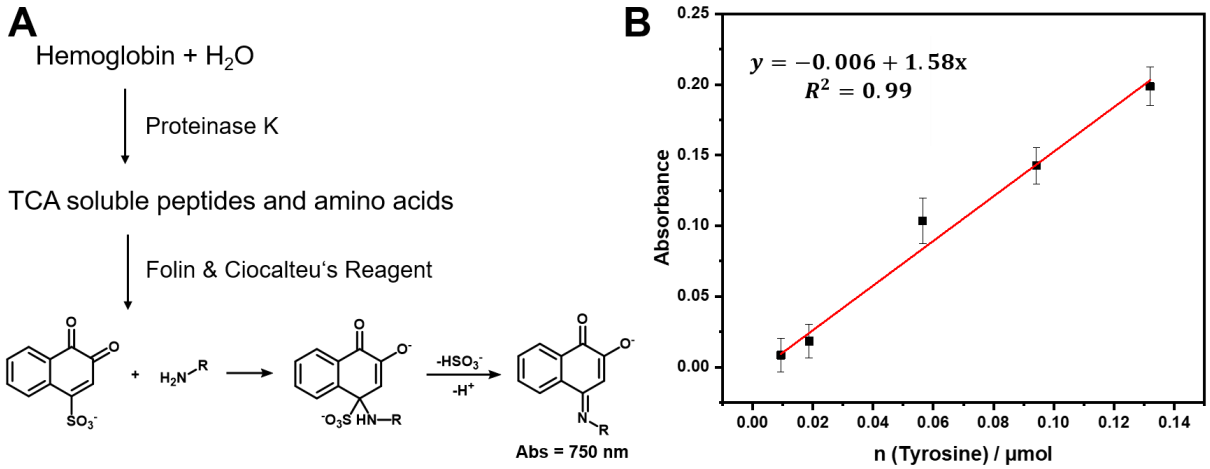

Figure 32. Enzymatic activity assay of proteinase K with Folin & Ciocalteu's Reagent and hemoglobin as substrate and tyrosine for the standard calibration.

The enzymatic assay of proteinase K treated with DTT revealed that the enzyme was not affected by the reducing agent (Table 7). Proteinase K possesses two disulfide bonds and apparently its enzymatic property was not inhibited by the loss of the disulfide bonds and no irreversible inactivation occurred. On the contrary, in case of 25 mM DTT to 0.1 UmL^{-1}

proteinase K the enzyme activity increased by 40 Umg^{-1}. The cleavage of the two disulfide bonds presumably increased the accessibility of the enzyme's substrate binding site as it has been demonstrated for the surfactant sodiumdodecyl sulfate (SDS) or calcium ions.[164] A reduction of the hemoglobin by DTT and thus easier accesibility of the protein to the enzyme was not possible since bovine hemoglobin does not possess cystein, i.e. disulfide bonds. In conclusion, degradation experiments using both stimuli to show an additive degradation of enzyme and DTT could be performed without risking loss of enzymatic activity.

Table 7. Enzymatic activity assay of proteinase K under the influence of DTT with hemoglobin as substrate. Proteinase K solution incubated with DTT at 37 °C for 10 min, 30 min and 2 h.

No.	Prot K /UmL^{-1}	DTT /$mmolL^{-1}$	Activity /Umg^{-1}	Error /Umg^{-1}	Activity /Umg^{-1}	Error /Umg^{-1}	Activity /Umg^{-1}	Error /Umg^{-1}
1	0.1	-	62	10	110	27	138	61
2	0.1	1	39	10	110	27	135	75
3	0.1	3	47	11	125	29	139	72
4	0.1	5	45	9	124	6	212	73
5	0.1	25	102	9	161	4	62	84
6	1	-	62	6	51	2	61	6
7	1	1	62	6	52	4	63	6
8	1	3	63	9	52	3	63	9
9	1	5	63	6	52	3	63	6
10	1	25	67	7	53	3	67	7

The dual degradation of PNCs was investigated by treating PNCs crosslinked with different amount of HDDP-SS with either proteinase K (5 U/mL), DTT (25 mM) or both at 37 °C in PBS buffer and the amount of released dextran-rhodamine B (10 kDa) was measured over time (Figure 33). A sample only treated with PBS buffer served as a control sample. Applying only enzymatic degradation led to partly degradation of PNCs after 1 h as a low amount of rhodamine-dye was released (Figure 33A). A slightly higher amount of dye was measured in the supernatant for PNCs crosslinked with the lowest amount of HDDP-SS (0.1 eq.). Degradation with 25 mM DTT proceeded very fast, since almost 80% of dye was already released after 0.5 h independent of crosslinking degree. Similar results were observed for treatment with both stimuli, indicating, that under chosen conditions of 5 U/mL proteinase K and 25 mM DTT, DTT was the main degradation stimuli and no additive degradation of both

could be proven. To demonstrate an additive degradation of both, enzyme and reducing agent, the conditions had to be optimized, that both degradation effects were visible.

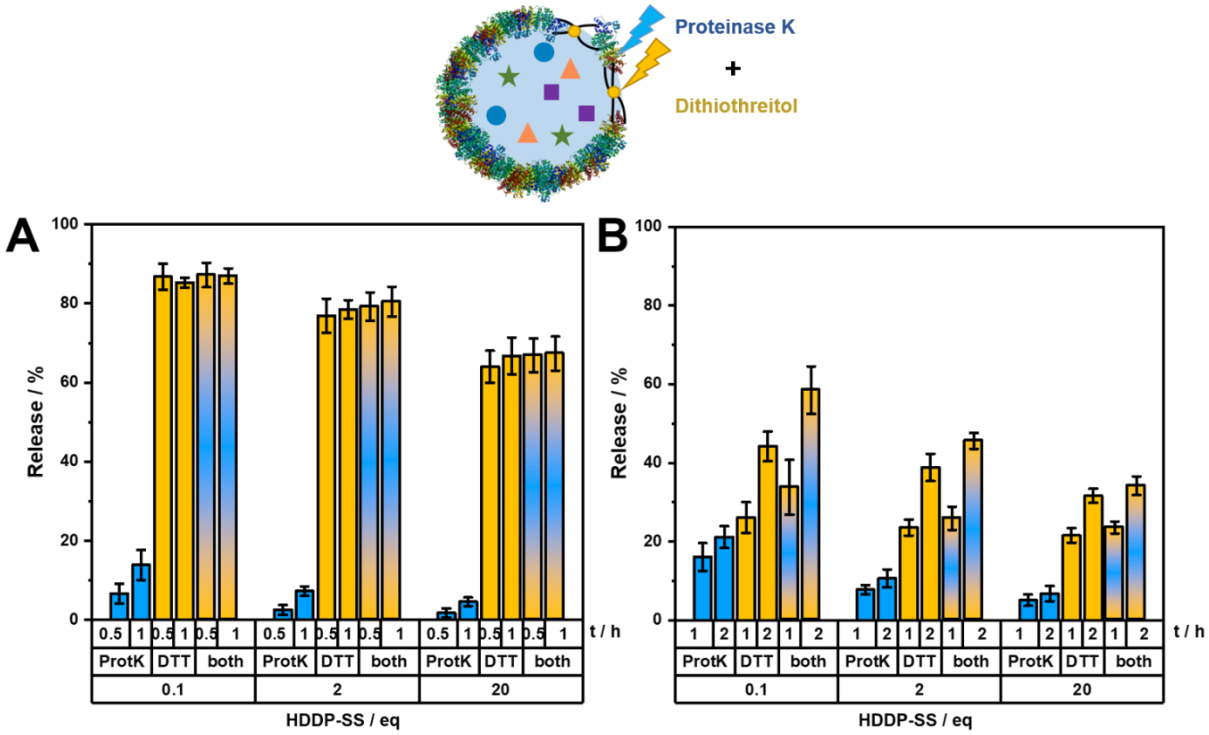

Figure 33. A) Release of dextran-rhodamine B 100K from HSA-HDDP-SS-nanocarriers crosslinked with 0.1, 2 and 20 eq HDDP-SS under treatment with A) 5 U/mL proteinase K B) 25 mM DTT and C) 5 U/mL proteinase K and 25 mM DTT for 0.5 and 1 h at 37 °C. B) Release of dextran-rhodamine B 100K from HSA-HDDP-SS-nanocarriers crosslinked with 0.1, 2 and 20 eq HDDP-SS under treatment with D) 5 U/mL proteinase K E) 10 mM DTT and F) 5 U/mL proteinase K and 10 mM DTT for 1 and 2 h at 37 °C. Protein structure was obtained from DrugBank online (https://go.drugbank.com/drugs/DB00062, 28.11.2021) and adapted.

In the next set of experiments, the amount of DTT was reduced to 10 mM and the degradation time was increased to 1 and 2 h to give more time for enzymatic degradation (Figure 33B). The amount of measured dye decreased significantly for 10 mM DTT compared to 25 mM. For enzymatic degradation, a higher release is obtained under the chosen conditions with 5 U/mL proteinase K at a longer reaction time. However, DTT remained the main degradation stimuli, as shown when treating PNCs with both stimuli. A difference in the released amount of dye with dual-degradation compared to single-degradation was only observed for the lowest amount of HDDP-SS (0.1 eq.), indicating a small additive degradation of enzyme and DTT. However, with a higher amount of crosslinker (2 eq. and 20 eq. HDDP-SS) the difference in release between single- and dual-stimuli was not significant enough to conclude additive degradation. Here again, the degradation conditions had to be optimized to demonstrate additive degradation with both stimuli.

With increasing degradation time and less DTT concentration, an increasing amount of released dye could be measured for HSA-NCs-HDDP-SS treated with proteinase K (5 U/mL) and DTT (3 mM) in combination (Figure 34). Under chosen conditions for enzyme and DTT the amount of released dye measured for PNCs-HDDP-SS treated with both stimuli was significantly higher after 3 h compared to only one stimulus, demonstrating an additive degradation of both enzyme and DTT. The PNCs crosslinked with different amounts of HDDP-SS treated with proteinase K and DTT, respectively and in combination, showed a significant difference in release, indicating the release kinetics were influenced by the crosslinking degree. The resulting PNCs crosslinked with HDDP-SS obtained the property of dual-degradation by reducing agent DTT and enzyme proteinase K.

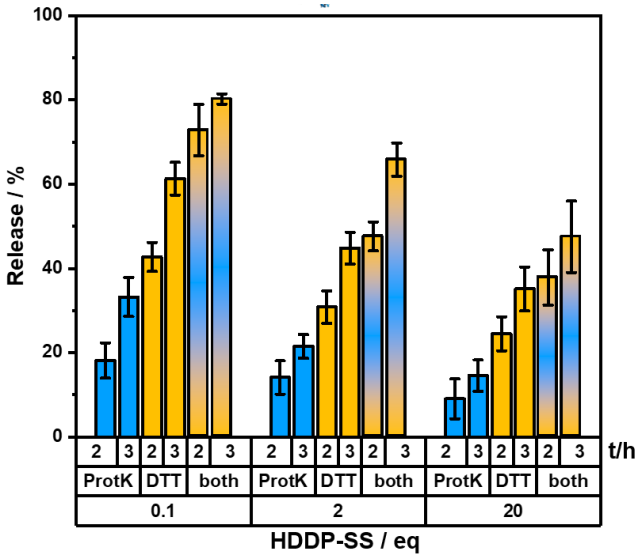

Figure 34. PNCs crosslinked with HDDP-SS and degraded with proteinase K (blue, 5 U/mL) and dithiothreitol (yellow, 3 mM).

Protein nanocarriers could be formed *via* the interfacial azide-alkyne click reaction of azide-modified proteins with a dialkyne crosslinker hexanediol dipropiolate in inverse miniemulsion. The ratio between azide moieties on the protein and alkyne groups of the crosslinker determined the crosslinking degree of the protein shell and thus the density and degradability of the protein nanocarriers. PNCs crosslinked with a reductive-responsive dialkyne crosslinker were degradable by enzymatic and reductive stimuli, enhancing the degradation degree of PNCs for high release effectivity. The developed process could enable a biorthogonal encapsulation of sensitive cargo molecules where the chemoselective crosslinking does not involve the cargo and preserve the cargo's activity. Additionally, the inverse miniemulsion process would allow encapsulation of multiple components at once during the interfacial nanocarrier shell formation. In the next section, the multicomponent encapsulation into developed protein nanocarriers was performed by using multiple immunotherapeutics with different physicochemical properties.

To demonstrate the bioorthogonality of the developed process, the stimulative activity of immunotherapeutics encapsulated into protein nanocarrier by azide-alkyne click reaction was investigated *in vitro*.

III. A4. Multicomponent Encapsulation of Therapeutics for Immunotherapy

Since anti-tumor vaccination still lacks the effective response of immune cells against tumors in most cases of vaccinated patients, the role of nanocarriers for co-delivery of vaccine components needs to step into focus. In the vaccination process, the vaccine, consisting of antigen and adjuvants, is taken up by dendritic cells and the antigens are presented on major histocompatibility complex (MHC) molecules of the DCs to the T cells.[165, 166] Subsequently, antigen-specific T cells are activated and proliferate to attack cells bearing the tumor-specific antigen eventually leading to tumor cell killing.[167] Crucial for the success of T cell priming is a strong activation of antigen-presenting cells (e.g. DCs) by adjuvants inducing expression of costimulatory molecules and the release of activating pro-inflammatory cytokines. Choosing the correct type and application route of adjuvants is of great importance for the induction of robust immune responses as each adjuvant binds to distinct receptors triggering different signaling pathways in antigen-presenting cells.[168, 169] Therefore, a combination of several different adjuvants simultaneously stimulates different receptors, leading to an additive DC activation.[170] To achieve a high local concentration of adjuvants in one DC, all components must be delivered simultaneously.[81]

A major challenge is to find a compatible protocol for the multicomponent encapsulation of cargo molecules with such different properties in terms of solubility and molecular weight. Here, the developed process for the formation of protein nanocarriers through azide-alkyne click reaction in inverse miniemulsion offered an excellent tool for the simultaneous encapsulation of multiple cargo molecules, such as adjuvants. For the investigation of additive stimulation of DCs by adjuvant-loaded PNCs, three adjuvants with different immune-stimulative properties and a dye for tracking the PNCs were encapsulated into PNCs crosslinked with HDDP (Figure 35).

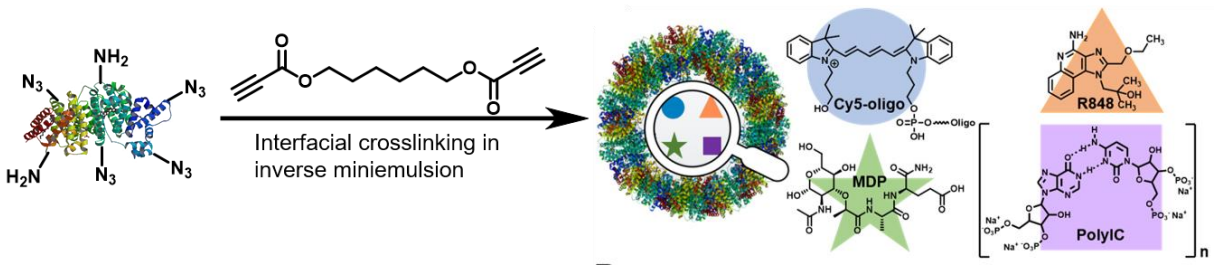

Figure 35. Multicomponent encapsulation of Cy5-Oligo, Resiquimod (R848), muramyl dipeptide (MDP) and polyinosinic-polycytidylic acid (Poly(I:C)) into protein nanocarriers by interfacial azide-alkyne crosslinking of azide-functionalized proteins with hexanediol dipropiolate (HDDP) in inverse miniemulsion. Protein structure was obtained from DrugBank online (https://go.drugbank.com/drugs/DB00062, 28.11.2021) and was adapted. Figure created by Natkritta Hüppe.

III. A4.1 Quantification of Adjuvants

For a precise comparison of the stimulative properties of different adjuvants and their combinations, the amounts of the different adjuvants encapsulated in the PNCs had to be quantified. The adjuvant-loaded PNCs were enzymatically degraded with proteinase K at a high rate as possible to ensure the release of all components. The adjuvants could either be quantified from the degraded mixture or the supernatant after separation by centrifugation. The challenge here was the different physicochemical properties (solubility, molecular weight) of the three adjuvants, where one method was not sufficient to precisely quantify each component. Therefore, a quantification method was established for each adjuvant.

a) Resiquimod (R848)

Resiquimod (R848) is a small molecule (M = 350.8 g/mol) with low water-solubility (> 1 mg/mL) and acts as an agonist for the toll-like receptors (TLR) 7 and 8.[171]

Since R848 possesses an aromatic moiety, its quantification can be performed by fluorescence measurements. A standard calibration curve for R848 was recorded through fluorescence at λ_{em} = 360 nm (λ_{ex} = 260 nm) (Figure 36). The limitation of the quantification method was as low as 0.01 nmolL^{-1}. The encapsulation efficiency of R848 was measured from the supernatant after the transfer of PNCs into water. The actual amount of R848 in the PNCs was quantified from the supernatant after enzymatic degradation of PNCs and separation from degraded protein fragments with centrifugal filters (MWCO 3 kDa).

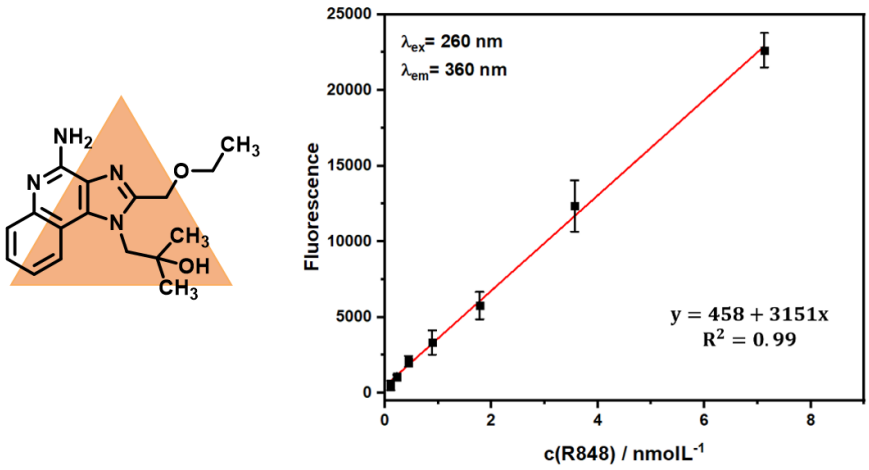

Figure 36. Chemical structure of Resiquimod (R848) and standard calibration curve of R848 by fluorescence measured at 360 nm.

b) Muramyl dipeptide (MDP)

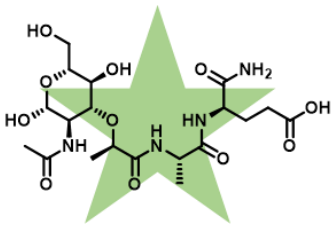

Scheme 5. Chemical structure of muramyl dipeptide.

The water-soluble peptidoglycan muramyl dipeptide (MDP; *M* = 492.5 g/mol) has been shown to be recognized by nucleotide-binding oligomerization domain-containing protein (NOD) 2.[172] Due to the *N*-acetylglucosamide moiety present within the MDP, a quantification by the colorimetric Morgan-Elson Reaction assay can be performed (Scheme 6). The Morgan-Elson reaction with *p*-dimethylaminobenzaldehyde (DMAB) is an assay for sugars bearing *N*-acetylglucosamide. The *N*-acetylglucosamide moiety is reduced under basic conditions at high temperatures and reacts with DMAB to a red-colored product.

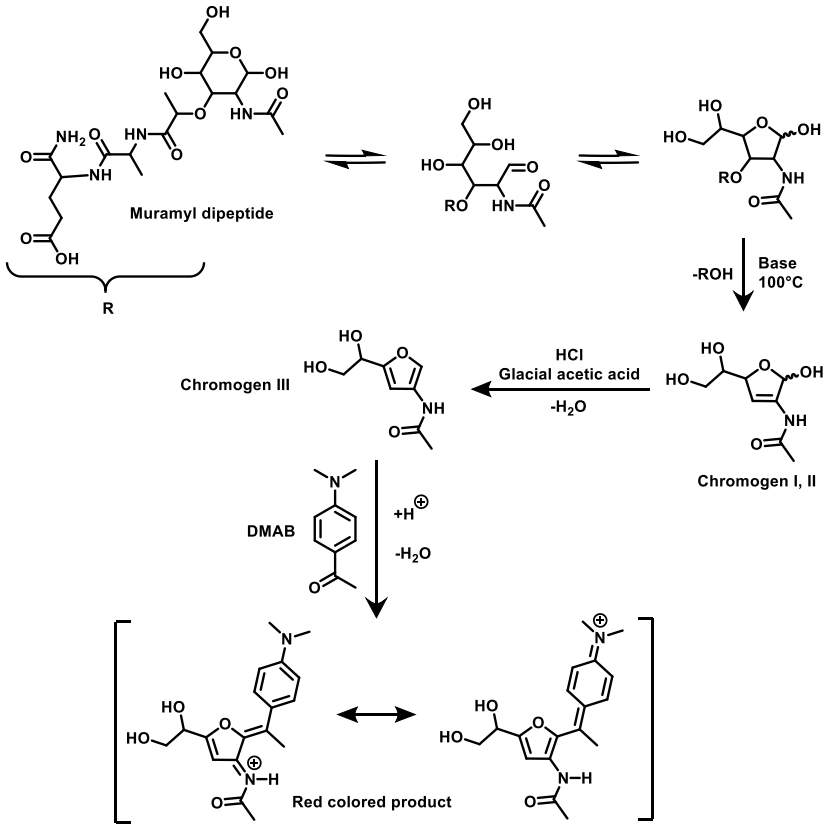

Scheme 6. Quantification of muramyl dipeptide with the Morgan-Elson reaction.

To obtain the optimal assay conditions for MDP, the pH value of the borate solution was varied, which influenced the reduction of the sugar, and the absorbance of the resulting colored product recorded at 546 nm (Figure 37). A pH value of 9 resulted in the highest absorbance for the assay with MDP substrate. Regarding the heating time of the sample at pH 9 at 100 °C, the absorbance peaked at 3 min and decreased with a longer heating time. The absorbance of the assay product plateaued after a DMAB concentration of 8 µgmL^{-1}. The highest absorbance was obtained at 12 min incubation time of the reduced sugar in DMAB solution at 38 °C. All conditions with a maximum absorbance at 546 nm were applied for the quantification of MDP with Morgan-Elson reaction.

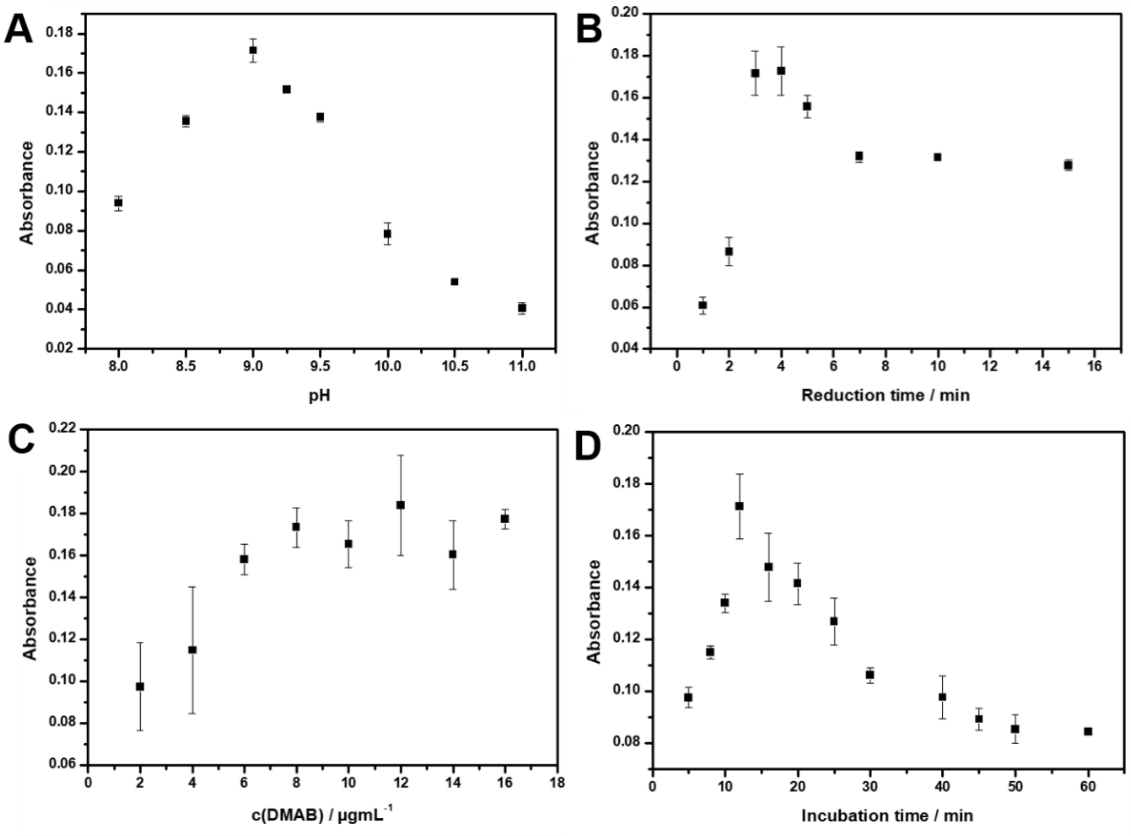

Figure 37. Optimization of MDP assay by variation of pH, heating time, DMAB concentration and incubation time.

With this optimized assay conditions, a standard calibration curve of MDP, measured with Morgan-Elson reaction, was recorded (Figure 38). The limiting concentration of this assay was as low as 0.02 mg/mL. The assay was very dependent on timing, as the absorbance was highly influenced by the incubation time. To ensure the applicability of the standard calibration curve for precise quantification incubation times had to adhere. This was especially difficult when measuring several samples at a time.

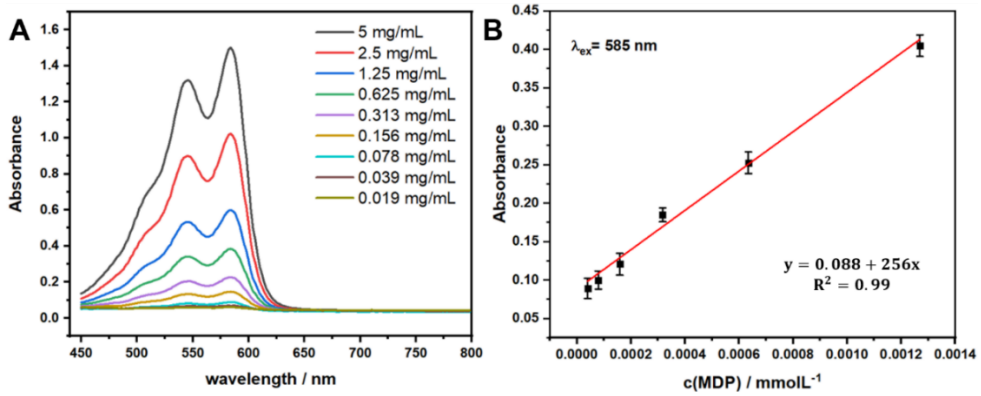

Figure 38. Morgan-Elson Assay of muramyl dipeptide (MDP) with *p*-dimethylaminobenzaldehyde (DMAB), measured by absorbance.

c) Polyinosinic-polycytidylic acid

The double-stranded RNA mimic polyinosinic-polycytidylic acid (Poly(I:C); 0.2-1 kb) acts as a TLR 3 ligand.[173] Poly(I:C) has a molecular weight between 100-500 kDa and cannot easily be separated from the nanocarrier dispersion after enzymatic degradation compared to the small molecules R848 and MDP. Therefore, a method had to be found, where PolyIC could be quantified in the degraded nanocarrier dispersion. Reverse-phase HPLC was used for the quantification of Poly(I:C). Adjusting the optimal HPLC setup was challenging since the dispersion contained a mixture of different components such as proteins, peptides, proteinase K, R848, MDP, surfactant and dye. For the quantification of Poly(I:C) in PNCs, the carriers were treated with 30 U/mL proteinase K for 24 h at 37 °C to ensure a high degree of degradation and full release of Poly(I:C). The dispersion turned completely clear, indicating a high degree of degradation. The full mixture of PNCs after degradation with proteinase K was eluted through a reverse phase HPLC column using a mixture of acetonitrile, 0.01% formic acid and 0.02 mol/L ammonium acetate. The amount of Poly(I:C) was quantified with a standard calibration curve (Figure 39).

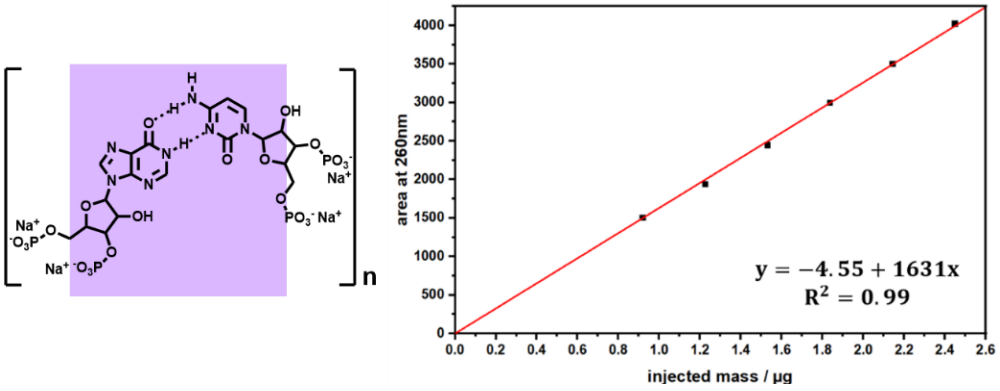

Figure 39. Standard calibration curve of Poly(I:C) measured by HPLC.

A quantification method of all three adjuvants after encapsulation into protein nanocarriers was established using different approaches. In the next step, multicomponent encapsulation of adjuvants into protein nanocarriers was performed and the stimulative property of adjuvant-loaded PNCs on dendritic cells was investigated.

III. A4.2 *In Vitro* Stimulation

In this study, adjuvants R848, MDP, and Poly(I:C) were combined and encapsulated into PNCs. Cy5-Oligo (5 kDa) as an additional cargo acted as a fluorescent dye (Figure 40A), allowing the investigation of the cellular uptake of PNCs by DCs. All four components were successfully encapsulated into PNCs through the azide-alkyne click reaction in inverse miniemulsion

demonstrating the excellent feasibility of developed nanocarrier formation for the encapsulation of multiple components (Figure 40B). Even though dimethylsulfoxide (DMSO) was used as a solvent for R848 (14 vol.-% in the disperse phase) stable droplets could be formed with no influence on the interfacial protein shell formation and stable PNCs with core-shell morphology were obtained (Figure 40C).

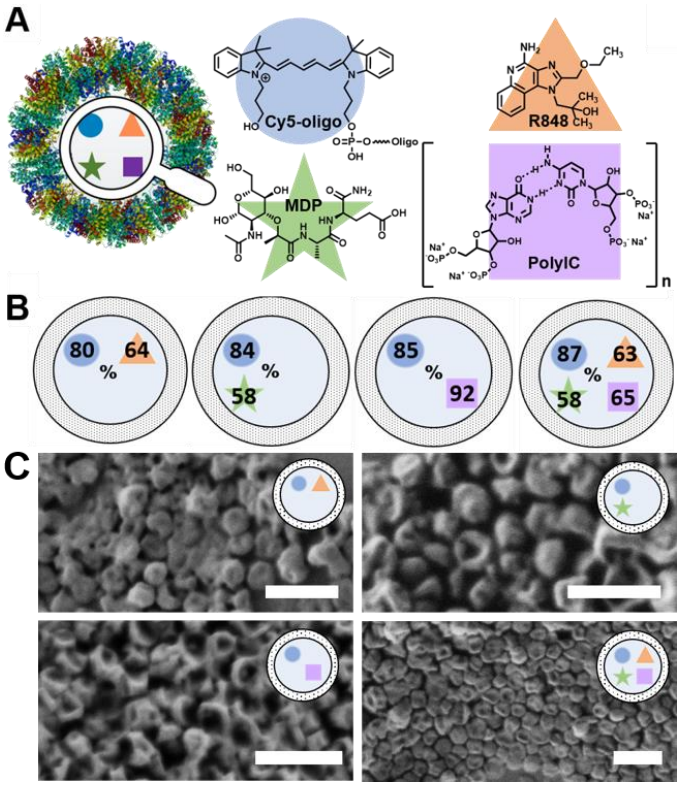

Figure 40. A) Chemical structures of Resiquimod (R848), muramyl dipeptide (MDP) and polyinosynic-polycytidylic acid (Poly(I:C)), B) Encapsulation efficiencies of dye and adjuvants into HSA-NCs crosslinked with HDDP. C) Scanning electron micrographs of adjuvant-loaded HSA-HDDP-NCs (scale bar: 0.5 µm). Protein structure was obtained from DrugBank online (https://go.drugbank.com/drugs/DB00062, 28.11.2021) and was adapted. Figure created by Natkritta Hüppe.

The PNCs were degraded by proteinase K (30 U/mL, 24 h, 37 °C), filtered, and the amount of each cargo was measured in the supernatant. Comparable EEs were obtained for the small molecules R848, and MDP (up to 65%) and Cy5-Oligo (over 80%) independent from cargo-loading (Figure 41B and Table 8). Only the EE of the high molecular weight Poly(I:C) decreased significantly from approx. 90% for single-loaded PNCs to approx. 60% for multiple-loaded PNCs. The encapsulation efficiency is influenced by the concentration in the disperse phase and at higher concentrations, the osmotic pressure in the water droplet is so high that part of the cargo will be pressed out of the aqueous phase and not encapsulated during the protein shell formation. Therefore, encapsulation efficiencies decreased with increasing cargo load. Table 8 summarizes the encapsulation efficiencies and the characterization data for all

HSA-NCs prepared herein: In all cases, similar zeta potentials between -30 mV and -40 mV were determined, indicating a similar shell formation regardless of the cargo molecule or its charge, i.e. an efficient encapsulation inside of the NCs was achieved. The diameters for all "clicked" NCs were similar and detected between 200-300 nm (after redispersion in water, measured by DLS).

Table 8. Encapsulation efficiencies of dye and adjuvants into human serum albumin nanocapsules crosslinked with HDDP.

No.	Linker	Adj.	$EE_{Cy5\ Oligo}$ / %	$c_{R848,theo}$ / molmL^{-1}	c_{R848} / molmL^{-1}	c_{R848} / %	$c_{MDP,theo}$ / molmL^{-1}	c_{MDP} / molmL^{-1}	c_{MDP} / %	$c_{PolyI:C,theo}$ / molmL^{-1}	$c_{PolyI:C}$ / molmL^{-1}	$c_{PolyI:C}$ / %	$d_{h,H2O}$ / nm	PDI	ζ / mV
1	HDDP	-	86	-	-	-	-	-	-	-	-	-	203	0.16	-32
2		R848	80	$4.50*10^{-8}$	$2.88*10^{-8}$	64	-	-	-	-	-	-	245	0.17	-40
3		MDP	84	-	-	-	$1.02*10^{-7}$	$5.92*10^{-8}$	58	-	-	-	212	0.22	-38
4		PolyI:C	85	-	-	-	-	-	-	$2.00*10^{-10}$	$1.84*10^{-10}$	92	215	0.20	-42
5		All 3	85	$8.91*10^{-8}$	$3.15*10^{-8}$	35	$1.02*10^{-7}$	$3.73*10^{-8}$	37	$2.00*10^{-10}$	$5.20*10^{-11}$	26	302	0.25	-34
6		All 3	87	$4.50*10^{-8}$	$2.84*10^{-8}$	63	$1.02*10^{-7}$	$5.55*10^{-8}$	53	$2.00*10^{-10}$	$1.30*10^{-10}$	65	218	0.21	-38
7		All 3	73	$2.23*10^{-8}$	$1.77*10^{-8}$	79	$1.02*10^{-7}$	$5.68*10^{-8}$	56	$2.00*10^{-10}$	$1.30*10^{-11}$	65	356	0.35	-28
8		All 3	90	$4.50*10^{-8}$	$2.84*10^{-8}$	64	$5.08*10^{-8}$	$3.59*10^{-8}$	71	$2.00*10^{-10}$	$1.46*10^{-11}$	73	366	0.18	-29
9		All 3	91	$4.50*10^{-8}$	$3.05*10^{-8}$	69	$2.54*10^{-8}$	$1.86*10^{-8}$	73	$2.00*10^{-10}$	$1.60*10^{-11}$	80	252	0.07	-32
10		All 3	52	$4.50*10^{-8}$	$3.23*10^{-8}$	74	$1.02*10^{-7}$	$7.06*10^{-8}$	69	$5.00*10^{-11}$	$4.65*10^{-11}$	93	194	0.27	-31
11	HDDP-SS	-	57	-	-	-	-	-	-	-	-	-	258	0.16	-34
12		R848	57	$4.50*10^{-8}$	$3.34*10^{-8}$	75	-	-	-	-	-	-	254	0.14	-33
13		All 3	73	$4.50*10^{-8}$	$2.93*10^{-8}$	65	$1.02*10^{-7}$	$6.43*10^{-8}$	63	$2.00*10^{-10}$	$1.22*10^{-10}$	61	304	0.19	-32

Flow cytometric and confocal laser scanning analysis revealed an efficient uptake of the adjuvant-loaded PNCs by the bone marrow-derived dendritic cells (BMDC) *in vitro*, as detected through the fluorescence of Cy5 (Figure 41). Control samples and soluble adjuvants solution did not show Cy5-binding, as expected.

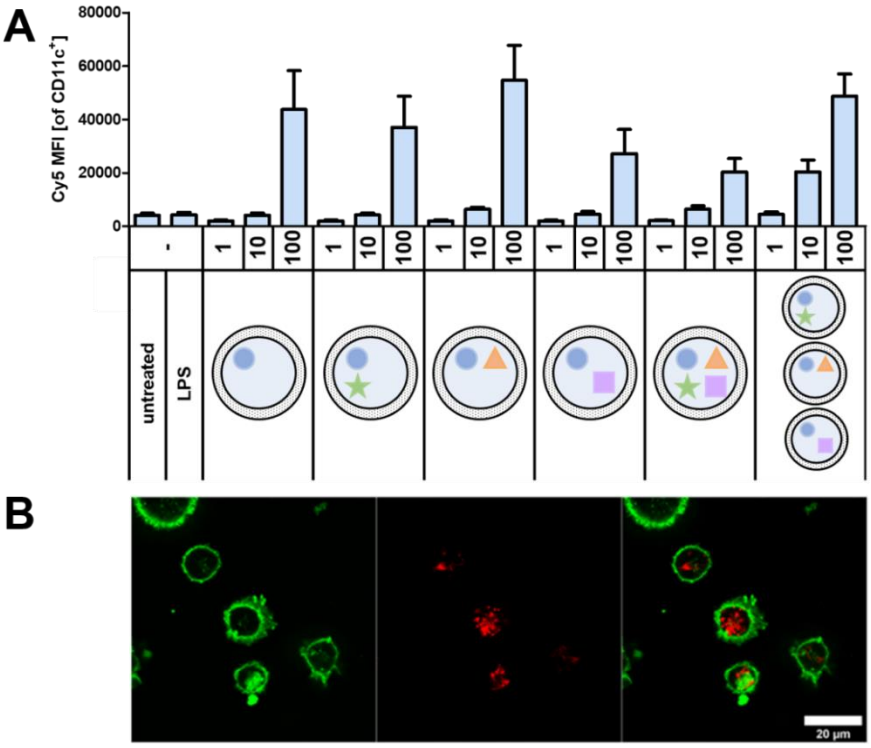

Figure 41. A) Cell binding/uptake into BMDC of Cy5-oligo-loaded HSA-click nanocapsules measured by flow cytometry. B) Confocal image of bone-marrow derived dendritic cells (green) and taken up human serum albumin nanocarriers (red). Cell experiment data and confocal images measured by [redacted].

The co-delivery of the adjuvant combination by PNCs was evaluated by the amount of cell surface-expressed activation markers CD80 and CD86 on the BMDCs after incubation with PNCs for 24 h (Figure 42). Untreated cells served as a negative control whereas cells treated with lipopolysaccharide (LPS), a potent TLR4 agonist inducing high expression of DC maturation, served as a positive control. The expression of CD80 and CD86 increased after treatment with adjuvant-loaded PNCs compared to untreated cells or cells treated with empty PNCs. Among the single-loaded PNCs with either R848, MDP or Poly(I:C), the TLR7/8 ligand R848 yielded the highest stimulation of BMDCs. The expression of the surface markers increased with PNCs loaded with the triple-combination of adjuvants compared to single-loaded PNCs. Moreover, a mixture of single-loaded PNCs with R848, MDP and Poly(I:C), respectively, exhibited a lower expression of surface markers compared to equimolar amounts of all three adjuvants encapsulated into one PNCs demonstrating a higher stimulation through co-delivery.

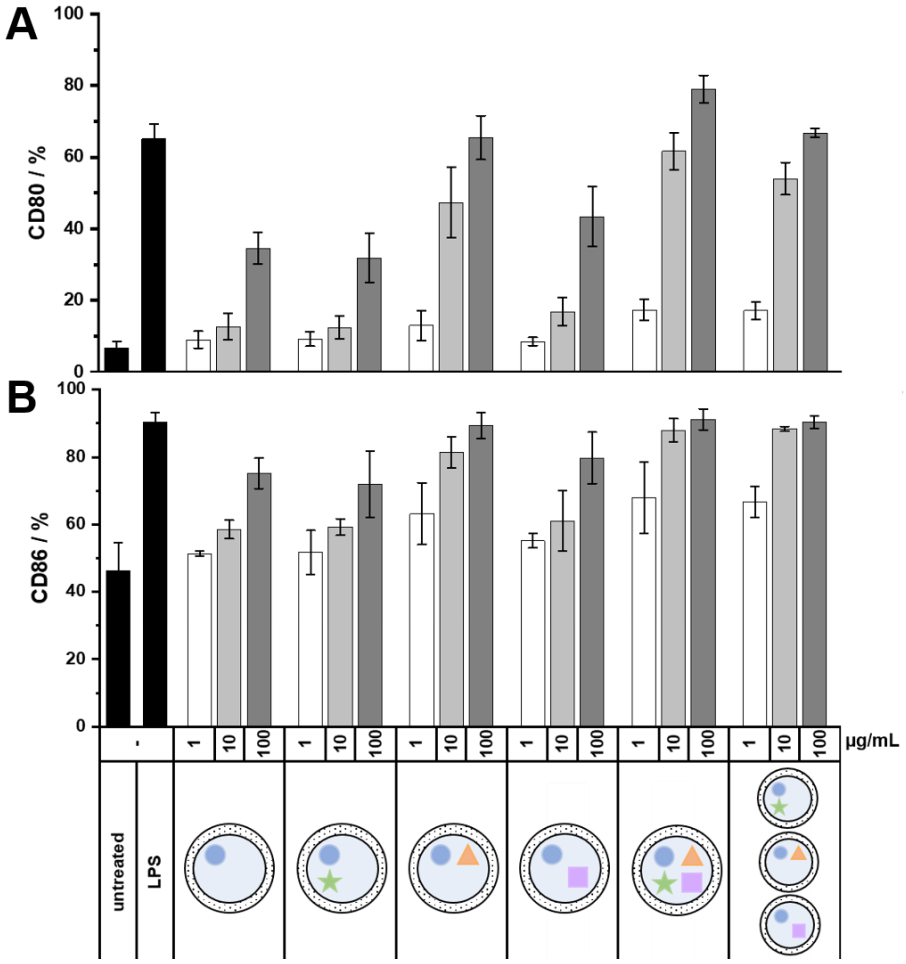

Figure 42. Upregulation of DC maturation markers CD80 and CD86 after stimulation with adjuvant-loaded HSA NCs with single loading, triple loading and mixture of single-loaded NCs. BMDCs (2×10^5 cells/mL) were incubated with differently loaded HSA-NC formulations (1–100 µg/mL) or LPS (100 ng/mL) as a positive control for 24 h. Surface expression of CD80 and CD86 of PNC-treated BMDCs was measured by flow cytometry. Data measured by [redacted].

The *in vitro* results underline the importance of simultaneous delivery of adjuvants by multicomponent encapsulation into nanocarrier to achieve higher effectivity in nanocarrier-based vaccination approaches. With our developed protein nanocarriers combining all the nanocarrier design requirements, we could encapsulate and co-deliver multiple components into cells independent of molecular weight (low-high) or solubility with high efficiency and preserved activity. Besides applying protein nanocarriers to deliver therapeutics into cells, PNCs can be loaded with a variety of cargo molecules, opening up a wide range of possibilities.

III. A5. Encapsulation of Protein Nanocarriers into Polymeric Cell Mimics

The loaded protein nanocarriers offer a variety of applications where it is necessary, that cargo molecules are delivered to a specific target or material has to be provided on-demand. Especially for the latter application, it could be useful to encapsulate loaded and degradable PNCs into other systems. For example, synthetic biology aims to mimic cell compartments to reproduce the function and behavior of cells.[106] Polymeric vesicles demonstrated cell-like characteristics and are a promising tool to create artificial cells.[106, 174] The vesicles are formed through self-assembly of amphiphilic block copolymers, resulting in vesicles with a semipermeable core-shell structure, similar to the phospholipid bilayer of cell membranes.[175] Encapsulation of loaded protein nanocarriers into those polymeric vesicles enables the possibility to mimic different compartments and functions of cells. One ability of a cell is to grow their cell membranes. The cellular growth could be realized in polymeric vesicles by inserting additional chains into the assembled vesicle wall. Long chain dialkylcarbocyanines such as Vybrant™ DiO are lipophilic dyes for cell membrane labeling, which diffuse into the cell membrane. The incorporation of Vybrant™ DiO into the phospholipid bilayer might be used to grow polymeric vesicles by incorporating the dye into the self-assembled polymer wall. To deliver the dye within the polymeric vesicle upon a stimulus, Vybrant™ DiO was encapsulated into protein nanocarriers (Scheme 7). Since the release of dye should be induced externally, an enzymatic degradation cannot be realized, as the enzyme is too large to pass through the vesicle wall. Therefore, the DiO-dye has to be loaded into reductive-responsive PNCs-HDDP-SS. The DiO-loaded PNCs should then be encapsulated into polymeric vesicles by the simple double emulsification (SDE) approach. Upon external addition of DTT, the PNCs should degrade and the DiO-dye released into the polymeric vesicle. The dye could diffuse to the vesicle membrane and incorporate into the polymeric assembly, possibly resulting in growth of the membrane.

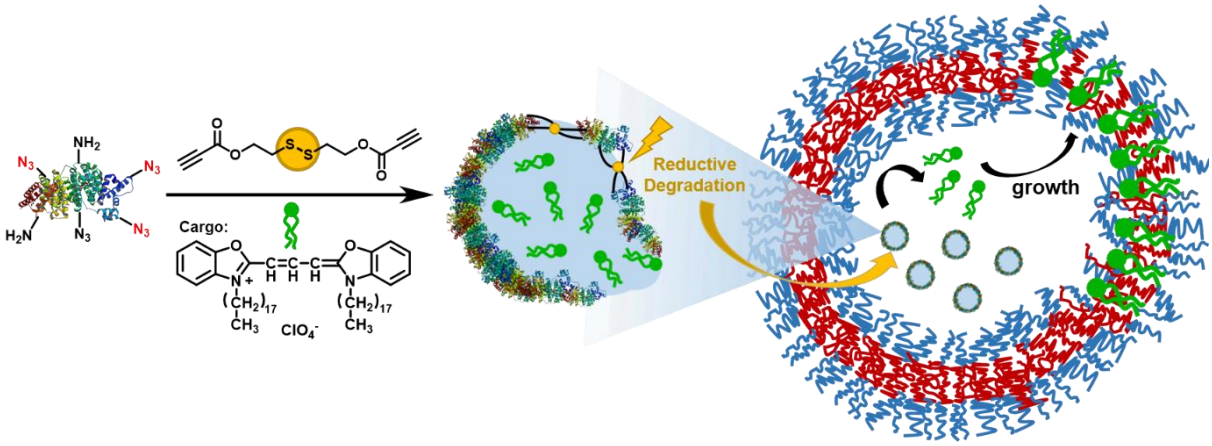

Scheme 7. Encapsulation of Vybrant™ DiO dye into reduction-responsive protein nanocarriers (PNCs), followed by encapsulation of PNCs into polymeric vesicles. Dye is released upon reductive degradation of PNCs and lipophilic dye is integrated into the vesicle membrane. Protein structure was obtained from DrugBank online (https://go.drugbank.com/drugs/DB00062, 28.11.2021) and was adapted. Scheme created by Natkritta Hüppe.

Vybrant™ DiO was encapsulated into HSA-NCs *via* azide-alkyne click reaction with HDDP-SS in inverse miniemulsion (Scheme 7). The lipophilic DiO-dye was not water-soluble and dimethylformamid (DMF) acted as a solvent. Despite the organic solvent in the aqueous disperse phase, the azide-functionalized protein stayed stable and soluble in water and an interfacial protein shell crosslinking could be performed successfully. The resulting DiO-loaded PNCs showed comparable sizes and size distributions to previously described PNCs in cyclohexane as well as after transfer into water (Figure 43A). A core-shell morphology was observed for PNCs in cyclohexane with scanning electron microscopy (SEM) (Figure 43C). Over 90% of Vybrant™ DiO was encapsulated into PNCs. The reductive degradation of HSA-NCs-HDDP-SS with DTT (25 mM) was monitored with DLS. The derived count rate, e.g. the scattering of the dispersion, decreased over time upon addition of DTT, indicating a reductive degradation of PNCs (Figure 43B). The size of PNCs decreased with DTT treatment from 241 nm to 88 nm after 23 h (Figure 43A).

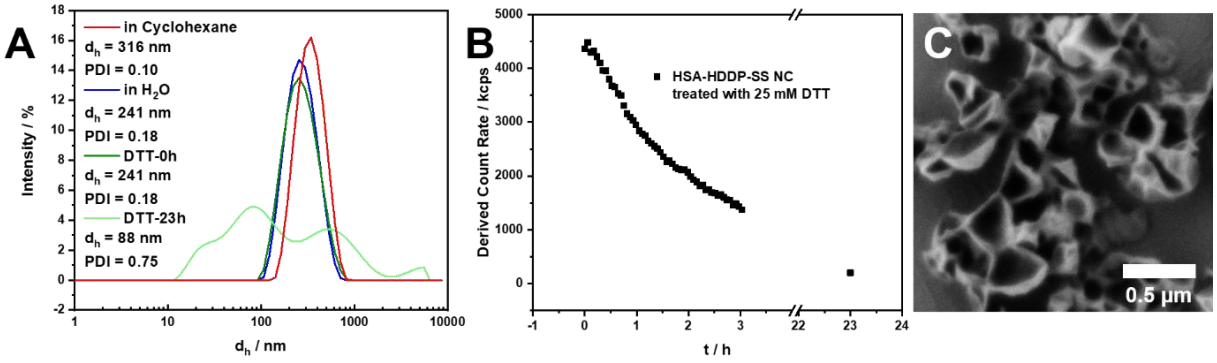

Figure 43. A) DLS of protein nanocarriers crosslinked with HDDP-SS and loaded with Vybrant DiO in cyclohexane (red), water (blue), after treatment with dithiothreitol for 0 h (dark green) and 23 h (light green). B) Change in the derived count rate over time after addition of 25 mM DTT to the HSA-HDDP-SS nanocarriers. C) Scanning electron micrograph of HSA-HDDP-SS with Vybrant™ DiO in cyclohexane.

After the successful formation and reductive degradation of DiO-loaded HSA-NCs-HDDP-SS, the PNCs were encapsulated into polymeric vesicles by SDE, according to literature.[107] The confocal images of the polymeric vesicles (Figure 44A, stained in red) showed a successful encapsulation of Vybrant™ DiO-loaded PNCs (green) into the vesicles (Figure 44B) in high quantity. Upon addition of DTT to the vesicle dispersion, the PNCs degraded and released the green-fluorescent dye. The DiO-dye successfully accumulated at the vesicle membrane (Figure 44C), but no significant growth of the vesical membrane could be observed with confocal microscopy. One reason could be that the amount of delivered and released dye was not sufficient to promote a membrane growth. As seen in the confocal images, a lot of green dye could be found within the vesicle core, which were either not released or not diffused to the outer shell. Moreover, green-fluorescent aggregated could be observed in the vesicle core, which hindered the diffusion of dye to the membrane.

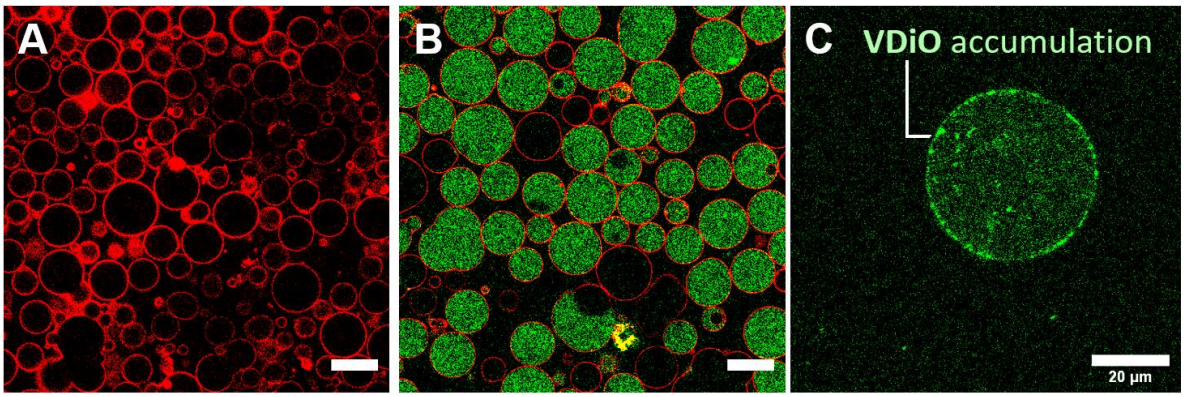

Figure 44. Confocal images of polymeric vesicles with A) membrane stained by Nile Red B) HSA-HDDP-SS NCs with Vybrant™ DiO (green) encapsulated into polymeric vesicles (red) and C) Vybrant DiO accumulation at membrane after reductive degradation of PNCs with dithiothreitol (25 mM). Images measured by [redacted].

It can be assumed that upon reductive degradation of PNCs degraded protein components aggregated and part of the lipophilic dye adsorbed to degraded protein. In order to realize a membrane growth in vesicles, higher amounts of Vybrant^{TM} DiO would need to be released into the vesicle membrane and vesicular conditions have to be found, where the dye and protein does not aggregate upon DTT treatment. Another approach would be to use another stimulus for the degradation of PNCs in the polymeric vesicles such as pH. A change in pH might maintain a higher stability of the dye after release compared to the reducing agent, so the dye might incorporate into the shell in higher quantity to achieve significant growth of the vesicle wall. Nevertheless, it could be demonstrated that developed reduction-responsive PNCs-HDDP-SS can be applied when water-soluble cargo molecules have to be encapsulated, delivered and released with high efficiency. Moreover, PNCs proved high stability during encapsulation into the vesicles, offering further application of PNCs by embedding or encapsulating them into other materials to achieve multi-functional systems.

III. A6. Conclusion

We developed a bioorthogonal protocol for the multicomponent encapsulation and co-delivery of fully biodegradable protein nanocarriers. For the synthesis of the PNCs, we applied a metal-free protocol to modify the protein's amine groups to azide groups with 1-sulfurylimidazol hydrochloride in water. With an azide-modified protein on hand, human serum albumin nanocarriers were prepared by metal-free azide-alkyne click reaction with activated hexanediol dipropiolate in an inverse miniemulsion. The developed process enabled the simultaneous encapsulation of multiple cargo molecules with different physicochemical properties such as molecular weights and solubility. A high encapsulation efficiency and a preserved bioactivity of the cargo was obtained. Varying the crosslinker amount not only allowed to tailor the density of the shell to entrap different adjuvants, but also the degradation and release rates of the nanocarriers. PNCs were further equipped with disulfide bonds by using HDDP-SS as the crosslinker, which resulted in nanocarriers releasing the cargo enzymatically and under reductive conditions. We demonstrated a successful encapsulation of the adjuvants R848, MDP, and Poly(I:C) into PNCs yielding a higher stimulation of immune cells with co-delivery of all three adjuvants encapsulated into one nanocarrier compared to single-loaded PNCs. In summary, this protocol might be used to develop efficient immunotherapies, which rely on the combination of several drugs and adjuvants with highly different physical properties. Further, the bioorthogonal formation of the nanocarriers with a guaranteed release upon proteolysis might be a powerful tool for the delivery of nucleic acids.

Chapter B – Dendritic Cell-Mediated T Cell Stimulation by Adjuvant-Loaded Ovalbumin Nanocarriers for Anti-Tumor Vaccination

Chapter B is part of the manuscript:

[redacted], N. Hüppe, [redacted], *manuscript in preparation*. For the thesis, this chapter was extended with preliminary results, additional experiments, optimizations and details.

Contributions:

Natkritta Hüppe synthesized and characterized the modified protein and resulting adjuvant-loaded protein nanocarriers as well as the azide-transfer agent and crosslinker involved as stated in the experimental part. Natkritta Hüppe performed the quantification of Resiquimod, PEG-R848, diABZI and muramyl dipeptide. For quantification of polyinosinic-polycytidylic acid, Natkritta Hüppe performed the degradation and release of Poly(I:C) from the protein nanocarriers. Natkritta Hüppe performed sample preparation for SEM. [redacted] performed *in vitro* as well as *in vivo* experiments with the adjuvant-loaded protein nanocarriers and evaluated the data.

Abstract

Tumor vaccination relies on three processes in the dendritic cell (DC)-mediated T cell stimulation: 1) DCs present tumor-specific antigens to T cells 2) For a strong immune response, adjuvants trigger antigen-independent upregulation of costimulatory marker molecules and 3) For enhanced T cell activation; cytokines are secreted from the stimulated DCs. If all three processes proceed sufficiently, T cells are activated and proliferate to specifically attack the antigen-bearing tumor cells. To achieve a high immune stimulation by antigen and adjuvants, the vaccine components were formulated into a nanovaccine composed of adjuvant-loaded ovalbumin nanocarriers (OVA-NCs). A multicomponent encapsulation of adjuvants, which target different pattern recognition receptors, promoted a synergistic stimulation of DCs leading to antigen-presentation on MHC class I and II, high expression of costimulatory molecules CD80/86 and secretion of pro-inflammatory cytokines, such as TNFα, IL-6 and IL-12. The dual-loaded OVA-NCs with a combination of TLR7/8 ligand Resiquimod (R848) and NOD2 ligand muramyl dipeptide (MDP) successfully achieved a DC-mediated T cell stimulation with high proliferation of OT-I/II T cells. In a mouse model bearing OVA-expressing melanoma tumor, OVA-R848/MDP-NCs demonstrated the highest tumor treatment efficacy through a low tumor growth rate and high probability of survival. The *in vivo* results underlined the superiority of a nanocarrier formulation to a soluble formulation due to simultaneous delivery of the vaccine components with enhanced synergistic stimulation effect.

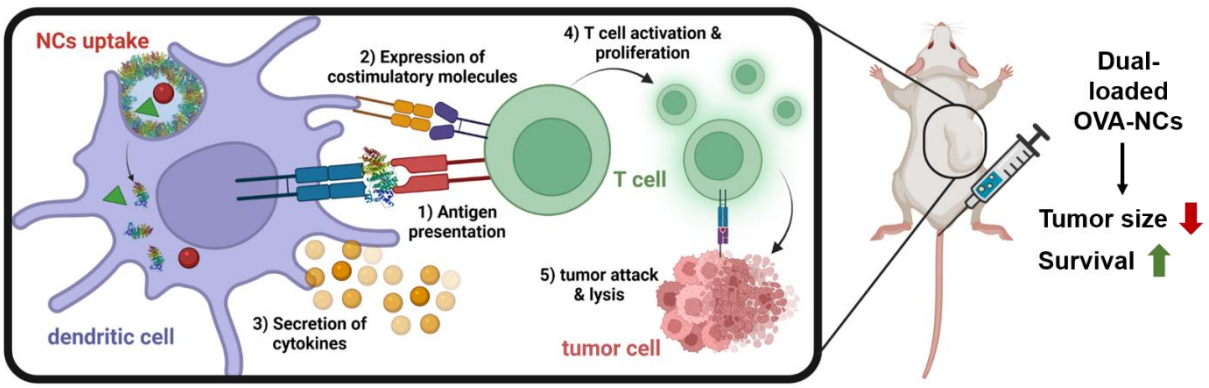

Figure 45. Dendritic cell-mediated T cell stimulation promoted by adjuvant-loaded ovalbumin nanocarriers leads to decrease in tumor growth/size and longer survival of melanoma-bearing mice. Figure created in Biorender.com by Natkritta Hüppe.

In further optimization experiments *in vitro*, a triple combination of R848, MDP and Poly(I:C) loaded into OVA-NCs further enhanced the stimulatory properties of the nanovaccine compared to dual-loaded NCs. Moreover, a lower crosslinking degree allowed faster intercellular degradation and release of adjuvants, leading to a higher DC stimulation.

Especially, the high degradation rate enabled higher release of large molecules such as Poly(I:C), promoting the synergistic effect of the adjuvant combination through simultaneous release. STING-agonist diABZI demonstrated a high stimulatory effect as well, especially the secretion of pro-inflammatory cytokine interferon (INF), which is not induced by the previous chosen adjuvants, could enhance the synergistic immune stimulation of the adjuvant combination. OVA-NCs loaded with a combination of multiple adjuvants proved to be a promising nanovaccine for the treatment of tumors.

III. B1. Introduction

The immune system is a remarkable machinery of cells that interact in a complex communication pathway to fight against threats to our body.[176, 177] If the body is exposed to pathogens such as bacteria or viruses the immune cells detect the intruder and invoke an attack. In most cases, the immune cells memorize the pathogen's identity on specific molecules, such as proteins or peptides and can eliminate the pathogen faster upon repeated exposure.[178-180] Those pathogen-related molecules, so-called antigens, play a crucial role in vaccination processes.[181, 182] A prophylactic vaccination trains the immune system to recognize specific pathogens and prepare for an attack before a potential intrusion happens.[183-185] Prophylactic vaccination helped to fight numerous bacterial or viral diseases up to eradication of some such as small pox.[186] However, threats to our body does not always come from outside but from within our body as well. Cancer is still the number one cause of deaths worldwide with one in six deaths are due to cancer.[187] Cancerous cells originate from mutation of our own cells and often intrudes our body slowly and quietly.[188-190] Often common tumor therapies such as chemotherapy lack the long term efficiency to fight the cancer and come with severe side effects for the patients due to highly toxic drugs.[191, 192] Immunotherapy aims for prophylactic or therapeutic treatment against tumors by training the immune system against the tumor cells.[193, 194] A successful activation of an adaptive immune response depends on 1) the antigen-presentation on MHC 2) expression of costimulatory marker molecules and 3) release of cytokines.[195] Several cells and signaling receptors and molecules are involved in a vaccination process. Dendritic cells (DCs) belong to the innate immune system and are the first defenders against pathogens.[165, 196] DCs can be found in all tissues and organs where they scan for potential threats. As one of the main antigen-presenting cells (APCs), DCs signal other immune cells like T cells to attack the pathogens by presenting the pathogenic antigen to the T cells.[197-199] In case of tumor therapy, a vaccine formulation would consist of the tumor-specific antigen for recognition and adjuvants for immune cell activation.[200-202] Adjuvants are stimulating molecules that induce immune cell activation and boost the immune response against the antigen.[203] The higher the stimulating property of the adjuvants the higher is the effectivity of the vaccination against the tumor-specific antigen.[204] As a first step in the vaccination process, the DCs internalize the vaccine components. The antigen is degraded and its peptide chains presented on the major histocompatibility complex (MHC) molecules of the DC to the T cells. The T cells recognize antigen-MHC complexes by antigen-specific T cell receptors (TCR) in combination with their TCR-co receptors CD4 or CD8α. The antigen presentation induces T cell activation and proliferation to attack the tumor bearing the specific antigen.[198] DCs not only

are APCs, but offer numerous pattern recognition receptors (PRRs) on their cell surface and in the endosome to sense all kind of pathogenic components.[205, 206] One of the best studied PRRs are toll-like receptors (TLR), which detect various pathogen- and damage-associated molecular patterns (PAMP and DAMP) such as proteins, lipoproteins and nucleic acids.[207, 208] NOD-like receptors (NLRs) detect PAMP and DAMP as well but especially bacterial peptidoglycans and cytosolic RNA viruses.[209, 210] The PRRs play a crucial role in DC maturation and T cell activation as they induce the expression of costimulatory marker molecules on the DC cell surface.[211] The maturation marker molecules, mainly CD80 and CD86, are as well recognized by the T cells through its CD28 molecule and enhance the adaptive T cell response.[212] A high expression of costimulatory molecules is indispensable for successful T cell activation as insufficient expression of costimulatory molecules leads to anergy or even apoptosis of the T cells.[213, 214] Different adjuvants act as ligands for different PRRs and induce different signaling pathways and expression of costimulatory marker molecules. Using several adjuvants in combination leads to an additive stimulation.[1, 149-151] In some cases, the right combination of adjuvants creates an enhanced cross-talk between the receptors achieving a superadditive stimulation and increased expression of costimulatory molecules. Another important signaling mechanism that promotes adaptive immune responses is the release of cytokines. Different cytokines trigger the activation of different T cell subtypes, for example cytokines tumor necrosis factor (TNF) α and interleukin (IL)-12 are known to promote polarization of naïve $CD4^+$ T cells into Th1.[215-217] The type of adjuvants influence the induction of different cytokines and thus effects the T cell proliferation. Therefore, adjuvants and their right combinations are important components for activating adaptive immune responses and should be well chosen for the design of a vaccination formulation. If all three processes, 1) antigen-presentation, 2) co-stimulation and 3) cytokine release, proceed effectively, the dendritic cell mediates T cell activation and proliferation. The T cells then attack the antigen-bearing tumor cell, leading to tumor lysis (Figure 46).

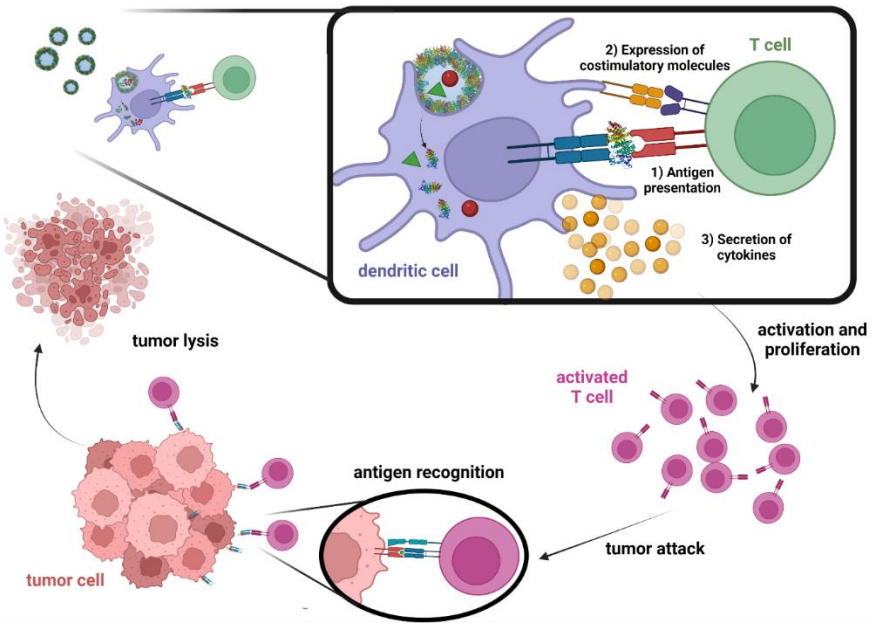

Figure 46. Induction of DC-mediated T cell activation for tumor treatment by a vaccination with tumor-specific antigen and adjuvants. Figure created with BioRender.com. Protein structure was obtained from DrugBank online (https://go.drugbank.com/drugs/DB00062, 28.11.2021) and was adapted. Figure created in Biorender.com by Natkritta Hüppe.

Besides the right combination of adjuvants in the vaccine formulation, a high concentration of the components in the DCs should be achieved to ensure an effective immune response. The adjuvants molecules have to cross the plasma membrane to reach the targeted endosomal PRRs. Usually the vaccine components are internalized by endocytosis.[218] Common vaccine formulations based on liquid mixture of the components lack the uptake efficiency into DCs due to systemic distribution and fast excretion upon administration. Nanocarriers as a delivery tool offer the opportunity to transport the vaccine components protected and efficiently to the DCs.[219, 220] An encapsulation of the vaccine components into nanocarriers could mediate and even increase the internalization of the molecules to the intracellular compartments, where the associated PRRs are present. Therefore, a high local concentration of antigen and adjuvants could be achieved in the cells leading to higher vaccination effectivity. Furthermore, encapsulation of vaccine components into nanocarriers enables the simultaneous transport of multiple components and thus promotes an additive stimulation effect when multiple adjuvants are encapsulated. Not only multiple but also different components can be encapsulated into nanocarriers, allowing the use of components that cannot be use in common formulations due to toxicity or solubility. Nanocarrier-based vaccine formulations, so-called nanovaccines, are the major focus in the development of new strategies for tumor treatments.[221, 222] For example, liposomes are already approved as drug delivery systems by the Food and Drug Administration (FDA) and are in focus as delivery systems for vaccine components.[67] Although liposomes offer

a broad range of lipids as nanocarrier materials, many liposome preparation methods suffer from low encapsulation efficiencies.[223] Another major class of nanocarriers are polymeric nanoparticles (NPs).[224] Polymeric NPs as well offer a broad range of synthetic polymers, such as polylactic acid (PLA) or polylactic-co-glycolic acid (PLGA), to name degradable and biocompatible ones.[225, 226] However, many nanocarrier procedures lack the ability to encapsulate multiple cargo molecules simultaneously in a controlled and biorthogonal manner.

In chapter A, the development of protein nanocarriers (PNCs) for the encapsulation and transport of multiple components was described. Multicomponent encapsulation of different adjuvants could be achieved with the established process in inverse miniemulsion and an additive stimulation of dendritic cells could be demonstrated. The PNCs are an optimal tool to formulate a nanovaccine for tumor treatment. Previously, the PNCs were prepared with human serum albumin (HSA) as the shell material since HSA is an endogenous protein offering high biocompatibility and biodegradability. However, for the formulation of a nanovaccine an antigen is needed to induce antigen-specific T cell activation. Ovalbumin (OVA) as an egg-white protein can be used as a model antigen for vaccine formulations. The formation of protein nanocarriers from ovalbumin is performed according to the previously developed protocol for HSA-NCs. The adjuvants are loaded into the antigen-consisting nanocarrier creating an all-in-one nanovaccine.

III. B2. Preparation of Ovalbumin Nanocarriers

Protein nanocarriers from ovalbumin were prepared through an interfacial crosslinking of azide-modified ovalbumin with hexanediol dipropiolate (HDDP) in an water-in-oil inverse miniemulsion (similar to the protocol reported in chapter A for HSA-NCs). The adjuvants were dissolved in the water-droplet and were encapsulated during the protein shell formation, allowing multicomponent encapsulation with high control and efficiency. For a formation of ovalbumin nanocarriers (OVA-NCs) by azide-alkyne click chemistry, OVA was functionalized with azide groups by 1-imidazol-sulfuryl azide hydrochloride, as previously described in chapter A (Scheme 8).[158, 160]

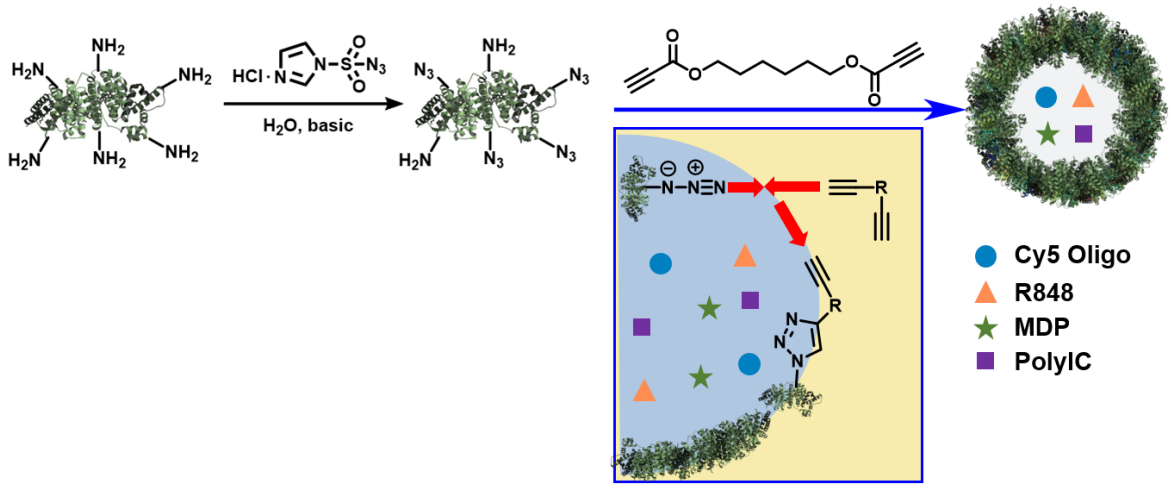

Scheme 8. Ovalbumin is functionalized with azide groups by 1-imidazole sulfurylazide hydrochloride in basic condictions (pH 8.3-11). Formation of ovabumin nanocarriers (OVA-NCs) through azide-alkyne crosslinking of azide-functionalized protein with hexanediol dipropiolate (HDDP). Multicomponent encapsulation of adjuvants into OVA-NCs during the protein shell formation. Protein structure was obtained from DrugBank online (https://go.drugbank.com/drugs/DB00062, 28.11.2021) and was adapted. Figure created in ChemDraw by Natkritta Hüppe.

After the reaction of OVA with the azide transfer agent at pH 11 for 24 h, the azide-modified OVA (OVA-N_3) showed a prominent azide signal 2100 cm^{-1} in the infrared (IR) spectra compared to the native protein (Figure 47). However, after lyophilization OVA-N_3 was not water-soluble anymore. The sensibility of OVA towards high basic pH led to denaturation and decreased water-solubility of the protein. Without high water solubility, OVA-N_3 could not be used to successfully prepare nanocarriers in inverse miniemulsion. Therefore, the azide functionalization protocol was tailored to optimize the reaction conditions and obtain water-soluble OVA-N_3.

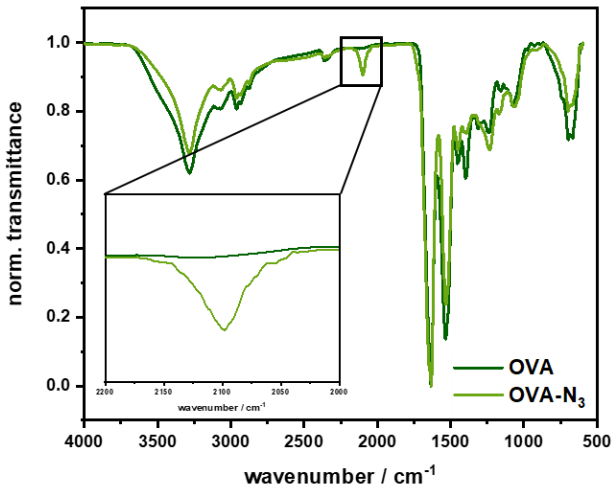

Figure 47. A) Infrared spectra of ovalbumin (OVA) before and after azide-functionalization (OVA-N_3) with 1-imidazol-sulfuryl azide hydrochloride under basic conditions (pH 11).

The azide-functionalization reaction with 1-imidazol-sulfuryl azide hydrochloride is a transfer reaction of amines to azides and depends on the nucleophilicity of the amine moiety. As demonstrated in chapter A, the pH value during the reaction influenced the number of transferred amines to azides. Ovalbumin was modified by 1-imidazol-sulfuryl azide hydrochloride at different pH values and reaction times and the resulting number of reacted amines was determined by fluorescamine assay with glycine as a standard substrate (Table 9). A successful azide-modification was achieved already at a pH of 8.2, resulting in seven azide groups after one day of reaction time. At increased pH values, i.e. pH 9.5 and 11, no dependence of reacted amines on the reaction time could be observed, indicating high reactivity of amines at pH > 9.

For *in vivo* experiments, the azide-modification had to be performed under endotoxin-free conditions to prevent fouling of the modified OVA upon storage. In general, high sterility and stability of proteins are difficult to maintain in solution and proteins should be stored as dried powders. Using a salt-containing solution for the lyophilization of the modified protein was crucial to maintain the water-solubility of OVA-N_3. Several optimization steps (pH, reaction time, salt concentration during lyophilization) were taken to obtain water-soluble OVA-N_3 and to successfully prepare stable OVA-NCs, as described in detail in the Supplementary Information (SI) of chapter B.

Table 9. Azide-functionalization of ovalbumin at different pH value and time. Number of azide groups ($N_{ex}(N_3)$) quantified by the theoretical ($N_{theo}(NH_2)$) and experimental ($N_{ex}(NH_2)$) number of amines, measured with the fluorescamine assay.

	pH	**t/d**	$N_{theo}(NH_2)$	$N_{ex}(NH_2)$	$N_{ex}(N_3)$
OVA, nat.	-	-	20	19	-
OVA-N_3	8.2	1	-	12	7
OVA-N_3	8.2	2	-	11	8
OVA-N_3	8.2	3	-	6	13
OVA-N_3	9.5	1	-	6	13
OVA-N_3	9.5	2	-	6	13
OVA-N_3	9.5	3	-	7	12
OVA-N_3	11	1	-	3	16
OVA-N_3	11	2	-	3	16
OVA-N_3	11	3	-	3	16

The optimal condition to obtain water-soluble OVA-N_3 was as follows: OVA was first dissolved in a K_2CO_3 solution of pH 11 and 1-imidazolesulfuryl azide hydrochloride solution was added dropwisely, while the pH value decreased to 9.5. The protein was left at higher basic pH for 30 min to gain high nucleophilicity of the amines and promote the azide transfer reaction. To minimize the harsh conditions of the azide transfer reaction, the pH value of the reaction solution was adjusted to pH 8.3 and the reaction proceeded for 8 h. With this milder procedure, water-soluble OVA-N_3 was obtained after purification (dialysis in sterile water) and lyophilization (with addition of NaCl (14.4 mg/mL)). With a water-soluble OVA-N_3 in hand, ovalbumin nanocarriers could be prepared similar to the method established in chapter A for HSA-NCs (Figure 48). Since OVA-NCs should be applied *in vivo*, the method was modified to a sterile and endotoxin-free procedure (sterile solvents and glassware, handling under flow bench), as described in the SI of chapter B. The endotoxin concentration of obtained OVA-NCs dispersion was measured with the LAL assay (see SI). With adjusting the protocol, OVA-NCs with a prominent core-shell morphology could successfully be prepared and Cy5-Oligo was encapsulated with 46% efficiency. The size of resulting OVA-NCs was with ~300 nm in cyclohexane and ~240 nm after transfer to water with narrow size distributions comparable to the results obtained for HSA-NCs.

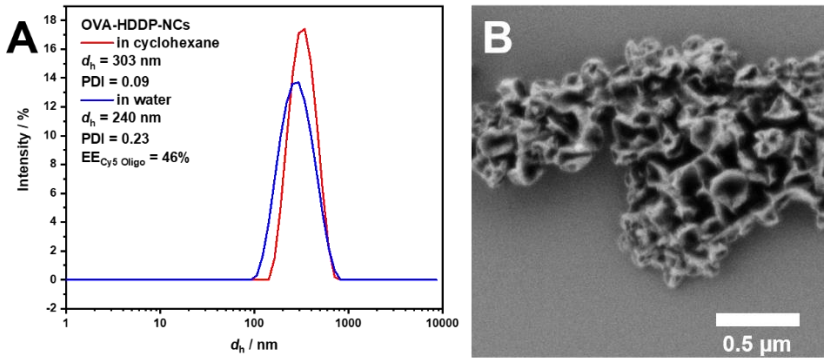

Figure 48. A) Dynamic light scattering and B) scanning electron micrograph of ovalbumin nanocarriers obtained from azide-modified ovalbumin crosslinked with hexanediol dipropiolate in inverse miniemulsion.

Solubility of Ovalbumin in Presence of DMSO

Ovalbumin is, like most proteins, sensible to organic solvents such as DMSO and temperature.[227, 228] Since some adjuvants are not water-soluble and have to be dissolved in DMSO for the encapsulation process, the stability of OVA in presence of DMSO with increasing temperature was investigated (Table 10). A stock solution of OVA was prepared and set to temperature and respective amount of DMSO was slowly added under stirring. With increasing temperature, the OVA solution formed a gel after addition of 59% (35 °C) and 39% (45 °C) DMSO. All solutions with added DMSO formed a gel after several days, indicating slow denaturation of OVA. The concentration of DMSO in the disperse phase should not exceed 50% for 25 °C and 14% for 45 °C to ensure stability of the protein in the water droplet and successful encapsulation of DMSO-soluble cargo molecules into OVA-NCs.

Table 10. Solubility of ovalbumin with addition of dimethylsulfoxide at different temperatures.

Sample	*T* / °C	DMSO / %	OVA dissolved
1	15	14	Y
2	15	19	Y
3	15	24	Y
4	15	29	Y
5	15	39	Y
6	15	59	gelated*
7	25	14	Y
8	25	19	Y
9	25	24	Y
10	25	29	Y
11	25	39	Y

12	25	59	gelated*
13	35	14	Y
14	35	19	Y
15	35	24	Y
16	35	34	Y
17	35	59	gelated
18	45	14	Y
19	45	19	gelated
20	45	24	gelated
21	45	29	gelated
22	45	39	gelated

*gelated after 30 min

With a successful transfer of the PNCs preparation procedure from HSA to OVA, OVA-NCs could be used for the DC-mediated T cell stimulation as an adjuvant-carrier and antigen all-in-one. Therefore, different combinations of adjuvants were encapsulated into OVA-NCs to investigate the DC stimulation.

III. B3. *In Vitro* Stimulation of DCs with Adjuvant-Loaded OVA-NCs

Adjuvants are key components in vaccines as they mediate stronger adaptive immune responses by inducing costimulatory marker molecules and release of cytokines from DCs.[168] There are several signaling pathways in the DC-mediated T cell activation that can be triggered by using different adjuvants. Some in combination even provide stimulatory synergies, further enhancing the vaccination effect.[151] Different combinations of adjuvants were loaded into OVA-NCs to create a nanovaccine with high stimulatory properties and to reduce tumor growth in *in vivo* mice models.

III. B3.1. R848 versus PEGylated R848-Loaded OVA Nanocarriers

Resiquimod (R848) as a TLR 7/8 ligand proved to be an effective adjuvant to promote high expression of CD80 and CD86 markers in DCs.[171] However, the small molecule is rather hydrophobic (solubility in water < 1 mg/mL) and only soluble in DMSO (20 mg/mL). OVA was susceptible to organic solvents and denatured with at higher concentration of DMSO, as described in section 2. Therefore, it would be beneficial to increase the water-solubility of R848 by attaching hydrophilic components such as poly(ethylene glycol) (PEG) to prevent the use of

DMSO for the nanocarrier preparation. R848 and PEGylated R848 of different molecular weights were encapsulated into OVA-NCs and their stimulatory effect in DCs compared (Scheme 9).

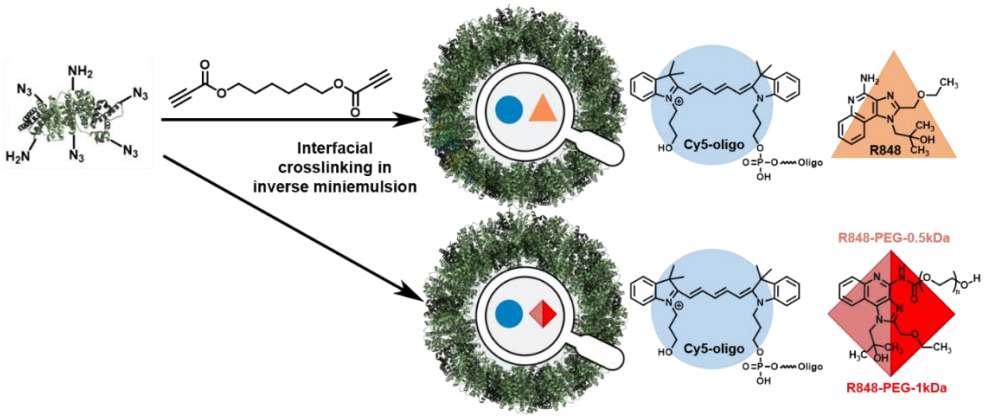

Scheme 9. Encapsulation of R848, R848-PEG-0.5kDa or R848-PEG-1kDa into ovalbumin nanocarriers crosslinked with hexanediol dipropiolate in inverse miniemulsion. Cy5-Oligo was additionally encapsulated as a fluorescent dye. Protein structure was obtained from DrugBank online (https://go.drugbank.com/drugs/DB00062, 28.11.2021) and was adapted.

R848 was functionalized with PEG through a reaction of the amine group of the R848 with poly(ethylene glycol)-*N*-hydroxysuccinimid ester (PEG-NHS) in DCM (Scheme 10).

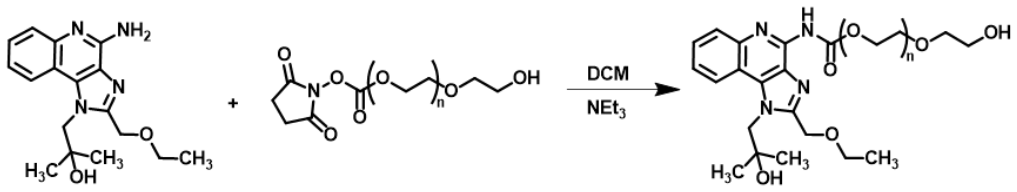

Scheme 10. PEGylation of Resiquimod (R848) with polyethyleneglycol-N-hydroxysuccinimid ester (PEG-NHS) in dichlormethane (DCM) with trimethylamine (NEt_3).

Both products with PEG-0.5 kDa and PEG-1 kDa were water-soluble (> 20 mg/mL). The ^{1}H-NMR spectrum of the product showed the presence of aromatic groups from the R848 as well as the signals from the PEG-chain (Figure 46). The functionalization degree of PEG to R848 was 20% for PEG-0.5 kDa and 10% for the PEG-1 kDa. The functionalization degree of PEG on R848 was rather low with a high amount of unreacted PEG chains. Free R848 should be completely removed by dialysis (MWCO 1 kDa). Unfortunately, PEGylated R848 was difficult to separate from free PEG chains due to the small difference in molecular weight and solubility. Therefore, a higher amount of R848-PEG was needed to obtain the same molar amount of R848 in the OVA-NCs compared to unmodified R848. Additionally, a high amount of free PEG chains had as well be encapsulated into the NCs.

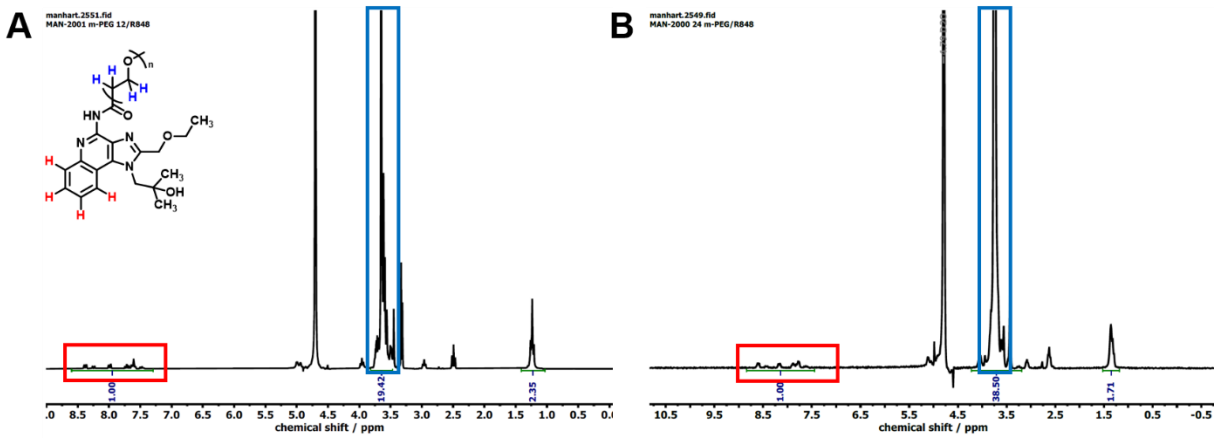

Figure 49. ^{1}H NMR spectrum of A) R848-PEG-0.5kDa and B) R848-PEG-1kDa in D_2O.

The stimulatory properties of PEG-R848 were compared to unmodified R848 by investigating the expression of MHC-II, CD80 and CD86 markers on bone-marrow-derived dendritic cells (BMDCs) (Figure 50). In all cases, PEGylated R848 induced a higher expression of markers compared to unmodified R848, while R848-PEG-1kDa gave the highest stimulation. We assumed, that the higher water-solubility of R848 achieved higher uptake into BMDCs and more effective ligation to PRRs to induce a stronger stimulation and expression of markers.

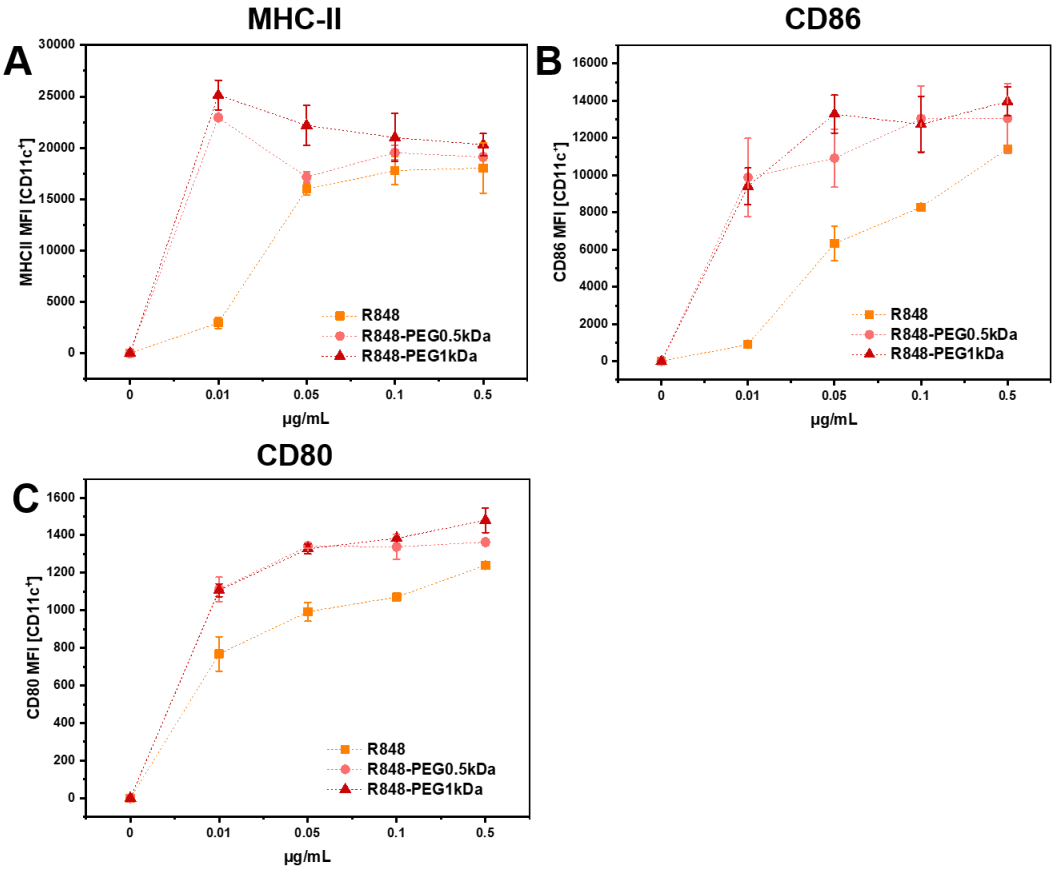

Figure 50. Upregulation of DC receptor MHC-II and maturation markers CD80 and CD86 after stimulation with R848, R848-PEG-0.5kDa and R848-PEG-1kDa in solution. BMDCs (2×10^5 cells/mL) were incubated with different concentrations of adjuvants (1–100 µg/mL) for 24 h. Surface expression of CD80 and CD86 of BMDCs was measured by flow cytometry. Data from [redacted].

The PEGylated R848 dissolved in the aqueous OVA solution and were encapsulated into OVA-NCs through interfacial crosslinking in inverse miniemulsion. As a comparison, unmodified R848 dissolved in DMSO was encapsulated into OVA-NCs as well. There was no significant difference in size and size distribution observable between R848- and R848-PEG loaded OVA-NCs (Table 11). All NCs had a size of approx. 300 nm with a PDI of ~ 0.1 in cyclohexane and after transfer into water by surfactant exchange the size decreased to approx. 230 nm. The encapsulation efficiencies of dye Cy5-Oligo as well as R848 were comparable at approx. 40% for unmodified as well as PEGylated R848.

Table 11. Analytical data of ovalbumin nanocarriers loaded with A) Cy5-Oligo+R848-PEG-0.5kDa, B) Cy5-Oligo+R848-PEG-1kDa and C) Cy5-Oligo+R848.

No.	Adjuvants	d_h (CH) / nm	PDI	d_h(H_2O) / nm	PDI	EE_{Cy5} / %	EE_{R848} / %
1	R848-PEG-0.5kDa	286	0.08	236	0.27	43	42
2	R848-PEG-1kDa	305	0.14	251	0.28	40	39
3	R848	301	0.10	203	0.31	45	34

A difference was only significant in the morphology of the OVA-NCs loaded with the different R848 derivatives, since R848-PEG-loaded OVA-NCs had visually thinner and softer protein shell, even more prominent for R848-PEG-0.5kDa (Figure 51A and B). A reason could be the high concentration of PEGylated R848 in the disperse phase, since a higher amount had to be used to reach a similar molar concentration in the OVA-NCs compared to unmodified R848. A high amount of free PEG chains could have influenced the protein shell formation during the interfacial crosslinking, leading to less amount of crosslinked protein and a thinner shell. In comparison, OVA-NCs loaded with unmodified R848 demonstrated a prominent protein shell (Figure 51C). Despite the addition of 14 vol.-% DMSO to the disperse phase, the OVA-N_3 remained sufficiently stable and soluble to perform an interfacial crosslinking with HDDP in an inverse miniemulsion.

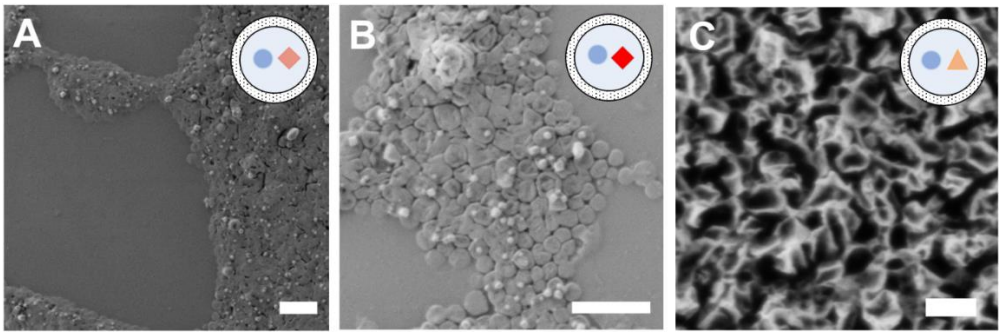

Figure 51. Scanning electron micrograph of ovalbumin nanocarriers loaded with A) Cy5-Oligo+R848-PEG-0.5kDa, B) Cy5-Oligo+R848-PEG-1kDa and C) Cy5-Oligo+R848, in cyclohexane. Scale bar: 0.5 µm.

The uptake into BMDCs measured by the Cy5-Oligo signal decreased from empty OVA-NCs to R848-loaded to R848-PEG-1kDa-loaded OVA-NCs (Figure 52A). Since the encapsulation efficiency of Cy5-Oligo was similar for all OVA-NCs, the lower uptake of R848-PEG-1kDa-loaded OVA-NCs could possibly be a result of a stealth effect by the PEG chains. The scanning electron micrographs revealed a change in shell morphology for OVA-NCs loaded with PEGylated R848. It could be assumed, that at high concentration of R848-PEG or free PEG chains were entrapped or adsorbed protein shell, creating an unwanted stealth effect to DCs. All adjuvant-loaded OVA-NCs achieved a high expression of antigen-presenting MHC-II receptors on the BMDCs. BMDCs treated with R848 and R848-PEG-loaded OVA-NCs showed a higher stimulation and expression of CD80 and CD86 markers for NCs loaded with unmodified R848 compared to PEGylated R848 (Figure 52B-D). Comparing the two PEGylated R848 samples, the OVA-NCs loaded with the smaller R848-PEG-0.5kDa led to higher expression of stimulatory molecules compared to R848-PEG-1kDa. The results for the stimulation of DCs by soluble R848-PEG compared to encapsulated R848-PEG were reversed, as R848-PEG gave a higher stimulation compared to unmodified R848 in solution while encapsulated R848 lead to higher stimulation. The encapsulation process *via* the inverse miniemulsion process influenced the activity of the adjuvant, where a PEGylation of R848 was not beneficial for the stimulative property of adjuvant-loaded OVA-NCs in BMDCs.

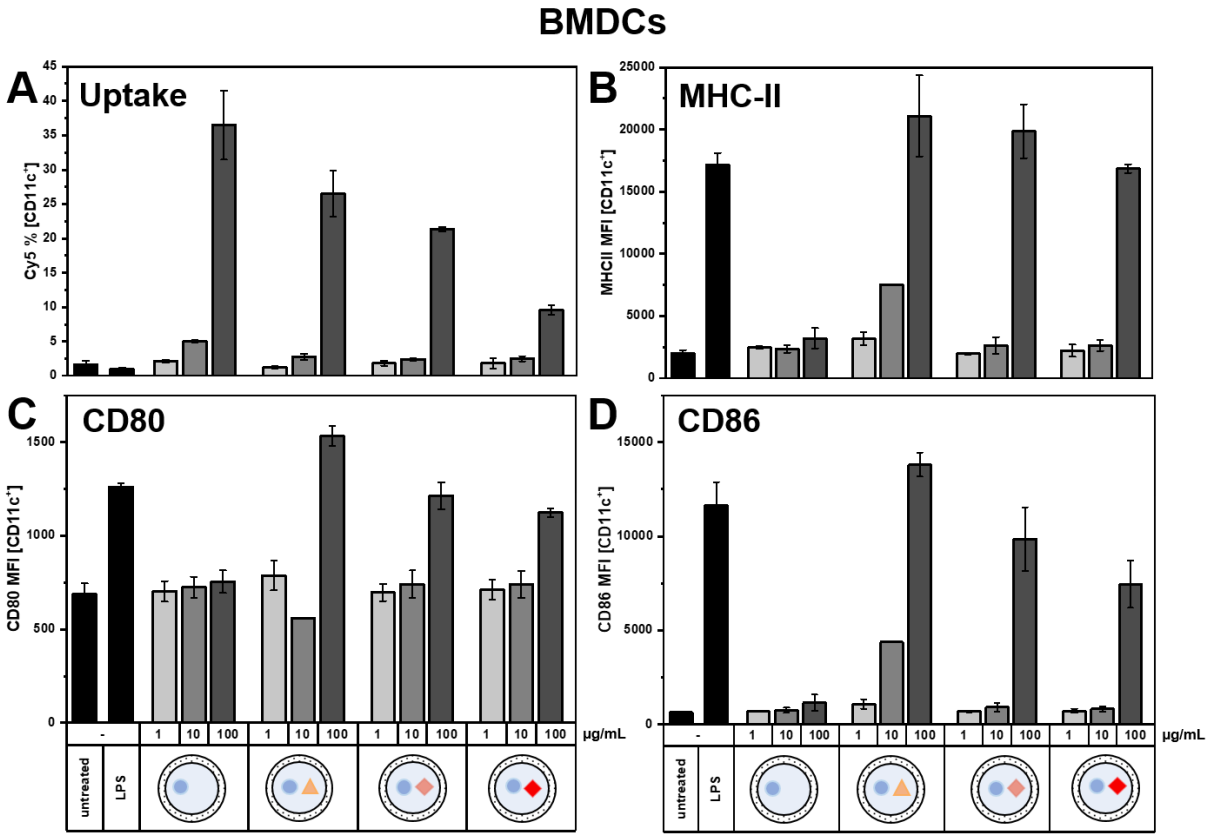

Figure 52. A) Cell binding/uptake into BMDC of Cy5-Oligo-loaded ovalbumin nanocarriers (OVA-NCs) measured by flow cytometry. B-D) Upregulation of DC receptor MHC-II and maturation markers CD80 and CD86 after stimulation with OVA-NCs loaded with R848, R848-PEG-0.5kDa and R848-PEG-1kDa. BMDCs (2×10^5 cells/mL) were incubated with differently loaded OVA-NCs formulations (1–100 µg/mL) or LPS (100 ng/mL) as a positive control for 24 h. Surface expression of CD80 and CD86 of NC-treated BMDCs was measured by flow cytometry. Data from [redacted].

Although the PEGylation of R848 achieved a water-soluble adjuvant and higher stimulatory properties in solution, no benefits to the stimulatory properties of adjuvant-loaded OVA-NCs could be gained from PEGylation under these conditions. Despite the use of DMSO for dissolving R848 in the disperse phase, stable OVA-NCs could be obtained and high stimulation of BMDCs was achieved resulting in high expression of costimulatory markers. For the following development of adjuvant-loaded OVA-NCs, unmodified R848 was used in combination with different adjuvants to create an optimal nanovaccine with superadditive stimulation properties.

III. B3.2. R848 and MDP-Loaded OVA Nanocarriers

A combination of TLR 7/8-agonist R848 and NOD2-ligand muramyl dipeptide (MDP) have proven to create a synergistic effect in DC-mediated T cell activation.[1, 81] Four different OVA-NCs were synthesized by interfacial azide-alkyne crosslinking with HDDP in inverse miniemulsion, namely OVA-NCs without adjuvants as a blank control (OVA-blank-NCs),

R848-loaded OVA-NCs (OVA-R848-NCs), MDP-loaded OVA-NCs (OVA-MDP-NCs) and dual-loaded OVA-NCs (OVA-R848/MDP-NCs). In all cases, Cy5-Oligo was encapsulated as a fluorescence dye for the detection *via* flow cytometry (Scheme 11).

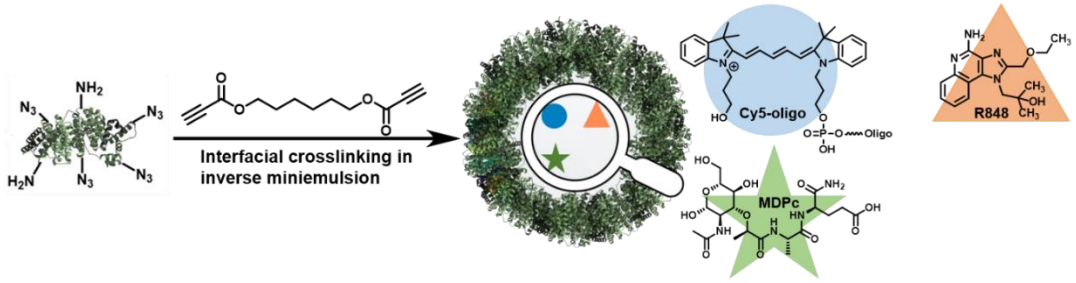

Scheme 11. Multicomponent encapsulation of Cy5-Oligo, Resiquimod (R848) and muramyl dipeptide (MDP) into ovalbumin nanocarriers crosslinked with hexanediol dipropiolate in inverse miniemulsion. Protein structure was obtained from DrugBank online (https://go.drugbank.com/drugs/DB00062, 28.11.2021) and was adapted.

Stable adjuvant-loaded OVA-NCs were prepared with all cargo combination, even the dual-loaded ones. In DLS measurements in cyclohexane, the diameters of the OVA-NCs were approx. 330 nm in cyclohexane with a relatively low PDI of 0.1 (Table 12). In water, the sizes differed about 100 nm from OVA-NCs formed with and without R848/DMSO in the disperse phase (Table 12, no. 2 and 4). The zeta potential was with approx. -38 mV, similar for empty and loaded OVA-NCs. The encapsulation efficiency of Cy5-Oligo, measured with fluorescence, was around 80%, besides MDP-loaded OVA-NCs were EE of Cy5-Oligo was considerably lower with a moderate 39%. The EEs of R848 were in single-loaded and dual-loaded NCs comparable, while EE of MDP significantly decreased by 40%.

Table 12. Analytical data of ovalbumin nanocarriers loaded with Cy5-Oligo and variations of adjuvants R848 and MDP.

No.	Adjuvants	d_h (CH) / nm	PDI	d_h(H_2O) / nm	PDI	ζ / mV	EE_{Cy5} / %	$EE_{Adj.}$ / %
1	-	333	0.12	382	0.54	-32	76	-
2	R848	385	0.16	211	0.18	-40	79	48
3	MDP	312	0.15	325	0.60	-38	39	73
4	R848/MDP	295	0.13	216	0.23	-38	87	57/33

The resulting adjuvant-loaded OVA-NCs demonstrated a prominent core-shell morphology comparable to each other according to scanning electron micrographs of NCs in cyclohexane (Figure 53).

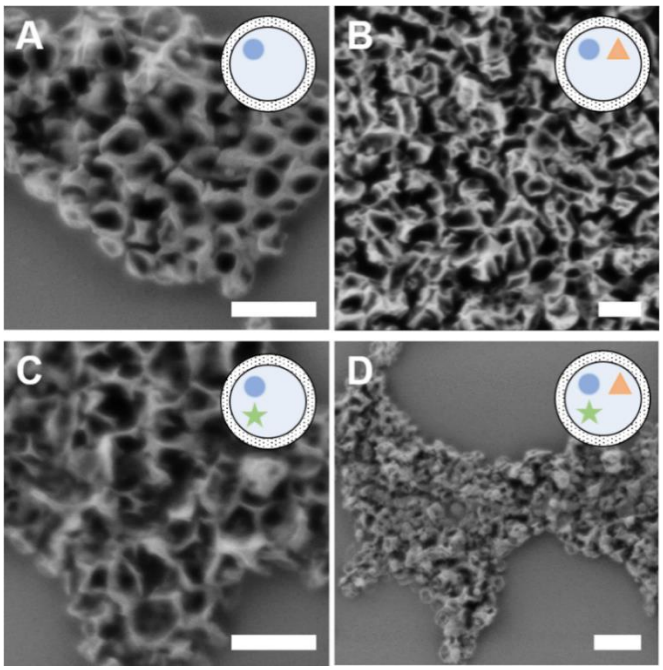

Figure 53. Scanning electron micrographs of ovalbumin nanocarriers crosslinked with hexanediol dipropiolate loaded with A) Cy5-Oligo B) Cy5-Oligo+R848 C) Cy5 Oligo+MDP D) Cy5-Oligo+R848/MDP; in cyclohexane, scale bar 0.5 µm.

In vitro experiments on BMDCs and splenocytes were performed with the prepared adjuvant-loaded OVA-NCs to investigate their stimulative properties. Special focus was on the achievement of a synergistic stimulation effect of the dual-loaded OVA-NCs with R848 and MDP.

a) Stimulation of BMDCs by R848 and MDP-Loaded OVA-NCs

BMDCs were treated with the adjuvant-loaded OVA-NCs to investigate their stimulative properties and induction of costimulatory marker molecules. Empty OVA-NCs acted as a negative and lipopolysaccharide (LPS) as a positive control. The OVA-NCs demonstrated a dose-dependent uptake into BMDCs with no significant differences between the OVA-NCs variants (Figure 54A). Antigen-presenting MHC-II molecules were expressed on the surface of BMDCs in adjuvant-loaded as well as empty OVA-NCs (Figure 54B). As expected, the antigen-NCs were internalized and degraded by BMDCs and the antigen-peptides presented on the extracellular MHC receptors. Using OVA as a shell material and antigen all in one allowed an effective uptake and antigen-delivery to BMDCs. The adjuvant-loaded OVA-NCs triggered a dose-dependent expression of costimulatory molecules CD80 and CD86, measured by flow cytometry (Figure 54C and D). OVA-blank-NCs showed, as expected, no significant stimulatory effect on BMDCs. OVA-MDP-NCs induced an expression of CD80 and CD86 only for the highest concentration of 100 µg/mL, while expression of markers was already significant for 10 µg/mL OVA-R848-NCs and OVA-R848/MDP-NCs, respectively. In case of

CD86 expression, dual-loaded OVA-NCs demonstrated the highest marker expression, indicating an additive stimulation effect when combining R848 and MDP. An additive effect could not be observed for expression of CD80. The stimulatory effect of OVA-R848-NCs and OVA-R848/MDP-NCs was similar or even higher than that of LPS.

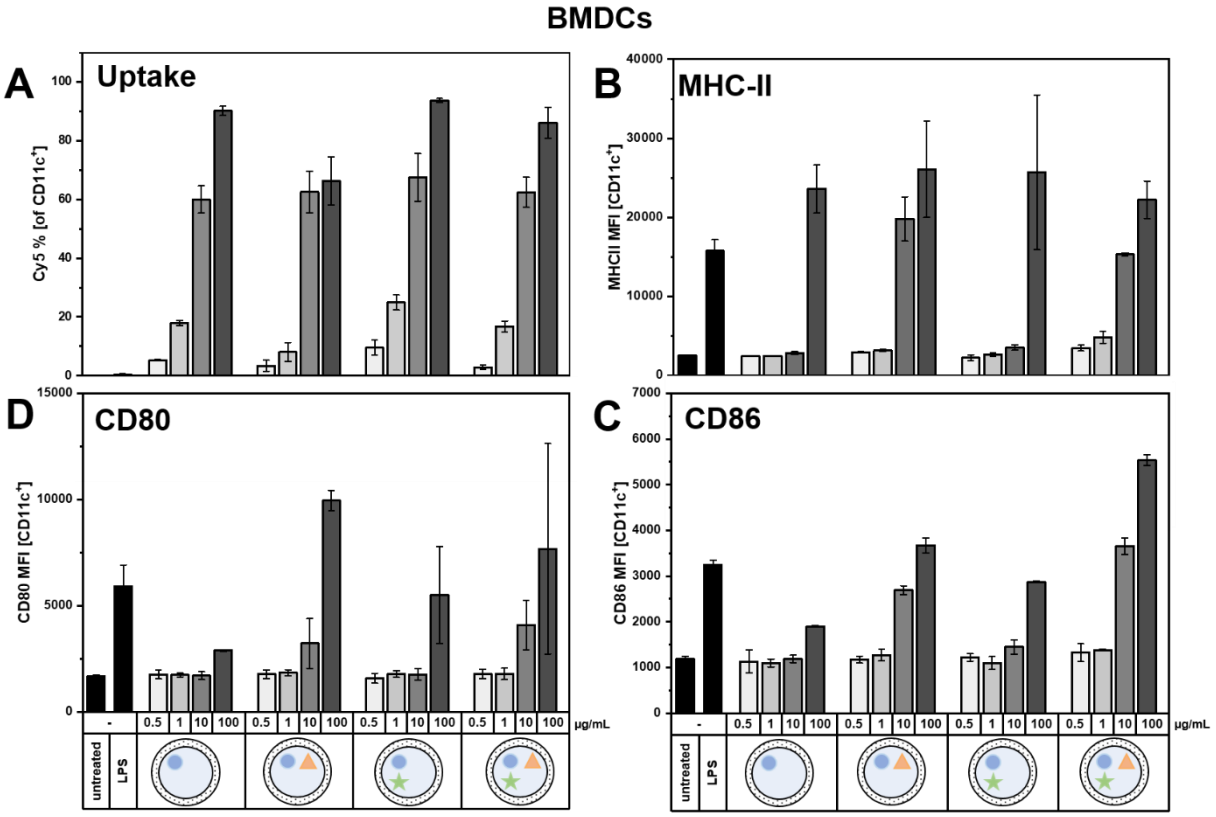

Figure 54. A) Cell binding/uptake into BMDC of Cy5-oligo-loaded ovalbumin nanocarriers (OVA-NCs) measured by flow cytometry. B-D) Upregulation of DC receptor MHC-II and maturation markers CD80 and CD86 after stimulation with OVA-NCs loaded with R848 and MDP, respectively and in combination. BMDCs (2×10^5 cells/mL) were incubated with differently loaded OVA-NCs formulations (1–100 µg/mL) or LPS (100 ng/mL) as a positive control for 24 h. Surface expression of CD80 and CD86 of NC-treated BMDCs was measured by flow cytometry. Data from [redacted].

The secretion of cytokines plays an important part in the signaling interplay of DC-mediated T cell activation.[217] The cytokine pattern allows an assumption about the effect and character of stimulation (pro- or anti-inflammatory) induced by the adjuvants as well as the type of T cell polarization associated to the stimulatory pattern. As different adjuvants bind to different PRRs and induce different signaling pathways, they can as well influence the secretion of different cytokines. Different combinations of adjuvants can trigger cytokine secretion in a synergistic manner. Therefore, the cytokine pattern in the supernatant of OVA-NCs treated BMDCs were analyzed by cytometric bead array and concentration of pro-inflammatory cytokines TNFα, IL-12 and IL-6 determined (Figure 55). The secretion of anti-inflammatory cytokines such as IL-10 induced by adjuvant-loaded OVA-NCs was consistently low comparable to cytokine concentration of the untreated samples. Empty OVA-NCs and MDP-loaded OVA-NCs

triggered no significant amount of cytokine secretion in BMDCs. The pro-inflammatory cytokines were secreted with highest concentration when treated by OVA-R848-NCs and OVA-R848/MDP-NCs. Dual-loaded NCs demonstrated the highest cytokine secretion already at 10 µg/mL NCs-concentration, indicating a synergistic stimulation of the adjuvant combination, although MDP alone did not induce significant cytokine secretion.

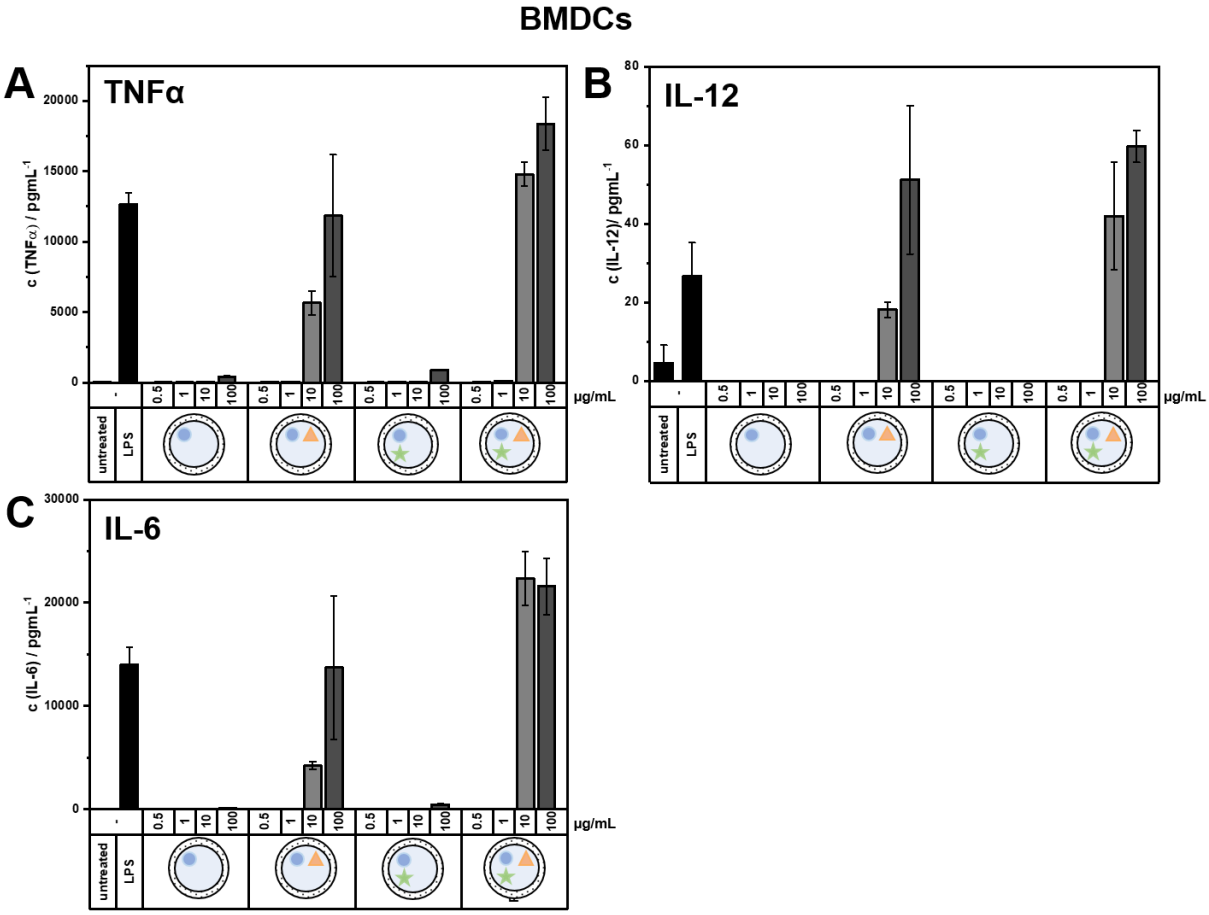

Figure 55. Cytokine secretion triggered by adjuvant-loaded ovalbumin nanocarriers. Cytokine contents in supernatants of BMDCs (1 x 106 cells/ml) treated with different concentrations of OVA-NCs for 24 h were analyzed by CBA. LPS treated BMDCs were used as positive control. Data from [redacted].

Adjuvant-loaded OVA-NCs demonstrated the induction of all three processes, important for DC-mediated T cell stimulation. First, the nanocarriers composed of the model-antigen OVA lead to a successful internalization and antigen-presentation on MHC-II receptors of BMDCs. Secondly, the adjuvants were successfully delivered into the BMDCs by OVA-NCs. There the adjuvants bonded to intracellular PRRs, triggering the expression of costimulatory marker molecules. Thirdly, adjuvant-loaded OVA-NCs stimulated BMDCs to secrete different pro-inflammatory cytokines in high concentrations. With all three pathways proceeded with adjuvant-loaded OVA-NCs, they could be used to trigger a DC-mediated T cell proliferation as an antigen-directed immune response. Here, the OVA-NCs acted as an antigen source to

activate proliferation of OVA-peptide-specific transgenic OT-I ($CD8^+$) and OT-II ($CD4^+$) T cells. OT-I T cells recognize OVA-presenting MHC-I and OT-II T cells recognize OVA-presenting MHC-II receptors. The T cell populations give an indication about the efficiency of antigen-presentation. BMDCs were treated with OVA-NCs and afterwards pre-treated BMDCs were co-cultured with OT-I and OT-II T cells in different ratios (Figure 56). The DC-mediated T cell proliferation was quantified by the incorporation of radioactive nucleoside, 3H-thymidine, into new strands of DNA during proliferation. Independent of the DC-concentration, untreated and LPS-treated BMDCs did not mediate a T cell proliferation. BMDCs treated with an OVA solution resulted in a proliferation of OT-I but not of OT-II T cells. Empty OVA-NCs induced a higher OT-I and OT-II proliferation than MDP-loaded OVA-NCs. OVA-MDP-NCs led to significant OT-I proliferation, but OT-II proliferation only at the highest DC:TC ratio of 1:5. The highest proliferation rate for OT-I and OT-II was obtained for OVA-R848-NCs and OVA-R848/MDP-NCs as expected from the results of marker expression and cytokine secretion. Here, the dual-loaded OVA-NCs demonstrated a slightly higher proliferation of T cells than OVA-R848-NCs. OT-I T cell proliferation was higher than OT-II T cell proliferation, especially significant for lower concentration of pre-treated BMDCs in the co-culture with T cells. The higher proliferation of OT-I ($CD8^+$) indicated that adjuvant-loaded OVA-NCs would direct a more prominent differentiation of T cells to Tc1 killer cells than to $CD4^+$ promoted Th differentiation.

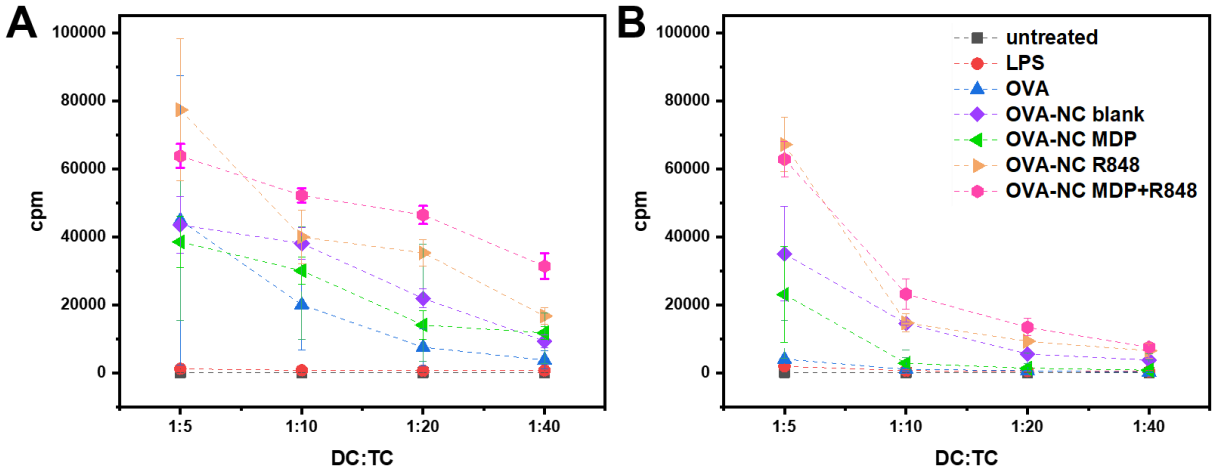

Figure 56. Dendritic cell mediated T cell proliferation upon treatment with adjuvant-loaded ovalbumin nanocarriers. LPS as control. BMDCs (1 x 106 cells/ml) were incubated with OVA-NCs for 24 h. Aliquots were co-treated with LPS. Titrated numbers of pre-treated BMDCs (starting with 105 cells) were co-cultured with OVA peptide-specific OT-I (CD8+) and OT-II (CD4+) T cells (each 5 x 105 cells) in triplicates in 96 well plates. T cell proliferation was measured in counts per minute (cpm) by 3H-thymidine incorporation, applied after three days of BMDC/T cell co-culture for 16 h (mean ± SD; n = 3). Data from [redacted].

Encapsulation of adjuvants into OVA-NCs enabled a successful DC-directed T cell stimulation. Dual-loaded OVA-NCs with a combination of R848 and MDP demonstrated the highest

expression of marker molecules and cytokines, leading to the highest proliferation rate of OT-I and OT-II T cells in BMDCs-directed proliferation. The developed dual-loaded OVA-NCs are a promising nanovaccine formulation for the tumor treatment of *in vivo* mice models. Although BMDCs are excellent cell models to study *in vitro* stimulation, in *in vivo* a mixture of cells are present in immune cell-regulating organs such as the spleen, which can change the interaction of adjuvant-loaded OVA-NCs with the cells and lead to different stimulation patterns. Therefore, the stimulative properties of adjuvant-loaded OVA-NCs were investigated in splenocytes, mononuclear cells from the spleen.

b) Stimulation of Splenocytes by R848 and MDP-Loaded OVA-NCs

The spleen is an important lymphoid organ with a rich and complex cell composition including dendritic cells, macrophages as well as T- and B-lymphocytes.[229] Splenocytes are ideal test populations to investigate the interaction of OVA-NCs with immune cells in a more realistic setup. OVA-NCs showed a concentration-dependent uptake into splenocytes, measured by the fluorescent Cy5-signal from the encapsulated dye (Figure 57A). No significant differences in uptake was observed for OVA-NCs with different loading. The expression of marker molecules on splenocytes treated with adjuvant-loaded OVA-NCs was analyzed with flow cytometry. MHC-II expression on splenocytes was not significantly increased upon OVA-NCs treatment in comparison to high MHC-II expression in BMDCs (Figure 57B). OVA-R848-NCs and OVA-R848/MDP-NCs obtained the highest expression of CD80 (Figure 57C). MDP-loaded OVA-NCs induced a high CD80 expression at a high dosage of 100 µg/mL, while empty OVA-NCs did not induce marker expression at all. For expression of CD86, no significant expression was observed for empty and single-loaded OVA-NCs. Only a combination of R848 and MDP in OVA-NCs yielded an increased CD86 expression, indicating an enhanced expression due to synergistic effects of the adjuvant combination (Figure 57D).

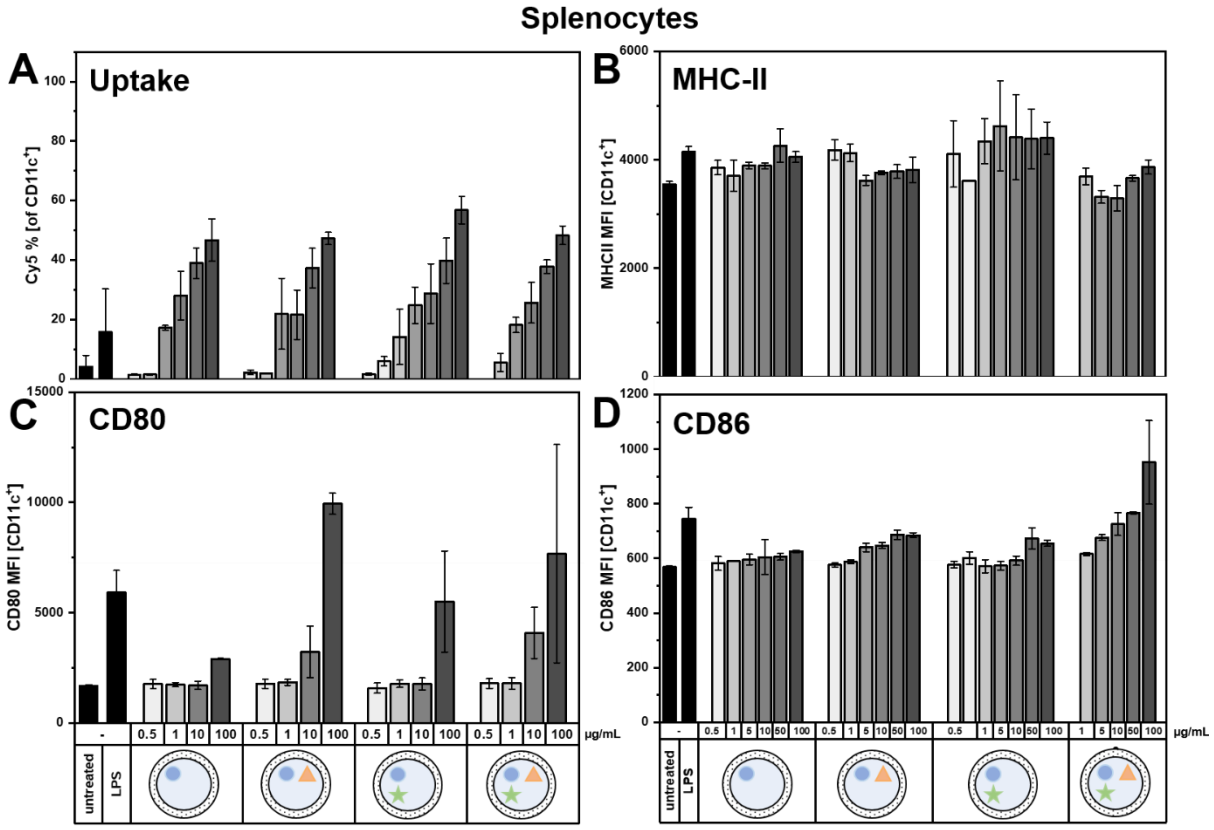

Figure 57. A) Cell binding/uptake into splenocytes of Cy5-oligo-loaded ovalbumin nanocarriers (OVA-NCs) measured by flow cytometry. B-D) Upregulation of receptor MHC-II and maturation markers CD80 and CD86 after stimulation with OVA-NCs loaded with R848 and MDP, respectively and in combination. Splenocytes were incubated with differently loaded OVA-NCs formulations (1–100 µg/mL) or LPS (100 ng/mL) as a positive control for 24 h. Surface expression of CD80 and CD86 of NC-treated Splenocytes was measured by flow cytometry. Data from [redacted].

The effect of adjuvant-loaded OVA-NCs on the cytokine excretion in splenocytes were investigated by cytometric bead array. Similar to the cytokine pattern in NCs-treated BMDCs, mainly pro-inflammatory cytokines, especially TNFα, IL-12 and IL-6 were found in the supernatant of NCs-treated splenocytes (Figure 58). As a control, no cytokine secretion was observed for untreated and LPS-treated splenocytes. The cytokine secretion induced by OVA-blank-NCs and OVA-MDP-NCs were consistently low, comparable with the results in BMDCs. Single-loaded OVA-NCs with R848 showed a concentration-dependent expression of pro-inflammatory cytokines, however considerably lower (500 pg/mL) than in BMDCs (10.000 pg/mL). The synergistic effect of the adjuvant combination on the cytokine secretion was much more prominent in splenocytes than BMDCs as the cytokine concentration for all three increased by more than double with OVA-R848/MDP-NCs.

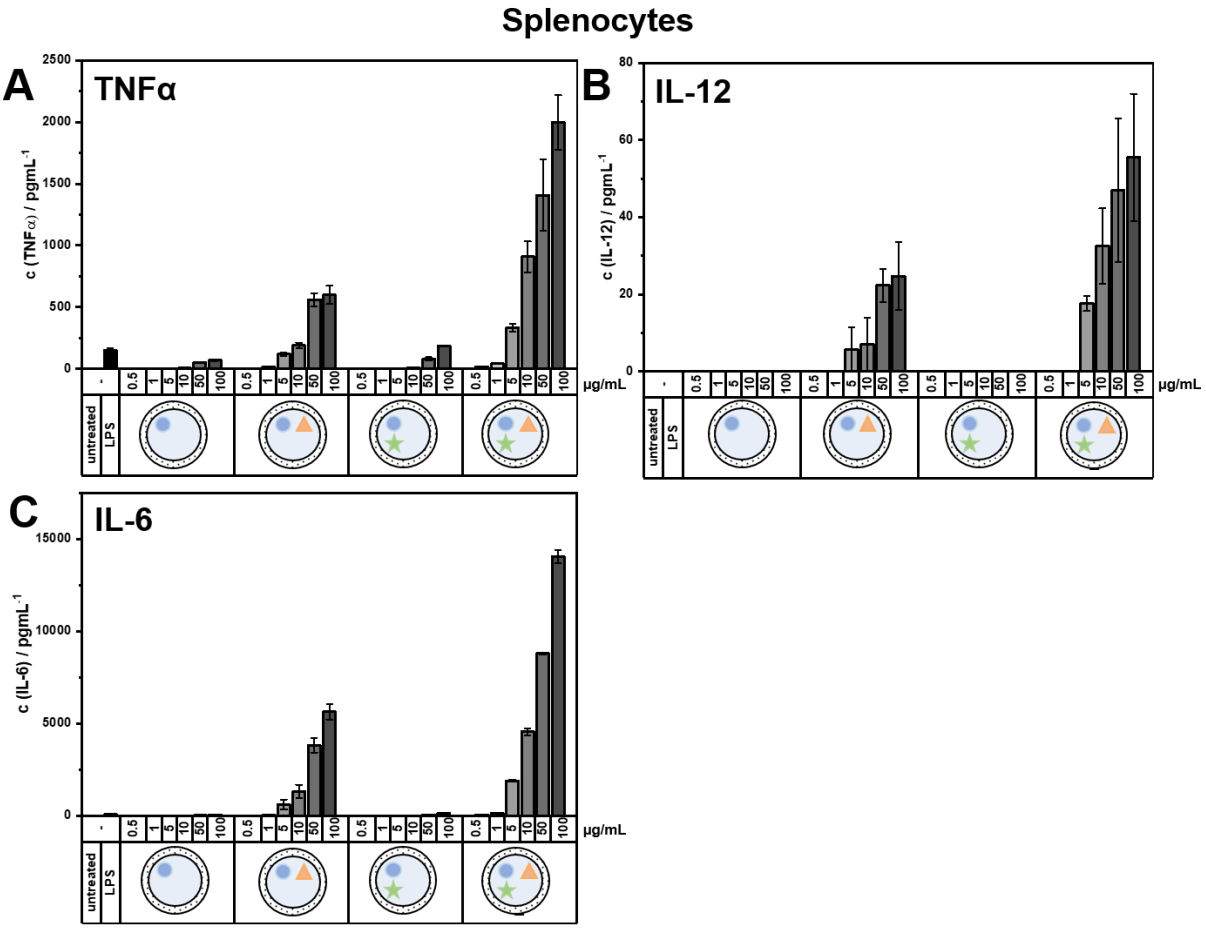

Figure 58. Cytokine secretion triggered by adjuvant-loaded ovalbumin nanocarriers. Cytokine contents in supernatants of splenocytes treated with different concentrations of OVA-NCs for 24 h were analyzed by CBA. LPS treated splenocytes were used as positive control. Data from [redacted].

Although, the stimulative response of splenocytes by OVA-NCs were not as high as in BMDCs, an effect of adjuvant-loaded OVA-NCs compared to untreated, LPS-treated and OVA-blank-NCs treated cells was still significant. Additionally, the highest expression of surface marker molecules and even more significant cytokine expression was obtained for dual-loaded OVA-NCs, underlining the superiority of an adjuvant combination compared to single-loaded NCs. Therefore, dual-loaded OVA-NCs with a combination of TLR-ligand R848 and NOD-ligand MDP offer great potential as a nanovaccine for the treatment of tumors in *in vivo* models. Since a multicomponent encapsulation of adjuvants achieved an enhanced immune response in DC-mediated T cell stimulation, an addition of another adjuvant should reach an even higher stimulation. Therefore, three different adjuvants were encapsulated into OVA-NCs and there stimulative properties investigated compared to dual-loaded OVA-NCs.

III. B2.3. R848, MDP and Poly(I:C) –Loaded OVA Nanocarriers

Dual-loaded OVA-NCs with a combination of R848 and MDP increased the immune response in DC-mediated T cell activation. An even higher stimulation of DCs could be achieved with addition of another adjuvant. As described in chapter A, a triple combination of R848, MDP and Poly(I:C) was encapsulated into HSA-HDDP-NCs and an additive effect of adjuvants on the expression of marker molecules in BMDCs could be obtained. Polyinosinic-polycytidylic acid (Poly(I:C)) is a double-stranded RNA analog which binds to endosomal TLR 3 receptors.[173] In addition to TLR7/8 ligation by R848 and NOD2 binding by MDP, Poly(I:C) could enhance a synergistic stimulation by higher cross-talk between PRRs. According to the protocol established for multicomponent encapsulation into HSA-NCs, the triple combination of R848, MDP and Poly(I:C) along with fluorescent dye Cy5-Oligo was encapsulated into OVA-NCs during the interfacial crosslinking of OVA-N_3 with HDDP in inverse miniemulsion (Scheme 12).

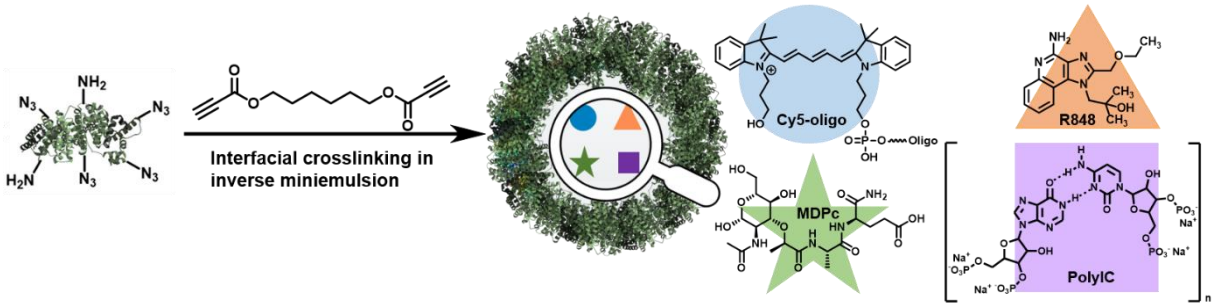

Scheme 12. Multicomponent encapsulation of Cy5-Oligo, Resiquimod (R848), muramyl dipeptide (MDP) and polyinosinic-polycytidylic acid (Poly(I:C)) into ovalbumin nanocarriers crosslinked with hexanediol dipropiolate in inverse miniemulsion. Protein structure was obtained from DrugBank online (https://go.drugbank.com/drugs/DB00062, 28.11.2021) and was adapted.

The OVA-NCs loaded with the different adjuvants and their combinations achieved stable NCs with a prominent core-shell morphology as observed in SEM (Figure 59). The adjuvant-loaded OVA-NCs showed a similar hydrodynamic radius of around 300 nm with a PDI of 0.1 in cyclohexane to empty NCs and previous HSA-NCs (Table 13). After transfer into water, the size of the Poly(I:C)-loaded NCs, in single and triple combination, decreased significantly to under 100 nm. The encapsulation efficiency of Poly(I:C) was considerably low, for the triple combination even under 10%. The EEs for R848 and MDP decreased significantly as well in the triple-loaded OVA-NCs, indicating that the high concentration of cargo molecules resulted in high osmotic pressure in the droplets and lower encapsulation efficiencies, especially of high molecular weight Poly(I:C). The EE of Cy5-Oligo was comparable for all OVA-NCs.

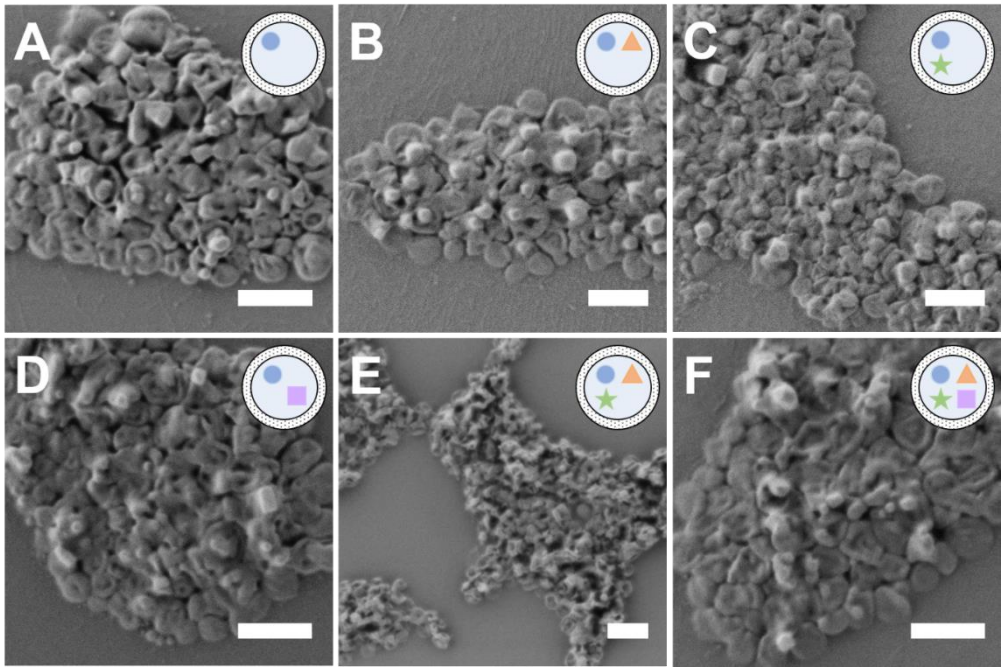

Figure 59. Scanning electron micrographs of ovalbumin nanocarriers loaded with A) Cy5-Oligo, B) Cy5-Oligo+R848, C) Cy5-Oligo+MDP, D) Cy5-Oligo+Poly(I:C), E) Cy5-Oligo+R848+MDP, F) Cy5-Oligo+R848+MDP+Poly(I:C), in cyclohexane. Scale bar: 0.5 µm.

Table 13. Analytical data of ovalbumin nanocarriers loaded with Cy5-Oligo and variations of adjuvants R848, MDP and Poly(I:C).

No.	Adjuvants	d_h (CH) / nm	PDI	d_h(H_2O) / nm	PDI	EE_{Cy5} / %	$EE_{Adj.}$ / %
1	-	333	0.12	382	0.54	76	-
2	R848	385	0.16	211	0.18	79	48
3	MDP	312	0.15	325	0.60	39	73
4	Poly(I:C)	294	0.11	95	0.41	63	12
5	R848/MDP	295	0.13	216	0.23	87	57/33
6	R848/MDP/Poly(I:C)	283	0.11	100	0.30	74	16/20/9

BMDCs treated with adjuvant-loaded OVA-NCs internalized the NCs concentration-dependent, measured by the Cy5-Oligo fluorescence in flow cytometry (Figure 60A). The measurement of MHC-II expression on the BMDCs after treatment with adjuvant-loaded OVA-NCs revealed synergistic influences (Figure 60B). The dual- and triple-loaded OVA-NCs achieved the highest MHC-II expression, already at a medium concentration of 10 µg/mL, compared to single-loaded NCs. There was no significant difference in MHC-II expression

between the dual and triple combination, as both were considerably high. Similar to untreated samples, OVA-MDP-NCs however showed no MHC-II expression, independent of NCs-concentration. Since uptake measurements revealed a high uptake of OVA-MDP-NCs and thus an effect of NCs should be possible, MDP alone did not induce antigen-presentation by MHC-II at all. In combination with R848, there seemed to be a synergistic stimulation as OVA-R848/MDP-NCs triggered higher expression of MHC-II compared to OVA-R848-NCs. The triple-loaded OVA-NCs lead to the highest CD80 expression compared to single and dual combination (Figure 60C). The synergistic effect of the triple combination was even more significant for CD86-expression. Here, the combination of R848, MDP and Poly(I:C) in the OVA-NCs lead to the highest upregulation of CD86, followed by the double combination and R848-loaded OVA-NCs as expected (Figure 60D). MDP-loaded OVA-NCs again did not induce a strong expression of marker molecules. The effect of MDP was only visible in combination with the other adjuvants, where the combination achieved a synergistic effect compared to single-loaded NCs.

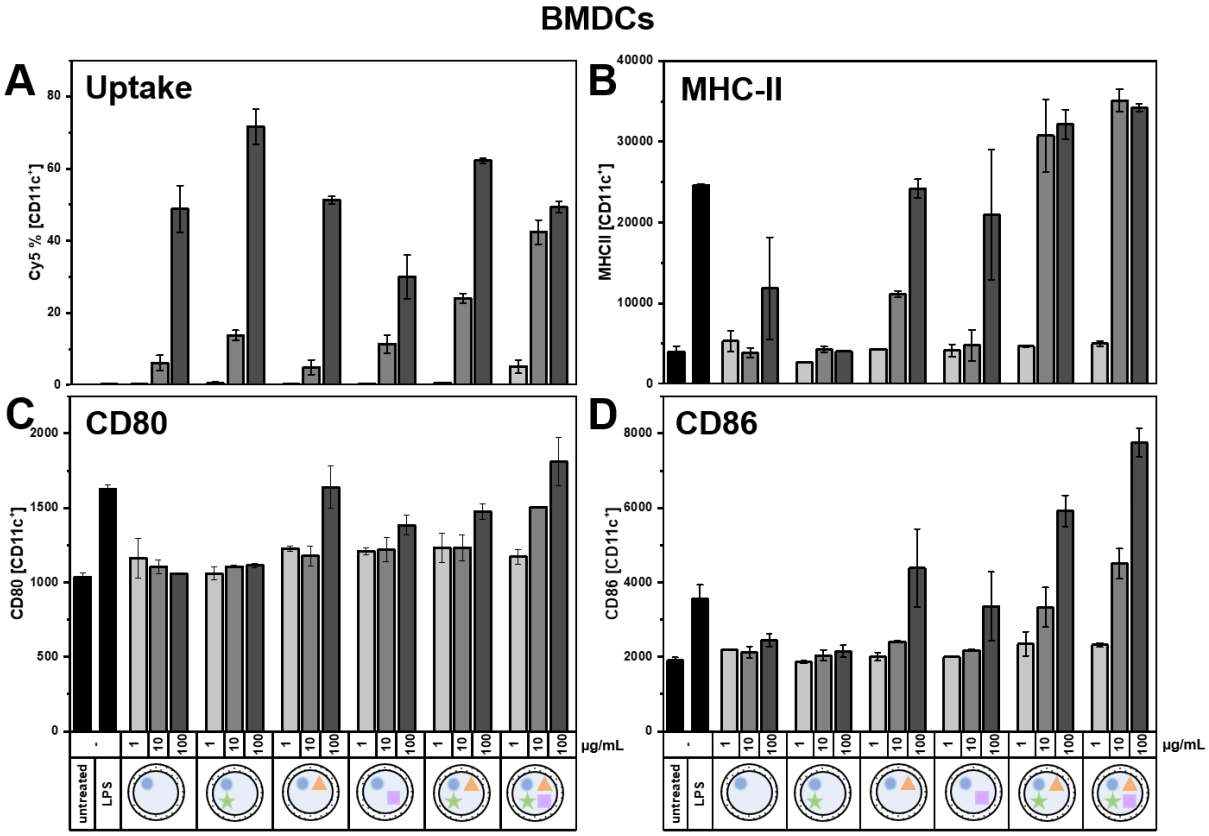

Figure 60. A) Cell binding/uptake into BMDC of Cy5-oligo-loaded ovalbumin nanocarriers (OVA-NCs) measured by flow cytometry. B-D) Upregulation of DC receptor MHC-II and maturation markers CD80 and CD86 after stimulation with OVA-NCs loaded with R848, MDP, Poly(I:C), respectively and in combinations. BMDCs (2×10^5 cells/mL) were incubated with differently loaded OVA-NCs formulations (1–100 µg/mL) or LPS (100 ng/mL) as a positive control for 24 h. Surface expression of CD80 and CD86 of NC-treated BMDCs was measured by flow cytometry. Data from [redacted].

Since a stimulation of BMDCs by OVA-NCs loaded with MDP alone was not significant and could only be seen in combination with other adjuvants, a different adjuvant was tested, that could achieve a higher stimulation alone and even higher synergistic effect in combination.

III. B2.4. R848 and DiABZI – Loaded OVA Nanocarriers

The encapsulation of adjuvants into OVA-NCs were successfully performed with R848, MDP and Poly(I:C) in single and combination. A synergistic stimulation of DCs could be achieved by combining adjuvants, which target different receptors. However, the NOD2 ligand MDP gave no significant stimulation of BMDCs alone, only in combination with R848, an effect could be observed compared to single-loaded OVA-R848-NCs. Therefore, another possibly more potent second adjuvant was chosen to achieve a higher superadditive effect on the immune stimulation. The diamidobenzimidazole compound (diABZI) is a potent non-nucleotide STING agonist, which induces interferon type 1 (IFN) expression as well as the secretion of cytotoxins IL-6 and TNF.[230, 231] In comparison to R848 and MDP, diABZI also triggers the secretion of INF cytokines, which are important for the maturation of immune cells. Therefore, an addition of diABZI to the adjuvant combination could increase the synergistic effect in DC-mediated T cell-stimulation with a tremendous potential to improve treatment of tumor cells. With the encapsulation of this compound into protein nanocarriers, further improvement on the immune activating performance of adjuvant-loaded OVA-NCs could be achieved. OVA-NCs loaded with diABZI were prepared similar to R848, as diABZI is only soluble in DMSO (Scheme 13).

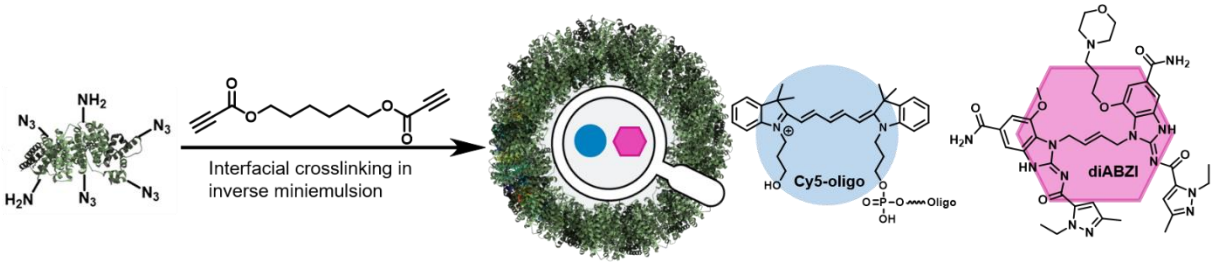

Scheme 13. Multicomponent encapsulation of Cy5-Oligo and diABZI STING agonist 3 into ovalbumin nanocarriers crosslinked with hexanediol dipropiolate in inverse miniemulsion. Protein structure was obtained from DrugBank online (https://go.drugbank.com/drugs/DB00062, 28.11.2021) and was adapted.

The STING agonist diABZI was soluble in DMSO in high concentration (100 mg/mL) and only small amounts of DMSO (16%) were needed, which should not influence the formation of protein nanocarriers in inverse miniemulsion. For optimizing the amount of diBAZI to achieve a high marker molecule upregulation and cytokine secretion, two amounts (0.8 mg and 0.08 mg)

were encapsulated into OVA-HDDP-NCs. The quantification of encapsulated diABZI into OVA-NCs could be performed with a standard calibration by fluorescence (Figure 61).

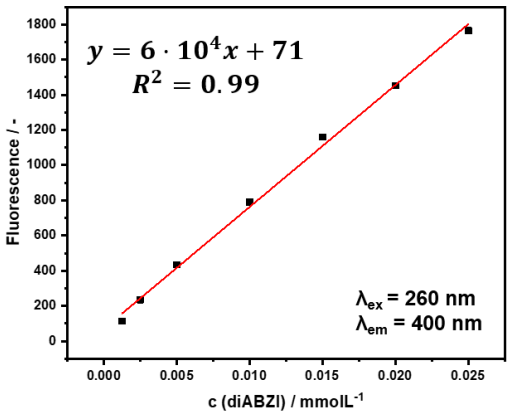

Figure 61. Standard calibration curve of diABZI in DMSO by fluorescence at 260/400 nm.

The ovalbumin solution maintained stable upon addition of diABZI, dissolved in DMSO, and stable OVA-NCs could be prepared with presence of diABZI. Scanning electron microscopy of the OVA-diABZI-NCs in cyclohexane revealed successful formation of nanocarriers with a prominent core-shell morphology (Figure 62). Compared to the NCs with less diABZI, OVA-NCs loaded with 0.8 mg diABZI showed a softer shell morphology due to the influence of more DMSO on the protein's structure. In DLS measurements in cyclohexane similar values were obtained for OVA-diABZI-NCs compared to previous OVA-R848-NCs, formed as well with DMSO (16 vol.-%) (Table 14). The hydrodynamic diameter after transfer into water was with 500-600 nm double the size and broad PDI compared to OVA-R848-NCs, indicating bigger nanocarriers or partly aggregated NCs due to change in the protein structure by DMSO. The encapsulation efficiency of Cy5-Oligo measured with fluorescence was as high as 70%. According to the quantified amount of diABZI in the NCs, over 90% diABZI was encapsulated into the OVA-NCs in both cases.

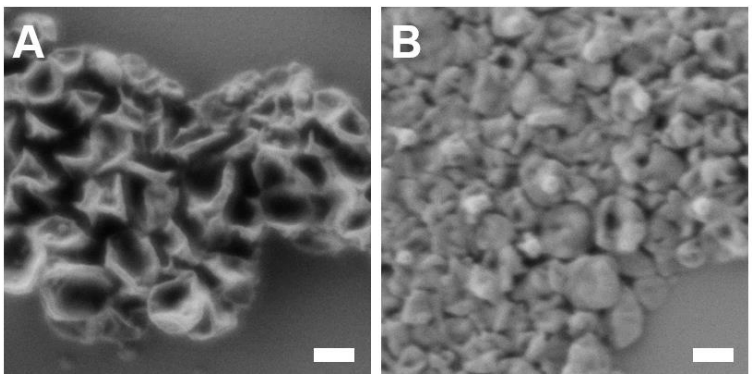

Figure 62. Scanning electron micrograph of ovalbumin nanocarriers loaded with A) Cy5-Oligo, 0.08 mg diABZI B) Cy5-Oligo, 0.8 mg diABZI; in cyclohexane. Scale bar: 0.2 µm.

Table 14. Analytical data of ovalbumin nanocarriers loaded with Cy5-Oligo and diABZI.

No.	m (diABZI)	d_h (CH) / nm	PDI	d_h(H_2O) / nm	PDI	ζ / mV	EE_{Cy5} / %	$EE_{Adj.}$ / %
1	0.08 mg	375	0.21	654	0.97	-37	73	95
2	0.8 mg	311	0.16	523	0.67	-44	74	90

In vitro experiments on BMDCs were performed with diABZI-loaded OVA-NCs. The expression of CD86 and CD80 markers in BMDCs upon treatment with OVA-diABZI-NCs showed the highest stimulation with the higher amount of encapsulated agonist, while no stimulation was observed for empty OVA-NCs (Figure 63). For lower concentration of OVA-diABZI-NCs the upregulation of CD80 and CD86 was lower compared to BMDCs treated with a solution of diABZI. It has to be noted, that the added mass was of NCs not diABZI, therefore the concentration of diABZI in OVA-NCs was significantly lower compared to solution of diABZI. The amount of diABZI in the NCs was 16 µg/mg NCs, therefore the amount of diABZI in solution was around 60 times higher than encapsulated diABZI, resulting in a lower stimulation. Therefore, the stimulation of diABZI-loaded OVA-NCs would be significantly higher than unencapsulated diABZI. The applied amount of diABZI was optimal to achieve an increased stimulation of BMDCs compared to untreated or empty OVA-NCs.

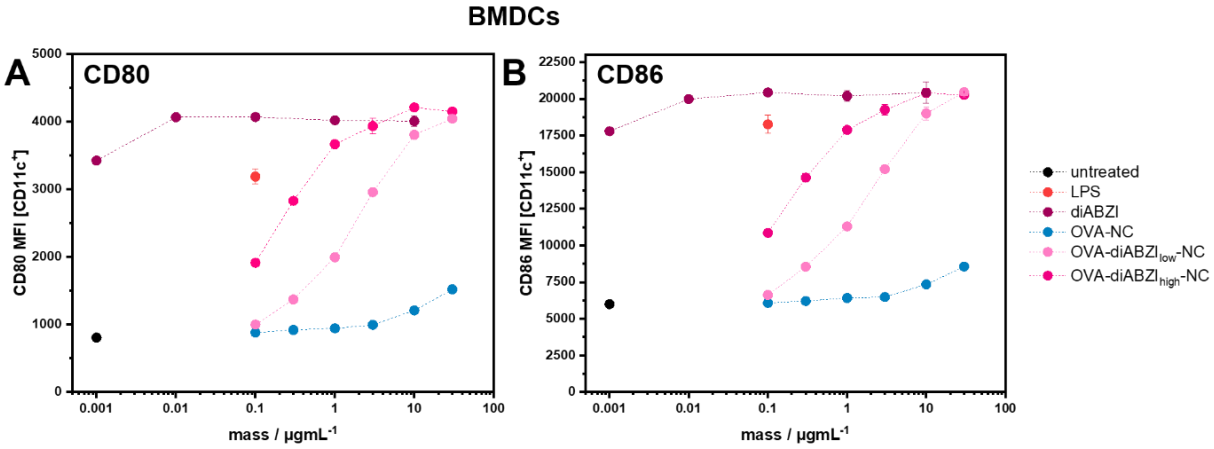

Figure 63. Expression of CD86 and CD80 markers on BMDCs (right) upon treatment with diABZI or OVA nanocarriers loaded with 0.08 mg diABZI (low) and 0.8 mg diABZI (high). LPS as control. Data from Dr. Michael Fichter.

An increased cytokine secretion was achieved for the diABZI-loaded OVA-NCs. The cytokine measurements revealed a high amount of INF α and β in the supernatant of BMDCs treated with OVA-diABZI-NCs compared to OVA-blank. High secretion of TNF-α and IL-6 was

observed as well, even concentration-dependent and significantly higher than soluble diABZI (Figure 64).

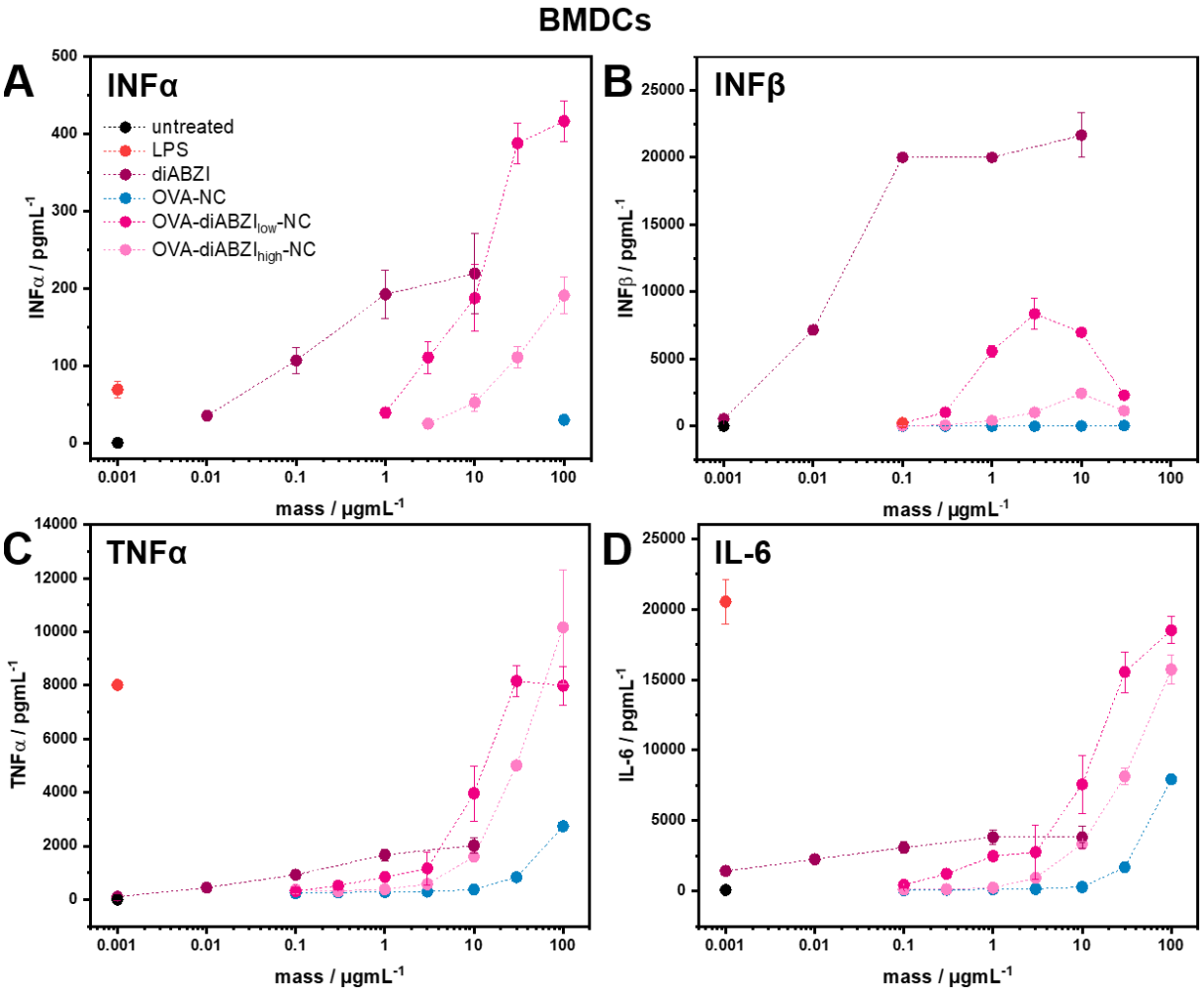

Figure 64. Expression of cytokines in BMDCs upon treatment with diABZI or OVA nanocarriers loaded with 0.08 mg diABZI (low) and 0.8 mg diABZI (high). LPS as control. Data from [redacted].

An increased immune response could be obtained in BMDCs treated with OVA-diABZI-NCs, leading to higher expression of marker molecules CD80 and CD86 and high secretion of pro-inflammatory cytokines. In comparison to MDP, diABZI alone could achieve a significant stimulation of BMDCs. Additionally, diABZI-loaded NCs triggered the secretion of INF cytokines, which are not induced by adjuvants R848 or MDP. Therefore, a combination of TLR7/8 ligand R848 with STING-agonist diABZI could give an improved adjuvant combination, resulting in a high superadditive effect in DC-mediated T cell stimulation. As a possible third component Poly(I:C) proved to effectively stimulate BMDCs for higher marker upregulation. However, Poly(I:C) as a double-strand RNA mimic is a high molecular weight molecule and its release into the cell is dependent on the degradability of the nanocarrier. As discussed in chapter A, the degradability of protein nanocarriers crosslinked by azide-alkyne

click chemistry was also influenced by the crosslinking degree. Therefore, the influence of the crosslinking degree of PNCs on the stimulative property of adjuvant-loaded OVA-NCs was investigated.

III. B2.5. Influence of Crosslinking Degree of OVA-NCs on DC Stimulation

The crosslinking degree influences the degradation of the protein nanocarriers. With lower crosslinking degree, the crosslinked protein shell is higher hydrated and is more accessible to proteases and is degraded faster. A higher degradation rate would lead to more effective release, especially of large cargo molecules such as double-strand RNA mimic Poly(I:C). With a faster and complete degradation of nanocarriers a higher stimulation of dendritic cells by adjuvants could be achieved and a high synergistic effect could be obtained by more simultaneous release of low and high molecular weight adjuvants. OVA-NCs were crosslinked with either 20 eq. or 2 eq. dialkyne crosslinker HDDP in the interfacial azide-alkyne crosslinking. During the formation of OVA-NCs low (R848), medium (R848-PEG-10kDa) and high molecular weight (Poly(I:C)) adjuvants were encapsulated, respectively and in combination, to study the effect of the crosslinking degree on intercellular degradation, measured by the resulting stimulation of BMDCs.

The DLS of OVA-NCs crosslinked with different amount of HDDP showed no significant difference in hydrodynamic diameter, measured in cyclohexane (Figure 65A, Table 15). After transfer into water the NCs crosslinked with 2 eq. HDDP revealed a decreased size to under 100 nm and broadening of size distribution, indicating protein parts that were not sufficiently crosslinked and disassembled after transfer into water. The decreased size in water was observed for all OVA-NCs independent of loading. The lower degree of crosslinking was also demonstrated in SEM as rather soft nanocarriers with thin shells were obtained for NCs crosslinked with 2 eq. HDDP (Figure 65B). Increasing the amount of crosslinker by 10-fold led to OVA-NCs with a more prominent shell, resulting in minimal change in NCs size after the transfer in water due to sufficient crosslinking (Figure 65A+C).

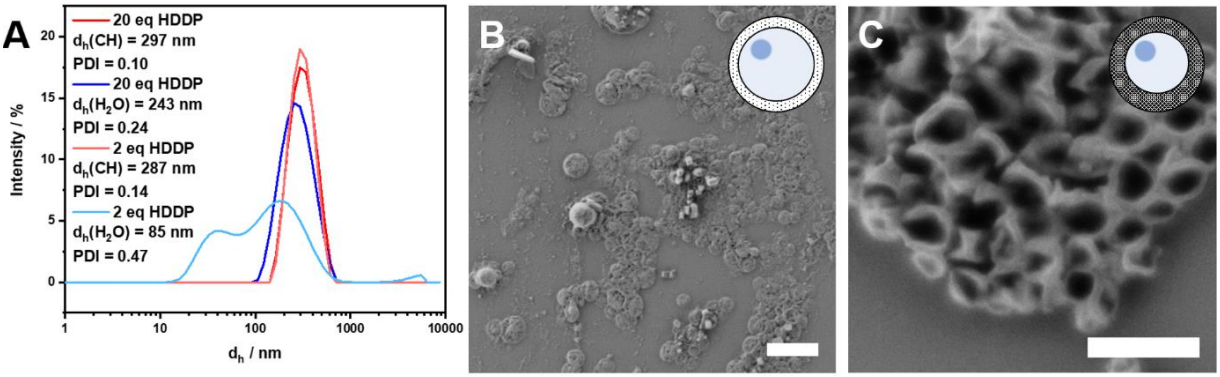

Figure 65. A) DLS of ovalbumin nanocarriers crosslinked with 2 eq. or 20 eq. of HDDP in cyclohexane (red) and water (blue); scanning electron micrograph of OVA-NCs crosslinked with A) 20 eq. HDDP and B) 2 eq. HDDP in cyclohexane.

The encapsulation efficiencies of Cy5-Oligo were double as high for OVA-NCs crosslinked with 20 eq. HDDP compared to 2 eq. HDDP (Table 15). The crosslinking degree influenced the encapsulation efficiency of the adjuvants as well, where in most cases lower EEs were obtained for OVA-NCs crosslinked with 2 eq. HDDP. Especially the EE of hydrophilic small molecule MDP decreased significantly with reduced amount of crosslinker due to a more permeable shell and thus higher diffusion of MDP out of the OVA-NCs in water.

Table 15. Analytical data of ovalbumin nanocarriers loaded with Cy5-oligo and adjuvants R848, R848-PEG-1 kDa and a combination of R848+MDP+Poly(I:C) crosslinked with 2 eq. or 20 eq. of HDDP.

No.	eq. HDDP	Adjuvants	d_h (CH) / nm	PDI	d_h(H_2O) / nm	PDI	EE_{Cy5} / %	EE_{Adj} / %
1	2	-	316	0.14	91	0.44	21	-
2	2	R848	297	0.11	89	0.50	17	34
3	2	R848-PEG-1kDa	277	0.12	100	0.54	20	3
4	2	R848/MDP/Poly(I:C)	287	0.13	85	0.47	19	34/9/11
5	20	-	303	0.09	340	0.23	46	-
6	20	R848	301	0.10	203	0.31	45	19
7	20	R848-PEG-1kDa	305	0.14	251	0.28	40	39
8	20	R848/MDP/Poly(I:C)	297	0.10	243	0.24	45	16/20/9

To investigate the influence of crosslinking degree and release rate of adjuvants from OVA-NCs on the immune stimulation, BMDCs were treated with adjuvant-loaded OVA-NCs crosslinked with either 2 eq. or 20 eq. HDDP. All NCs were internalized successfully by

BMDCs, demonstrated by the prominent Cy5 fluorescence in the cells (Figure 66A). The OVA-NCs induced a high expression of MHC-II receptors independent from crosslinking degree and loading (Figure 66B). The expression of CD80 and CD86 marker revealed that OVA-NCs loaded with R848, MDP and Poly(I:C) lead to a stronger stimulation compared to single-loaded NCs (Figure 66C+D). Additionally, OVA-NCs crosslinked with 2 eq. HDDP demonstrated a higher stimulation compared to 20 eq. crosslinker, which was especially significant for the OVA-R848-PEG 10kDa-NCs and triple-loaded OVA-NCs, where a higher expression was already achieved with a lower concentration of NCs (10 µg/mL).

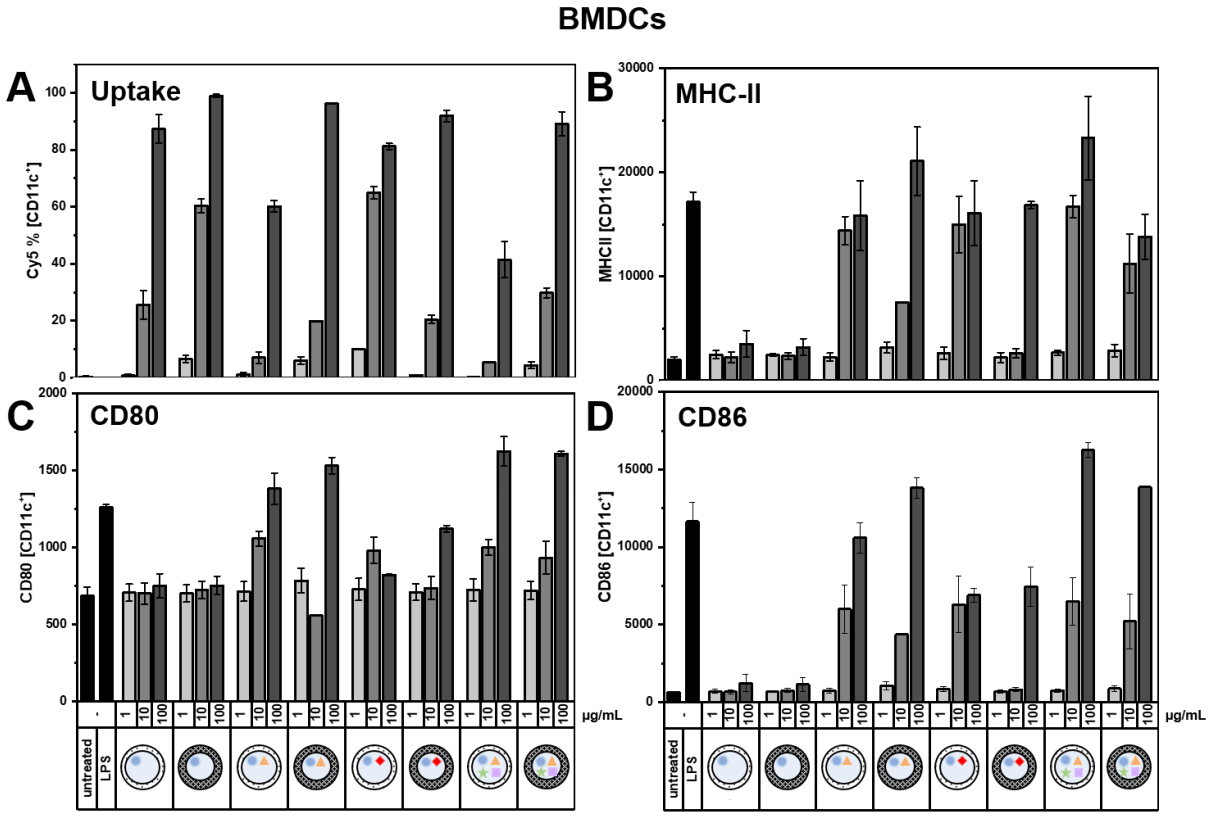

Figure 66. A) Cell binding/uptake into BMDC of Cy5-oligo-loaded ovalbumin nanocarriers (OVA-NCs) measured by flow cytometry. B-D) Upregulation of DC receptor MHC-II and maturation markers CD80 and CD86 after stimulation with adjuvant-loaded OVA-NCs crosslinked with either 2 or 20 eq. HDDP. BMDCs (2×10^5 cells/mL) were incubated with differently loaded OVA-NCs formulations (1–100 µg/mL) or LPS (100 ng/mL) as a positive control for 24 h. Surface expression of CD80 and CD86 of NCs-treated BMDCs was measured by flow cytometry. Data from [redacted].

The higher marker expression for OVA-NCs crosslinked with lower amount of HDDP indicated a faster and higher enzymatic degradation of OVA-NCs in the BMDCs. A faster and higher degree of degradation allowed a more simultaneous release of all adjuvants, promoting a synergistic stimulation of BMDCs.

III. B4. *In Vivo* Tumor Treatment with Adjuvant-Loaded OVA-NCs

The DC-mediated T cell stimulation is an important pathway to treat tumor cells.[232] For a successful activation of the immune cells against tumor cells three processes have to occur. For one, the DCs presents the tumor-specific antigen on the MHC receptor to the T cells for recognition. Second, the adjuvants trigger an antigen-independent expression of costimulatory marker molecules such as CD80 and CD86 that are recognized by CD28 and CTLA-4 receptors of the T cell. Lastly, the adjuvants induce the secretion of cytokines from the DCs that enhance the stimulation of T cells. If all three processes proceed successfully, the T cells are activated against antigen-specific tumor cells and proliferate to attack. To enhance the vaccination effect, the vaccine components antigen and adjuvants were formulated into adjuvant-loaded OVA-NCs, which enables a simultaneous delivery of antigen and multiple adjuvants to DCs. In *in vitro* experiments with BMDCs as well as splenocytes, adjuvant-loaded OVA-NCs demonstrated high immune stimulating properties, expressed in the upregulation of MHC-II, CD80 and CD86 receptors as well as secretion of cytokines. A combination of R848 and MDP loaded into OVA-NCs obtained high stimulation of DCs through a synergistic effect of the TLR7/8 and NOD2 ligand. The stimulation of DCs and antigen-presentation by adjuvant-loaded OVA-NCs resulted in activation and proliferation of OT-I and OT-II T cells, indicating a high immune stimulating property of the developed nanovaccine. The vaccination ability of dual-loaded OVA-NCs with a combination of R848 and MDP was investigated in an *in vivo* model with tumor-bearing mice. A high immune stimulating property of the adjuvant-loaded OVA-NCs should lead to a DC-mediated T cell stimulation and attack of the tumor cells. For the *in vivo* setup, mice were inoculated with OVA-specific B16 melanoma cells (B16/OVA-Luc cells) in the right flank to promote tumor growth (Figure 64). When the tumor reached a significant size of 25-50 mm^3, the mice were treated every seven days with different vaccine formulations, including the adjuvant-loaded OVA-NCs. The tumor growth and probability of survival gave an indication over the effectivity of the tumor treatment with the different vaccine formulations. Mice with a tumor size over 800 mm^3 were eliminated from the test. If the vaccine treatment is successful and T cells are sufficiently activated to recognize ovalbumin as the antigen on the melanoma cells, the tumor cells should be attacked resulting in decrease of tumor size and higher probability of survival of the mice.

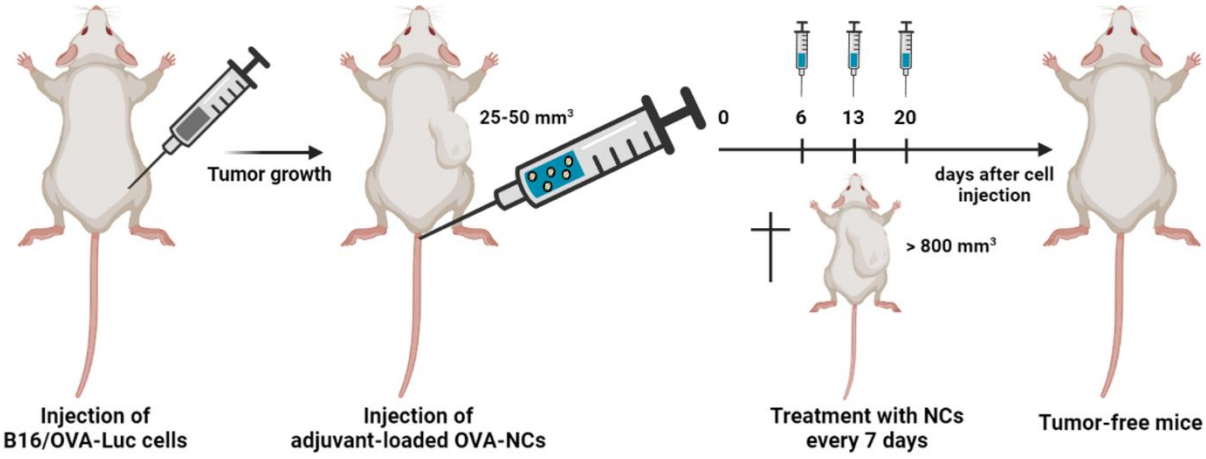

Figure 67. *In vivo* tumor treatment of tumor-bearing mice with adjuvant-loaded ovalbumin nanocarriers. Figure created with BioRender.com by Natkritta Hüppe.

OVA-NCs containing R848 and MDP, respectively and in combination, were prepared following the developed procedure in inverse miniemulsion. Empty OVA-NCs was prepared as a control sample. The scanning electron micrographs of the OVA-NCs in cyclohexane revealed successful preparation of NCs with a prominent core-shell morphology (Figure 68). The sizes of the nanocarriers measured by DLS gave a size of around 300 nm in cyclohexane (Table 16). After transfer into water, the OVA-NCs remained in size, besides the ones loaded with R848, where DMSO in the disperse phase, influenced the protein structure during the shell formation leading to a decreased size of R848-containing OVA-NCs. The encapsulation efficiency of R848 as well as MDP did not change in the single- or dual-loaded OVA-NCs.

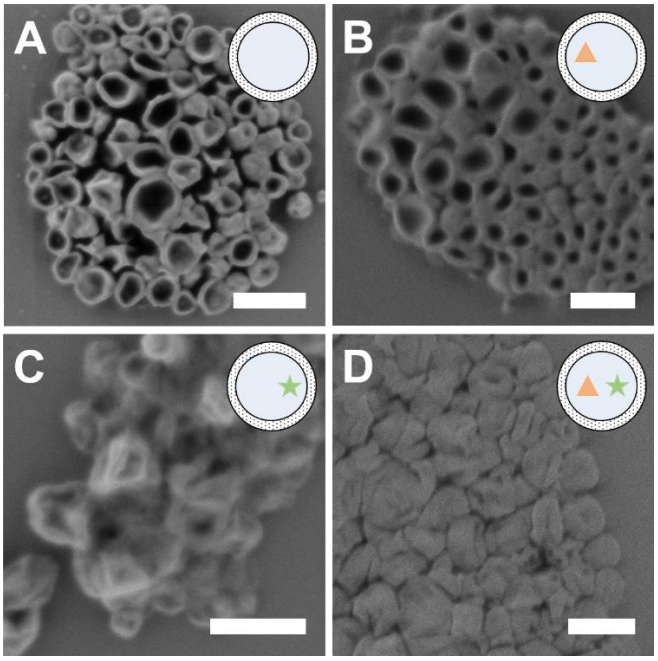

Figure 68. Scanning electron micrographs of ovalbumin nanocarriers loaded with A) no cargo, B) R848, C) MDP and D) R848+MDP; in cyclohexane. Scale bar: 0.2 µm.

Table 16. Analytical data of ovalbumin nanocarriers loaded with adjuvants R848 and MDP, respectively and in combination.

No.	Adjuvants	d_h (CH) / nm	PDI	$d_h(H_2O)$ / nm	PDI	EE_{R848} / %	EE_{MDP} / %
1	-	332	0.14	382	0.54	-	-
2	R848	385	0.16	211	0.18	61	-
3	MDP	312	0.15	325	0.60	-	55
5	R848/MDP	295	0.13	216	0.23	61	42

Tumor-bearing mice were treated with adjuvant-loaded OVA-NCs with R848 and MDP, respectively and in combination. As a comparison, OVA-NCs and OVA solutions containing unencapsulated adjuvants were applied as vaccine formulations as well. PBS, OVA and OVA-NCs without adjuvants acted as control samples. The measurement of tumor size after the inoculation of B16/OVA-Luc cells revealed a decreased tumor growth for the vaccine formulation with a combination of R848 and MDP (Figure 69).

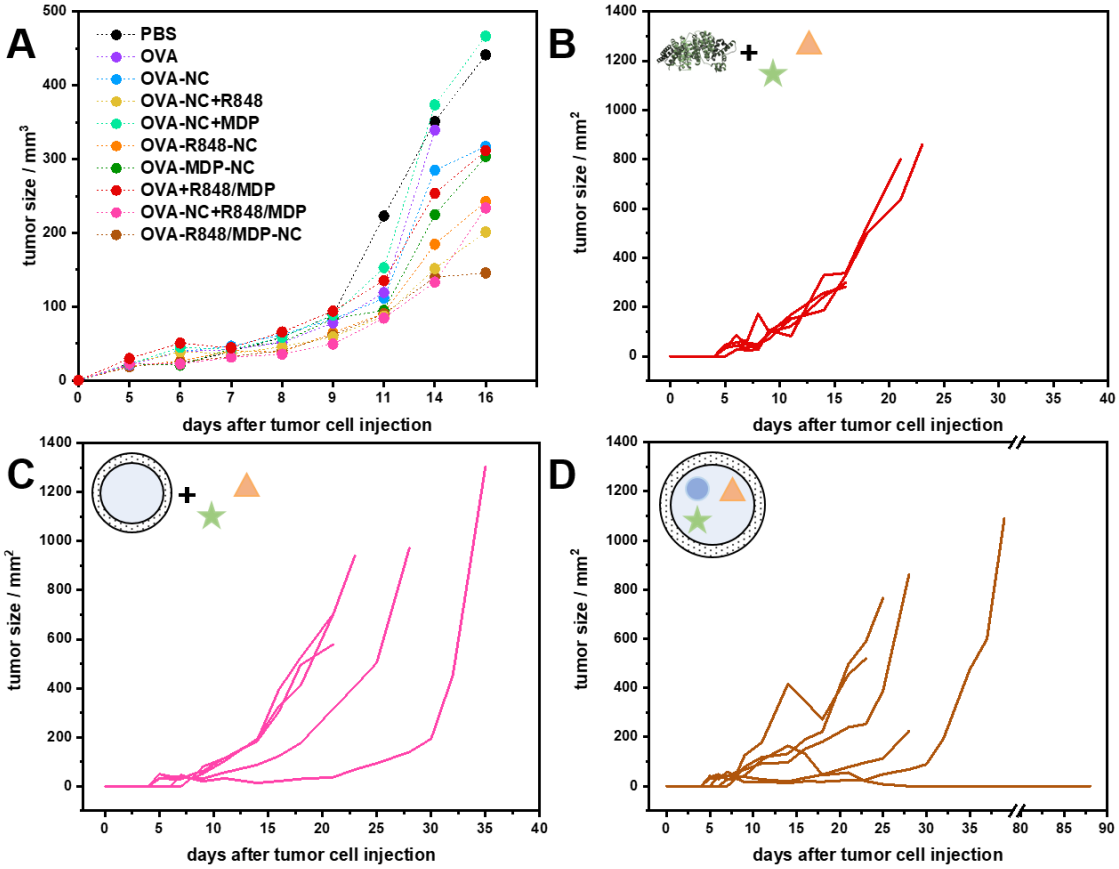

Figure 69. Tumor growth on mice treated with different formulations of antigen ovalbumin and adjuvants R848 and MDP as solutions or nanocarriers. Protein structure was obtained from DrugBank online (https://go.drugbank.com/drugs/DB00062, 28.11.2021) and was adapted. Data from [redacted].

The treatment efficacy of single-loaded OVA-NCs with MDP was comparable to a soluble formulation with OVA, R848 and MDP, demonstrating that already one adjuvant encapsulated into nanocarriers stimulated the immune more efficiently. Moreover, low synergistic effect of R848 and MDP was obtained when administered in soluble form and the tumor growth consistently with the soluble formulation. OVA-NCs with unencapsulated MDP did not achieve a tumor reduction at all and the tumor growth was comparable to mice treated with PBS. Mice treated with the PBS control had a probability of survival until day 19 and for OVA-NCs+MDP until day 21 where even the third treatment on day 20 had already no effect on the survival anymore (Figure 70). The treatment efficacy of OVA-R848-NCs was similar to OVA-NCs with unencapsulated R848 and MDP, underlining the necessity of encapsulation to achieve high concentrations of adjuvants for high stimulation and a synergistic effect. Nevertheless, the OVA-NCs with unencapsulated R848 and MDP delayed a significant tumor growth for over 30 days. In one mouse, tumor growth increased significantly when the treatment was stopped after the third injection on day 20, indicating a sufficient immune stimulation during treatment but no long lasting effect. The dual-loaded OVA-NCs achieved the highest effect on immune cell stimulation indicated by the slowest tumor growth. Especially compared to the soluble formulation of OVA+R848/MDP, an encapsulation of adjuvants into nanocarriers decreased the tumor size by half at 16 days after tumor cell injection. Moreover, during the treatment minimal tumor growth was observed for 50% of mice treated with OVA-R848/MDP-NCs and the mice survived up to 30 days. One mouse treated with the dual-loaded OVA-NCs did not grow a significant tumor and stayed tumor-free even after the last NCs injection on day 20, resulting in a long survival of the mouse through the complete test phase of 90 days.

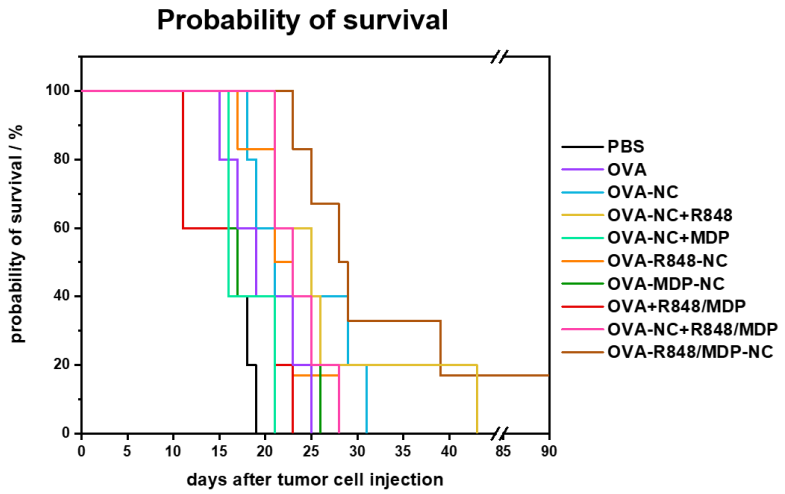

Figure 70. Probability of survival of mice injected with tumor cells and treated with different formulations of antigen ovalbumin and adjuvants R848 and MDP as solutions or nanocarriers. Data by [redacted].

The high treatment efficacy of the nanocarriers formulation compared to the soluble formation underlined the superiority of adjuvant encapsulation, where the adjuvants are delivered simultaneously and create a higher synergistic effect. Even a formulation of the antigen ovalbumin as a nanocarrier resulted in a higher immune stimulation and slowed tumor growth, demonstrating that the delivery of antigen in high concentrations as a nanocarrier had a significant effect on the immune response compared to soluble ovalbumin. The tumor treatment with adjuvant-loaded OVA-NCs with a combination of R848 and MDP proved to be successful and a high positive effect on the tumor growth and probability of survival was observed. Even if MDP alone had no strong immune stimulating properties as shown in the *in vitro* and confirmed by weak effect *in vivo*, a combination of R848 and MDP with encapsulation into OVA-NCs achieved the desired high immune stimulating properties and tumor treatment efficacy due to synergistic effect. As already demonstrated in the *in vitro* experiments, an exchange of MDP with the more potent STING agonist diABZI could create an even stronger immune stimulation by dual-loaded OVA-NCs in combination with R848. Next, OVA-NCs loaded with R848 and diABZI should be tested for their tumor treatment efficacy in mouse models.

III. B5. Conclusion

Nanocarriers composed of the antigen ovalbumin were successfully prepared using the interfacial azide-alkyne crosslinking in inverse miniemulsion and multiple cargo molecules were efficiently encapsulated. Adjuvant-loaded OVA-NCs with a combination of R848 and MDP resulted in a successful DC-directed T cell stimulation by a synergistic effect of the TLR7/8 and NOD 2 ligand. The induction of a high DC stimulation by dual-loaded OVA-NCs lead to activation and proliferation of OT-I and OT-II T cells in BMDC-directed proliferation. The dual-loaded OVA-NCs with R848 and MDP were applied in *in vivo* mouse models with a melanoma tumor. The tumor growth of mice treated with different formulations revealed the highest treatment efficacy for adjuvants encapsulated into OVA-NCs. The nanocarriers formulations demonstrated superior immune stimulation compared to soluble formulations due to simultaneous delivery of the vaccine components to immune cells. The higher concentration of internalized vaccine components into DCs resulted in a higher immune response thus higher decrease of tumor cells and higher survival of mice. In conclusion, adjuvant-loaded OVA-NCs proved to have high potential as nanovaccines for the treatment of tumors.

The combination of three adjuvants (R848, MDP and Poly(I:C)) achieved an even higher stimulation of DCs *in vitro* compared to the dual-loaded NCs. OVA-diABZI-NCs showed higher stimulation properties than MDP. Further optimization of adjuvant-loaded OVA-NCs could achieve even higher anti-tumor effect, increasing their potential as nanovaccines in immunotherapy.

Chapter C – Protein Nanocarriers *via* Interfacial Denaturation

Chapter C is part of the manuscript:

N. Hüppe, [redacted], *manuscript in preparation*. For the thesis, this chapter was extented with preliminary results, additional experiments, optimizations and details.

Contributions:

Natkritta Hüppe synthesized and characterized the protein nanocarriers as stated in the experimental part. Natkritta Hüppe performed the NanoDSF and DLS measurements as well as sample the preparation for SEM. She also performed the degradation and release experiments of the protein nanocarriers.

Abstract

Denaturation of proteins were applied for the preparation of protein nanocarriers (PNCs) without use of chemical reactions. Established methods such as desolvation lack high control and efficiency to encapsulate cargo molecules. Inverse W/O miniemulsion allows the entrapment of multiple cargo molecules in the water droplet upon shell formation. Thermal denaturation of protein at the water droplet interface resulted in formation of protein nanocarriers and encapsulation of dye. A decreased melting temperature (T_m) at the W/O interface lead to formation of a protein nanocapsules instead of nanoparticles. The type of protein and solvent influenced the thermal denaturation process and ovalbumin in a water-in-cyclohexane was revealed to efficiently form PNCs. A two-step heating profile with heating first $T > T_m$ (80 °C) then $T<T_m$ (40 °C) leads to a stable protein shell even after transfer to water and high encapsulation efficiencies (EE > 80%) could be obtained. Often the formed protein shell was susceptible to the ultrasonication in the water transfer step. With formation of PNCs by thermal denaturation in a double W/O/W emulsion the redispersion step could be left out and transfer of PNCs into water was performed by solvent evaporation after thermal denaturation. Dependent on the surfactant and emulsification technique, stable PNCs with EE > 90% could be achieved in double emulsion. As demonstrated, the crosslinker type and crosslinking degree influences the degradation of PNCs. Unselective crosslinking with highly reactive 1,4-toluene diisocyanate lead to formation of unwanted polyurea in the nanocarrier shell, decreasing the enzymatic degradability and release. In comparison, PNCs from thermal denaturation demonstrated high enzymatic degradability and dye release, similar to PNCs crosslinked with hexanediol dipropiolate in a bioorthogonal azide-alkyne click reaction. Interfacial denaturation of proteins in inverse miniemulsion showed high potential for multicomponent encapsulation into PNCs with high control and efficiency without using chemical reactants.

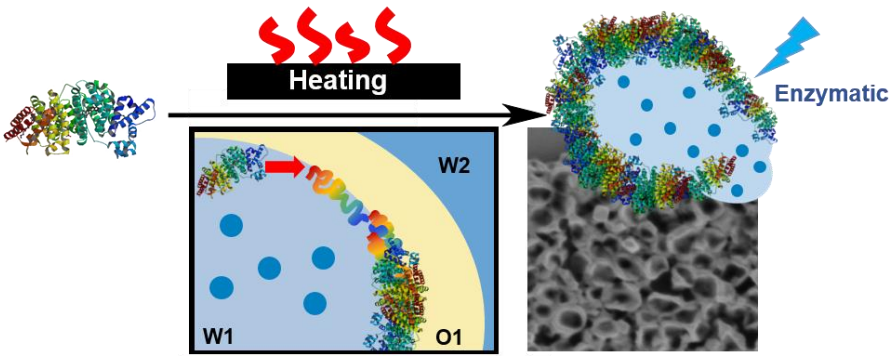

Figure 71. Biodegradable protein nanocarriers prepared *via* interfacial denaturation by heating in a W/O/W double emulsion. Image created by Natkritta Hüppe.

III. C1. Introduction

Medical regulations expect quality products with high biocompatibility, definition and reproducibility before approval. Only a few nanocarrier-based drug formulations were approved by the Food and Drug Administration (FDA), including Abraxane®, a protein-based drug conjugate.[233] To the motto "less is more", nanocarrier design should focus on basic principles to achieve quality products instead of designing more and more complex synthetic systems. The major challenge is to prepare nanocarriers without synthetic materials, without modification of materials, in principle without chemical reactions at all, but still maintain high definition and reproducibility of the product. In food industry, the regulations for products are very strict as well and only few substances are allowed for food applications. For example, proteins are biocompatible, degradable and come from a broad range of sources, making them abundant and cost-effective materials. Nanocarriers based on proteins have proven to be efficient biocompatible delivery systems for food actives and are successfully applied in food applications.[65, 234] Broad commercial use of protein nanocarriers (PNCs) in medical applications is yet to achieve as medical regulations require even higher precision in size and size distribution for nanocarriers. Additionally, encapsulation of cargo molecules should proceed with high control and efficiency. Over the past years, various strategies for the preparation of PNCs were developed for medical applications.[16, 17, 37] A majority of the methods are based on precipitation or denaturation of proteins under certain chemical (e.g. anti-solvent) or physical (e.g. heat or pressure) changes.[19, 235, 236] One of the main methods to form protein nanocarriers is a desolvation or coacervation method, at which upon change in solvent, pH or ionic strength the reduction of solubility leads to a protein aggregation. Other techniques to induce protein particle formation are thermal denaturation/gelation or self-assembly upon addition of hydrophobic compounds.[24, 237] Although those established methods have demonstrate successful formation of PNCs, methods based on coacervation lack high reproducibility due to difficult control over size and lack high encapsulation efficiencies (EEs) due to passive entrapment.[19, 236, 238] Furthermore, they still require crosslinking of the nanocarriers to achieve high stability and entrapment efficiency, e.g. with glutaraldehyde[13] or genipin (more biocompatible), which are not bioorthogonal.[239, 240] Therefore, preparation of PNCs without the use of chemical reactions have to be optimized, if they were to be used in medical applications and fulfil demanding medical regulations.

Emulsions as an active encapsulation strategy offer higher control over the encapsulation process compared to passive entrapment in coacervation or self-assembly approaches.[49] Protein

nanocarriers were successfully prepared through interfacial crosslinking in inverse miniemulsions and cargo molecules (even multiple) could be encapsulated with high efficiency, as demonstrated by Piradashvili *et al.* or previously in chapter A.[71, 82, 84] Although chosen chemistries were bioorthogonal and the cargo's activity could be maintained, bioorthogonal reactions always require the modification of the material with the respective reacting groups. Proteins are prone to any structural changes, leading to instability. Even with a mild and minimal modification reaction such as the azide transfer by 1-imidazolsulfuryl azide hydrochloride, several optimization steps had to be done to maintain the water-solubility of sensitive proteins. The questions are whether an interfacial crosslinking is necessary to form a protein shell or if an interfacial denaturation for example with temperature is sufficient to induce a protein shell formation in inverse miniemulsion. The combination of an emulsion-based strategy with physical nanocarrier preparation by denaturation has high potential to prepare fully biocompatible and biodegradable protein nanocarriers without the use of chemical reagents and modifications, while achieving high control over the encapsulation process. Therefore, the preparation of protein nanocarriers formed through an interfacial denaturation *via* heating in inverse miniemulsion was studied to design a reaction-free approach (Scheme 14).

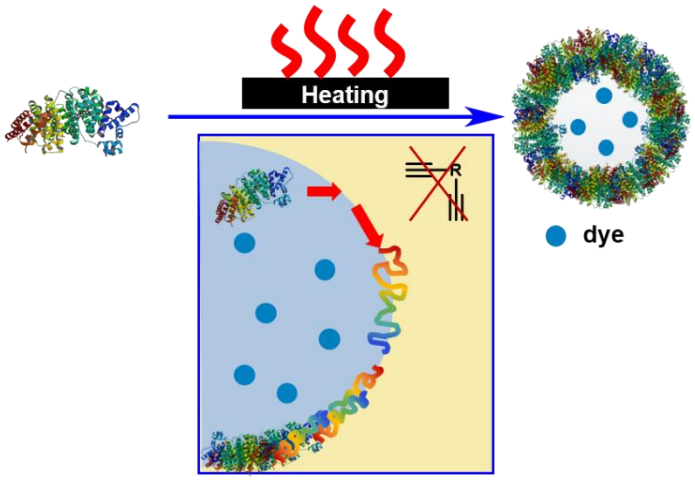

Scheme 14. Preparation of protein nanocarriers *via* interfacial thermal protein denaturation at the nanodroplet interface of an inverse miniemulsion. Image created by Natkritta Hüppe.

III. C2. Interfacial Denaturation in W/O Inverse Miniemulsion

Protein nanocarriers were prepared through an interfacial denaturation of the proteins upon heating. The organic solvent used as the continuous phase for the formation of W/O miniemulsions mediates the interfacial behavior of proteins. There is a broad range of proteins with different denaturation temperatures that influence their interfacial denaturation. Therefore, both factors, solvent and denaturation temperature, were studied in the formation of a protein shell by interfacial denaturation.

III. C2.1. Proteins with Different Melting Temperatures

Denaturation describes the process when non-covalent bonds (e.g. hydrogen bonds) of protein structures break under the influence of a stimuli (e.g. temperature, pH, ionic strength).[241] These non-covalent bonds are responsible for the ordered protein folding and upon unfolding the protein chains change, leading to decreased solubility and aggregation. However, proteins are partly unfolded and partly maintain their native structure, which can lead to a refolding process when the denaturing stimuli ceased. Most proteins, such as ovalbumin, demonstrated reversible denaturation or so-called renaturation and only denature irreversibly under drastic conformational changes at extreme conditions like frying an egg at high temperatures.[227, 242] The unfolding of proteins is described with the melting temperature (T_m).[243] At the melting temperature, half of the protein is unfolded (i.e. denatured), which can be measured by label-free nano differential scanning fluorimetry (NanoDSF). In NanoDSF, the protein solution is heated and upon unfolding of the protein-chain, the fluorescent aromatic side-chains of tryptophan and tyrosine are exposed to the solvent. The fluorescence of the exposed aromatic moieties change and can be correlated to the rate of unfolding, where the melting temperature is expressed in the maxima. The interfacial denaturation was studied in an inverse miniemulsion of water as dispersed phase and cyclohexane as continuous phase. Proteins with different melting temperatures, ranging from hemoglobin (46 °C), ovalbumin (77 °C) to casein (>100 °C) (measured by NanoDSF), were studied, if they could be used to generate protein nanocarriers in inverse miniemulsion (Table 17). Proteins possess hydrophilic and hydrophobic domains and can denature in the presence of organic solvents.[244, 245] Since the protein nanocarriers were prepared in an inverse miniemulsion, the unfolding of the proteins was measured in a water-in-cyclohexane miniemulsion. In most cases, the determined T_m were lower in the emulsion compared to pure water, for example, the T_m of ovalbumin in the emulsion was determined to be 69 °C compared to T_m = 77 °C in water (Table 17).

Table 17. Analytical data of protein nanocarriers from proteins with different melting temperatures. Melting temperatures measured by NanoDSF. Size, size distributions and DCR measured by dynamic light scattering. Encapsulation efficiency measured by fluorescence of dextran-rhodamine B (570/590 nm).

Protein	$T_{m,H2O}$ / °C	$T_{m,emul}$ / °C	T /°C	$d_{h,reac}$ / nm	PDI	$d_{h,CH}$ / nm	PDI	$d_{h,H2O}$ / nm	PDI	DCR	EE / %
Hemo-globin	46	49	40	143	0.23	328	0.08	101	0.43	234	-
			80	139	0.20	380	0.25	304	0.21	9435	5
Oval-bumin	77	69	40	120	0.18	257	0.17	467	0.73	663	17
			80	425	0.85	596	0.35	349	0.34	1241	56
Casein	>100*	56	40	116	0.22	301	0.11	133	0.41	330	-
			80	108	0.22	261	0.07	106	0.28	256	34

T_m: melting temperature in H_2O or inverse miniemulsion (emul); d_h: hydrodynamic radius; $d_{h,reac}$: hydrodynamic size of miniemulsion dispersion droplets after heating and before purification, measured by DLS at 173°; CH: cyclohexane; PDI: polydispersity index, DCR: derived count rate, EE: encapsulation efficiency. *NanoDSF measured from 25-100 °C

To observe the nanocarriers after interfacial denaturation by heating, an inverse miniemulsion was prepared and heated to 40 °C (formation temperature under T_m) and above T_m at 80 °C for 24 h. When hemoglobin was used as a shell material at 40 °C protein nanocarriers with a core-shell morphology were obtained as visualized in SEM (Figure 72), however the shell thickness seemed to be thin and cracks were observed. At 80 °C, well above the T_m, particle-like PNCs were obtained. Dynamic light scattering (DLS) of the dispersion in cyclohexane indicated diameters of 328 and 380 nm, respectively (Table 17). However, for hemoglobin nanocarriers prepared below T_m, transfer into water resulted in a very low scattering intensity in DLS measurements, indicating disassembly of the protein particles. The hemoglobin particles prepared at 80 °C remained insoluble, indicating formation of stable PNCs. However, when dextran-rhodamine B as a dye was dissolved within the disperse phase, no or very low amount of dye was detected in the PNCs for both temperatures. In case of ovalbumin (OVA) with a higher T_m of 69 °C, similar observations were made. While at 40 °C ovalbumin formed PNCs with a prominent core-shell morphology, at 80 °C particle-like structures were obtained. Similar to hemoglobin, PNCs, formed under T_m, partly disassembled resulting in a lower EE of 17% compared to 56% at 80 °C. The melting temperature of high temperature stable protein casein with T_m = 280 °C decreased significantly to 56 °C in inverse miniemulsion. At both heating temperatures, below and above T_m, casein showed particle rather than capsule morphologies. Moreover, after transfer into water the casein NCs almost completely dissolved, expressed in the low derived count rate (DCR) for both cases. Nevertheless at 80 °C, 34% dye could be

encapsulated into casein NCs of small sizes in water ($d_{h,water}$ = 106 nm). Disassembly of PNCs, prepared under T_m, could be expected after transfer into water as only a small fraction of protein chains unfolded and refolding of the protein chains could have occurred as soon as the denaturing stimuli (temperature and organic solvent) were removed. Heating of the proteins in inverse miniemulsion however lead to higher denaturation degree of the protein chains and formation of stable aggregates.

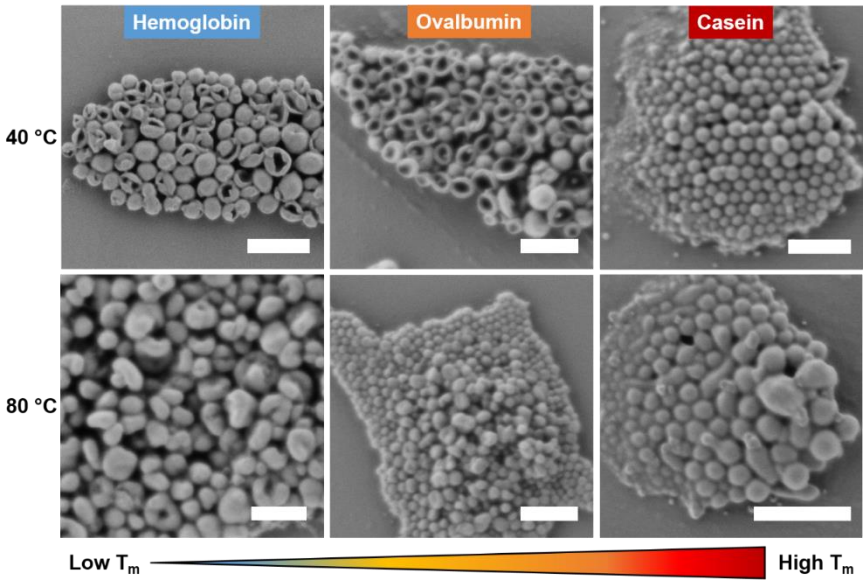

Figure 72. Scanning electron micrographs of protein nanocarriers of proteins hemoglobin, ovalbumin and casein with different melting temperatures formed through interfacial denaturation at 40 °C ($T < T_m$) or 80 °C. Scale bar: 0.5 µm.

The investigation of different proteins for the formation of PNCs through interfacial denaturation revealed OVA to be the most promising to form nanocapsules and entrap cargo. In the next section, the influence of the organic solvent on the protein denaturation and protein shell formation was investigated with cyclohexane and toluene.

III. C2.2. Different Organic Solvent for Inverse Miniemulsion

Organic solvent impact the stability and denaturation of proteins.[246] For ovalbumin, the melting temperature decreased from 77 °C in water to 69 °C in an inverse water-cyclohexane-emulsion, while toluene further reduced the T_m to 50 °C (Figure 73).

OVA-NCs formed in an inverse miniemulsion at 40 °C with toluene yielded no prominent PNCs with a core-shell morphology but rather deformed nanoparticles (NPs) (Figure 73B). Comparing the DLS data, in toluene the size distribution was bimodal with significant amount of species between 500-1000 nm, indicating formation of bigger aggregates (Figure 73D). After

transfer into water, those aggregated separated, resulting in mean sizes around 200 nm. Compared to cyclohexane, a significant amount of dye (EE = 64%) could be encapsulated, owing to the higher denaturation and thus more efficient entrapment of dye.

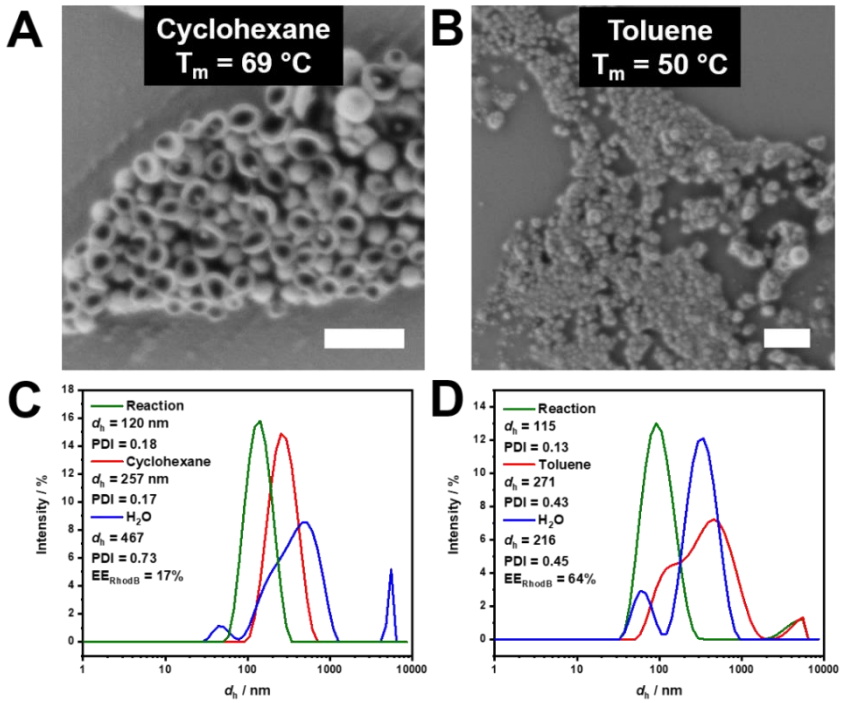

Figure 73. Scanning electron micrographs (upper row) and dynamic light scattering (bottom row) of ovalbumin nanocarriers formed through thermal denaturation at 40 °C in a water-in-cyclohexane (A+C) and water-in-toluene (B+D) miniemulsion. Scale bar: 0.5 µm.

Heating to 40 °C led to the formation of OVA-NCs with a prominent core shell morphology comparable to the morphology observed for OVA-NCs crosslinked with HDDP. However, the temperature was not high enough to denature the protein irreversibly leading to renaturation and disassembly in water. As a result, dye was only encapsulated with low EEs. Next, the heating temperature was changed to promote stronger interfacial denaturation and obtain OVA-NCs with a stable shell.

III. C2.3. Ovalbumin NCs from Interfacial Denaturation in W/O Miniemulsion

In a water-in-cyclohexane miniemulsion the melting temperature of ovalbumin was 69 °C. Therefore, heating to 40 °C was not sufficient to form a stable protein shell by irreversible denaturation. In comparison, heating above T_m at 80 °C in emulsion led to formation of full particles, where the proteins inside the droplet denatured as well (Figure 71B). The complete denaturation resulted in higher stability of PNCs after transfer to water and higher EEs. However, the morphology was deformed with high sizes and broad distribution in emulsion due to strong aggregation (Figure 74E). To find the optimal heating profile, the miniemulsion was

heated to 80 °C for 5 min first to induce unfolding in the majority of protein chains. Then the emulsion stirred overnight at 40 °C to mediate the denaturation only at the interface. The resulting PNCs possessed a prominent core-shell morphology with 257 nm size. The protein shell maintained stable after transfer to water and 88% EE could be achieved. Although the size distribution after transfer into water was bimodal with a size around 500 nm, the strategy to first induce denaturation at $T > T_m$ was successful for the preparation of stable PNCs through interfacial denaturation in inverse miniemulsion.

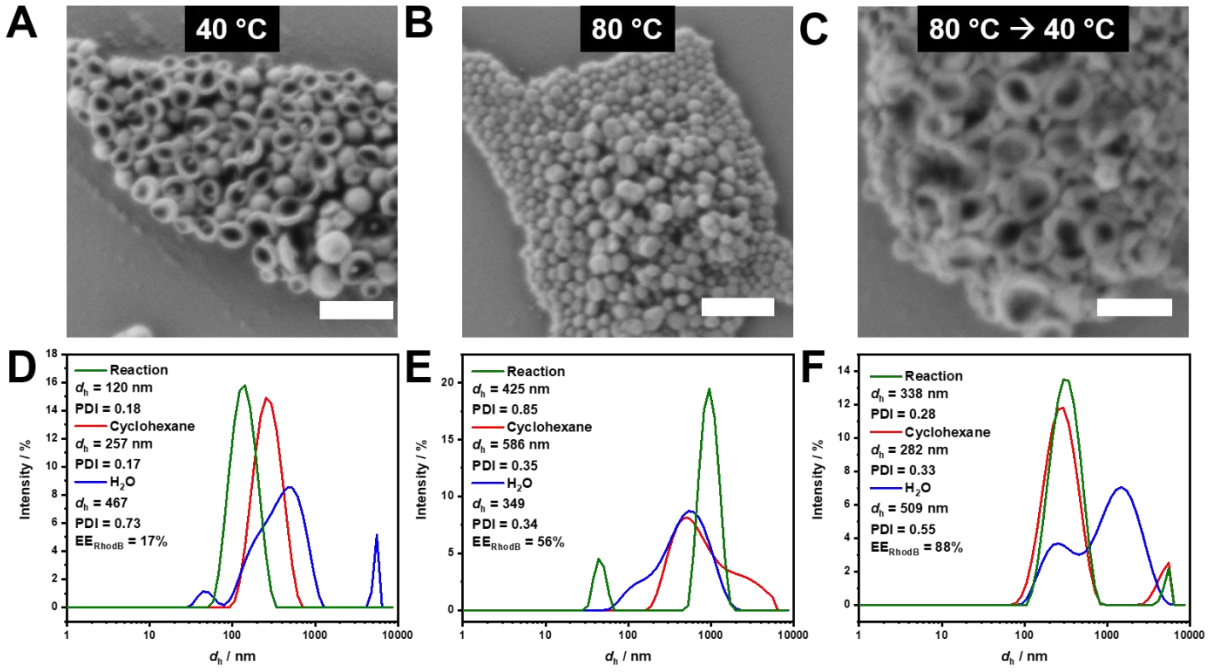

Figure 74. Scanning electron micrographs (upper row) and dynamic light scattering (bottom row) of ovalbumin nanocarriers formed through thermal denaturation in a water-in-cyclohexane miniemulsion at 40 °C (A+D), 80 °C (B+E) and 80 °C, cooled to 40 °C after 5 min. Scale bar: 0.5 µm.

The transfer of PNCs into water was performed by emulsifying the NCs dispersion in cyclohexane into a SDS-containing solution through ultrasonication. Upon cyclohexane evaporation the surfactant was exchanged and the PNCs stabilized in water. Although the transfer technique worked for crosslinked PNCs, the more labile PNCs tend to disassemble upon ultrasonication, especially if not irreversibly denatured, leading to a broad and bi-modal size distribution in DLS. Therefore, another strategy had to be found to maintain the protein shell upon transfer into water.

III. C3. Interfacial Denaturation in W/O/W Emulsion

Ovalbumin nanocarriers were successfully formed by interfacial denaturation in inverse miniemulsion. However, after transfer to water the PNCs showed a broad and bimodal size

distribution compared to PNCs in cyclohexane. Therefore, the water transfer step is a crucial and limiting step for the preparation of PNCs by interfacial denaturation. Double emulsions offer preparation of nanocarriers and transfer into aqueous dispersion in one pot, providing a direct approach without ultrasonication after interfacial denaturation. By emulsifying the W/O miniemulsion in water prior to denaturation, the water transfer could proceed just by solvent evaporation. Therefore, the PNCs were prepared by heating in a W/O/W emulsion, followed by solvent evaporation to stabilize the PNCs in water (Scheme 15).

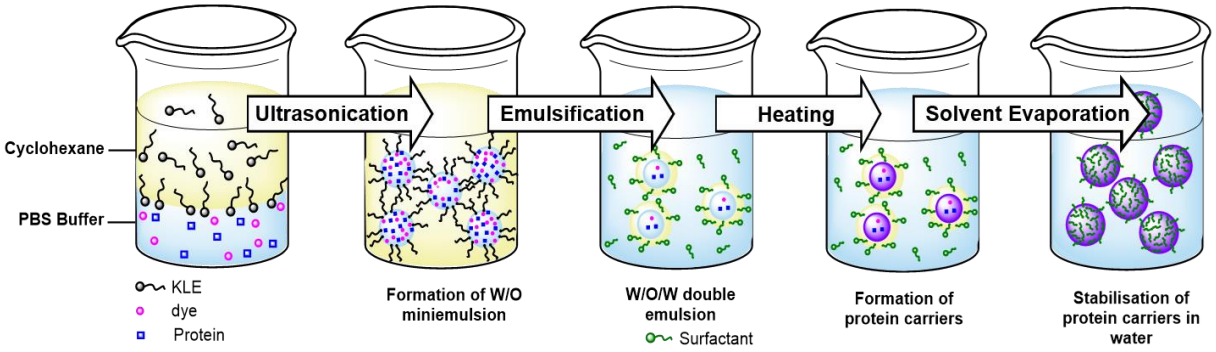

Scheme 15. Process steps for the preparation of protein nanocarriers through interfacial denaturation in a water-in-oil-in-water (W/O/W) double emulsion upon heating. Dextran-RhodaminB-10 kDa was encapsulated as a model cargo. P((E/B)-*b*-EO)) was used to stabilized the W/O miniemulsion, which was emulsified in a second aqueous phase with different surfactants. Scheme prepared with ChemDraw 20.1 by Natkritta Hüppe.

The O/W miniemulsion with ovalbumin in the disperse phase was prepared as established and the resulting miniemulsion was emulsified again in an aqueous solution with different surfactants (anionic, cationic and non-ionic) and by using different techniques (US bath, Ultraturrax, US Tip). Then the double emulsion was stirred at 40 °C overnight to form OVA-NCs and afterwards the cyclohexane was removed by evaporation. Resulting NCs demonstrated a prominent core-shell morphology as observed in SEM (Figure 75A). After transfer into water, the DLS showed presence of two species (green), one below and one above 100 nm, resulting in a mean size of approx. 110 nm and a multi-modal distribution (Figure 75B).

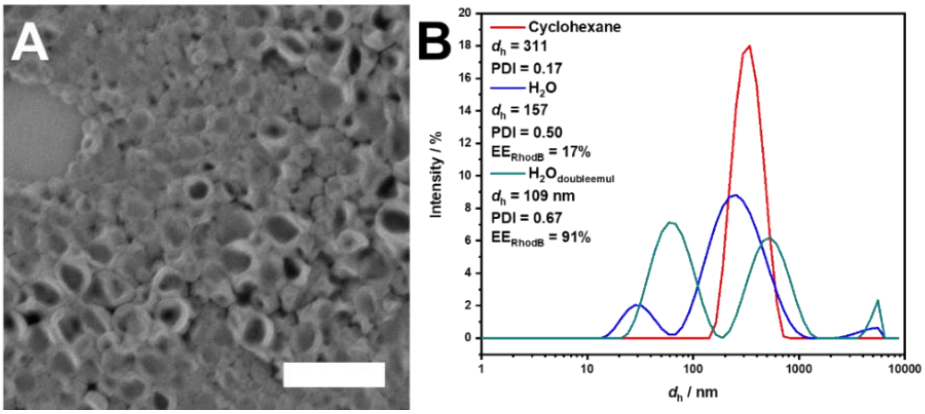

Figure 75. A) Scanning electron micrographs of ovalbumin nanocarriers formed through interfaciel denaturation in a water-in-cyclohexane-in-water double emulsion at 40 °C and B) dynamic light scattering of ovalbumin nanocarriers in cyclohexane (red), water after redispersion into 0.1 wt% SDS solution (blue) and water after interfacial denaturation in double emulsion (green). Scale bar: 0.5 µm.

Different techniques were used to form a W/O/W double emulsion (Table 18). Only the emulsion formed in the ultrasonication (US) bath had comparable sizes to PNCs in cyclohexane. Whereas the other two techniques, ultrasonication tip (amplitude 10%, 1 min) and ultraturrax (20 000 rpm), lead to smaller PNCs under 100 nm as measured from the unpurified dispersion. After purification by washing through a centrifuge filter (MWCO 50 kDa) the PNCs from the double emulsion *via* an ultraturrax aggregated. In all three cases, encapsulation efficiency of dye was over 90%, significantly higher than in W/O miniemulsion and comparable to EEs obtained for crosslinked PNCs. The approach with the US bath showed the most promising results to form stable PNCs from interfacial denaturation in a double emulsion. Next, different surfactants were used in the second aqueous phase to stabilize the W/O/W emulsion. The PNCs size in the unpurified dispersion was lower than 200 nm, with cationic cetyltrimethylammoniumbromid (CTAB) even smaller than 50 nm. After purification the results for polymeric LutA50 stood out, as it formed large PNCs and the encapsulation efficiency was very low (not detectable), whereas for the other nonionic surfactants over 70% encapsulation efficiency was achieved. While PNCs from Brij78 and Tween80 maintained their diameters after purification, the dispersion from CTAB cleared up and almost no scattering could be observed, indicating no presence of PNCs. The high encapsulation efficiency seemed to be caused by ionic interaction of the cationic surfactant CTAB with the anionic Cy5-dye. In conclusion, SDS or one of the polymeric non-ionic surfactants gave the best results for formation of PNCs through thermal denaturation in double emulsion and achieved high encapsulation efficiencies.

Table 18. Analytical data of ovalbumin nanocarriers formed through interfacial denaturation at 40 °C in a W/O/W double emulsion stabilized with different surfactants (0.1 wt%). W/O miniemulsion were stabilized with P((E/B)-*b*-EO)). Double emulsion formed with different methods. Dynamic light scattering (DLS) of nanocarriers in cyclohexane was measured from the base W/O miniemulsion after heating at 40 °C and purification by centrifugation. DLS after heating at 40 °C in W/O/W emulsion measured after evaporation of cyclohexane from unpurified and purified dispersions.

No.	Surfactant of W/OW/	Method	$d_{h,CH}$ / nm	PDI	$d_{h,unpure}$ / nm	PDI	$d_{h,water}$ / nm	PDI	EE / %
1	-	-	318	0.17	-	-	157	0.50	-
2	SDS	US-Bath	318	0.17	232	-	109	-	91
3	SDS	US-Tip	318	0.17	89	0.37	82	-	90
4	SDS	Ultraturrax	318	0.17	78	0.34	(4158)	-	90
5	CTAB	US-Bad	318	0.17	48	0.40	92	0.40	77
6	Brij78	US-Bad	318	0.17	110	0.42	147	0.44	72
7	Lut-A50	US-Bad	318	0.17	182	-	499	-	3
8	Tween80	US-Bad	318	0.17	181	-	197	-	88

* PDI without values: DLS curve had no Gaussian distribution.

III. C4. Degradation of Protein Nanocarriers: Crosslinked vs. Denatured

As shown in chapter A and B, the crosslinking degree influenced the degradation rate of protein nanocarriers. A high degradation degree is important to ensure efficient release of cargo molecules, especially large ones, at the target site. PNCs were prepared with different shell formation techniques and the degradation behavior of crosslinked and denatured PNCs was compared (Table 19).

Table 19. Analytical data of ovalbumin nanocarriers prepared through crosslinking in W/O miniemulsion with 1) 30 mg 1,4- toluene diisocynate (TDI), 2) 3 mg TDI and 3) hexanediol dipropiolate (HDDP); 4) through interfacial denaturation in a W/O/W emulsion at 40 °C; before and after enzymatic degradation. Release of dextran-rhodamine B-10 kDa was determined in the supernatant after 24 h treatment with proteinase K (5 U/mL).

No.	Method	$d_{h,CH}$ / nm	PDI	$d_{h,water}$ / nm	PDI	EE / %	NCs yield / %	$d_{h,degraded}$ / nm	PDI	Release / %
1	$TDI_{30\ mg}$	258	0.07	305	0.36	69	56	312	0.36	4
2	$TDI_{3\ mg}$	273	0.08	306	0.28	58	50	245	0.47	25
3	HDDP	294	0.12	271	0.30	63	28	77	0.42	63
4	Denat.	288	0.17	354	0.52	83	66	80	0.39	72

Ovalbumin nanocarriers prepared by crosslinking with 1,4-toluene diisocyanate (TDI) or hexanediol dipropiolate (HDDP) or by interfacial denaturation in inverse miniemulsion resulted

in PNCs of comparable sizes between 258 and 294 nm as determined by DLS in cyclohexane. SEM revealed in all cases a prominent core-shell morphology; the TDI-crosslinked PNCs appeared stiffer, which could be explained by H-bonding polyurea units in the crosslinked shell, while PNCs-HDDP and the denatured PNCs seemed softer materials (Figure 76). After transfer to water, the diameters of PNCs-TDI and PNCs-HDDP remained relatively unchanged (Table 19). The size distribution of PNCs-denatured increased in water, which might be related to aggregation due to cyclohexane evaporation. In all cases, encapsulation efficiencies (of dextran-rhodamine B-10 kDa) over 50% were obtained, interestingly the denatured PNCs resulted in the highest EE of 83%, probably because dye remained entrapped without the additional centrifugation step in cyclohexane and redispersion into water by ultrasonication.

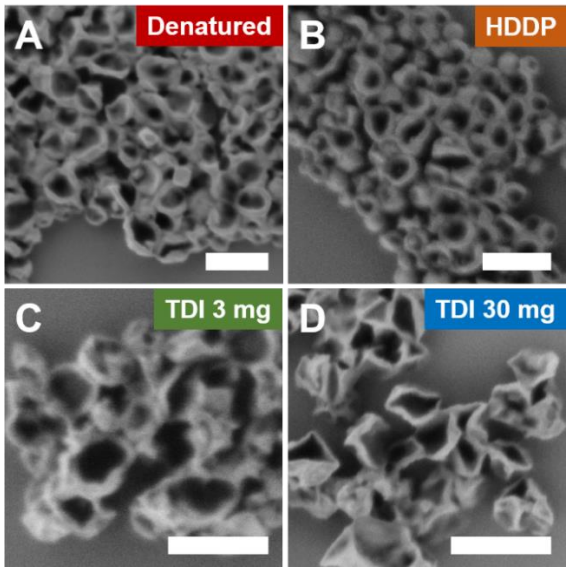

Figure 76. Scanning electron micrographs of ovalbumin nanocarriers formed through A) interfacial denaturation in a W/O/W emulsion at 40 °C; crosslinking in W/O miniemulsion with B) hexanediol dipropiolate (HDDP), C) 3 mg 1,4- toluene diisocynate (TDI) and D) 30 mg TDI. Scale bar: 0.5 µm.

Enzymatic Degradation

The enzymatic degradation of crosslinked and denatured PNCs was followed over time after treatment with proteinase K (5 U/mL) by measuring the derived count rate (DCR) *via* DLS (Figure 77A). The DCR is the scattering intensity of the sample and indicates the degradation of PNCs, as the dispersion cleared up during enzymatic degradation to a homogeneous solution approaching a DCR of 0. In all cases, the scattering intensity decreased over time, indicating that parts of the nanocarriers dissolved during enzymatic hydrolysis. However, the different preparation methods resulted in different degradation rates. The DCR of PNCs crosslinked with a high amount of TDI decreased only slowly during 20 h after the addition of the enzyme,

indicating a slow degradation. In case of unselective crosslinkers such as TDI, not only the protein is crosslinked during reaction at the water droplet interface, but TDI reacts as well with water to a diamine. Then the diamine reacts in a following polyaddition reaction with itself, forming polyurea.[247, 248] Since polyurea is not enzymatically degradable, parts of the nanocarrier shell will not be as well. Thus, the presence of polyuria units in the protein shell could slow down the enzymatic degradation of the PNCs-TDI. When PNCs were crosslinked with less TDI (3 mg), the enzymatic degradability increased, as observed by a decrease of DCR after addition of proteinase K. Therefore, the amount of crosslinker mediates the amount of polyuria formation and thus biodegradability of protein nanocarriers crosslinked with TDI. For PNCs crosslinked by azide-alkyne click chemistry with HDDP, the DCR significantly decreased in a matter of 5 min, indicating a fast enzymatic degradation. Afterwards, only a minimal change in scattering was measured, indicating that most of PNCs were disassembled in 2 h and then protein parts were further degraded. In comparison to the highly reactive and unselective TDI, the HDDP reacts selectively with azide-modified proteins without formation of side products. As demonstrated in chapters A and B, PNCs-HDDP proven high enzymatic degradability controlled by the crosslinking degree. Protein nanocarriers formed without crosslinking but through interfacial denaturation demonstrated a quickly decreasing DCR after addition of enzyme to the PNCs dispersion similar to PNCs-HDDP. This implicates, that the degradation of PNCs prepared by crosslinking with HDDP or by interfacial denaturation do offer similar degradability independent of the preparation method.

In addition, the release of the dye dextrane-rhodamine B-10 kDa was monitored during the enzymatic degradation (Figure 77B). Proteinase K was added to the PNCs and samples were taken from dispersion at specific time points. The released dye in the supernatant was measured by fluorescence after separation from the remaining PNCs by filtration through centrifuge filters (MWCO 50 kDa). Low degradability of PNCs-TDI-30 mg was underlined by release experiments, where below 5% dye (dextrane-RhodB-10kDa) was released after 24 h treatment with proteinase K (5 U/mL) (Figure 77B). Even after a second addition of higher concentrations of enzyme (30 U/mL) after 24 h, no significant dye release could be observed for PNCs-TDI-30 mg. These results underline the previous observations, that PNCs-TDI have a low degradability due to the proportion of non-degrabdable polyurea as a side product in the protein shell. In fact, when decreasing the amount of TDI to 3 mg, the release of dye was around 10% and a significant increase in release over 20% could be obtained for PNCs-TDI-3 mg with a second addition of enzyme after 24 h. With less TDI less polyurea is formed and the PNCs

became more degradable and more dye could be released. However, even with 3 mg of TDI, a significant part of the PNCs was still not degradable, hindering a high release of the large dye.

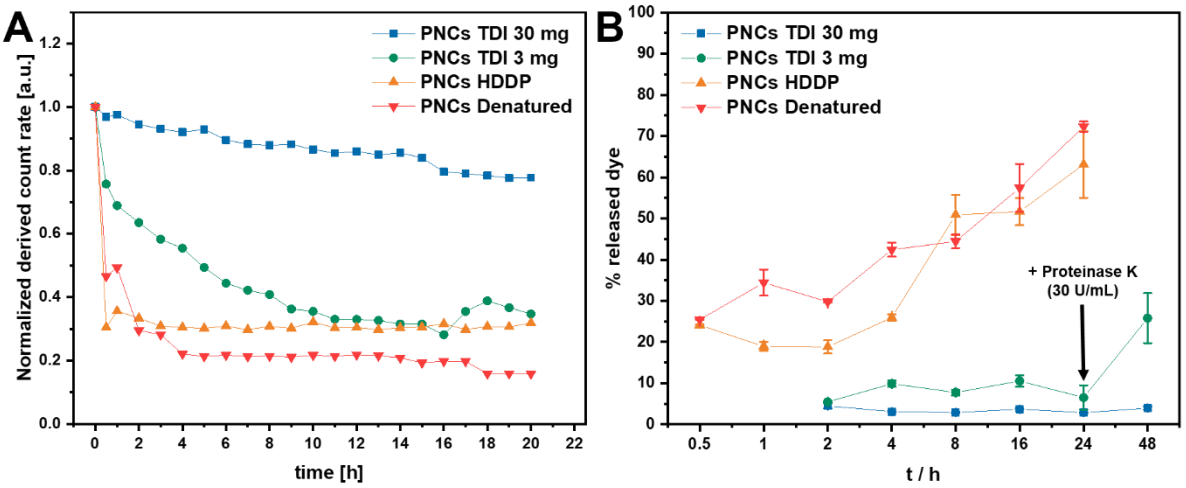

Figure 77. Enzymatic degradation and release of PNCs: A) Derived count rates (DCR) measured by dynamic light scattering of protein nanocarriers (2 mg/mL) with different preparation strategies (TDI 30 mg, TDI 3 mg, HDDP, interfacial denaturation) after the addition of proteinase K(5 U/mL); Note: the DCR was normalized to the initial DCR of respective dispersion as the maximum and DCR of the proteinase K solution as minimum. B) Release of dextran-rhodamine B (10 kDa) from protein nanocarriers (2 mg/mL) during the enzymatic degradation with proteinase K (5 U/mL) (n = 3), measured by fluorescence (570/590 nm). After 24 h proteinase K (30 U/mL) was added to PNCs-TDI-3 mg (green) and PNCs-TDI-30 mg (blue).

The release experiments for both PNCs-HDDP and PNCs-denatured revealed an increased release of dye over time up to approx. 70% after 24 h. As observed in the DLS measurements, where in both cases, the DCR dropped quickly after addition of enzyme, it was expected, that PNCs crosslinked with HDDP or prepared by denaturation would have a higher amount of released dye compared to PNCs-TDI. Since similar results were obtained for PNCs-HDDP and PNCs-denatured, crosslinking with HDDP might not have a significant effect on the degradability of PNCs in comparison to denatured protein. Therefore, both methods are suitable for the preparation of highly degradable protein nanocarriers. However, degradability is not the only factor that could be influenced by the preparation method. The use of a crosslinker could change the surface characteristics of PNCs compared to PNCs prepared by interfacial denaturation. Different surface properties mediate different interactions of the nanocarriers with cells or components of biological fluids such as proteins. Therefore, the surface characteristics play an important role for the fate of the nanocarriers in the body. PNCs prepared by interfacial denaturation without additional use of reactants such as crosslinkers could offer another strategy to obtain the desired nanocarrier-cell interaction and thus efficient drug delivery systems. Moreover, different surface characteristics of PNCs enable different possibilities for surface modification, achieving multifunctional PNCs.

III. C5. Conclusion

Interfacial denaturation of proteins by heating in a W/O miniemulsion allowed the preparation of fully degradable protein nanocarriers (PNCs) with dye encapsulation during protein shell formation. The preparation of protein nanocarriers by interfacial denaturation was influenced by the melting temperature T_m of proteins, which decreased at the interface of a water-in-cyclohexane miniemulsion. Ovalbumin (OVA) was revealed the most promising protein to prepare PNCs with a core-shell morphology by interfacial denaturation. Since the transfer into water was the weak spot of the strategy, a double emulsion (W/O/W) was generated from the W/O miniemulsion prior to interfacial denaturation. The water transfer of PNCs in the double emulsion proceeded in one-pot by solvent evaporation. Stable protein nanocarriers could be obtained by the double emulsion technique with high EE of dye (> 90%). The degradation of PNCs prepared by crosslinking with TDI or HDDP or interfacial denaturation demonstrated the influence of the crosslinker on the degradation and release of cargo molecules. Unselective crosslinking with TDI lead to decreased enzymatic degradability due to the formation of polyurea. Bioorthogonal crosslinking with hexanediol dipropiolate (HDDP) achieved similar high enzymatic degradation and release results as denatured PNCs, proving as well that crosslinking by click reaction does not influence the degradability significantly. In conclusion, PNCs could be prepared successfully by interfacial denaturation in inverse miniemulsion with efficient dye loading and enzymatic degradability. In the next step, PNCs could be applied for the multicomponent encapsulation of therapeutics as described for crosslinked PNCs, moving forward in the development of a fully biocompatible drug delivery system without the use of chemical reactions and reactants.

Chapter D – Modification of Protein Nanocarriers for Cell Trafficking, Stealth and Targeting

Chapter D, III. D2. "Protein Nanocarriers to Study Cell-Carrier Interaction" is part of the manuscript:

[redacted], N. Hüppe[redacted], *manuscript in preparation*. For the thesis, this chapter was extended with preliminary results, additional experiments, optimizations and details.

Contributions:

Natkritta Hüppe synthesized and characterized the modified protein and resulting protein nanocarriers as well as the azide-transfer agent and crosslinker involved as stated in the experimental part. The iron oxide nanoparticles were synthesized and encapsulated by Natkritta Hüppe. [redacted] performed the *in vitro* plasma protein corona and cell uptake experiments. [redacted] performed the intracellular protein corona experiments as well as the cell uptake experiments, transmission electron microscopy (TEM) and confocal laser scanning microscopy (cLSM) for the proteomics-guided intracellular trafficking analysis. For the surface modification, Natkritta Hüppe performed and analyzed the modification. [redacted] functionalized the antibodies and modification of nanocarriers as well as all *in vitro* experiments regarding the stealth and targeting experiments.

Abstract

The development of nanocarriers as drug delivery systems requires investigation on their behavior and interaction in physiological environment. The knowledge gained from studying protein corona formation and cell-carrier interaction can be used to improve the nanocarrier system by tailored modification. Protein nanocarriers proved to be promising delivery systems for vaccine components. Modification of protein nanocarriers with magnetic CMPVA-coated iron oxide nanoparticles enabled to study the formation of protein corona from blood as well as intracellular corona. Furthermore, due to the higher contrast of loaded magnetic nanoparticles in electron microscopy, the cell uptake mechanism and intracellular pathway of PNCs could be visualized. Cell-carrier interaction experiments revealed the need for stealth and targeting properties in PNCs to promote their specific uptake into dendritic cells. Therefore, PNCs were modified with stealth polymer polyethylene glycol and a decreased uptake into macrophages could be achieved. The modification with azide-bearing antibodies by a specific site-click reaction to DBCO-functionalized PNCs resulted in a higher uptake of CD11c-modified PNCs into dendritic cells. However, a contribution of Fc-mediated uptake was observed, indicating an unspecific uptake mechanism *via* Fc receptors. The site-selective conjugation of antibodies to PNCs have to be improved to ensure a specific Fab-directed targeting to CD11c receptors of DCs. Protein nanocarriers loaded with adjuvants and modified with stealth and targeting properties are promising delivery systems to promote a high anti-tumor immune response through DC-mediated T cell stimulation.

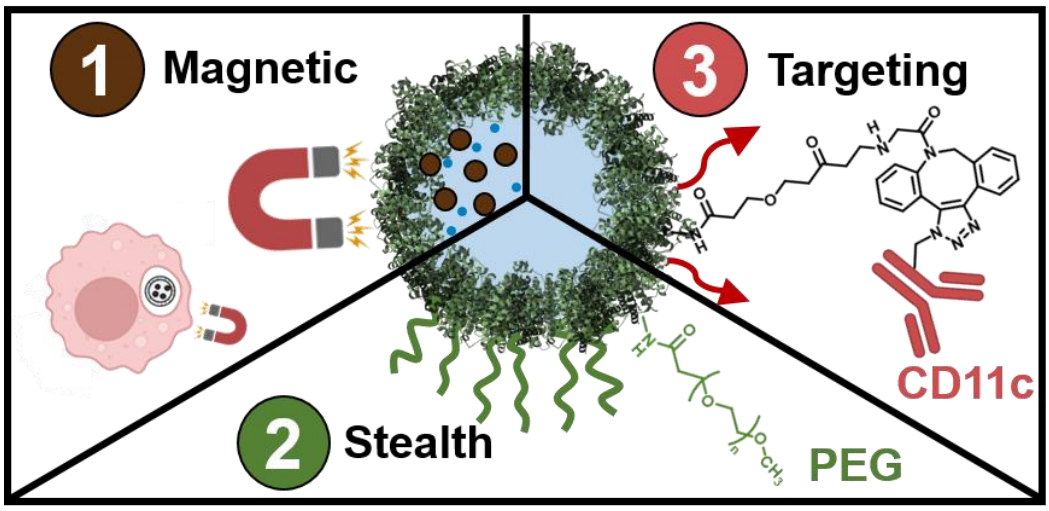

Figure 78. Modification of Protein Nanocarriers for Cell Trafficking, Stealth and Targeting. Figure created in BioRender.com by Natkritta Hüppe.

III. D1. Introduction

Nanocarriers as drug delivery systems protect the cargo from systemic distribution and fast excretion, increasing the therapeutic efficacy and lowering side effects by protecting the body from toxic cargo molecules. Encapsulation of vaccine components, i.e. antigen and adjuvants, into nanocarriers have proven to increase the vaccination effect by simultaneous delivery into dendritic cells (DCs).[81, 249] Up to now, many nanovaccines have been reported to be taken up by "passive targeting" into DCs.[250] An even higher efficiency, especially *in vivo*, could be achieved by specifically targeting the dendritic cells and reduce competitive uptake into undesired cells such as macrophages.[251, 252] Nanocarriers offer numerous possibilities for modification towards stealth and targeting functions. Over the past decade, many targeting strategies to dendritic cells were developed at which the surface of the nanocarriers are functionalized with targeting ligands such as carbohydrates[253, 254], antibodies or proteins.[255] Especially, the novel site-specific conjugation technique to the Fc part of antibodies allowed higher specific targeting of antibody-functionalized nanocarriers to dendritic cells by the Fab region.[256] The decrease of targeting through the Fc part is important to hamper unspecific uptake into Fc-receptor bearing cells like macrophages. Although many have proven the targeting specificity of surface-modified nanocarriers *in vitro*, none of the nanocarriers have been clinically approved due to failed *in vivo* studies.[257, 258] One major reason is the adsorption of blood proteins onto the nanocarriers surface leading to coverage of the targeting ligands on the surface.[259] The formation of a protein corona and their influence on the fate of nanocarriers in the body have been studied extensively in the past years.[260-262]. Many strategies have been developed to decrease protein adsorption and enhance blood circulation time by modifying the nanocarriers' surface with stealth polymers such as polyethylene glycol[40], polyphosphoesters[263] or polysarcosines[264].[265] Surface-functionalization of nanocarriers with stealth and targeting moieties is a crucial step to achieve high treatment efficacy. Once arrived at the targeting cell, the nanocarriers are internalized, degraded and the therapeutic cargo released to take effect. However, little is known about what actually happens with the nanocarriers in cells. Blood is not the only biological medium that the nanocarriers encounter on their way to the target. It has been reported that nanocarriers content with different cell milieus upon internalization into cells where a new biological environment with a different protein composition could change the existing plasma protein corona.[7] The formation of the so-called intracellular protein corona (IPC) alike the blood protein corona influences the intracellular fate of the nanocarriers.[266, 267] Moreover, the IPC acts like a tracing mark of where the nanocarriers travelled through the cells

and analysis of the IPC could give an insight into cellular processing of nanocarriers.[268] Studying the intracellular fate of nanocarriers would benefit their design on how to improve their functionality and increase treatment efficacy.

Great developments were achieved in the last years towards specific targeting of dendritic cells with modified nanocarriers. The next step is to transfer the approaches gained for intracellular trafficking, stealth and targeting from model nanocarriers to nanocarriers, which have clinical potential, such as protein nanocarriers, developed in this work. The combination of biodegradable nanocarriers loaded with therapeutics and modified with stealth and targeting properties could achieve high therapeutic efficiency and paves the way towards clinical application of anti-tumor nanovaccines. Furthermore, the knowledge gained from intracellular studies could lead to precise design of optimal multifunctional drug delivery systems. Therefore, protein nanocarriers, prepared through interfacial crosslinking in inverse miniemulsion, were loaded with magnetic nanoparticles to study intracellular trafficking and were surface-functionalized with stealth and targeting moieties to enhance specific uptake into DCs.

III. D2. Protein Nanocarriers to Study Cell-Carrier Interaction

Magnetic separation of cells containing nanocarriers is a convenient method to study cell-carrier interaction, especially for PNCs, which are too soft to be collected by centrifugation without damage. Therefore, superparamagnetic iron oxide nanoparticles (SPIONs) were encapsulated into PNCs during their interfacial formation in inverse miniemulsion. To study the influence of unselective and biorthogonal crosslinking on the nanocarrier's surface composition and thus influence on carrier-cell interaction, the nanocarriers were prepared with toluene diisocyanate (TDI) and hexanediol dipropiolate (HDPP), respectively.

III. D2.1. Synthesis of CMPVA-Coated Fe_3O_4-Nanoparticles

The superparamagnetic Fe_3O_4-NPs were synthesized through co-precipitation of iron(II) and iron(III) chloride under high basic conditions and stabilized with oleic acid (Scheme 16A), according to literature.[269] Since the protein nanocarriers are prepared in an inverse water-in-oil miniemulsion, the SPIONs were transferred to an aqueous phase by exchanging the oleic acid. Tetramethylammonium hydroxide (TMAOH) was reported to be a good stabilizer for SPIONs in water, but due to its ionic charge it is also sensitive to higher salt concentrations, leading to aggregation of SPIONs. Therefore, as additional polymeric stabilizer carboxymethylated

polyvinyl alcohol (CMPVA) (Scheme 16B) was used to prevent aggregation of SPIONs upon encapsulation and achieve a higher loading into PNCs.

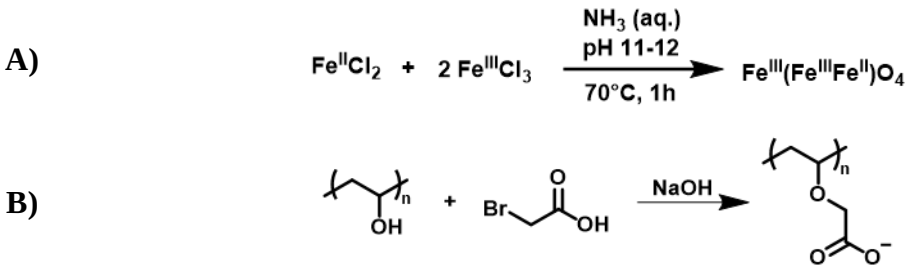

Scheme 16. A) Synthesis of iron oxide nanoparticles by co-precipitation. B) Synthesis of carboxymethylated polyvinyl alcohol.

Polyvinyl alcohol could successfully be functionalized with carboxymethyl groups (Scheme 16B; Figure 79A). The molecular weight increased from 8000 $gmol^{-1}$ to 12000 $gmol^{-1}$ after carboxymethylation. CMPVA was obtained as a colorless powder and with 65% yield. The oleic acid-stabilized Fe_3O_4-NPs were redispersed in an aqueous solution of TMAOH (10 wt%) and CMPVA was added to obtain CMPVA-coated Fe_3O_4-NPs (CMPVA@Fe_3O_4-NPs), stable in aqueous media. Transmission electron microscopy (TEM) revealed spherical NPs with a size of around 20 nm.

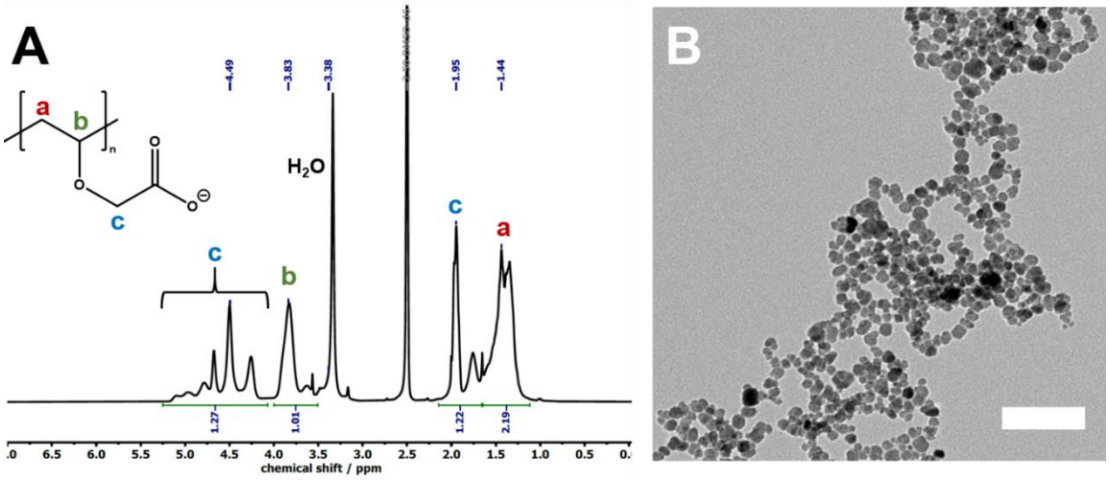

Figure 79. A) ^1H NMR of carboxymethylated polyvinyl alcohol (CMPVA). B) Transmission electron micrograph of CMPVA@Fe_3O_4 nanoparticles in water. Scale bar: 100 nm.

CMPVA@Fe_3O_4-NPs were highly stable in high concentrations (100 mg/mL) in aqueous phase up to several months and could be used to modify protein nanocarriers with magnetic properties by encapsulation of CMPVA@Fe_3O_4-NPs into PNCs.

III. D2.2. Encapsulation of CMPVA@Fe_3O_4-NPs into PNCs

Protein nanocarriers were prepared by interfacial crosslinking in an inverse miniemulsion. Depending on the crosslinker, the reaction could be performed unselectively or bioorthogonally. In chapter A, a biorthogonal strategy for PNCs formation was realized with azide-alkyne click chemistry, leading to preservation of the cargoe's activity and high therapeutic effectivity. Not only does the crosslinking chemistry affect the encapsulation of the cargo, but the resulting nanocarrier surface composition as well. As previously described by Frey *et al*., the surface composition, influenced by the crosslinker, impacts the protein adsorption and cell-carrier interaction.[84] The influence of unselective crosslinking with 1,4-toluene diisocyanate (TDI) and biorthogonal crosslinking with hexanediol dipropiolate (HDDP) on interaction of protein nanocarriers with proteins and cells were investigated. Encapsulation of CMPVA@Fe_3O_4-NPs into PNCs allowed a magnetic cell separation of PNCs-containing cells to study cell-carrier interaction.

a) PNCs Crosslinked with 1,4-Toluene Diisocyanate (TDI)

For an unselective crosslinking of proteins in an inverse miniemulsion, TDI was chosen as the crosslinker. TDI is a highly reactive compound that reacts mainly with nucleophiles such as amines to urea bond (Scheme 17). However, TDI also hydrolyzed upon reaction with water at the interface of the inverse miniemulsion and reacts with another TDI to polyurethanes.[270] The unwanted side reaction of TDI with itself creates polyurethane patches in the shell of the protein nanocarriers, leading to a different surface composition. To investigate the cell-carrier interaction of PNCs-TDI, CMPVA@Fe_3O_4-NPs were encapsulated into PNCs during the interfacial crosslinking with TDI in inverse miniemulsion (Scheme 17).

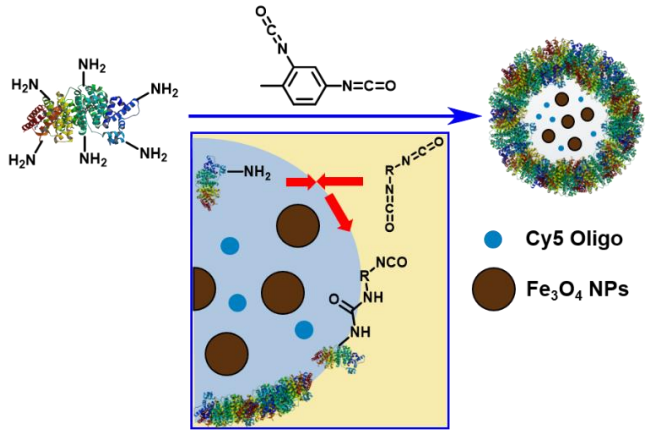

Scheme 17. Encapsulation of CMPVA@Fe_3O_4-nanoparticles into PNCs by interfacial crosslinking with 1,4-toluene diisocyanate (TDI) in inverse miniemulsion. Protein structure was obtained from DrugBank online (https://go.drugbank.com/drugs/DB00062, 28.11.2021) and was adapted. Figure created by Natkritta Hüppe.

Different methods were tested to find the optimal encapsulation strategy for magnetic nanoparticles with high encapsulation efficiency and minimal amount of free CMPVA@Fe_3O_4-NPs (Table 20). Since usually magnetic stir bars were used for the reaction, a mechanical stirrer was used instead to prevent accumulation of SPIONs on the magnetic stir bar. Encapsulation of CMPVA@Fe_3O_4-NPs by method 1 resulted in almost no formation of protein nanocarriers as seen in electron microscopy (Figure 80A+E). Instead, most of the proteins aggregated as well as the SPIONs, which was not encapsulated into PNCs and hard to separate from PNCs. High amount of free SPIONs in the dispersion is not desirable for the protein corona studies, as the protein corona of free magnetite might falsify the results. It was observed that upon addition of highly concentrated CMPVA@Fe_3O_4-NPs dispersion to the protein solution, both aggregated. Therefore, in method 2 the amount of SPIONs was decreased to 5 mg. The protein mostly stayed stable and some CMPVA@Fe_3O_4-NPs could be encapsulated into PNCs-TDI with a prominent core-shell morphology (Figure 80B+F). However, as observed in TEM, a lot of PNCs-TDI were empty and there was still aggregates of CMPVA@Fe_3O_4-NPs outside of the PNCs. Due to mechanical stirring, a bigger flask had to be used, which promoted the evaporation of solvent from the miniemulsion during the reaction, leading to instability of the nanodroplets, aggregation of proteins and CMPVA@Fe_3O_4-NPs.

Table 20. Comparison of method 1, 2, 3 and 4 for encapsulation of CMPVA@Fe3O4-nanoparticles into protein nanocarriers in inverse miniemulsion.

	Method 1	**Method 2**	**Method 3**	**Method 4**
Amount of magnetite	50 mg	5 mg	0.3 mg	25 mg
Reaction vessel	100 mL-flask	100 mL-flask	40 mL-vial	40 mL-vial
Mechanical stirrer for reaction	yes	yes	no	no
Magnetic stirrer for reaction	no	no	yes	yes
Magnetic stirrer for redispersion	no	no	yes	yes
Hydrodynamic radius / nm	320	240	320	378
PDI	0.10	0.14	0.18	0.15

Encapsulation of magnetic NPs was performed with the previous established method by stirring with a magnetic stirrer in a 40 mL vial. The amount of CMPVA@Fe_3O_4-NPs was further decreased to 0.3 mg to prevent free magnetite after the PNCs formation. PNCs-TDI, formed according to method 3, resulted in stable NCs with a prominent core-shell morphology and comparable size to previous PNCs. However, due to the small amount of CMPVA@Fe_3O_4-NPs most of the PNCs were empty (Figure 80C+G). Empty PNCs could be separated from SPIONs-

loaded ones, but with high yield loss. In method 4, the amount of magnetite was increased to 25 mg and the encapsulation into PNCs performed as established before. Due to the high stability of the iron oxide-NPs coated with CMPVA, no protein or NPs aggregated upon mixing. With method 4, stable PNCs evenly loaded with CMPVA@Fe_3O_4-NPs could be obtained and no free NPs was observed in EM (Figure 80D+H). Moreover, energy dispersive X-ray spectroscopy (EDX) measurements revealed successful encapsulation of SPIONs into PNCs (SI to chapter D, Figure 174).

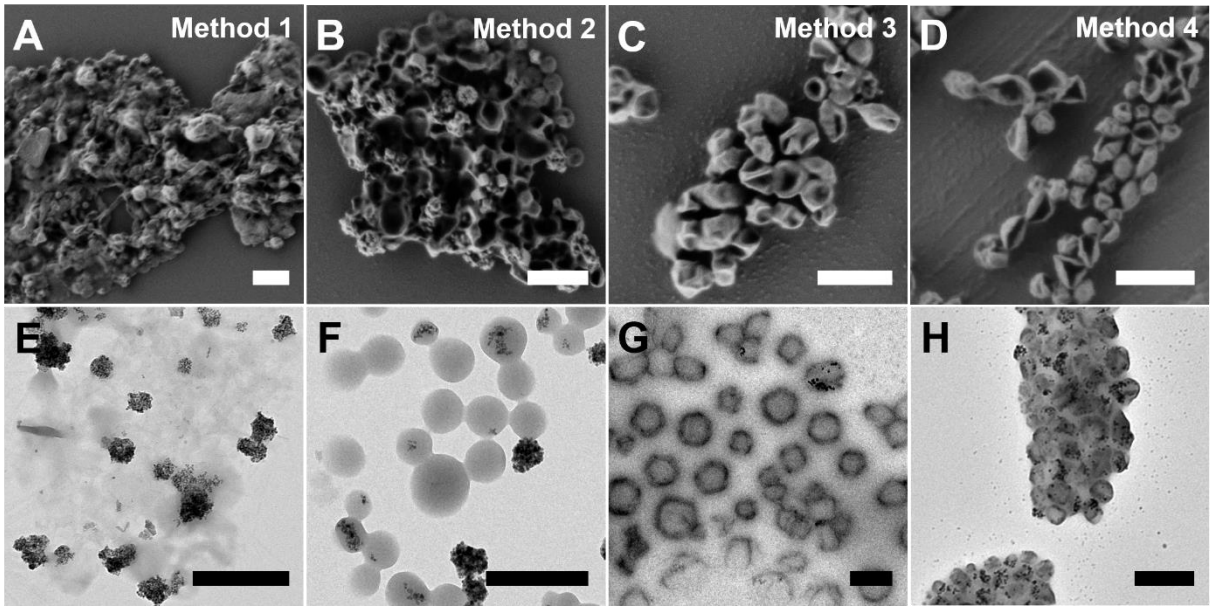

Figure 80. Scanning (upper row) and transmission (lower row) electron micrographs of protein nanocarriers loaded with CMPVA@Fe_3O_4-nanoparticles prepared with A/E) Method 1, B/F) Method 2, C/G) Method 3 and D/H) Method 4; in cyclohexane. Scale bar: 0.5 µm.

The CMPVA@Fe_3O_4-NPs-loaded PNCs were purified by centrifugation. After centrifugation at 1500*g*, a significant amount of PNCs were left in the supernatant. To investigate the PNCs in the supernatant, the dispersion was centrifuged at higher speed (3000*g*) to collect all NCs. As expected, the PNCs from the supernatant contained a high amount of empty and lightly loaded PNCs compared to the PNCs from the main fraction (Figure 81D). The size of PNCs from the supernatant fraction was about 100 nm smaller than the main fraction (Table 21). To increase the yield, loaded PNCs were separated from empty ones by magnetic decantation. Despite their heavy loading with SPIONs, the PNCs in water were still too soft to be collected efficiently by centrifugation. Therefore, to prevent loss of PNCs during purification in aqueous dispersion a centrifuge filter was used for purification of NPs-loaded PNCs.

Table 21. Analytical data of CMPVA@Fe_3O_4-loaded protein nanocarriers crosslinked with TDI.

Sample	Centrifuge speed	d_h (CH) / nm	PDI	d_h (H_2O) / nm	PDI	ζ /mV	EE_{Cy5} / %
1	1500*g*	345	0.13	371	0.24	-30	36
2*	3000*g*	265	0.17	-	-	-	-

*nanocarriers from supernatant of sample 1

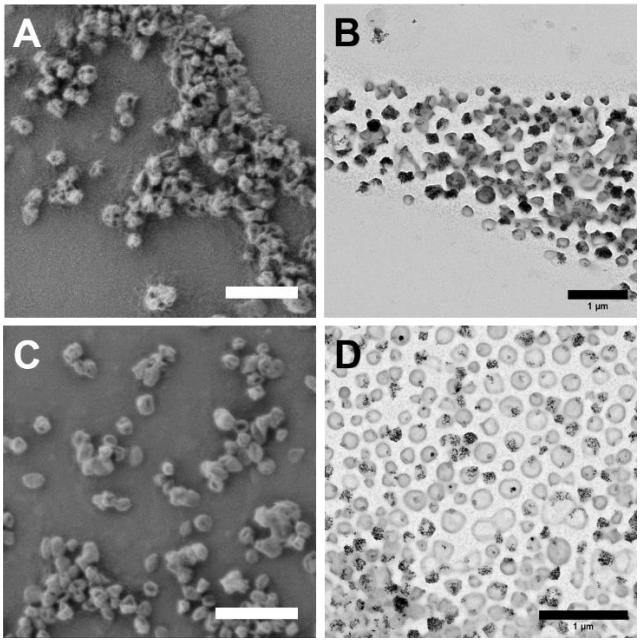

Figure 81. Scanning (left) and transmission (right) electron micrographs of A/B) Protein nanocarriers (PNCs) loaded with CMPVA@Fe_3O_4-nanoparticles, centrifuged at 1500*g* and C/D) PNCs from the supernatant of A, centrifuged at 3000*g*; in cyclohexane. Scale bar: 1 µm.

PNCs-TDI could successfully be prepared and loaded with CMPVA@Fe_3O_4-NPs with minimal amount of free NPs as proven by EM. Additionally, the fluorescent dye Cy5-Oligo was as well encapsulated into PNCs-TDI with moderate encapsulation efficiency of 36%. PNCs with magnetic and fluorescent modification could be used for studying the cell-carrier interaction.

b) PNCs Crosslinked with Hexanediol Dipropiolate (HDDP)

In comparison to TDI-crosslinked PNCs, crosslinking with the activated dialkyne HDDP in an azide-alkyne click reaction enables a chemoselective crosslinking strategy with no side products, resulting in nanocarriers composed mainly of the protein shell material. CMPVA@Fe_3O_4-NPs were encapsulated into PNCs-HDDP by interfacial crosslinking in inverse miniemulsion (Scheme 18).

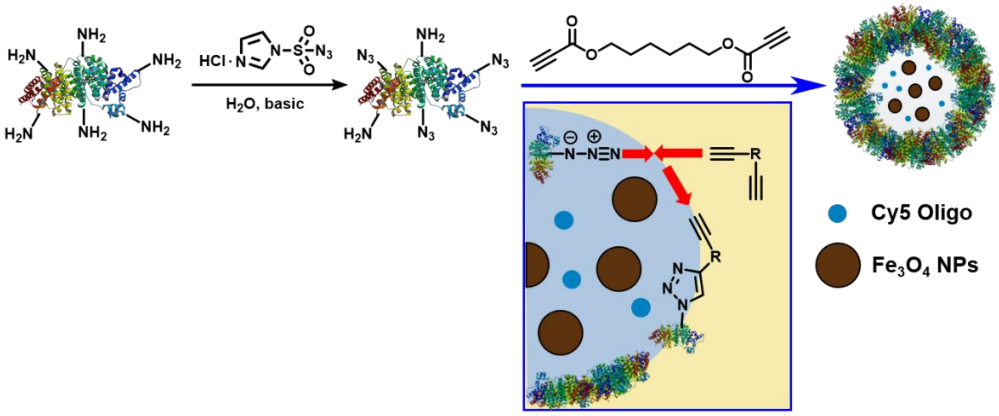

Scheme 18. Encapsulation of CMPVA@Fe_3O_4-nanoparticles into PNCs by interfacial crosslinking with hexanediol dipropiolate (HDDP) in inverse miniemulsion. Protein structure was obtained from DrugBank online (https://go.drugbank.com/drugs/DB00062, 28.11.2021) and was adapted. Figure created by Natkritta Hüppe.

The CMPVA@Fe_3O_4-NPs were added to the aqueous dispersed phase to encapsulate them into ovalbumin nanocarriers, crosslinked with HDDP. Upon addition of the NPs solution to the protein solution, it turned turbid, indicating protein or NPs aggregation. Nevertheless, PNCs with comparable size of 328 nm and partly loaded with CMPVA@Fe_3O_4-NPs could be obtained as observed in DLS and EM (Figure 82), indicating aggregation of NPs rather than protein in the disperse phase. Although loaded PNCs could be separated from empty ones by magnetic decantation, a high amount of CMPVA@Fe_3O_4-NPs were not encapsulated and accumulated on the surface of the PNCs as seen in the scanning electron micrograph (Figure 82B). Additionally, loaded PNCs could not be transferred into water by surfactant exchange (0.1 wt% SDS) and PNCs aggregated in water after evaporation of cyclohexane (Figure 82A, blue curve). One reason could be the adsorption of SPIONs on the PNCs surface, changing its interaction with the surfactant and surface stability in water.

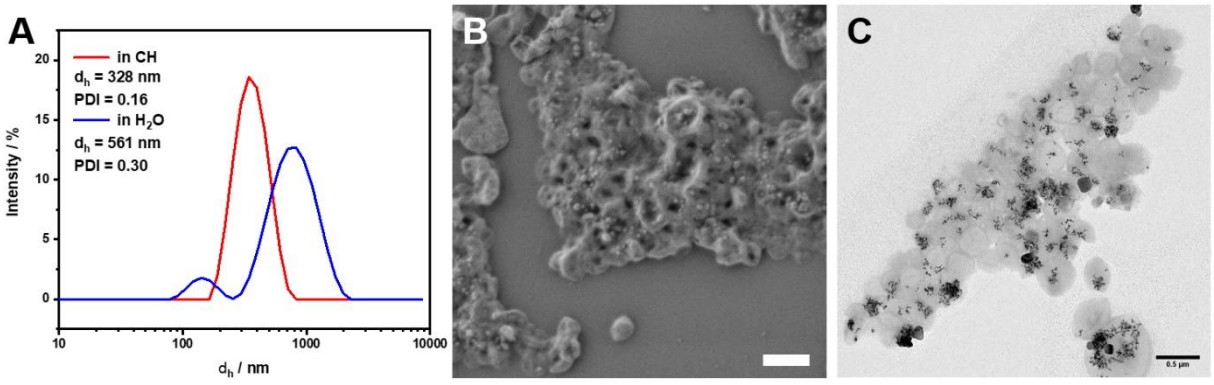

Figure 82. A) Dynamic light scattering; B) Scanning electron and C) Transmission electron micrograph of CMPVA@Fe_3O_4-NPs-loaded protein nanocarriers prepared with PBS, in cyclohexane (red) and water (blue). Scale bar: 0.5 µm.

In comparison to PNCs prepared with TDI, proteins for the crosslinking with HDDP were functionalized with azide-groups. To increase the stability of modified protein, the protein was dissolved in a phosphate buffer. A reason for the aggregation of CMPVA@Fe_3O_4-NPs upon addition to the protein solution could be their instability in salt-containing solutions. Therefore, the protein was dissolved in deionized water instead of PBS buffer and upon addition of CMPVA@Fe_3O_4-NPs, the dispersion maintained stable and no aggregated could be observed. The formation of PNCs crosslinked with HDDP with the salt-free protocol lead to stable PNCs, which could be transferred into water and a size of approx. 350 nm with 0.22 PDI was observed in DLS (Figure 83A). EM revealed a prominent core-shell morphology of PNCs and efficient loading of CMPVA@Fe_3O_4-NPs with almost no free magnetic NPs in the dispersion (Figure 83B+C).

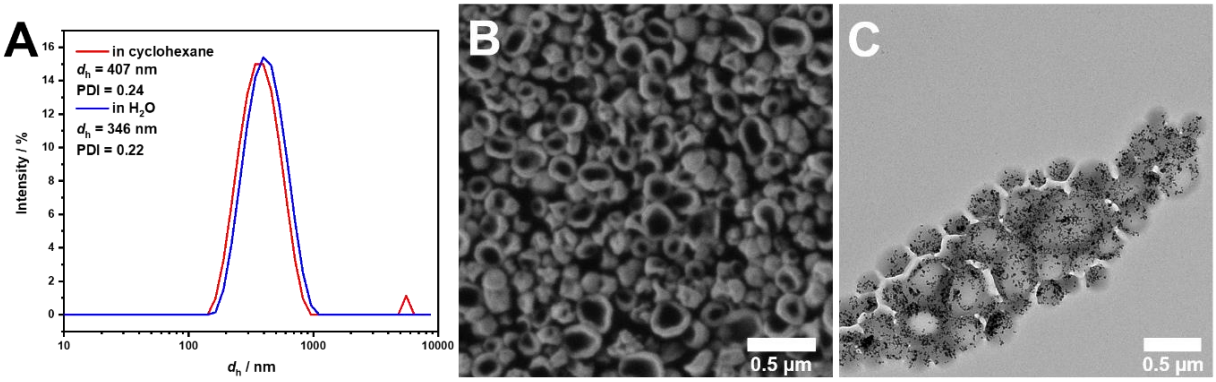

Figure 83. A) Dynamic light scattering; B) Scanning electron and C) Transmission electron micrograph of CMPVA@Fe_3O_4-NPs-loaded protein nanocarriers prepared without salt, in cyclohexane (red) and water (blue). Scale bar: 0.5 µm.

CMPVA@Fe_3O_4-NPs could successfully be encapsulated into PNCs crosslinked with unselective crosslinker TDI as well as selective dialkyne HDDP through interfacial shell formation in inverse miniemulsion. The modified PNCs could be used to investigate protein corona formation and cell-carrier in the next step.

III. D2.3. Plasma Protein Corona and Cellular Uptake of Protein Nanocarriers

If nanocarriers are to be applied for clinical therapy such as nanovaccines, their fate in the body and interaction with biological fluid and cells have to be investigated to increase their delivery efficiency. One of the in vivo phenomena after administration into the blood is the adsorption of proteins forming a so-called protein corona around the NCs. The formation and composition of the protein corona depends on the composition of the nanocarriers' surface and influences the bio-distribution and cell uptake of the NCs.[259, 261] Therefore, the formation of a protein

corona and its composition on the PNCs was investigated. PNCs crosslinked with unselective TDI should have another surface composition than crosslinking with selective HDDP, influencing the protein corona formation and cellular uptake. Due to modification of protein nanocarriers with magnetic properties by encapsulation of CMPVA@Fe_3O_4-NPs, PNCs could easily be magnetically separated from blood media as well as after uptake into cells.

The amount of adsorbed protein on the PNCs surface after incubation into human blood plasma was determined by Pierce assay (Figure 84A). Protein nanocarriers in general adsorbed low amount of proteins with less than 0.2 mgm^{-2} compared to model nanocarriers such as polystyrene (PS) nanoparticles (300 mgm^{-2}) and even PS-NPs already functionalized with stealth polymer PEG (1.1 mgm^{-2}). No difference in amount of protein adsorption could be observed for PNCs crosslinked with TDI or HDDP. The formed protein corona of the PNCs was investigated by SDS-PAGE and the protein composition revealed with LC-MS. After incubation of PNCs in blood plasma, the pattern of protein composition observed by SDS Page showed a richer composition for PNCs crosslinked with HDDP compared to TDI. For analysis of the protein corona composition, label-free mass spectrometry was used after detachment of the protein corona from the PNCs by SDS solution (Figure 84B). All identified proteins were divided into seven groups and the respective composition displayed in percentage. A significant difference in the protein corona composition between polystyrene NPs and protein NCs could be observed, where PS-NPs mostly adsorbed lipoproteins. Protein nanocarriers demonstrated a broader protein composition pattern with the dominant proteins being immunoglobulins and complement proteins. There was a slight difference between TDI and HDDP crosslinked PNCs as PNCs-HDDP revealed an enriched adsorption of complement proteins and PNCs-TDI enriched immunoglobulin Ig kappa. Proteins from the complement system and immunoglobulins might mediate the interaction with phagocytic cells leading to unspecific uptake and short blood circulation times.[261] Therefore, protein nanocarriers independent of crosslinker should be functionalized with stealth polymers such as polyethylene glycol to decrease protein adsorption and increase higher targeting efficiency with longer blood circulation time.

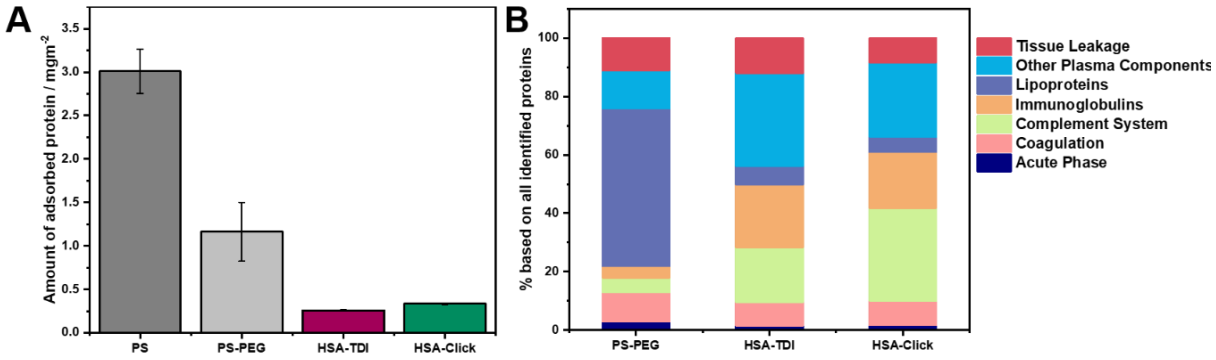

Figure 84. A) Absolute amount of corona proteins adsorbed onto nanocarriers after incubation in blood plasma (mgm^{-2} surface) determined by the Pierce assay (n = 3) B) Corona proteins adsorbed onto nanocarriers identified by quantitative LC-MS were classified into seven different groups according to their biological functions. Data from [redacted].

The cell uptake of PNCs crosslinked with unselective TDI compared to biorthogonal HDDP was investigated in different biological media. All PNCs interacted strongly with RAW264.7 macrophages as predicted from the protein corona composition with enriched complement proteins and immunoglobulins (Figure 85). PNCs crosslinked with HDDP demonstrated high uptake of over 90% already after 2 h independent of the incubation media. PNCs crosslinked with TDI were less uptaken by macrophages and showed a decrease in uptake after incubation with blood serum and plasma, respectively. The uptake experiments into macrophages revealed the findings in the corona composition where PNCs crosslinked with HDDP strongly enriched complement proteins on their surface compared to TDI crosslinked PNCs. The small difference in corona composition led to a significant difference in the unspecific uptake by macrophages. The results from the corona composition as well as cell uptake demonstrated that the surface composition of the PNCs crosslinked with TDI and HDDP, respectively, were not the same. As assumed, an unselective side reaction of TDI with itself lead to patches of polyurethane on the surface of PNCs, influencing the protein adsorption and cellular uptake of PNCs. If PNCs crosslinked with HDDP were to be used as nanocarriers to target dendritic cells, the PNCs have to be surface-functionalized with stealth polymers to hamper the high unspecific cell uptake of PNCs-HDDP into macrophages.

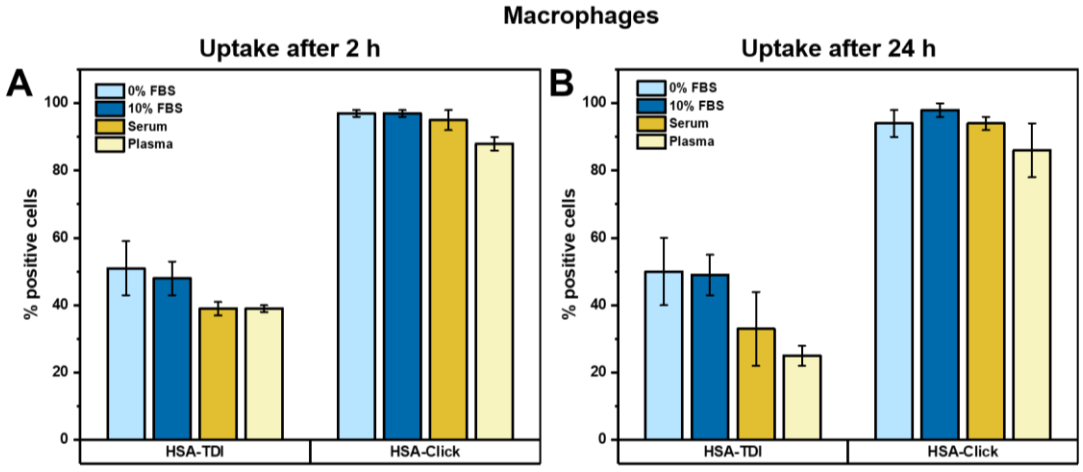

Figure 85. Cell uptake of protein nanocarriers crosslinked by click chemistry versus 1,4-toluene diisocyanate (TDI) into RAW264.7 after incubation in different media, A) uptake after 2 h and B) uptake after 24 h. Data from [redacted].

The cell uptake of PNCs into HeLa cells showed after 2h in both cases no interaction of PNCs and HeLa cells (Figure 86). After 24 h a significant increase of uptake could be observed for PNCs-HDDP without and with prior incubation in 10% FBS. In general, incubation of the PNCs in blood serum and plasma, respectively, reduced the cellular uptake towards HeLa cells. If PNCs were to be used as nanocarriers to target cancer cells, the PNCs have to be surface-functionalized with cancer-specific targeting moieties to promote uptake into cancer cells.

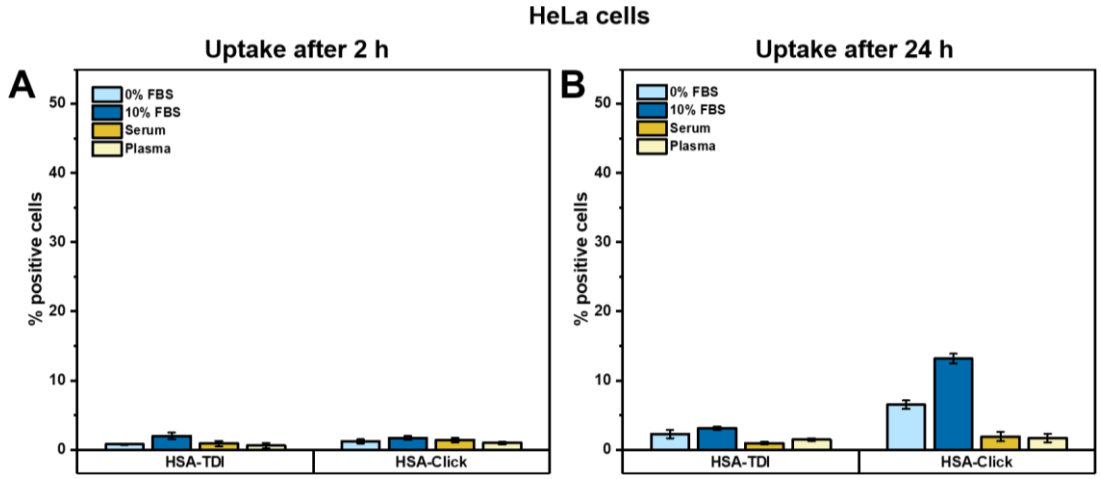

Figure 86. Cell uptake of protein nanocarriers crosslinked by click chemistry versus 1,4-toluene diisocyanate (TDI) into HeLa cells after incubation in different media, A) uptake after 2 h and B) uptake after 24 h. Data from [redacted].

The investigation of the protein corona formation and composition as well as the uptake of PNCs into macrophages and HeLa cells revealed the need for surface modification with stealth and targeting properties to enhance the delivery efficacy of PNCs. Since PNCs were applied successfully to analyze plasma protein formation and cellular uptake, PNCs loaded with

CMPVA@Fe_3O_4-NPs could be used to study the intracellular trafficking and formation of an intracellular protein corona.

III. D.2.4. Intracellular Protein Corona and Cellular Uptake of Protein Nanocarriers

The plasma protein corona mediated the uptake of PNCs into macrophages and HeLa cells. On their journey into the cell, PNCs encounter a change in biological environment and a change in the protein corona composition could be induced. A different protein corona could on one hand influence the uptake pathway of PNCs into the cells. On the other hand, the IPC indicates footprints, revealing in which cell compartments the PNCs have been present upon internalization. The information about the uptake mechanism and further processing of the PNCs in cells could assist in the tailored design of optimal nanocarriers. Therefore, PNCs were modified with magnetic and fluorescent properties by encapsulation of CMPVA@Fe_3O_4-NPs and fluorescent dye Cy5-Oligo to study cell uptake and intracellular trafficking in dendritic cells (DCs).

Viability experiments of DCs after incubation with CMPVA@Fe_3O_4-NPs-loaded PNCs revealed no cytotoxicity induced by PNCs, even with increased concentrations of PNCs, while the control treated with 20% DMSO decreased the viability greatly (Figure 87A). The use of proteins as nanocarrier materials promoted high biocompatibility of the PNCs. The cell uptake of CMPVA@Fe_3O_4-NPs-loaded PNCs increased concentration-dependent and time-dependent, measured by the Cy5 fluorescence in flow cytometry after DCs were incubated with PNCs for 2 h and 24 h, respectively (Figure 87B). The incubation of PNCs in cell culture medium supplemented with 5% fetal bovine serum (FBS) to form a protein corona during cell incubation did not affect the cell uptake after 2 h. After 24 h incubation, a protein corona on the PNCs induced a reduced cell uptake compared to PNCs in cell culture medium without FBS (Figure 87C). The cell uptake of PNCs (250 µg/mL) was performed with continuous incubation and removal of PNCs after 2 h (Figure 87D). Both experiments revealed fast uptake rates of PNCs during the first 2 h. A continuous incubation mediated continuous uptake until the cells internalized all PNCs, indicated with a plateau of Cy5-positive cells. Removal of PNCs after 2 h demonstrated exocytosis of PNCs after 4 h, indicated by decrease of Cy5-signal in PNCs-containing cells. The cell uptake experiments, analyzed by flow cytometry, already indicated a cell-carrier interaction where the PNCs were successfully taken up and processed in the DCs.

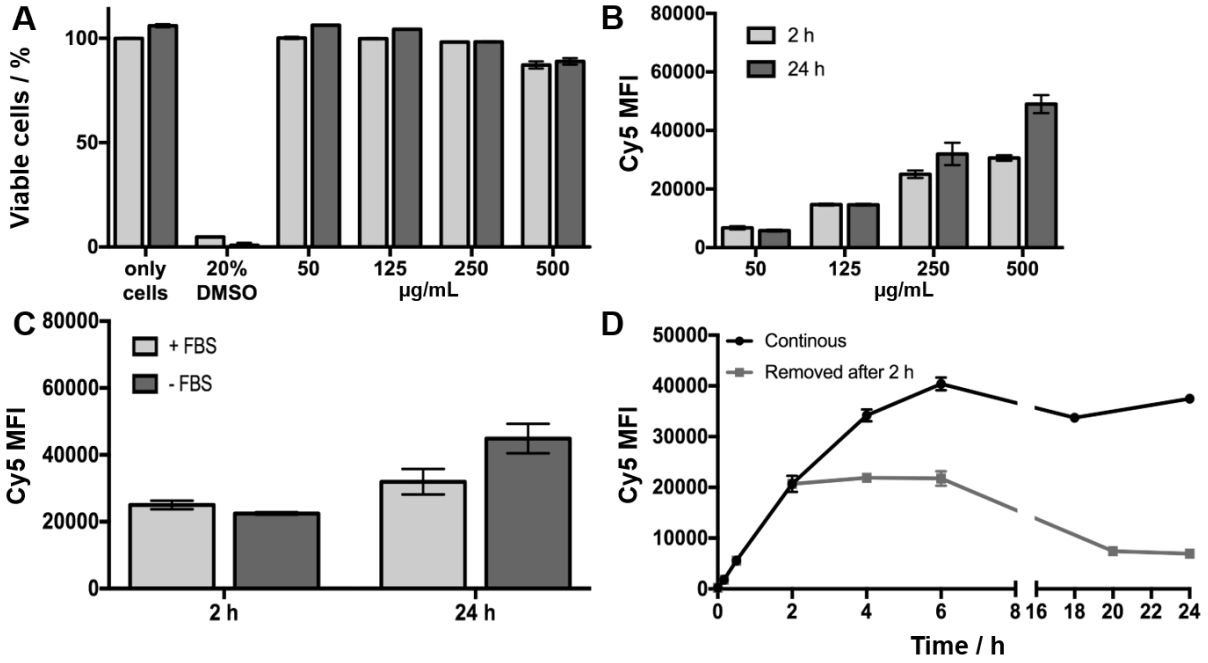

Figure 87. A) Viability of cells after incubation with CMPVA@Fe_3O_4-NPs-loaded protein nanocarriers. Uptake of CMPVA@Fe_3O_4-NPs-loaded protein nanocarriers B) with different concentrations into dendritic cells after 2 h and 24 h. C) treated with and without 5% FBS in the cell culture medium; NP concentration 250 µg/mL. D) Over time without (black) and with (grey) removal of NCs after 2h; measured by the median fluorescence intensity (MFI) of Cy5-Oligo. Data from [redacted].

Microscopic analysis with transmission electron microscopy (TEM) and confocal laser scanning microscopy (cLSM) visualized the cell-carrier interaction (Figure 88). The high contrast of CMPVA@Fe_3O_4-NPs encapsulated into the PNCs in TEM allowed identification and tracking of PNCs upon cell uptake and intracellular processing. Upon addition of CMPVA@Fe_3O_4-NPs-loaded PNCs to the cell medium, the uptake mechanism of DCs for PNCs could be observed as a zipper-like mechanism on the cell surface around the PNCs indicating an uptake by phagocytosis (Figure 88A), correlating with prior TEM visualizations of phagocytosis events.[7] The encapsulation of Cy5-Oligo enabled the identification of PNCs after internalization into DCs. As demonstrated by cLSM, the yellow-marked PNCs were detected inside the cells, whereas the cell membrane was marked pink and the cell nucleus blue (Figure 88B). After a successful uptake of PNCs into DCs, the intracellular fate of the PNCs was visualized by TEM. The PNCs could easily be identified due to the high contrast of encapsulated SPIONs. The evaluation of the micrographs of DCs treated with CMPVA@Fe_3O_4-NPs-loaded PNCs revealed presence of PNCs in endosomal compartments of the cell among others (Figure 88C). Moreover, after fusion of late endosomes with lysosomes to endolysomes (Lys) the PNCs came into a cell milieu with enzymes and acidic pH, where PNCs probably are degraded and cargo molecules released.

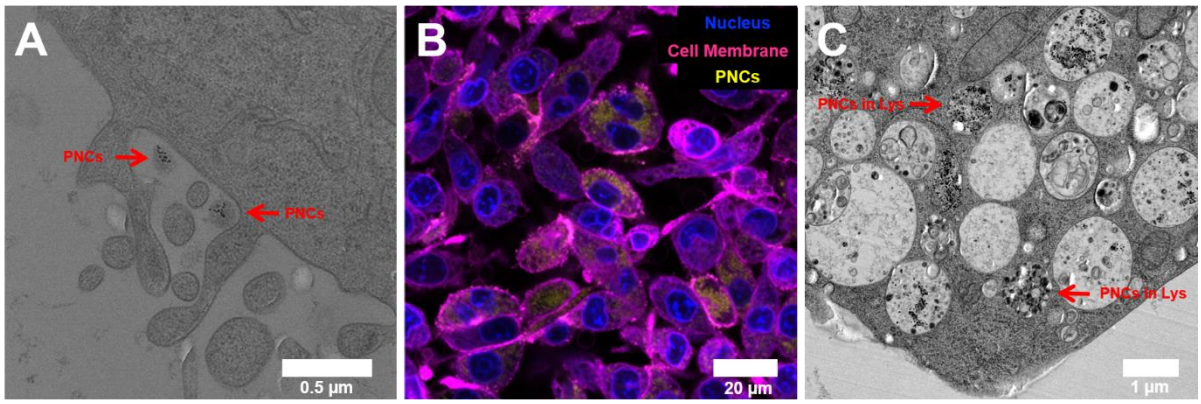

Figure 88. A) Transmission electron micrograph of cell about to internalize CMPVA@Fe_3O_4-NPs-loaded protein nanocarriers (mPNCs) by phagocytosis. B) mPNCs uptaken into cells and visualized by cLSM. C) Transmision electron micrograph of mPNCs internalized into endolysosomes (Lys) of cells. Images from [redacted].

While electron microscopy allows visual analysis of cell-carrier interaction, the intracellular protein corona formed during internalization of PNCs into DCs could give more information about the uptake and processing route. The magnetic properties of PNCs due to loading with CMPVA@Fe_3O_4-NPs enabled a magnetic separation of uptaken PNCs from cellular debris after cell lysis. After lysis of the PNC loaded DCs, the PNCs were collected magnetically after being released from the cells by cell lysis (Figure 89A). The protein-coated PNCs were purified from the cell media by magnetic decantation and the intracellular protein corona on the PNCs obtained through heating in SDS solution. An SDS-PAGE of the intracellular protein corona revealed a difference in protein composition between 2 h and 24 h uptake, indicating a dynamic protein corona and change of environment during internalization of PNCs into DCs (Figure 89B). Further proteomic analysis could give an overview over the protein composition of the ICP and correlating with knowledge over occurrence of proteins in specific compartments, a tracking profile of PNCs upon internalization into DCs could be created.

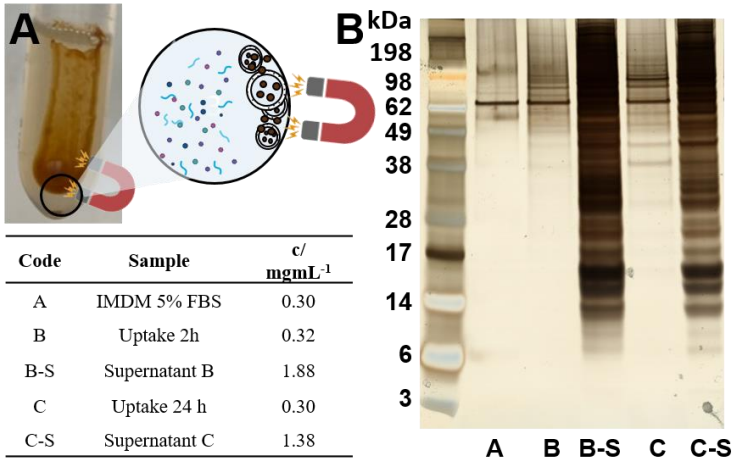

Code	Sample	c/ mgmL^{-1}
A	IMDM 5% FBS	0.30
B	Uptake 2h	0.32
B-S	Supernatant B	1.88
C	Uptake 24 h	0.30
C-S	Supernatant C	1.38

Figure 89. A) Magnetic collection of CMPVA@Fe_3O_4-NPs-loaded protein nanocarriers after uptake into cells and cell lysis. B) SDS-PAGE of intracellular protein corona on CMPVA@Fe_3O_4-NPs-loaded PNCs after uptake into cells. Figure partly created with BioRender.com by Natkritta Hüppe. Data from [redacted].

The modification of protein nanocarriers with CMPVA@Fe_3O_4-NPs provided a strategy to study intracellular uptake and protein corona formation of PNCs interacting with DCs. The high contrast of SPIONs in TEM allowed visualization of PNCs during the cell-carrier interaction and PNCs were easily separated from the cell debris after cell lysis. The intracellular protein corona could be studied due to the superparamagnetic properties of PNCs. Although *in vitro* cell uptake studies demonstrated high uptake rates of PNCs into DCs, *in vivo* targeting of DCs might fail due to high unspecific uptake into macrophages as revealed by plasma protein corona analysis. Therefore, PNCs were modified with stealth and targeting moieties on their surface to promote long circulation times and high targeting efficiency into DCs.

III. D3. Surface Modification of Protein Nanocarriers

Developed nanovaccine, composed of adjuvant-loaded ovalbumin nanocarriers, proved a high anti-tumor immune response due to efficient DC-mediated T cell stimulation *in vitro* as well as in an *in vivo* mouse model. Compared to a subcutaneous administration, an intravenous injection could mediate the accumulation of therapeutic PNCs in the lymph nodes where the immune cells are located, increasing the stimulating efficiency of adjuvant-loaded PNCs. However, injection into the blood circulation systems means contact of PNCs with blood components including proteins and phagocytic cells that could lead to unspecific uptake and fast excretion of PNCs. Efficient delivery of nanovaccines is crucial to induce a robust anti-tumor immune response. Therefore, the PNCs had to be modified with stealth moieties to enhance blood circulation time and prevent unspecific uptake. Additionally, dendritic-cell specific antibodies, such as CD11c, promote receptor-mediated uptake of antibody-modified PNCs into DCs.[271, 272]

III. D3.1. Modification with Stealth Polymers

Low affinity to blood proteins affects the formation of protein corona on nanocarriers and mediates the cell-carrier interaction. The importance of the protein corona in understanding the biological fate of the nanocarriers has opened up a new field to control the protein corona formation by modifying the nanocarriers.[273] Many studies have proven the ability of polymers such as PEG to promote stealth properties when functionalized on the surface of NCs. Therefore, protein nanocarriers were modified with polyethylene glycol and the influence of surface modification on the unspecific cell uptake into macrophages was investigated. Due to the naturally high number of amine groups on proteins, PNCs could be modified with PEG

through NHS-reaction of *N*-hydroxysuccinimid-polyethylene glycol-methylene oxide (NHS-PEG-MeO) with the amines on the NCs surface under basic conditions (Scheme 19).

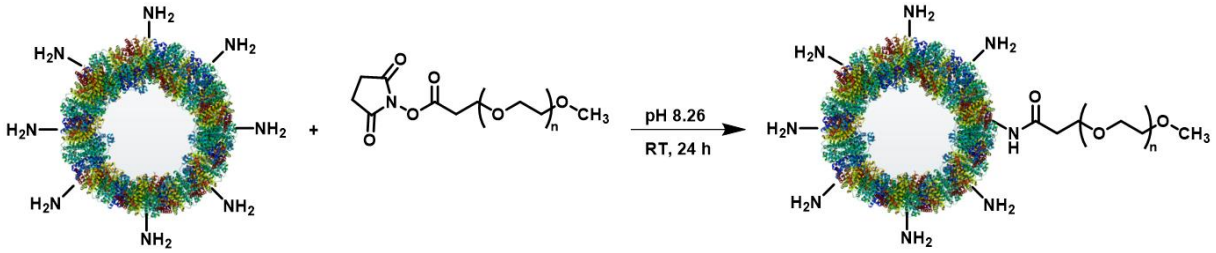

Scheme 19. Surface functionalization of protein nanocarriers with *N*-hydroxysuccinimid-polyethylene glycol-methylene oxide under basic conditions (NHS-PEG-MeO). Protein structure was obtained from DrugBank online (https://go.drugbank.com/drugs/DB00062, 28.11.2021) and was adapted.

PEG with two molecular weights, namely 2 and 5 kDa, were chosen and added to the PNCs in different PEG/NH_2 ratios to obtain different densities of PEG chains on the PNCs surface (Table 22). Successful PEGylation of PNCs was confirmed by fluorescamine assay, where a decreased number of amines could be determined for PNCs after reaction with NHS-PEG-MeO. A higher ratio of PEG to amines achieved higher PEGylation rates of PNCs in both cases with PEG-2kDa and PEG-5 kDa. Therefore, the density of PEG chains per nm^2 carrier was 0.3 chains for 0.5 eq. PEG and 1.5 chains for 50 eq. PEG. There was no significant difference for the PEGylation efficiency between the PEG with different molecular weights.

Table 22. Analytical data of surface-functionalized protein nanocarriers with *N*-hydroxysuccinimid-poly(ethylene glycol-methylene oxide) (NHS-PEG-MeO) in different ratios and molecular weights.

Sample	**M_w (PEG) /gmol^{-1}**	**PEG:NH_2**	**NH_2 /carrier**	**PEG chain / carrier**	**PEG chain / nm^2**
$OVA_{pristine}$	-	-	$2.82 \cdot 10^5$	-	-
OVA_{PEG}	2 000	0.5	$2.42 \cdot 10^5$	40 000	0.32
OVA_{PEG}	2 000	50	$9.30 \cdot 10^4$	189 000	1.50
OVA_{PEG}	5 000	0.5	$2.37 \cdot 10^5$	45 500	0.36
OVA_{PEG}	5 000	50	$9.01 \cdot 10^4$	191 900	1.52

The uptake of PNCs functionalized with PEG into RAW264.7 cells was investigated for the different PEG densities (Figure 90). In case of the low PEG density of 0.32 chains/nm^2, no stealth effect and decreased uptake was observed and over 50% for PEG-2 kDa and almost 80% for PEG-5 kDa of PNCs were taken up into the macrophages. In fact, pristine PNCs showed

lower unspecific uptake than PNCs modified with a low density of PEG. As described by Li *et al.*, the density of PEG chains on the NCs surface influences the conformation of the chains on the surface and thus mediates the stealth effect towards phagocytic cells.[274] The authors revealed that the PEG conformation changed from a mushroom brush to a dense brush with increasing the PEG chain density. A dense brush above 0.5 chains/nm^2 demonstrated a decreased unspecific cell uptake into macrophages. A significant stealth effect and decreased uptake was observed for PNCs with 1.5 PEG chains/nm^2 due to the described formation of a dense PEG brush on the PNCs, influencing the protein corona formation. The highest stealth effect was achieved for PEG-5 kDa with a PEG density of 1.5 chains/nm^2 and less than 5% PNCs were uptaken into RAW264.7 cells.

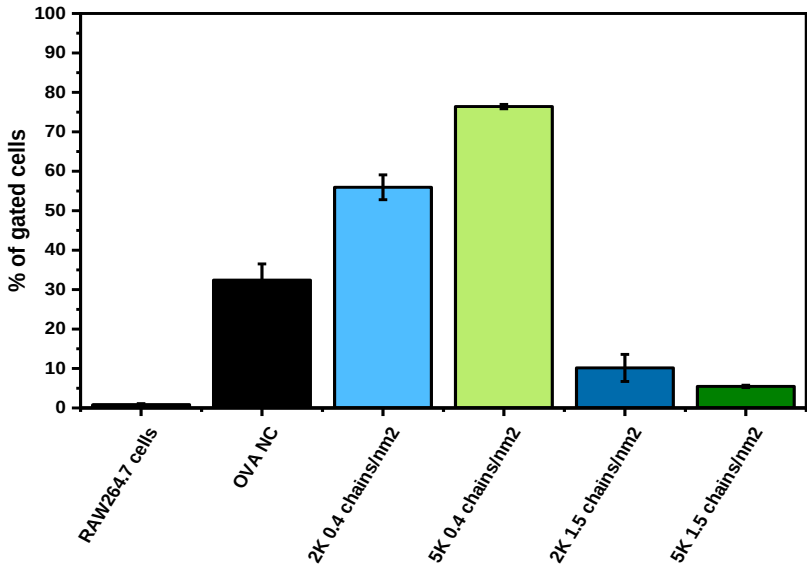

Figure 90. Uptake of protein nanocarriers with and without polyethylene glycol (2 and 5 kDa) on the surface into RAW264.7 cells, measured by fluorescence of Cy5-positive cells. Data from [redacted].

Surface functionalization of PNCs with PEG led to higher stealth effect with inhibited unspecific uptake into macrophages. A higher density of PEG chains on NCs surface (1.5 chains/nm^2) achieved the highest stealth effect. PEG was until recently the gold standard as a stealth polymer, but the polymer has risen concerns about its degradability and immugenicity. Therefore, more biocompatible and degradable alternatives should be found as stealth polymers. Polyphosphoesters (PPEs) have demonstrated their high stealth ability comparable with PEG.[263] PPEs have the advantage that they are biocompatible and compared to PEG degradable.[275] So far, PPEs have only been used on model nanocarriers such as polystyrene nanoparticles. Next, the stealth property of PPEs should be transferred to nanocarriers that could be used in clinical applications such as developed protein nanocarriers.

III. D3.2. Targeting with Antibodies

Modification of nanocarriers with cell-specific antibodies enhances specific targeting to desired cells and increases the delivery efficiency. Dendritic cells as antigen-presenting cells play a crucial role in antigen-specific anti-tumor responses.[232] Different surface receptors on the cell promote specific uptake, for example, on dendritic cells, those include, CD11c, CLEC 9A, or DC-SIGN.[253, 276] The orientation of antibodies on the nanocarriers' surface mediates the specificity of uptake, where the Fc part of the antibody promotes an unspecific uptake through Fc receptors, present also on phagocytic cells. To ensure a specific targeting of dendritic cells, the respective antigen-binding region, namely the Fab part, of the antibody has to be accessible. Therefore, Brückner *et al.* developed an efficient strategy for site-specific functionalization of antibodies onto nanocarriers.[256] The antibodies were functionalized with azide moieties at a characteristic *N*-gylcosylation pattern at the Fc part. The antibody was attached to the surface through a chemoselective azide-alkyne click reaction, where a site-specific conjugation promotes an orientation of the Fab region outwards and thus a specific dendritic cell targeting. Further, *in vivo* studies demonstrated a successful antibody-mediated cell uptake through the CD11c surface receptor on DCs, despite the formation of a protein corona upon intravenous injection.[252] The site-specific antibody functionalization was now transferred from the model nanocarrier mgHES (hydroxyethylstarch coated magnetite nanoparticles) to protein nanocarriers to achieve a specific targeting of adjuvant-loaded PNCs to DCs and enhance anti-tumor vaccination.

a) Surface Functionalization with DBCO Groups

For the functionalization with antibodies *via* site-click reaction, alkyne groups are needed on the surface of the nanocarriers. The protein nanocarriers bearing amino-groups on the surface were functionalized *via* NHS chemistry with dibenzocyclooctine (DBCO) moieties (Scheme 20).

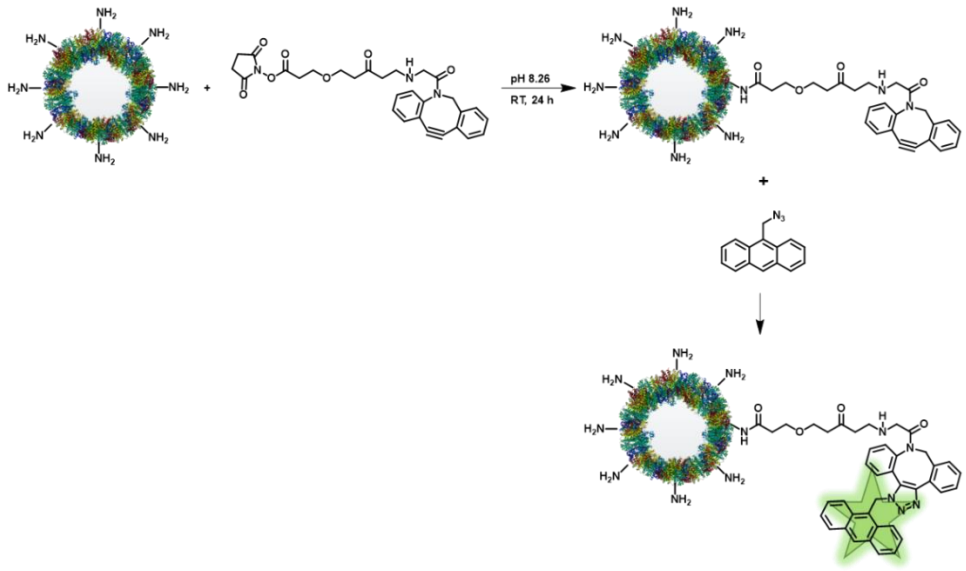

Scheme 20. Surface functionalization of protein nanocarriers with DBCO groups by dibenzocyclooctin-N-hydroxysuccinimidylester (DBCO-NHS) and quantification of DBCO groups by anthracene-azide. Protein structure was obtained from DrugBank online (https://go.drugbank.com/drugs/DB00062, 28.11.2021) and was adapted.

The number of alkyne groups on the PNCs can be determined with anthracene-azide, which forms a fluorescent product (λ_{ex} = 370 nm, λ_{em} = 418 nm) when reacting with alkyne-groups by azide-alkyne click chemistry.[277] The increase in fluorescence corresponds to the amount of reacted alkyne groups (equation 1):

$$n_{\text{reacted azido}} = \left(\frac{\Omega}{48}\right) \cdot n_{\text{Anth}-N_3} \text{ with } \Omega = \frac{I}{I_0} \qquad \text{eq.1}$$

First, the amount of remaining amines on the PNCs surface was determined by fluorescamine assay using glycine as a standard substrate and lysozyme as a reference substrate. The ovalbumin nanocarriers were crosslinked with 10 eq. HDDP and afterwards possessed $2 \cdot 10^6$ amines per nanocarrier (Table 23).

Table 23. Amount of amines on the surface of ovalbumin nanocarriers determined with fluorescamine assay.

	M /gmol^{-1}	**HDDP / eq.**	**$N_{theo}(NH_2)$/ protein**	**$N_{ex}(NH_2)$ /protein**	**$N_{ex}(NH_2)$ /mg NC**	**$N_{ex}(NH_2)$ /NC**
OVA, nat.	42800	-	20	19	-	-
OVA-N_3	42800	-	20	6	-	-
OVA-NC	42800	10	20	5	$5 \cdot 10^{16}$	$2 \cdot 10^6$
Lysozyme	14300	-	6	6	-	-

The OVA-HDDP NCs were functionalized with DBCO-PEG4-NHS ester (2 eq. to amine groups) over night and after washing through a centrifuge filter (MWCO 3K), the amount of

DBCO on the surface was determined with the anthracene-azide. The increase in fluorescence corresponds to the amount of reacted alkyne groups (equation 1). An increase in fluorescence was observed after the reaction of PNCs-DBCO with anthracene azide, indicating the presence of alkynes on the NCs surface. The amount of reacted azide groups corresponded to $7 \cdot 10^5$ DBCO groups per nanocarrier and 35% of amines were conjugated with DBCO moieties (Table 24). Additionally, the supernatant from the reaction dispersion was analysed and an excess of DBCO groups corresponding to $1.5 \cdot 10^{16}$ reacted azides were determined. The blank nanocarriers did not result in an increase of fluorescence, meaning no anthracene azides were attached to the PNCs without DBCO.

Table 24. Fluorescence intensity measured for anthracene azide ($23*10^{-3}$ mg), blank (0.2 wt% NC dispersion) and sample ($23*10^{-3}$ mg Anth-N3 + 0.2 wt% NC-DBCO dispersion); λ_{ex} = 370 nm, λ_{em} = 418 nm.

Sample	**HDDP**	$N_{ex}(NH_2)$/NC	I_0 (Anth-N_3)	I_{blank}	I	N(reac.N_3)	N(DBCO)/NC
1	10 eq.	$2 \cdot 10^6$	2600	1100	3800	$2.8 \cdot 10^{15}$	$7 \cdot 10^5$
2*	10 eq.	$2 \cdot 10^6$	2600	-	19800	$1.5 \cdot 10^{16}$	-

*supernatant of sample 1

DBCO-NHS ester were added to the PNCs in different ratios to the amount of amine groups (Table 25). A ratio of 0.5 eq. DBCO with 2% led to the lowest conversion of amine groups and approx. 38000 DBCO groups were quantified on the PNCs. With an increasing amount of DBCO, the conversion of amines increased, while the conversion of DBCO was between 20-30% in all cases. With an excess of 4 eq. DBCO, 70% amine groups were conjugated with DBCO corresponding to approx. 106 groups. However, when a ratio of 6:1 was used, the number of DBCO determined on the PNCs exceeded the number of amines, resulting in 125% amine conversion. The exceeding amount of DBCO indicates that at high excess the DBCO moieties adsorb to the PNCs surface and could not be removed by three times centrifugation.

Table 25. Amount of DBCO groups on protein nanocarriers with $2 \cdot 10^6$ amine groups, determined with anthracene assay.

Ratio DBCO / eq.	DBCO / NC	Conversion DBCO / %	Conversion NH_2 / %
0.5	$3.75 \cdot 10^4$	39	2
1	$1.63 \cdot 10^5$	35	8
2	$5.50 \cdot 10^5$	25	28
4	$1.40 \cdot 10^6$	21	70
6	$2.51 \cdot 10^6$	25	125

b) Surface Functionalization with Antibodies

To study the antibody-mediated specific targeting of dendritic cells, protein nanocarriers were functionalized with purified anti-mouse CD11c-antibodies, binding to CD11c-expressing DCs. An isotype antibody, here the purified Armenian hamster IgG Isotype Ctrl antibody, was used as a control, because its composition (class and type) matches to the CD11c-antibodies, with a lack of specificity to the target. For this reason, the isotype control allowed the differentiation between non-specific Fc-directed uptake from specific Fab-mediated uptake. Due to the DBCO groups on the PNCs surface, azide-modified antibodies could be attached site-specifically to the surface metal-free *via* strain-promoted azide-alkyne click chemistry (Scheme 21). The PNCs were loaded with CMPVA@Fe_3O_4 NPs to allow magnetic purification of antibody-modified PNCs from the reaction solution with unreacted antibodies.

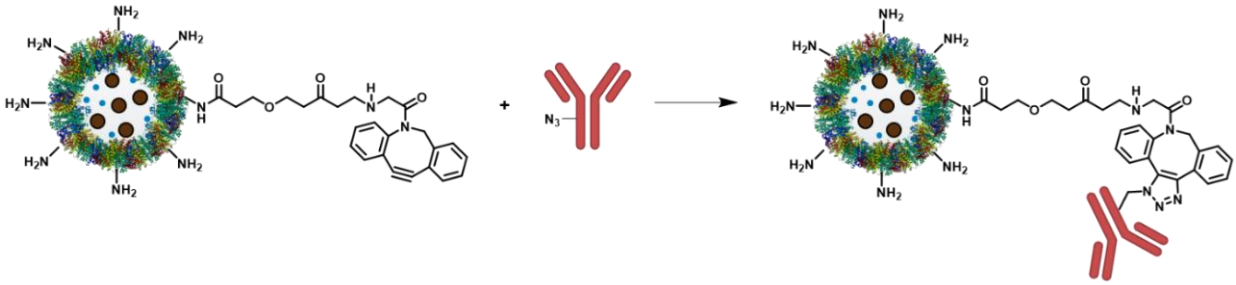

Scheme 21. Site-specific antibody functionalization of CMPVA@Fe_3O_4 nanoparticles-loaded protein nanocarriers bearing DBCO groups *via* strain-promoted azide-alkyne click chemistry. Protein structure was obtained from DrugBank online (https://go.drugbank.com/drugs/DB00062, 28.11.2021) and was adapted. Figure (antibody) partly created in BioRender.com by Natkritta Hüppe.

The amount of CD11c-antibodies on the PNCs surface was verified with a fluorescein isothiocyanate-labelled (FITC) secondary antibody test by flow cytometry (Figure 91A). A concentration-dependent increase of FITC fluorescence was observed with increased amount

of antibody added to the PNCs. A negative control with naked OVA-NCs and DBCO-functionalized OVA-NCs only weakly bound anti-hamster FITC, displayed in almost no fluorescence observed by flow cytometry. The DBCO-functionalized PNCs were conjugated with the targeting antibody CD11c as well as the isotype control IgG in two concentrations to investigate a concentration-dependent specific uptake into DCs. The CD11c-targeting experiments showed an increased uptake of OVA-NCs into DC2.4 cells when functionalized with the antibody (Figure 91B). No concentration-dependent uptake was observed as the NCs reacted with 10 µg antibodies lead to a similar uptake compared to 50 µg, for CD11c and IgG, respectively. In comparison, no significant increase in uptake was obtained for naked and DBCO-functionalized PNCs. Incubation of antibody-modified PNCs in FBS resulted in comparable uptake as PNCs without FBS, indicating that a formation of a protein corona around the PNCs did not have an effect on their uptake. However, high specific Fab-directed uptake could not been proven as PNCs functionalized with the isotype control resulted in an increased uptake as well, not significantly less than with the targeting antibody.

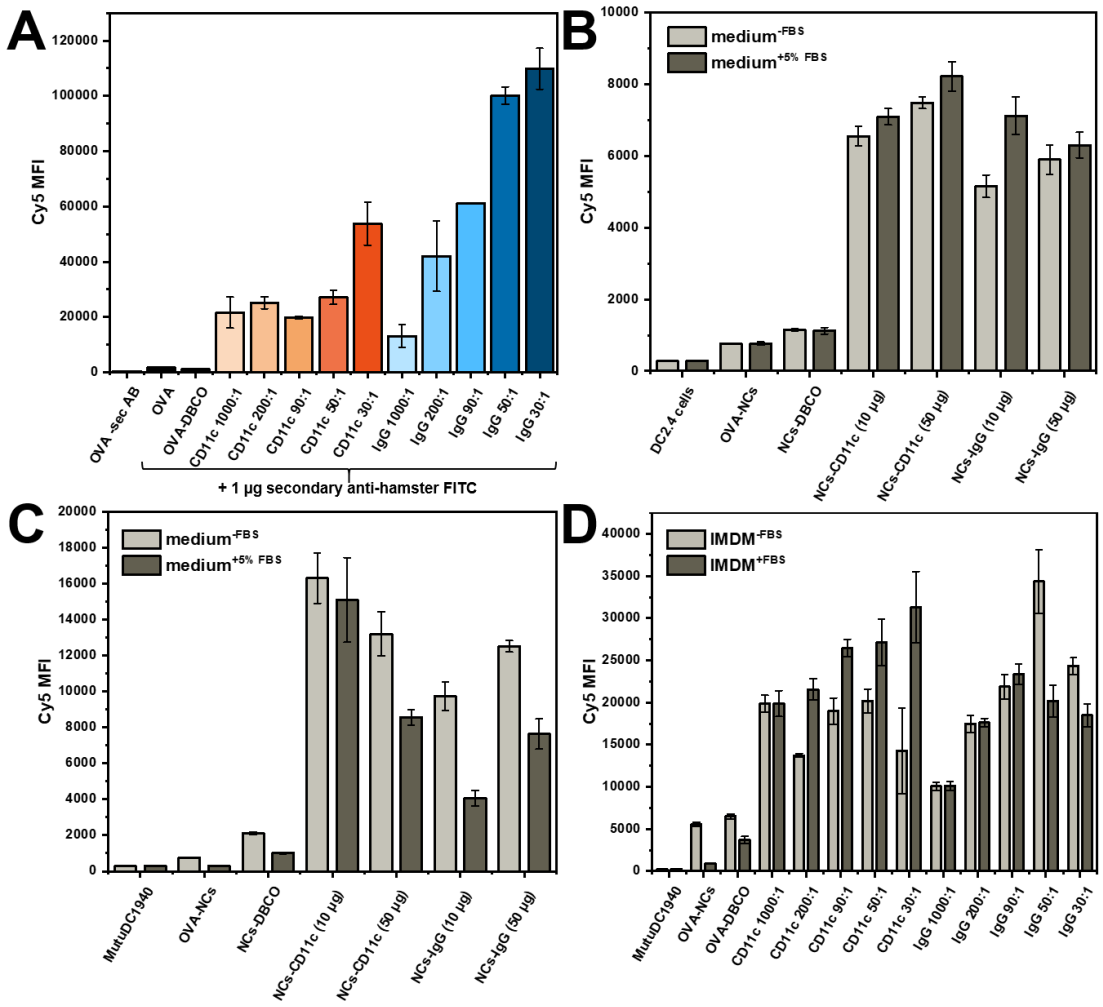

Figure 91. A) Antibody detection on protein nanocarriers by secondary antibody test. Uptake of CD11c-antibody-functionalized protein nanocarriers treated with and without FBS into B) DC2.4 cells. C) MutuDC1940 cells D) into MutuDC1940 after Fc-receptor blocking. Data from [redacted].

Because no specific CD11c-promoted uptake into DC2.4 cells could be proven for PNCs, another dendritic cell line was tested. The MutuDC1940 are splenic dendritic cells derived from CD11c:SV40LgT transgenic mice, expressing a high concentration of CD11c-receptors. The uptake experiments of antibody-modified OVA-NCs into MutuDC1940 revealed an increased uptake of NCs into DCs (Figure 91C). Here, the lower concentration of CD11c lead to a higher uptake compared to 50 µg antibody. While FBS incubation had no influence on the uptake of NCs-CD11c (10 µg), a decreased uptake was observed for NCs-CD11c (50 µg) with a protein corona. The isotype control achieved as well increased uptake of NCs-IgG into MutuDC1940 with a significant concentration-dependence and influence of FBS. More importantly, the uptake of NCs-CD11c into MutuDC1940 was significantly higher compared to IgG-modified NCs, indicating an increased contribution of specific Fab-directed uptake compared to DC.2.4 cells. The higher expression of CD11c-receptors on MutuDC1940 promoted a CD11c-specific uptake of PNCs (Figure 91D). However, the contribution of Fc-directed unspecific uptake was still significant as demonstrated with the IgG control. Therefore, the contribution of Fc-directed uptake was investigated by blocking the Fc receptors on DCs prior to incubation with antibody-modified PNCs. If the Fc receptors are blocked, there should not be unspecific uptake by the Fc part and uptake into DCs should be promoted only through targeting by the Fab region of antibody-modified PNCs. Different ratios of antibody to the DBCO concentration were applied to study the minimal and optimal ratio where the highest targeting specificity is achieved. The uptake into MutuDC1940 was significantly higher for NCs-CD11c with the highest ratio of DBCO:antibody (2000:1) compared to IgG with the same ratio, indicating a higher contribution of Fab-directed targeting. Many studies have demonstrated that even a low number of antibodies on the NCs surface can enhance the targeting specificity. Sometimes according to the motto “Less is more”, higher site-specific conjugation of antibodies could be achieved, when lower concentrations of antibodies are not sterically hindered in the conjugation. However, as seen from the high uptake of IgG-modified PNCs for the other ratios, Fc-directed uptake was still possible and complete blocking of Fc receptors failed with this setup. Therefore, no clear information could be gained from these blocking experiments. Changes on the setup could promote successful blocking og Fc receptors and prove specific Fab-directed targeting of CD11c-functionalized PNCs to DCs. Regarding the high contribution of Fc-directed uptake, it has to be considered that there might be azide groups on the PNCs surface left unreacted after the interfacial azide-alkyne crosslinking of azide-modified proteins with HDDP. The excess of azides could react in a side reaction with the DBCO-NHS ester in the same strain-promoted azide-alkyne click reaction as with the azide-modified antibody, conjugating the PNCs surface

with unwanted NHS moieties (Scheme 22). The NHS moieties could then react unselectively with the amine groups on the antibody, leading an uncontrolled orientation of the antibody on the PNCs. Most likely, the side reaction lead to a higher number of Fab-specific conjugation, decreasing the number of accessible target sites and increasing number of accessible Fc-regions.

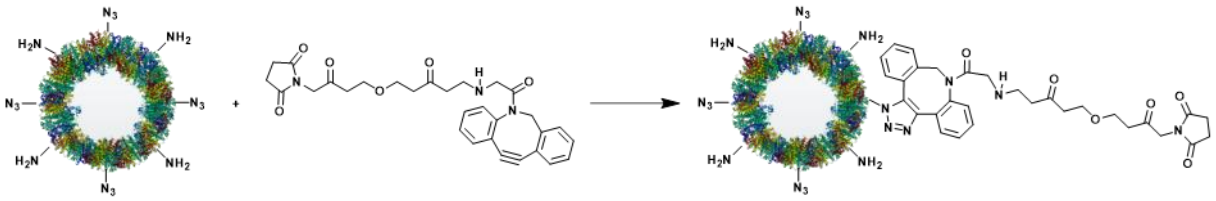

Scheme 22. Side reaction of DBCO functionalization by reaction of DBCO with remaining azide groups on the surface of protein nanocarriers. Protein structure was obtained from DrugBank online (https://go.drugbank.com/drugs/DB00062, 28.11.2021) and was adapted.

Nevertheless, higher uptake into DCs could be achieved with modifying the PNCs with antibodies compared to naked PNCs. The most promising results were obtained for specific targeting of splenic MutuDC1940 cells as the antibody-modified OVA-NCs achieved the highest difference of CD11c-targeted uptake compared to the IgG isotype control. Antibody-modification of PNCs can offer a high potential to improve the therapeutic efficiency of the nanovaccine by an increased and more selective uptake into DCs. Thus, transfer of the successful results achieved for site-specific antibody modification on model NCs mgHES should be of high focus for further development of PNCs as nanovaccines.

III. D4. Conclusion

Modification of protein nanocarriers with enabled studying the interaction of PNCs with cells to enhance their delivery efficiency into DCs and thus therapeutic efficiency. PNCs-TDI and PNCs-HDDP could successfully be loaded with CMPVA@Fe_3O_4-NPs with minimal amount of free NPs. Encapsulation of the Cy5-Oligo added fluorescent properties to the magnetic PNCs, so that the modified PNCs could be used for studying cell-carrier interactions. The results from the protein corona composition and cell uptake into macrophages as well as HeLa cells demonstrated the necessity for surface modification of protein nanocarriers with stealth and targeting properties to achieve high specific uptake into dendritic cells. Additionally, the difference in corona composition of TDI compared to HDDP crosslinked PNCs revealed the effect of the crosslinker on the surface composition of PNCs and thus affects their interaction with proteins and cells. The high contrast of magnetic PNCs could be used to visualize intracellular uptake and study intracellular protein corona formation of PNCs upon internalization into DCs. The modification of PNCs with stealthy polyethylene glycol, obtaining high density of PEG brushes (1.5 chains/nm^2) on the surface, significantly decreased

the unspecific cell uptake into macrophages compared to naked PNCs. PNCs were functionalized with DBCO groups to enable site-specific modification with azide-bearing antibodies. CD11c-modified PNCs obtained a higher uptake into DCs compared to unmodified PNCs. Although, unspecific uptake by the isotype control revealed Fc-directed internalization, the contribution of specific Fab-directed targeting was significantly increased, especially in splenic MutuDC1940. Further optimization of stealth and targeting properties of PNCs by surface modification could advance the potential of adjuvant-loaded PNCs as anti-tumor nanovaccines for clinical use.

IV. Conclusion

This thesis presents the development of multifunctional nanocarriers for co-delivery of therapeutics. Interfacial azide-alkyne click reaction between the activated dialkyne hexane diol dipropiolate and azide-modified protein in an inverse miniemulsion enabled successful preparation of protein nanocarriers without the use of metal catalysts or the formation of side products, making it a mild and biorthogonal approach. Dissolving cargo molecules in the disperse phase of an inverse miniemulsion allowed multicomponent encapsulation during the nanocarrier shell formation with high efficiency and control. With the developed method, four and possibly even more cargo molecules could be encapsulated simultaneously into protein nanocarriers without significantly compromising the encapsulation efficiency of each cargo. Developed nanovaccine composed of dual-adjuvant-loaded ovalbumin nanocarriers demonstrated efficient anti-tumor properties in *in vivo* experiments with melanoma-bearing mice. Here, co-encapsulation and co-delivery of adjuvants lead to higher decrease of tumor growths and longer survival of mice. The *in vivo* results underline the importance of nanocarriers as drug delivery systems to achieve high local concentrations of therapeutics at the target site and enhance treatment efficacy. The high stimulation efficiency of adjuvant-loaded protein nanocarriers demonstrated, that all adjuvants maintained their bioactivity during the encapsulation process, underlining the advantage of the mild and biorthogonal preparation method. Interfacial denaturation of proteins in W/O/W emulsions also proved to be an efficient bioorthogonal strategy to prepare protein nanocarriers without the use of chemical reactants. The prepared protein nanocarriers not only allow multicomponent encapsulation, but also surface modification with stealth and targeting moieties. The additional functionalities promoted a higher uptake of the nanocarriers into dendritic cells, which could facilitate an even higher treatment efficacy of the nanovaccine. In this thesis, the protein nanocarriers were modified successfully at the surface with stealth polymer PEG *via* NHS chemistry and targeting antibodies *via* site-specific strain-promoted azide-alkyne reaction. The developed procedure for the preparation of multifunctional protein nanocarriers can be adapted to numerous materials, cargo molecules and surface functionalization. The versatile PNCs are not only promising for vaccination, but for various biomedical applications such as theranostics. Integration of several functionalities into one system enables multitherapies, revolutionizing biomedical treatments. Furthermore, the tailored design of a fully biocompatible and biodegradable nanocarrier with high treatment efficacy could fulfill the strict requirements of the FDA, paving the way for broad application of nanocarriers in biomedicine.

V. Supplementary Information

V. 1. Supplementary Information to Chapter A

Materials

All chemicals and materials were used as received. Human serum albumin (> 99% purity) was purchased from Sigma Aldrich as well as 1,6-hexanediol (99%), propiolic acid, sulfuryl chloride and imidazole. Cyclohexane (HPLC grade) was purchased from VWR. Fluorescamine was purchased from Alfa Aesar. The block copolymer poly((ethylene-co-butylene)-*b*-(ethylene oxide)) P((E/B)-*b*-EO) used as the oil-soluble surfactant was synthesized as described in literature and consists of a poly((ethylene-co-butylene) block (NMR: M_n = 3900 g/mol) and a poly(ethylene oxide) block (NMR: M_n = 2700 g/mol).[161] The anionic surfactant sodium dodecyl sulfate (SDS) was purchased from Sigma Aldrich. Cy5-Oligo was purchased from IBA Lifesciences. Proteinase K from tritirachium album (≥ 30 units/mg) and peroxidase from horseradish (≥ 50 units/mg) was purchased from Sigma Aldrich. Resiquimod (R848), Muramyldipeptide (MDP) and Polyinosinic-polycytidylic acid (Poly(I:C) LMW) was purchased from Invivogen. Amicon Ultra-2 centrifugal filter devices were purchased from Merck Millipore (100 kDa) nominal molecular weight limit (NMWL). The magnesium and calcium-free phosphate-buffered saline was purchased from Life Technologies. Demineralized water was used for all experiments.

Experimentals

1. Synthesis of 1,6-Hexandiol Dipropiolate (HDDP)

The dialkyne crosslinker was synthesized by esterification following the literature. Briefly, hexandiole (4 g, 33.85 mmol), propiolic acid (9.48 g, 135.39 mmol) and *p*-TsOH (333.33 mg, 5 mol%) were dissolved in 120 mL toluene and stirred at 135 °C under reflux for 3 days using a dean-stark apparatus. Afterwards, the reaction solution was washed twice with 100 mL saturated $NaHCO_3$ solution and twice with 100 mL water. The solvent was removed and the product purified by column chromatography (PE:EtOAc 10:1). The product was obtained as colorless crystals. Yield: 3.37 g, 45%.

^{1}H NMR (300 MHz, CD_2Cl_2) δ 4.10 (t, 4H, O-C$\underline{H}_2$), 2.87 (s, 2H, $\underline{H}$C≡C), 1.61 (m, 4H, C$\underline{H}_2$-CH_2-O), 1.32 (m, 4H, CH_2-C$\underline{H}_2$-CH_2) ppm. ^{13}C NMR (300 MHz, CD_2Cl_2) δ 153, 74.6, 66.6, 28.5, 25.8 ppm.

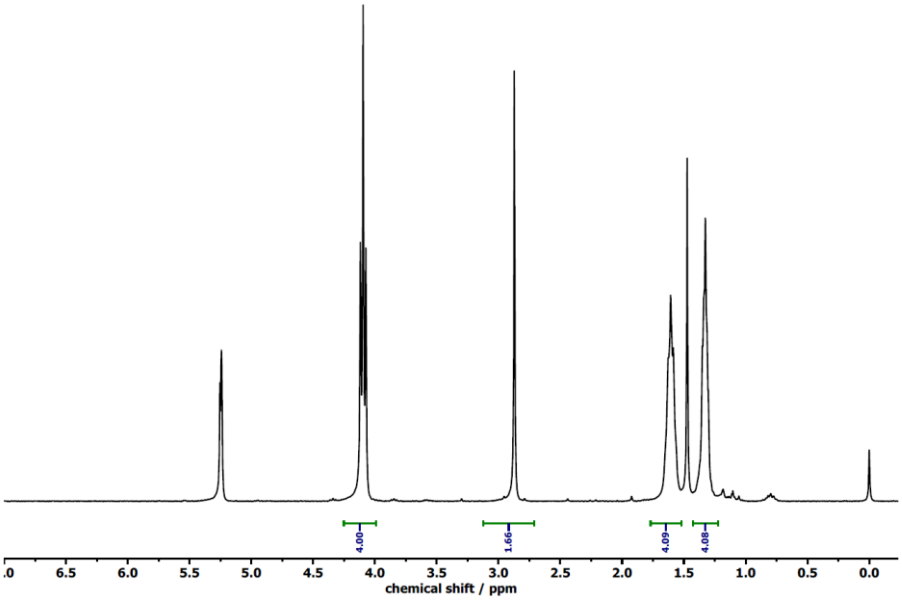

Figure 92. ^{1}H NMR spectrum of 1,6-hexandiol dipropiolate in CD_2Cl_2.

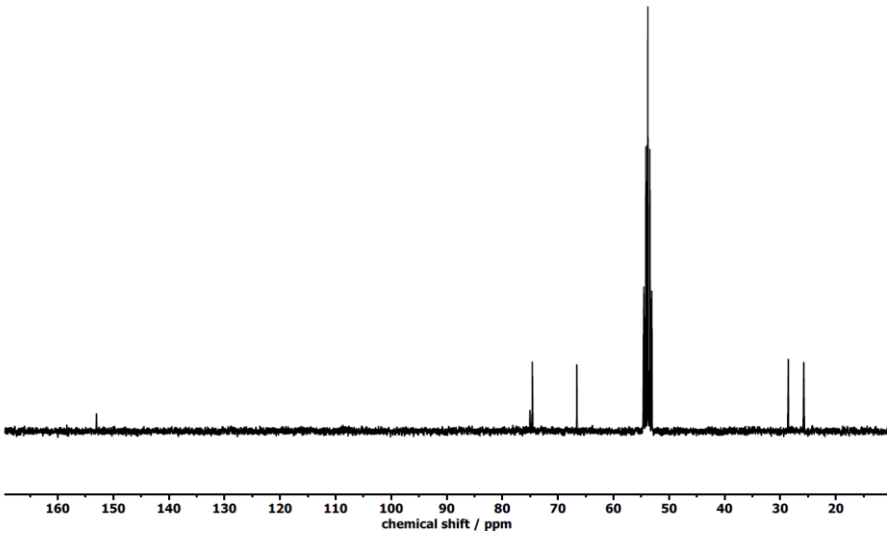

Figure 93. ^{13}C NMR spectrum of 1,6-hexandiol dipropiolate in CD_2Cl_2.

2. Synthesis of Disulfide 1,6-Hexanediole Dipropiolate (HDDP-SS)

The dialkyne crosslinker was synthesized by esterification following the literature. Briefly, bis(2-hydroxyethyl) disulfide (3.0 g, 19.5 mmol), propiolic acid (5.4 g, 78.0 mmol) and *p*-TsOH (360 mg, 2 mmol) were dissolved in 150 mL benzene and stirred under reflux for 3 days using a dean-stark apparatus. Afterwards, 100 mL saturated $NaHCO_3$ solution was added to the reaction solution and the organic phase separated. The aqueous phase was washed twice with

100 mL diethylether. The organic phases are combined and dried over Na_2SO_4. The solvent was removed and the product purified by column chromatography (n-hexane:EtOAc = 3:1). The product was obtained as colorless crystals. Yield: 2.3 g, 46%.

^{1}H NMR (300 MHz, $CDCl_3$) δ 4.41 (t, 4H, O-C<u>H</u>$_2$), 2.96-2.92 (m, 6H, S-CH_2 and <u>H</u>C≡C) ppm. ^{13}C NMR (300 MHz, CD_2Cl_2) δ 152.3, 75.5, 74.3, 74.3, 63.9, 36.7 ppm.

3. Synthesis of 1-Imidazole-Sulfonyl Azide Hydrochloride

The azide transfer agent was synthesized according to Goddard-Borger *et al.*[158] Briefly, sodium azide (1.63 g, 25 mmol) was suspended in 25 mL MeCN and cooled down to 0 °C. Under vigorous stirring sulfurylchloride (3.34 g, 25 mmol) was added drop-wisely. The reaction solution was slowly brought to room temperature and the reaction carried out at room temperature overnight. Again, the reaction solution is cooled down to 0 °C and imidazole (3.23 g, 47.5 mmol) added in small portions. The reaction is stirred at room temperature for 3 h. Afterwards, 50 mL EtOAc is added and the reaction solution is washed twice with 50 mL saturated $NaHCO_3$ solution and twice with 50 mL water. The organic phase is dried over $MgSO_4$ and filtered. A mixture of AcCl/EtOH is slowly added to the reaction solution at 0 °C. The product is filtered, washed with EtOAc and dried. Yield: 3.13 g.

^{1}H NMR (300 MHz, D_2O) δ 7.44 (dd, 1H, N-C<u>H</u>=CH), 7.85 (dd, 1H, HC=C<u>H</u>-N), 9.17 (dd, 1H, N=C<u>H</u>-N) ppm. ^{13}C NMR (300 MHz, CD_2Cl_2) δ 152.3, 75.5, 74.3, 74.3, 63.9, 36.7 ppm.

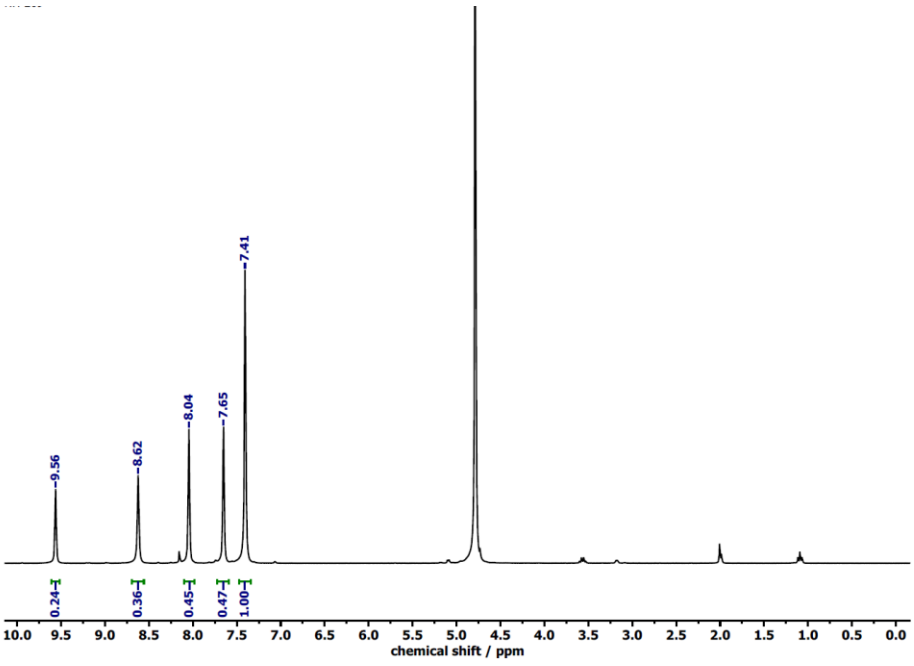

Figure 94. ^{1}H NMR spectrum of 1-imidazole-sulfonyl azide hydrochloride in D_2O.

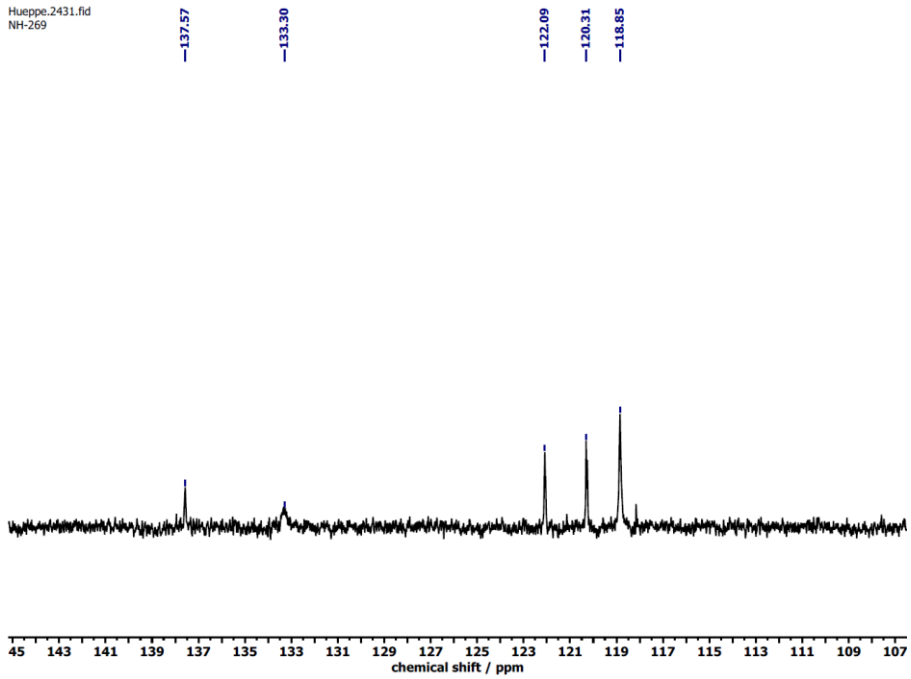

Figure 95. ^{13}C NMR spectrum of 1-imidazole-sulfonyl azide hydrochloride in D_2O.

4. Azidation of Proteins with 1-Imidazole-Sulfonyl Azide Hydrochloride

The human serum albumin (1 g) was dissolved in 20 mL K_2CO_3 solution of pH 11. The azide transfer agent (276 mg) was dissolved in 2 mL water and added dropwisely to the protein solution. The pH value of the reaction solution was adjusted to pH 11 with 1 M NaOH. The reaction solution was stirred at room temperature for 48 h. The product was purified by dialysis (MWCO 1K) and lyophilized. Yield: 0.93 g. Horse radish peroxidase (200 mg) was functionalized with azide moieties with the similar procedure. Amounts of reagents were adapted, 86 mg of azide transfer agent. Yield: 0.27 g. The amount of azide moieties was determined using the fluorescamine assay.

5. Fluorescamine Assay

The quantitative amount of azide groups was determined with the fluorescamine assay in borate buffer at pH 8.2.

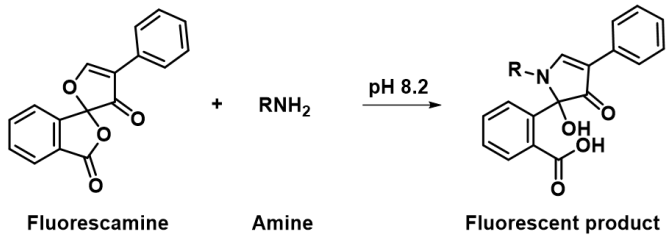

Scheme 23. Reaction of fluorescamine with amines to a fluorescent product at pH 8.2.

Glycine was used for the standard calibration curve and lysozyme was used as a reference. A decreased amount of amine groups was determined for the protein after azide-functionalization, indicating a successful reaction.

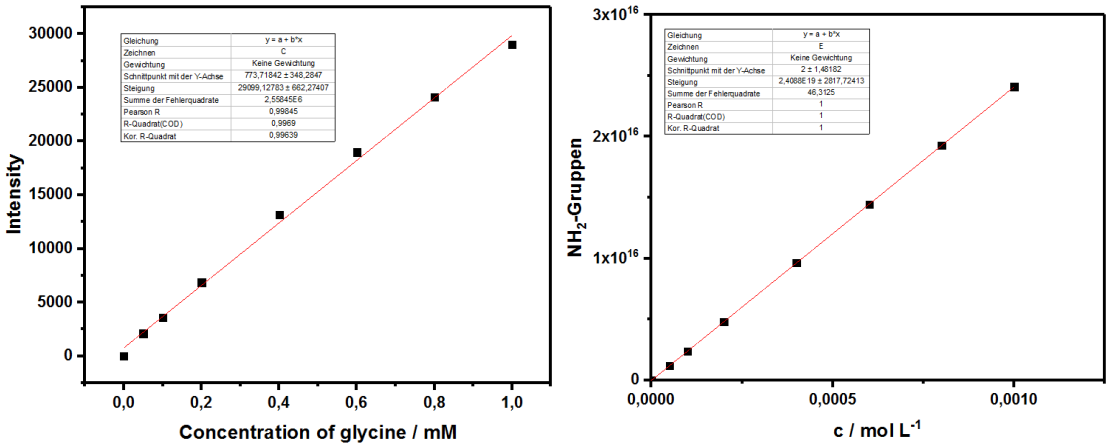

Figure 96. Fluorescamine assay, standard calibration with glycine.

6. Preparation of Protein Nanocarriers

First, the azide-functionalized protein (HSA and HRP, 50 mg) was dissolved in 0.4 mL NaCl solution (c = 14.4 mg/mL) and dye solution was added, either 100 µL Cy5-Oligo (c = 0.1 nmol/µL) or dextrane-rhodamine B (0.1 mg, 1 mg/ mL). 35.7 mg of surfactant poly((ethylene/butylene)-*block*-(ethylene oxide)) (P((E/B)-*b*-EO)) were dissolved in 7.5 g of cyclohexane and the mixture was added to the aqueous solution. The two phases were homogenized by ultrasound under ice-cooling (70% amplitude, 3 min, 20 s pulse, 10 s pause). A third solution containing of 10.7 mg P((E/B)-*b*-EO), 35.7 mg crosslinker in 5 g of cyclohexane and was then added dropwise to the stirred miniemulsion at 40 °C. The reaction was carried out at 40 °C for 24 h. Afterwards, the protein nanocarriers were purified by repetitive centrifugation (1500*g*, 20 °C) and redispersion in cyclohexane to remove excess of surfactant and crosslinker. For the transfer of the nanocarriers into aqueous media, 500 µL of concentrated nanocarrier dispersion in cyclohexane is added dropwise to 5 mL 0.1 wt% SDS solution under shaking in an ultrasonication bath for 3 min. Then, the emulsion was stirred open over night to evaporate the organic solvent. The protein nanocarriers in water were purified by repetitive centrifugation and washing in Amicon Ultra-2 centrifugal filters (500*g*, MWCO 100 kDa).

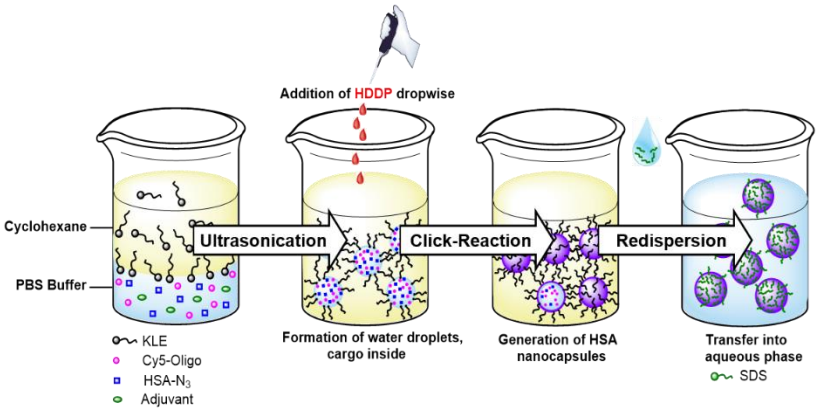

Scheme 24. Preparation of protein nanocarriers crosslinked with HDDP in inverse miniemulsion and transfer into water. Scheme created in ChemDraw 20.1 by Natkritta Hüppe.

PGPR surfactant: For the preparation of protein nanocarriers by using PGPR as a surfactant, PGPR (75 mg) was used instead of P((E/B)-*b*-EO) in the cyclohexane phase. The procedure for the inverse miniemulsion and following crosslinking maintained.

Vybrant DiO: For the encapsulation of Vybrant DiO dye into protein nanocarriers crosslinked with HDDP-SS, a solution of dye (1 mM in DMF, 20 µL) was added to the disperse phase containing HSA (50 mg) and 7.2 mg NaCl in 0.48 mL H_2O. The preparation of protein nanocarriers proceeded as described above.

7. Encapsulation of Protein Nanocarriers into Polymersomes

The encapsulation of protein nanocarriers into polymersomes by simple double emulsification (SDE) method was performed according to Houbrechts *et al.*[107] Briefly, protein nanocarriers were dispersed in an aqueous sucrose solution (250 mM). The PNCs in sucrose (5 µL) were added into a solution of polybutylene-polyethylene oxide in toluene (30 µL). Both solution were gently emulsified for 1 min using a micropipette. A double emulsion was formed by adding the W/O emulsion (5 µL) into more sucrose solution (200 µL) and gentle emulsification with a micropipette for 1 min. The double emulsion was left open to air for at least 2 h to evaporate the toluene. Then the dispersion (100 µL) was transferred into a microscope chamber slide containing a glucose solution (400 µL, 250 mM) for microscopic analysis. To degrade the protein nanocarriers encapsulated in the polymersomes, a solution of dithiothreitol (25 mM) was added to the dispersion.

8. Characterization of Protein Nanocarriers

Dynamic light scattering (DLS) was used to determine the average size and size distribution of the nanocarriers. A diluted dispersion (10 µL sample diluted in 1 mL cyclohexane or 50 µL

sample diluted in 200 µL H_2O) was measured on a Malvern Zetasizer Nano S (Malvern Panalytical) equipped with a detector at 90° scattering mode at 20 °C. The zeta potential of the nanocarriers were measured in 10^{-3} M potassium chloride solution with a ZetaNanosizer (Malvern Panalytical) at 20 °C. Scanning electron microscopy (SEM) studies were done on a field emission microscope (LEO (Zeiss) 1530 Gemini, Oberkochen, Germany) working at an accelerating voltage of 170 V. The silica wafers are cleaned in the plasma oven prior to use. Then, 2 µL of a diluted nanocarrier dispersion in cyclohexane or distilled water (concentration similar to samples for DLS) were dropped onto the wafers and dried under ambient conditions for 15 min. No additional contrast agent was applied. The solid content of the nanocarrier dispersion was measured gravimetrically. The fluorescence intensities for all mentioned experiments were measured using a microplate reader (Infinite M1000, Tecan, Switzerland).

9. Determination of Encapsulation Efficiency and Permeability

The encapsulation efficiency was determined by measuring the fluorescence intensity of using a microplate reader (Infinite M1000 Tecan, Switzerland). The unpurified nanocarrier dispersion after transfer into 0.1 wt% SDS were concentrated in an Amicon centrifuge filter 100 K for 30 min at 500 g. The amount of non-encapsulated dye was measured in the supernatant and the encapsulation efficiency determined in proportion to the fluorescence intensity of the un-purified dispersion. After washing the aqueous dispersion, the permeability of the nanocarriers was measured using the same method. The dispersion was concentrated in an Amicon Centrifuge filter at a certain time point and the amount of leaked dye measured in the supernatant.

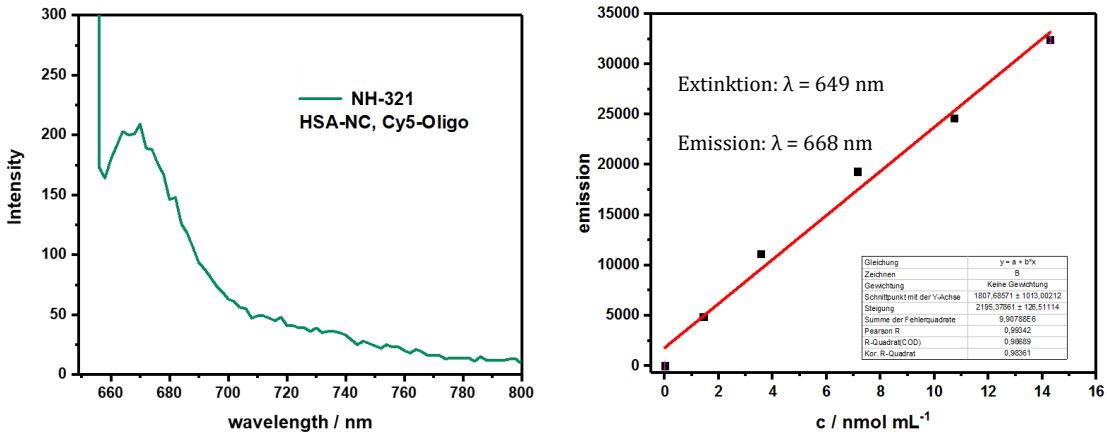

Figure 97. Fluorescence curve of HSA nanocarriers with encapsulated Cy5-Oligo (left). Standard calibration curve of Cy5-Oligo fluorescence (right).

10. Degradability of Protein Nanocarriers

The enzymatic degradation of the protein nanocarriers were performed with proteinase K and determined by release of Cy5-Oligo. A 0.1 wt% nanocarrier dispersion in PBS buffer was treated with a proteinase K solution (30 U/mL) at 37 °C. After the enzymatic degradation the dispersion is filtered by centrifugation in an Amicon centrifuge filter 3K at 500*g* for 30 min and the amount of released dye in the supernatant measured by fluorescence. The degradation of the nanocarriers by proteinase K is also monitored by DLS measurements every 5 min over 10 h. The reduction-responsive properties of HDDP-SS-crosslinked protein nanocarriers were investigated with dithiothreitol (DTT) by release of Cy5-Oligo. A 0.1 wt% nanocarrier dispersion in PBS was treated with a DTT solution (25 mM) at 20 °C. After the reductive degradation, the dispersion is filtered by centrifugation in an Amicon centrifuge filter 3K at 500*g* for 30 min and the amount of released dye in the supernatant measured by fluorescence. The degradation of the nanocarriers by DTT is also monitored by DLS measurements every 5 min over 10 h. In both cases, enzymatic and reductive degradation, a sample treated with PBS buffer serves as a control sample and every experiment was performed in triplets.

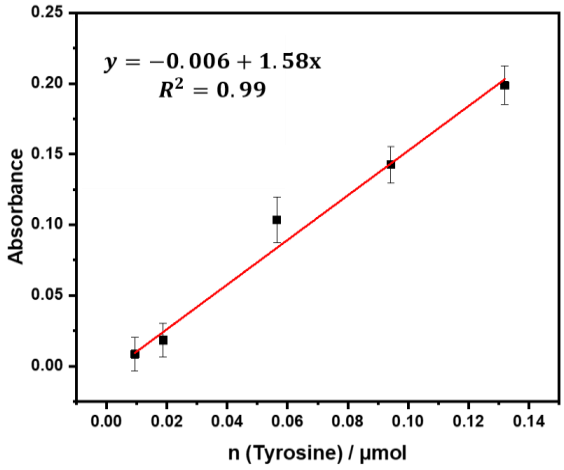

Figure 98. Tyrosine calibration curve for the determination of th enzyme activity of proteinase K.

11. Determination of Enzyme Concentration in Protein Nanocarrier

A protein assay with bicinchoninic acid (BCA) was used as the substrate to determine the concentration of the enzyme in the nanocarrier dispersion. Briefly, BCA (100 mg), sodium carbonate (200 mg), sodium hydrogen carbonate (95 mg) and sodium tartrate (16 mg) were dissolved in 10 mL of distilled water and the pH of the solution was adjusted to 11.3 by using 3.0 M NaOH. A solution of $CuSO_4$ x 5 H_2O (50 mg/mL, 200 µL) in distilled water was added to the substrate solution. 10 µL of protein or nanocarrier dispersion was mixed with 200 µL of

metal-containing substrate solution and incubated at 60 °C for 30 min. The absorbance of the sample was measured at 565 nm and the enzyme concentration determined by a standard calibration with native enzyme.

12. Enzymatic Activity

The enzymatic activity of HRP and HRP-HDDP nanocarriers were determined using 2,2'-azino-bis(3-ethylbenzothiazoline-6-sulphonic acid) (ABTS) as substrate. Briefly, the substrate was dissolved in 100 mM potassium phosphate buffer (pH 5.0) to a concentration of 5 mg/mL. The enzyme in different stages of the nanocarrier preparation were diluted to a concentration of 0.002 mg/mL protein in a solution of 0.5% Triton X-100 in 40 mM PBS buffer (pH 6.8). The ABTS solution (190 µL) was mixed with the enzyme solution (3.3 µL) in a 96-well plate and the reaction started with addition of 0.3% (w/w) hydrogen peroxide solution (6.6 µL). The absorbance at 405 nm was monitored by a UV/Vis spectrophotometer and the enzyme activity determined by a standard calibration with native HRP.

13. Quantification of Adjuvants in Protein Nanocarriers

For the quantification of adjuvants in the protein nanocapsules (PNCs), the PNCs were degraded by proteinase K (30 U/mL) at 37 °C overnight. The PNCs remains and the enzyme were separated from the released adjuvants through a centrifuge filter (MWCO 3K, 30 min, 1500*g*). The amount of Resiquimod (R848) was determined by fluorescence (λ_{ex} = 260 nm, λ_{em} = 360 nm) using a standard calibration curve (Figure 99). Muramyl dipeptide (MDP) was determined from the supernatant using the Morgan-Elson Reaction (Scheme 6). The supernatant (50 µL) was mixed with borate buffer (50 µL, pH 9) and incubated at 100 °C for 3 min. The mixture is cooled to room temperature and DMAB (500 µL) was added to the mixture. The mixture was incubated again at 37 °C for 15 min and afterwards the absorbance measured at 585 nm. The MDP was quantified by a standard calibration (Figure 100). Poly(I:C) was quantified from the full mixture after degradation as it has a too high molecular weight to be separated from the proteins. The full mixture of PNCs after degradation with proteinase K was eluted through a reverse phase HPLC column using a mixture of acetonitrile, 0.01% formic acid and 0.02 mol/L ammoniumacetate. The Poly(I:C) signal was quantified using a standard calibration curve (Figure 101).

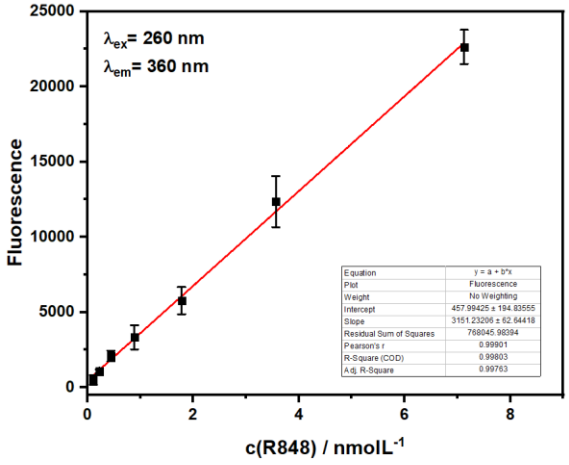

Figure 99. Standard calibration curve of R848 by fluorescence measured at 360 nm.

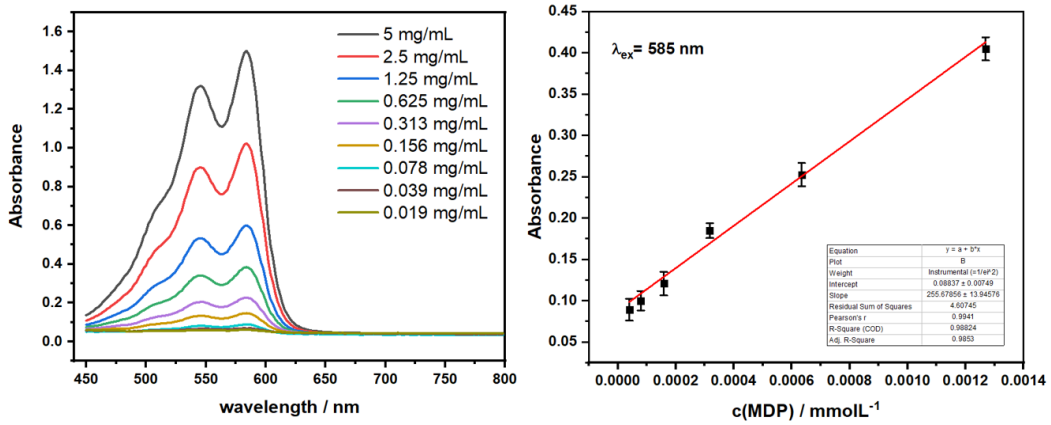

Figure 100. Absorbance measurements of MDP assay *via* Morgan-Elson reaction with DMAB.

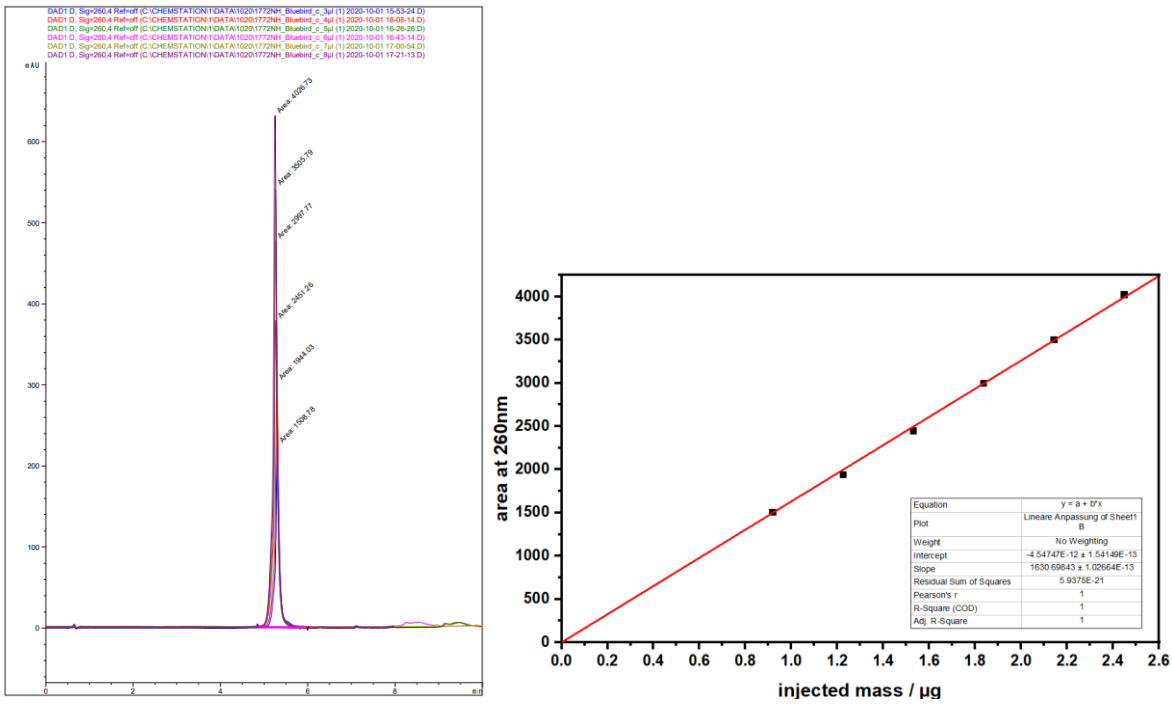

Figure 101. Standard calibration curve of Poly(I:C) measured by HPLC.

14. *In Vitro* Experiments with BMDCs

Bone marrow-derived dendritic cells (BMDC) were differentiated from bone marrow progenitors (BM cells) of 8- to 10-week-old C57BL/6mice. Briefly, the bone marrow was obtained by flushing the femur, tibia, and hip bone with Iscove's Modified Dulbecco's Medium (IMDM) containing 5% FCS (Sigma-Al-drich) and 50 μMβ-mercaptoethanol (Roth, Karlsruhe, Germany). For the analysis of DC maturation and nanocarrier uptake/binding and degradation *via* flow cytometry the BM cells (2 × 105cells/1.25 mL) were seeded in 12 well suspension culture plates (Greiner Bio-One,Frickenhausen, Germany) with culture medium (IMDM with 5% FCS, 2 mL-glutamine, 100 U/mL penicillin, 100 μg/mL streptomycin [all from Sigma-Aldrich], and 50 μM β-mercaptoethanol), supplemented with 5% of GM-CSF containing cell culture supernatant derived from X63.Ag8–653 myeloma cells stably transfected with a murine GM-CSF expression construct. On day 3, 500 μL of the same medium was added into each well. On day 6, 1 mL of the old medium was replaced with 1 mL fresh medium per well. For other DC based assays the BM cells (2 × 106cells/10 mL) were seeded on bacterial dishes (Ø 94 mm; Greiner Bio-One). On day 3 and 6, an additional 5 mL of culture medium was added into these dishes. Before usage, all nanoparticle solutions were checked for endotoxin contaminations by limulus amebocyte lysate (LAL) assay (Thermo Fisher Scientific) according to the manufacturer's instructions.

Confocal Imaging

Uptake of PNCs containing fluorescent Cy5-Oligo (red) was monitored by Confocal Laser Scanning Microscopy (cLSM). To this end, BMDC (3 × 105cells) on day 7 of culture were seeded in chamber slides(Thermo Fisher Scientific) and treated with 150 μg/mL PNCs for 3 h at 37 °C. After that, the chamber slides were washed, and the samples were incubated with DAPI (Sigma-Aldrich) to stain the cell nuclei (blue). Unbound dye was washed off. Samples were assayed using a Zeiss LSM710 (Carl Zeiss) and analyzed using ImageJ (NIH, Bethesda, USA) and ZEN 2009 (Carl Zeiss) software.

Flow Cytometry Assay

To detect cell-nanocarrier-interaction and to analyze the expression of surface markers, cells were harvested and washed in staining buffer (phosphate buffer saline [PBS]/2% FCS). To block Fc receptor-mediated staining, cells were incubated with rat anti-mouse CD16/CD32 Ab (clone 2.4G2), purified from hybridoma supernatant, for 15 min at room temperature. After that, cells were incubated with eFluor450-conjugated Ab specific for MHC class II I-Ab, d,q/I-

Ed, k(cloneM5/114.15.2), fluorescein isothiocyanate (FITC)-labeled Ab directed at CD80 (clone 16-10A1), phycoerythrin (PE) anti-CD86 (clone GL-1), PE-Cy7-labeled anti-CD11c (clone N418), for 30 min at 4 °C. Dead cells were stained by incubation with fixable viability dye (FVD) eFI506 for 30 min at room temperature in the dark. Samples were measured with a BD FACSCanto-II flow cytometer equipped with BD FACS Diva software (BDBiosciences). Data were generated based on defined gating strategies and analyzed using FlowJo software (FlowJo, Ashland, USA)

V. 2. Supplementary Informations to Chapter B

Materials

All chemicals and materials were used as received. Albumin from chicken egg white (> 99% purity) was purchased from Sigma Aldrich as well as 1,6-hexanediol (99%), propiolic acid, sulfurylchloride and imidazole. Cyclohexane (HPLC grade) was purchased from VWR. Fluorescamine was purchased from Alfa Aesar. The block copolymer poly((ethylene-co-butylene)-*b*-(ethylene oxide)) P((E/B)-*b*-EO) used as the oil soluble surfactant was synthesized as described in literature and consists of a poly((ethylene-co-butylene) block (NMR: M_n = 3900 g/mol) and a poly(ethylene oxide) block (NMR: M_n = 2700 g/mol).[161] The anionic surfactant sodium dodecyl sulfate (SDS) was purchased from Sigma Aldrich. Cy5-Oligo was purchased from IBA Lifesciences. Proteinase K from tritirachium album (≥ 30 units/mg) was purchased from Sigma Aldrich. Resiquimod (R848), muramyl dipeptide (MDP) and polyinosinic-polycytidylic acid (Poly(I:C) LMW) was purchased from Invivogen, diABZI compound 3 was purchased from Selleckchem. PEG-NHS was purchased from Sigma Aldrich. Amicon Ultra-2 centrifugal filter devices were purchased from Merck Millipore (50 kDa) nominal molecular weight limit (NMWL). The magnesium and calcium free phosphate-buffered saline, was purchased from Life Technologies. Demineralized water was used for all experiments.

Experimentals

1. Azidation of Ovalbumin with 1-Imidazole-Sulfonyl Azide Hydrochloride

Ovalbumin (1 g) was dissolved in 20 mL K_2CO_3 solution of pH 11 (for the optimization experiments pH value was adjusted accordingly to 8.2, 9.5 or 11). The azide transfer agent (276 mg) was dissolved in 2 mL water and added dropwisely to the protein solution. The reaction solution was stirred at pH 11 and room temperature for 30 min. Afterwards, the pH value of the reaction solution was adjusted to pH 8.3 with 1 M NaOH or 1 M HCl. The reaction solution was stirred at room temperature for 8 h (for the optimization experiments reaction time was adjusted accordingly to one, two or three days). The product was purified by dialysis (MWCO 1K) and lyophilized in NaCl (14.4 mg/mL). Yield: 0.78 g. The amount of azide moieties was determined using the fluorescamine assay (see chapter A experimental part).

2. Endotoxin-Free Preparation of Ovalbumin Nanocarriers

All glassware were baked at 200 °C over night. All plastic materials (caps, centrifuge tubes) were autoclaved at 120 °C. Other preparation equipment (spatula, sonicator tip) was sprayed

with 70% EtOH. All materials were dissolved in sterile and endotoxin-free solvents and handeled under the flow bench. First, the azide-functionalized ovalbumin (50 mg) was dissolved in cargo solution, according to table 26. 35.7 mg of surfactant poly((ethylene/butylene)-*block*-(ethylene oxide)) (P((E/B)-*b*-EO)) were dissolved in 7.5 g of cyclohexane and the mixture was added to the aqueous solution. The two phases were homogenized by ultrasound under ice-cooling (70% amplitude, 3 min, 20 s pulse, 10 s pause). A third solution containing of 10.7 mg P((E/B)-*b*-EO), 13 mg crosslinker hexanediol dipropiolate (for synthesis see chapter A experimental) in 5 g of cyclohexane and was then added dropwise to the stirred miniemulsion at 40 °C. The reaction was carried out at 40 °C for 24 h. Afterwards, the ovalbumin nanocarriers were purified by repetitive centrifugation (1500*g*, 30 min, 20 °C) and redispersion in cyclohexane to remove excess of surfactant and crosslinker. For the transfer of the nanocarriers into aqueous media, 500 µL of concentrated nanocarrier dispersion in cyclohexane was added layered onto 5 mL 0.1 wt% SDS solution and emulsified under shaking in an ultrasonication bath for 5 min. Then, the emulsion was stirred open over night under the flow bench to evaporate the organic solvent. The ovalbumin nanocarriers in water were purified by repetitive centrifugation (500*g*, 20°C, 30 min) and washing in Amicon Ultra-2 centrifugal filters (MWCO 50 kDa). The solid content of the dispersion was measured gravimetrically.

Table 26. Volume of cargo solution added to ovalbumin (50 mg) to obtain the disperse phase.

Cargo	**$V_{CyOligo}$ / µL[a]**	**c / mgmL^{-1}**	**V_{cargo} / µL**	**V_{water} / µL**
Cy5 Oligo	-	0.1[a]	100	500
R848	100	10	70	330
R848-PEG-0.5 kDa	100	3.75	400	-
R848-PEG-1 kDa	100	6.75	400	-
MDP	100	10	250	150
Poly(I:C)	100	20	250	150
diABZI	100	10	8	392
diABZI	100	10	80	320
R848+MDP	100	10+10	70+250	80
R848+MDP+Poly(I:C)	100	10+10+20[b]	70+250	80

[a]c / nmolµL^{-1}, [b]MDP (10mg/mL) dissolved in Poly(I:C) solution (20 mg/mL)

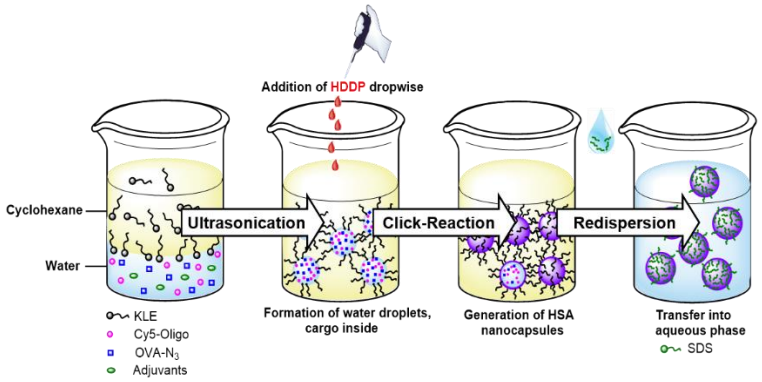

Scheme 25. Preparation of ovalbumin nanocarriers crosslinked with HDDP in inverse miniemulsion and transfer into water. Scheme prepared in ChemDraw 20.1 by Natkritta Hüppe.

Optimization of OVA-NCs Preparation Procedure

Number 1: A formation of OVA-NCs with partly dissolved OVA-N_3 resulted in broad size distribution with the majority of NCs had large particle-like morphologies (Table 27, no.1, Figure 102A).

Number 2: Since the modified OVA had a low water-solubility after lyophilization, OVA-N3 was kept in solution after purification and concentrated to achieve a high concentration of protein in the disperse phase. The resulting OVA-NCs were comparable to previously synthesized HSA-NCs in size, size distribution, and core-shell morphology in cyclohexane as well as after transfer to water. However, for encapsulation of cargo molecules that have to be added to the dispersed phase, OVA-N_3 has to be concentrated to higher than 100 mg/mL to fit into the fixed disperse phase volume of 500 µL. With higher concentrated OVA-N_3 solution it was observed that the protein began to gelate and precipitate (Table 27, no.2, Figure 102B).

Number 3: The azide-transfer reaction was performed at pH 8.2 for 24 h. The resulting OVA-N_3 possessedtwo2 azide groups, which reduced the effect on the protein structure and its stability, resulting in water-soluble OVA-N_3 after lyophilization. OVA-NCs formed from OVA-N_3 with two azide groups resulted in a morphology with a thin and soft shell in SEM, indicating low crosslinking efficiency of the protein due to the low number of azide groups (Table 27, no.3, Figure 102C). A lower crosslinking degree leads to higher permeability of the protein shell, unsuitable for efficient transport of small molecules.

Number 4: With adjusting the pH to 9.5 and decreased reaction time to 8 h, five azide groups per OVA were obtained (Table 27, no. 4). The modified protein was lyophilized in PBS solution (180 mg/mL) resulting in water-soluble OVA-N_3. The formation of OVA-NCs gave stable capsules with a core-shell morphology and comparable size and size distribution to HSA-NCs

in cyclohexane and water (Figure 102D). However, the high salt concentration in the protein solution affected the encapsulation efficiency (EE), especially of small molecule R848, leading to low EE of 3%.

Table 27. Analytical data of ovalbumin nanocarriers synthesized from azide-functionalized ovalbumin with different amounts of azide and salt.

No.	N_{ex} (N_3)	Salt /mgmL^{-1}	d_h(CH) /nm	PDI	d_h(H_2O) /nm	PDI	ζ /mV	EE_{Cy5} /%	EE_{R848} /%
1	16	-	344*	0.30*	n.d.	n.d.	n.d.	n.d.	n.d.
2	16	-	229	0.21	353	0.40	-38	n.d.	n.d.
3	2	-	309	0.15	170	0.62	n.d.	63	16
4	5	180	229	0.20	353	0.40	-38	43	3

*filtrated through 0.5 µm PTFE Filter

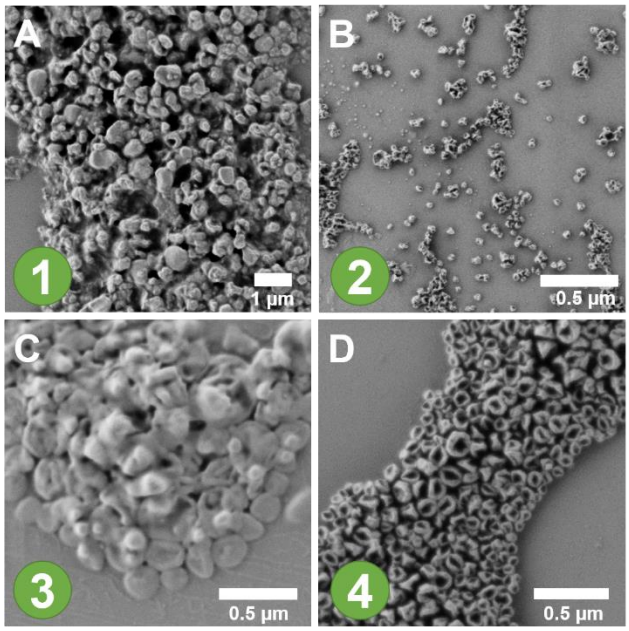

Figure 102. Scanning electron micrographs of ovalbumin nanocarriers synthesized from A) Low water-soluble azide-functionalized ovalbumin (OVA-N_3) A) OVA-N_3 concentrated in solution, B) OVA-N_3 with two azide groups lyophilized in water, C) OVA-N_3 with five azide groups lyophilized in PBS buffer, D) OVA-N_3 with five azide groups lyophilized with 14 mg/mL NaCl. All OVA-NCs were loaded with Cy5 Oligo.

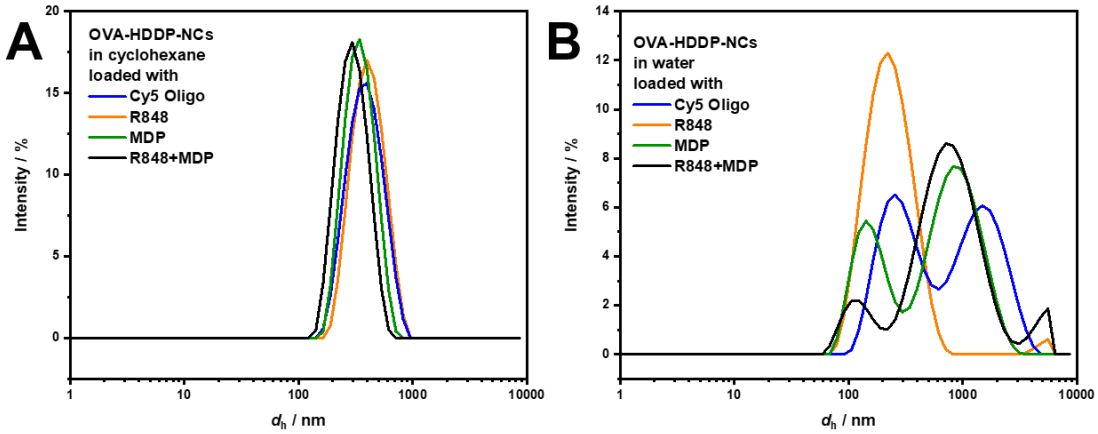

Figure 103. Dynamic light scattering of ovalbumin nanocarriers crosslinked with HDDP and loaded with Cy5-Oligo (blue), Resiquimod (R848, orange), muramyl dipeptide (MDP, green) and R848+MDP (black) in A) cyclohexane and B) water.

3. Characterization of Protein Nanocarriers

Dynamic light scattering (DLS) was used to determine the average size and size distribution of the nanocarriers. A diluted dispersion (10 µL sample diluted in 1 mL cyclohexane or 50 µL sample diluted in 200 µL H_2O) was measured on a Malvern Zetasizer Nano S (Malvern Panalytical) equipped with a detector at 90° scattering mode at 20 °C. The zeta potential of the nanocarriers were measured in 10^{-3} M potassium chloride solution with a ZetaNanosizer (Malvern Panalytical) at 20 °C. Scanning electron microscopy (SEM) studies were done on a field emission microscope (LEO (Zeiss) 1530 Gemini, Oberkochen, Germany) working at an accelerating voltage of 170 V. The silica wafers are cleaned in the plasma oven prior to use. Then, 2 µL of a diluted nanocarrier dispersion in cyclohexane or distilled water (concentration similar to samples for DLS) were dropped onto the wafers and dried under ambient conditions for 15 min. No additional contrast agent was applied. The solid content of the nanocarrier dispersion was measured gravimetrically. The fluorescence intensities for all mentioned experiments were measured using a microplate reader (Infinite M1000, Tecan, Switzerland).

4. Determination of Encapsulation Efficiency

The encapsulation efficiency was determined by measuring the fluorescence intensity of using a microplate reader (Infinite M1000 Tecan, Switzerland). The unpurified nanocarrier dispersion after transfer into 0.1 wt% SDS were concentrated in an Amicon centrifuge filter 100 K for 30 min at 500*g*. The amount of non-encapsulated dye was measured in the supernatant and the encapsulation efficiency determined in proportion to the fluorescence intensity of the un-purified dispersion.

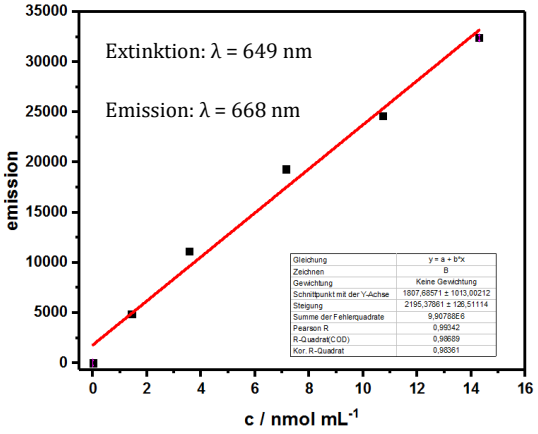

Figure 104. Standard calibration curve of Cy5-Oligo fluorescence.

For the quantification of adjuvants in the protein nanocarriers (PNCs), the PNCs were degraded by proteinase K (30 U/mL) at 37 °C overnight. The PNCs remained and the enzyme were separated from the released adjuvants through a centrifuge filter (MWCO 3K, 30 min, 1500*g*). The amount of Resiquimod (R848) and R848-PEG was determined by fluorescence (λ_{ex} = 260 nm, λ_{em} = 360 nm) using a standard calibration curve. Muramyl dipeptide (MDP) was determined from the supernatant using the Morgan-Elson Reaction. The supernatant (50 µL) was mixed with borate buffer (50 µL, pH 9) and incubated at 100 °C for 3 min. The mixture was cooled to room temperature and DMAB (500 µL) was added to the mixture. The mixture was incubated again at 37 °C for 15 min and afterwards the absorbance measured at 585 nm. The MDP was quantified by a standard calibration. Poly(I:C) was quantified from the full mixture after degradation as it has a too high molecular weight to be separated from the proteins. The full mixture of PNCs after degradation with proteinase K was eluted through a reverse phase HPLC column using a mixture of Acetonitrile, 0.01% formic acid and 0.02 mol/L ammoniumacetate. The Poly(I:C) signal was quantified using a standard calibration curve. For the calibration curves of the adjuvants see chapter A experimental part. The amount of STING agonist diABZI was determined by fluorescence fluorescence (λ_{ex} = 260 nm, λ_{em} = 400 nm) using a standard calibration curve.

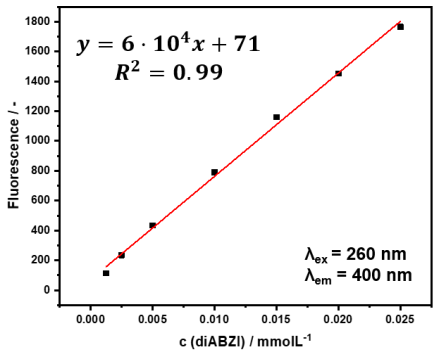

Figure 105. Standard calibration curve of diABZI.

5. *In Vitro* Experiments

Endotoxin Assay

Before usage of NCs for *in vitro* and *in vivo* experiments, the concentration of endotoxins in the OVA-NCs dispersions was determined with LAL assay (Pierce LAL Chromogenic Endotoxin Quantification Kit, Ref. No: 88282, Thermo Fisher), according to the manufacturer's instructions.

Isolation of BMDCs

Bone marrow-derived dendritic cells (BMDC) were differentiated from bone marrow progenitors (BM cells) of 8- to 10-week-old C57BL/6mice. Briefly, the bone marrow was obtained by flushing the femur, tibia, and hip bone with Iscove's Modified Dulbecco's Medium (IMDM) containing 5% FCS (Sigma-Al-drich) and 50 μMβ-mercaptoethanol (Roth, Karlsruhe, Germany). For the analysis of DC maturation and nanocarrier uptake/binding and degradation *via* flow cytometry the BM cells (2 × 105cells/1.25 mL) were seeded in 12 well suspension culture plates (Greiner Bio-One,Frickenhausen, Germany) with culture medium (IMDM with 5% FCS, 2 mL-glutamine, 100 U/mL penicillin, 100 μg/mL streptomycin [all from Sigma-Aldrich], and 50 μM β-mercaptoethanol), supplemented with 5% of GM-CSF containing cell culture supernatant derived from X63.Ag8–653 myeloma cells stably transfected with a murine GM-CSFexpression construct. On day 3, 500 μL of the same medium was added into each well. On day 6, 1 mL of the old medium was replaced with 1 mL fresh medium per well. For other DC based assays the BMcells (2 × 106cells/10 mL) were seeded on bacterial dishes (Ø 94 mm; Greiner Bio-One). On day 3 and 6, an additional 5 mL of culture medium was added into these dishes.

Isolation of Splenocytes

Splenocytes were collected from spleens of C57BL/6 mice by grinding the spleen though a cell strainer. The spleen cell medium was centrifuged (300*g*, 10 min, 4 °C) and lysis buffer (pH 7.4) was added to the cell pellet to lyse the erythrocytes for 1 min. Then spleen cell medium was added to stop the lysis and the splenocytes suspension was separated by centrifugation. For *in vitro* experiments, the splenocytes were seeded on suspension culture plates in spleen cell medium.

Isolation of OT-I and OT-II T cells

The T cells were isolated from the spleen of transgenic OT-I and OT-II mice. The splenocytes were isolated as described the previous section and suspended in T cell isolation buffer. The cell suspension was passed through a nylon wool column to separate T cells from undesired immune cells and T cells were collected from the column with T cell isolation buffer. The T cell suspension was centrifuged (300*g*, 10 min, 4 °C) and T cells were isolated and counted.

Confocal Imaging

Uptake of PNCs containing fluorescent Cy5-Oligo (red) was monitored by Confocal Laser Scanning Microscopy (cLSM). To this end, BMDC (3 × 105cells) on day 7 of culture were seeded in chamber slides(Thermo Fisher Scientific) and treated with 150 µg/mL PNCs for 3 h at 37 °C. After that, the chamber slides were washed, and the samples were incubated with DAPI (Sigma-Aldrich) to stain the cell nuclei (blue). Unbound dye was washed off. Samples were assayed using a Zeiss LSM710 (Carl Zeiss) and analyzed using ImageJ (NIH, Bethesda, USA) and ZEN 2009 (Carl Zeiss) software.

Flow Cytometry Assay

To detect cell-nanocarrier-interaction and to analyze the expression of surface markers, cells were harvested and washed in staining buffer (phosphate buffer saline [PBS]/2% FCS). Internalization of OVA-NCs into cells was measured by the fluorescent signal of Cy5 in NC-positiv cells in flow cytometry. To block Fc receptor-mediated staining, cells were incubated with rat anti-mouse CD16/CD32 Ab (clone 2.4G2), purified from hybridoma supernatant, for 15 min at room temperature. After that, cells were incubated with eFluor450-conjugated Ab specific for MHC class II I-Ab,d,q/I-Ed,k(cloneM5/114.15.2), fluorescein isothiocyanate (FITC)-labeled Ab directed at CD80 (clone 16-10A1), phycoerythrin (PE) anti-CD86 (clone GL-1), PE-Cy7-labeled anti-CD11c (clone N418), for 30 min at 4 °C. Dead cells were stained by incubation with fixable viability dye (FVD) eFI506 for 30 mi min at room temperature in the dark. Samples were measured with a BD FACSCanto-II flow cytometer equipped with BD FACSDiva software (BDBiosciences). Data were generated based on defined gating strategies and analyzed using FlowJo software (FlowJo, Ashland, USA).

Measurement of Cytokines Secretion

The amount of cytokines were measured from the supernatants of the cell culture. The BMDCs or splenocytes were treated with OVA-NCs and the supernatants were collected after 24 h by

centrifugation (300*g*, 10 min, 4°C). The cytokines were quantified using a Cytometric Bead Array Kit (CBA Flex Set (IL-1β, IL-5, IL-6, IL-10, IL-12p70, IFN-γ, TNF-α); BD Biosciences, Heidelberg) followed by data analysis using FCAP Array software (Soft Flow).

Ovalbumin-Specific T Cell Proliferation

T cell proliferation in BMDCs were performed with ovalbumin-specific OT-I and OT-II T cells. $CD8^+$ OT-I T cells recognize $OVA_{257-264}$ peptides in the context of H-$2K^b$, and $CD4^+$ OT-II T cells are specific for $OVA_{323-339}$ peptide in the context of H-2 I-Ab and I-A^d.[278]The BMDCs (10^5 cells/mL) were beforehand treated with adjuvant-loaded OVA-NCs and then co-cultured with OT-T/OT-II T cells ($5x10^4$/mL), respectively, for 72 h. The proliferation rate was measured by genomic incorporation of of radioactive [Methyl-3H] thymidine (^{3}HTdR). The co-culture was pulsed with ^{3}HTdR (0.25 µCi/well) for another 16 h. T cells were harvested and transferred to glass fiber filters. The incorporation of radioactive methyltritium was quantified with a liquid scintillation counter.

6. *In Vivo* Experiments

Mice

Six week old female B6 mice (C57BL/6J) were purchased from Charles River Laboratories and were kept under a 12 h dark, 12 h light cycle (with food and water supply ad libitum). OT-I/-II x Ly5.1 were bred in-house. All animal experiments were performed at the PKZI at University Medical Center in Mainz and have been approved by the Animal Care and Use Committee (Landesuntersuchungsamt Rheinland-Pfalz).

Tumor Cell Injection

B16/OVA-Luc cells, transfected and purchased from Translational Oncology Mainz (TRON) , were cultured in DMEM high glucose (4.5 g/l, Sigma-Aldrich) supplemented with 10% FCS (heat-inactivated), 100 U ml^{-1} penicillin, 100 µg ml^{-1} streptomycin and 10 µg/ml Blasticidin (InvivoGen). The cells were cultured at 37 °C and 7.5% CO_2. For injection, they were collected using trypsin-EDTA (Sigma-Aldrich) and $5*10^5$ cells (in sterile PBS, 100 µl) were injected subcutaneously into the right flank. Tumors were measured every other day with a caliper and tumor volume was calculated using the formula: width x length x length/2. Animals were killed when the tumor reached a size > 800 mm^3.

Immunization with OVA-NCs

All OVA-NCs were synthesized as described previously and prepared in sterile PBS (Gibco). They were injected subcutaneously in the tail base (500 µg in 100 µl) at day 6, 13 and 20 post tumor cell injection.

V. 3. Supplementary Informations to Chapter C

Materials

All chemicals and materials were used as received. Human serum albumin (> 99% purity) was purchased from Sigma Aldrich as well as 1,6-hexanediol (99%), propiolic acid, sulfuryl chloride and imidazole. Cyclohexane (HPLC grade) was purchased from VWR. Fluorescamine was purchased from Alfa Aesar. The block copolymer poly((ethylene-co-butylene)-*b*-(ethylene oxide)) P((E/B)-*b*-EO) used as the oil soluble surfactant was synthesized as described in literature and consists of a poly((ethylene-co-butylene) block (NMR: M_n = 3900 g/mol) and a poly(ethylene oxide) block (NMR: M_n = 2700 g/mol). [161] The anionic surfactant sodium dodecyl sulfate (SDS) was purchased from Sigma Aldrich. Cy5-Oligo was purchased from IBA Lifesciences. Proteinase K from tritirachium album (≥ 30 units/mg) and peroxidase from horseradish (≥ 50 units/mg) was purchased from Sigma Aldrich. Amicon Ultra-2 centrifugal filter devices were purchased from Merck Millipore (100 kDa) nominal molecular weight limit (NMWL). The magnesium and calcium free phosphate-buffered saline, was purchased from Life Technologies. Demineralized water was used for all experiments.

Experimentals

1. Synthesis of 1,6-Hexandiol Dipropiolate (HDDP)

The dialkyne crosslinker was synthesized by esterification following the literature. Briefly, hexandiol (4 g, 33.85 mmol), propiolic acid (9.48 g, 135.39 mmol) and *p*-TsOH (333.33 mg, 5 mol%) were dissolved in 120 mL toluene and stirred at 135 °C under reflux for 3 days using a dean-stark apparatus. Afterwards, the reaction solution was washed twice with 100 mL saturated $NaHCO_3$ solution and twice with 100 mL water. The solvent was removed and the product purified by column chromatography (PE:EtOAc 10:1). The product was obtained as colorless crystals. Yield: 3.37 g, 45%.

^{1}H NMR (300 MHz, CD_2Cl_2) δ 4.10 (t, 4H, O-C$\underline{H}_2$), 2.87 (s, 2H, $\underline{H}$C≡C), 1.61 (m, 4H, C$\underline{H}_2$-CH_2-O), 1.32 (m, 4H, CH_2-C$\underline{H}_2$-CH_2) ppm. ^{13}C NMR (300 MHz, CD_2Cl_2) δ 153, 74.6, 66.6, 28.5, 25.8 ppm.

2. Synthesis of 1-Imidazole-Sulfonyl Azide Hydrochloride

The azide transfer agent was synthesized according to Goddard-Borger *et al*.[158] Briefly, sodium azide (1.63 g, 25 mmol) was suspended in 25 mL MeCN and cooled down to 0 °C. Under

vigorous stirring sulfuryl chloride (3.34 g, 25 mmol) was added drop-wisely. The reaction solution was slowly brought to room temperature and the reaction carried out at room temperature overnight. Again, the reaction solution is cooled down to 0 °C and imidazole (3.23 g, 47.5 mmol) added in small portions. The reaction is stirred at room temperature for 3 h. Afterwards, 50 mL EtOAc is added and the reaction solution is washed twice with 50 mL saturated $NaHCO_3$ solution and twice with 50 mL water. The organic phase is dried over $MgSO_4$ and filtered. A mixture of AcCl/EtOH is slowly added to the reaction solution at 0 °C. The product is filtered, washed with EtOAc and dried. Yield: 94%.

^{1}H NMR (300 MHz, D_2O) δ 7.44 (dd, 1H, N-C<u>H</u>=CH), 7.85 (dd, 1H, HC=C<u>H</u>-N), 9.17 (dd, 1H, N=C<u>H</u>-N) ppm. ^{13}C NMR (300 MHz, CD_2Cl_2) δ 152.3, 75.5, 74.3, 74.3, 63.9, 36.7 ppm.

3. Azidation of Proteins with 1-Imidazole-Sulfonyl Azide Hydrochloride

Ovalbumin (1 g) was dissolved in 20 mL K_2CO_3 solution of pH 11 (for the optimization experiments pH value was adjusted accordingly to 8.2, 9.5 or 11). The azide transfer agent (276 mg) was dissolved in 2 mL water and added dropwisely to the protein solution. The reaction solution was stirred at pH 11 and room temperature for 30 min. Afterwards, the pH value of the reaction solution was adjusted to pH 8.3 with 1 M NaOH or 1 M HCl. The reaction solution was stirred at room temperature for 8 h (for the optimization experiments reaction time was adjusted accordingly to one, two or three days). The product was purified by dialysis (MWCO 1K) and lyophilized in NaCl (14.4 mg/mL). Yield: 0.78 g.

4. Preparation of Protein Nanocarriers by Interfacial Denaturation

A) Inverse W/O Miniemulsion

First, the (azide-functionalized) protein (50 mg) was dissolved in 0.4 mL NaCl solution (c = 14.4 mg/mL) and 100 µL Cy5-Oligo (c = 0.1 nmol/µL) or dextran-rhodamin B (0.5 mg). 35.7 mg of surfactant poly((ethylene/butylene)-*block*-(ethylene oxide)) (P((E/B)-*b*-EO)) were dissolved in 7.5 g of cyclohexane and the mixture was added to the aqueous solution. The two phases were homogenized by ultrasound under ice-cooling (70% amplitude, 3 min, 20 s pulse, 10 s pause). A third solution containing of 10.7 mg P((E/B)-*b*-EO), crosslinker (TDI 30 mg or 3 mg; HDDP 35.7 mg) in 5 g of cyclohexane and was then added dropwise to the stirred miniemulsion at 40 °C. In case of protein nanocarriers from thermal denaturation, the third solution was added without crosslinker. The reaction was carried out at 40 °C (or 80 °C) for 24 h. Afterwards, the protein nanocarriers were purified by repetitive centrifugation (1500*g*, 20 °C) and redispersion in cyclohexane to remove excess of surfactant and crosslinker. For the

transfer of the nanocarriers into aqueous media, 500 µL of concentrated nanocarrier dispersion in cyclohexane is added dropwise to 5 mL 0.1 wt% SDS solution under shaking in an ultrasonication bath for 3 min. Then, the emulsion was stirred open over night to evaporate the organic solvent. The protein nanocarriers in water were purified by repetitive centrifugation and washing in Amicon Ultra-2 centrifugal filters (MWCO 100 kDa, 500*g*).

B) Double W/O/W Emulsion

The W/O miniemulsion was prepared as described above in 4.A. The resulting inverse miniemulsion (2 mL) was emulsified in water containing different surfactants (0.1 wt%, 20 mL). Different techniques can be used for emulsification such as ultrasonication bath (shaking under dropwise addition of W/O miniemulsion for 10 min), Ultrasonication tip (10% amplitude, 1 min, 10 s pulse, 5 s pause) or ultraturrax (20000 rpm, 5 min). The double emulsion was heated to 40 °C (or 80 °C) under stirring for 24 h. Then, the emulsion was cooled down to room temperature and stirred open over night to evaporate the cyclohexane. Protein nanocarriers were obtained by washing through a centrifuge filter (MWCO 50 kDa, 500*g*, 30 min, three times).

5. Characterization of Protein Nanocarriers

Dynamic light scattering (DLS) was used to determine the average size and size distribution of the nanocarriers. A diluted dispersion (10 µL sample diluted in 1 mL cyclohexane or 50 µL sample diluted in 200 µL H_2O) was measured on a Malvern Zetasizer Nano S (Malvern Panalytical) equipped with a detector at 90° scattering mode at 20 °C. Scanning electron microscopy (SEM) studies were done on a field emission microscope (LEO (Zeiss) 1530 Gemini, Oberkochen, Germany) working at an accelerating voltage of 170 V. The silica wafers are cleaned in the plasma oven prior to use. Then, 2 µL of a diluted nanocarrier dispersion in cyclohexane or distilled water (concentration similar to samples for DLS) were dropped onto the wafers and dried under ambient conditions for 15 min. No additional contrast agent was applied. The solid content of the nanocarrier dispersion was measured gravimetrically. The fluorescence intensities for all mentioned experiments were measured using a microplate reader (Infinite M1000, Tecan, Switzerland).

6. Determination of Encapsulation Efficiency

The encapsulation efficiency is determined by measuring the fluorescence intensity of using a microplate reader (Infinite M1000 Tecan, Switzerland). The unpurified nanocarrier dispersion after transfer into 0.1 wt% SDS are concentrated in an Amicon centrifuge filter 100 K for 30 min at 500*g*. The amount of non-encapsulated dye was measured in the supernatant and the

encapsulation efficiency determined in proportion to the fluorescence intensity of the un-purified dispersion (Cy5-Oligo: λ = 649/670 nm; Dextran-rhodamine B: λ = 570/590 nm).

7. Degradation of Protein Nanocarriers

The enzymatic degradation of the protein nanocarriers were performed with proteinase K and determined by release of dextran-rhodamine B. A 0.2 wt% nanocarrier dispersion in PBS buffer was treated with a proteinase K solution (5 U/mL) at 37 °C. After the enzymatic degradation the dispersion is filtered by centrifugation in a centrifuge filter (MWCO 50 kDa) at 500*g* for 30 min and the amount of released dye in the supernatant measured by fluorescence. The degradation of the nanocarriers by proteinase K is also monitored by DLS measurements every 5 min over 20 h. Enzymatic degradation was performed in triplets.

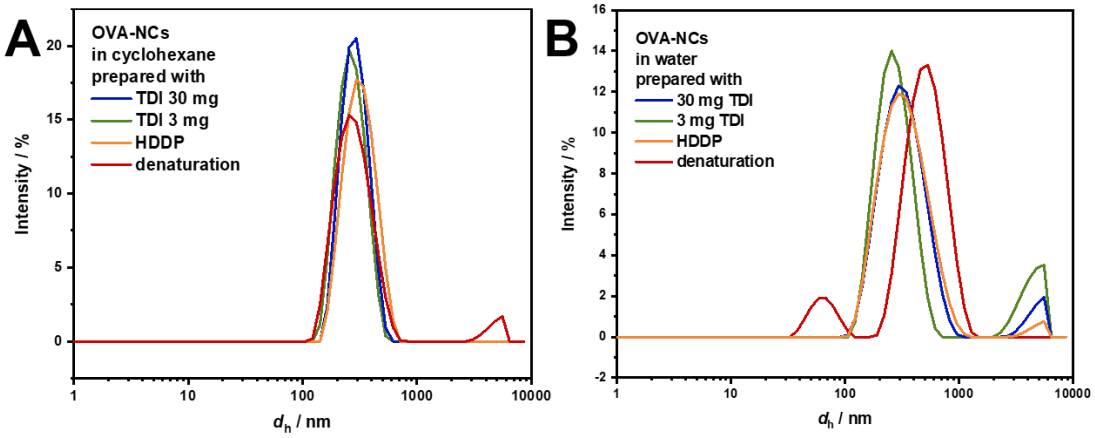

Figure 106. Dynamic light scattering of ovalbumin nanocarriers prepared by crosslinking with 30 mg TDI (blue), 3 mg TDI (green), HDDP (orange) or by interfacial denaturation (red) in A) cyclohexane and B) water.

V. 4. Supplementary Informations to Chapter D

Materials

All chemicals and materials were used as received. Human serum albumin and ovalbumin (> 99% purity) was purchased from Sigma Aldrich as well as 1,6-hexanediol (99%), propiolic acid, sulfurylchloride, imidazole, tetramethylammonium hydrochloride, Polyvinyl alcohol (PVA). 1,4-toluene diisocyanate was purchased from TCI chemicals. Cyclohexane (HPLC grade) was purchased from VWR. Fluorescamine was purchased from Alfa Aesar. The block copolymer poly((ethylene-co-butylene)-*b*-(ethylene oxide)) P((E/B)-*b*-EO) used as the oil soluble surfactant was synthesized as described in literature and consists of a poly((ethylene-co-butylene) block (NMR: M_n = 3900 g/mol) and a poly(ethylene oxide) block (NMR: M_n = 2700 g/mol).[161] The anionic surfactant sodium dodecyl sulfate (SDS) was purchased from Sigma Aldrich. Cy5-Oligo was purchased from IBA Lifesciences. Amicon Ultra-2 centrifugal filter devices were purchased from Merck Millipore (50 kDa) nominal molecular weight limit (NMWL). The magnesium and calcium free phosphate-buffered saline, was purchased from Life Technologies. Demineralized water was used for all experiments.

Experimentals

To Section 2.1: Preparation of CMPVA@Fe_3O_4

1. Synthesis of Carboxymethylated Polyvinyl Alcohol

Polyvinyl alcohol (PVA) was dissolved in 10 mL distilled water at 80 °C and cooled down to room temperature. Sodium hydroxide was dissolved in 20 mL distilled water and slowly added to PVA solution under stirring (750 rpm). Bromo acetic acid was dissolved in 10 mL distilled water and added to the reaction solution dropwisely. The reaction was stirred for three days at room temperature. Afterwards, the reaction solution was filtered and the supernatant adjusted to pH 6 with 1M HCl. Ethanol was added to the reaction solution and stirred for 30 min to precipitate the side product. The product solution was centrifuged to remove the side product and lyophilized to obtain carboxymethylated PVA (CMPVA) as a white powder. Yield = 63%.

2. Synthesis of CMPVA-Coated Iron Oxide Nanoparticles

Oleic acid-coated iron oxide nanoparticles (Fe_3O_4 NPs) were synthesized by co-precipitation.[269] Briefly, Iron(III) chloride hexahydrate (24.36 g, 90 mmol) and Iron(II) chloride tetrahydrate (12.01 g, 60 mmol) were dissolved in 100 mL water and an aqueous ammonia

solution (40 mL, 28 wt%) was added dropwise under vigorous stirring. Oleic acid (4.00 g, 14 mmol) was added to the solution and the reaction was stirred with a mechanical stirrer at 70 °C for one hour, followed by 110 °C for two hours. After purification with distilled water, the oleic acid-coated iron oxide nanoparticles were dried in an oven at 65 °C for storage. Oleic acid-coated iron oxide nanoparticles (0.10 g) were dispersed in 10 mL of 10 wt% tetramethylammonium hydroxide solution (TMAOH) in an ultrasonication bath for 1 h. The dispersed Fe_3O_4 NPs were centrifuged at 1400 rpm for 1 h. The pellet was redispersed in 0.1 wt% TMAOH solution. CMPVA (100 mg) was dissolved in 50 mL hot distilled water and added dropwisely to the dispersion of Fe_3O_4 NPs. The dispersion was stirred vigorously overnight. The dispersion of CMPVA-coated iron oxide nanoparticles (CMPVA@Fe_3O_4-NPs) is washed three times with 50 mL distilled water by centrifugation (1500*g*, 1 h). The pellet is redispersed in 1 mL distilled water.

To Section 2.2: Preparation of CMPVA@Fe_3O_4-Loaded Protein Nanocarriers

3. Azidation of Proteins with 1-Imidazole-Sulfonyl Azide Hydrochloride

Protein (1 g) was dissolved in 20 mL K_2CO_3 solution of pH 11. The azide transfer agent (276 mg) was dissolved in 2 mL water and added dropwisely to the protein solution. The reaction solution was stirred at pH 11 and room temperature for 30 min. Afterwards, the pH value of the reaction solution was adjusted to pH 8.3 with 1 M NaOH or 1 M HCl. The reaction solution was stirred at room temperature for 8 h. The product was purified by dialysis (MWCO 1K) and lyophilized. The amount of azide moieties was determined using the fluorescamine assay (see chapter A experimental part).

4. Formation of Protein Nanocarriers Loaded with CMPVA@Fe_3O_4 Nanoparticles

First, the protein, unmodified or azide-functionalized, (50 mg) was dissolved in 0.2 mL H_2O and 100 µL Cy5-Oligo (c = 0.1 nmol/µL) and 200 µL CMPVA@Fe_3O_4-NPs. 35.7 mg of surfactant poly((ethylene/butylene)-*block*-(ethylene oxide)) (P((E/B)-*b*-EO)) were dissolved in 7.5 g of cyclohexane and the mixture was added to the aqueous solution. The two phases were homogenized by ultrasound under ice-cooling (70% amplitude, 3 min, 20 s pulse, 10 s pause). A third solution containing of 10.7 mg P((E/B)-*b*-EO), crosslinker toluene diisocyanate (10 mg, for the unmodified protein) or hexanediol dipropiolate (13 mg, for the azide-functionalized protein) (for synthesis see SI chapter A) in 5 g of cyclohexane and was then added dropwise to the stirred miniemulsion at 40 °C. The reaction was carried out at 25 °C (TDI) or 40 °C (HDDP) for 24 h. Afterwards, the protein nanocarriers were purified by repetitive centrifugation (1500*g*,

20 °C, 30 min) and redispersion in cyclohexane to remove excess of surfactant and crosslinker. For the transfer of the nanocarriers into aqueous media, 500 µL of concentrated nanocarrier dispersion in cyclohexane was added dropwise to 5 mL 0.1 wt% SDS solution under shaking in an ultrasonication bath for 3 min. Then, the emulsion was stirred open over night to evaporate the organic solvent. The protein nanocarriers in water were purified by repetitive centrifugation (500*g*, 20°C, 30 min) and washing in Amicon Ultra-2 centrifugal filters (MWCO 50 kDa).

5. Characterization of Protein Nanocarriers

Dynamic light scattering (**DLS**) was used to determine the average size and size distribution of the nanocarriers. A diluted dispersion (10 µL sample diluted in 1 mL cyclohexane or 50 µL sample diluted in 200 µL H_2O) was measured on a Malvern Zetasizer Nano S (Malvern Panalytical) equipped with a detector at 90° scattering mode at 20 °C. The zeta potential of the nanocarriers were measured in 10^{-3} M potassium chloride solution with a ZetaNanosizer (Malvern Panalytical) at 20 °C. Scanning electron microscopy (**SEM**) studies were done on a field emission microscope (LEO (Zeiss) 1530 Gemini, Oberkochen, Germany) working at an accelerating voltage of 170 V. The silica wafers were cleaned in the plasma oven prior to use. Then, 2 µL of a diluted nanocarrier dispersion in cyclohexane or distilled water (concentration similar to samples for DLS) were dropped onto the wafers and dried under ambient conditions for 15 min. No additional contrast agent was applied. Scanning transmission electron microscopy (STEM) was performed in combination with an energy-dispersive X-ray spectroscopy (EDX) to verify the elemental composition (Hitatchi SU-8000). This provides precise elemental maps by means of locally recording the spectrum of emitted X-rays. It should be noted that the resulting elemental maps only yield a relative concentration distribution. Transmission electron microscopy (**TEM**) was performed using a Jeol 1400 transmission electron microscope with a voltage of 120 kV. Samples were prepared by placing a drop of the nanocarriers dispersion onto a 300 mesh carbon-coated copper grid and drying under ambient conditions.The **solid content** of the nanocarrier dispersion was measured gravimetrically. The **fluorescence** intensities for all mentioned experiments were measured using a microplate reader (Infinite M1000, Tecan, Switzerland).

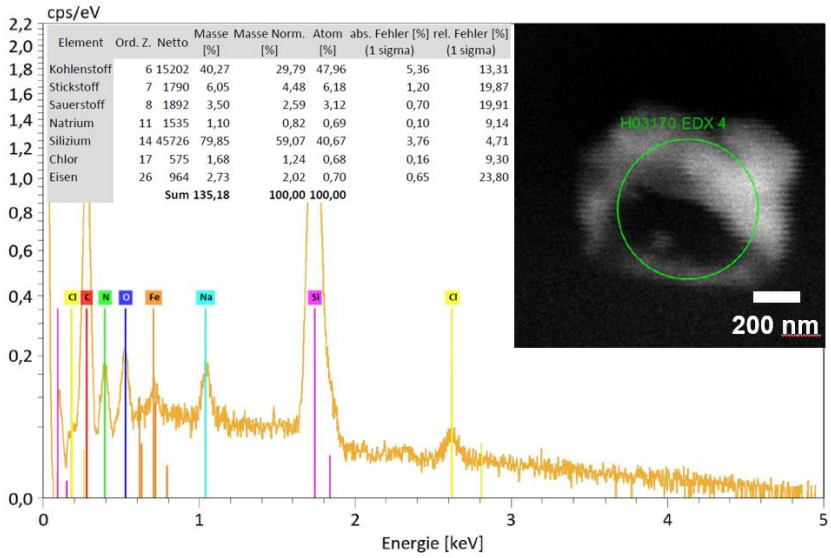

Figure 107. EDX measurements of magnetite encapsulated into HSA-TDI NC in cyclohexane.

6. Determination of Encapsulation Efficiency

The encapsulation efficiency of Cy5-Oligo (λ_{ex} = 649 nm, λ_{em} = 670 nm) was determined by measuring the fluorescence intensity of using a microplate reader (Infinite M1000 Tecan, Switzerland). The unpurified nanocarrier dispersion after transfer into 0.1 wt% SDS were concentrated in an Amicon centrifuge filter 100 K for 30 min at 500*g*. The amount of non-encapsulated dye was measured in the supernatant and the encapsulation efficiency determined in proportion to the fluorescence intensity of the un-purified dispersion.

To Section 2.3: Plasma Protein Corona and Cellular Uptake of Protein Nanocarriers

7. *In Vitro* Protein Corona

Human plasma was obtained from the Department of Transfusion Medicine Mainz from healthy donors. A plasma pool from ten volunteers was used and stored at - 20 °C. Human serum and plasma, prepared from blood by anti-coagulation with EDTA, heparin or citrate. PNCs were incubated with serum or plasma (1 mL) for 1 h at 37 °C. Afterwards, PNCs were separated from the blood medium by centrifugation (20000 rpm, 1 h, 4 °C) to obtain hard corona-coated PNCs. The protein-coated PNCs were washed from unbound proteins with PBS (1 mL) three times by centrifugation. The adsorbed protein were removed from the PNCs surface by treating them with 2% SDS with 62.5 mM Tris*HCl at 95 °C for 5 min. The PNCs were removed by centrifugation and the resulting protein-containing supernatant was analyzed by SDS-PAGE, Pierce-Assay and liquid chromatography-mass spectrometry (LC-MS).

8. SDS-PAGE

Protein-containing supernatant from protein corona experiments were incubated in NuPAGE™ LDS sample buffer and NuPAGE™ sample reducing agent at 70 °C for 10 min. The solution was applied on a NuPAGE™ 10% Bis-Tris protein gel (Thermo Fisher Scientific). The protein gel was run in NuPAGETM MES SDS running buffer at 100 V for 1 h with dithiothreitol. As a molecule marker SeeBlue Plus2 PreStained Standard was used and SilverQuestTM Silver Staining kit (Thermo Fisher Scientific) was used to visualize the protein according to the manufacturer's instruction.

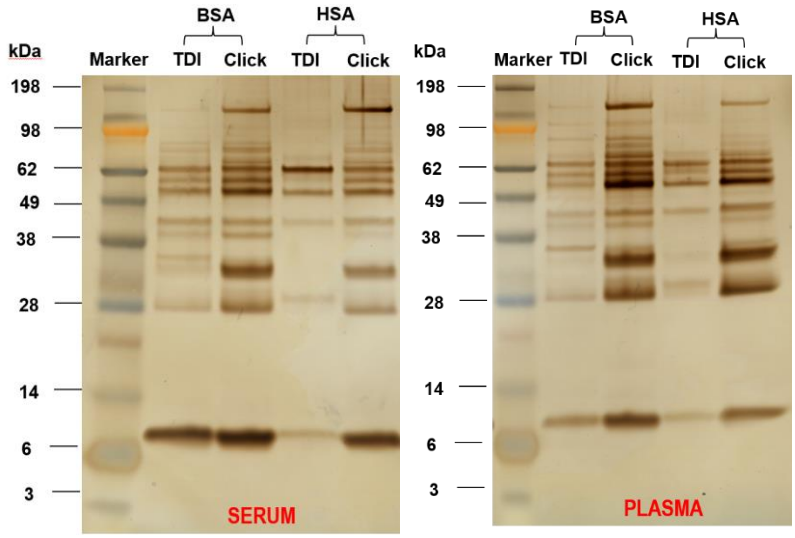

Figure 108. SDS page of the protein corona adsorbed to protein nanocarriers crosslinked with TDI or HDDP after incubation into serum (left) and plasma (right).

9. Protein Quantification

The protein concentration was determined by Pierce 600 nm protein assay (Thermo Fisher Scientific), according to the manufacturer's instruction.

10. In Solution Digestion

Proteins were digested according to literature.[268] Briefly, proteins were purified from SDS by applying Pierce detergent removal columns (Thermo Fisher Scientific). Then, the proteins were precipitated from the solution using the ProteoExtract® Protein Precipitation Kit (CalBioChem) according to the manufacturer's instruction. The precipitated protein was collected by centrifugation (14000 rpm, 10 min) and re-suspended in RapiGest SF (Waters Cooperation), dissolved in ammonium bicarbonate buffer (50 mM). Then, the proteins were reduced in DTT solution (5 mM) at 56 °C for 45 min and alkylated with iodoacetamide (15 mM) at room temperature for 60 min in the dark. The proteins were digested with trypsin in a ratio of 50:1 at

37 °C for 18 h. The digestion was quenched with HCl (2 µL) and the solubilized peptides were separated from the potential aggregates by centrifugation (14000 rpm, 15 min, 4 °C).

11. Liquid Chromatography-Electron Spray Ionization Mass Spectrometry (LC-MS)

The peptide samples were diluted with 0.1% formic acid and spiked with the reference peptide standard Hi3 E.coli (Waters Cooperation). The samples were separated in a C18 analytical reversed phase column and a C18 nanoACQUITY trap column using 0.1 vol.-% formic acid in water and acetonitrile, respectively. A nanoACQUITY UPLC coupled to a Synapt G2-Si mass spectrometer (Waters Cooperation) was used for the measurements. NanoLockSpray source in a positive ion mode was used for ionization and the Synapt G2-Si was operated in resolution mode performing data-independent acquisition (MSE) measurements. Data analysis was performed with MassLynx 4.1 and Progensis QI (2.0).[262] The proteins were quantified for 90 min with a mass to charge range of 50-2000 Da. For protein identification a human database was downloaded from Uniprot and modified with the sequence information of Hi3 Ecoli standard for absolute protein quantification. The absolute amount was quantified on the TOP3/Hi3 in fmol and the relative amount calculated in % based on all identified proteins.[279]

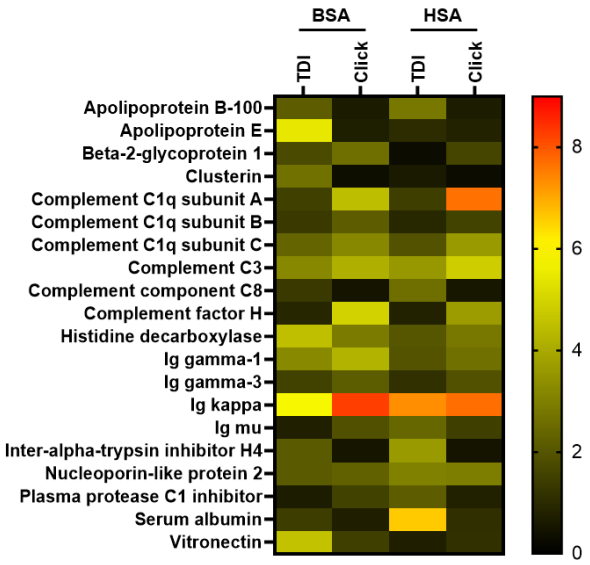

Figure 109. LC-MS analysis of the protein corona adsorbed to protein nanocarriers crosslinked with TDI or HDDP incubated in blood plasma. The relative amount of each protein in % is calculated based on the total amount of all identified proteins determined in fmol. Data from Dr. Johanna Simon.

12. *In Vitro* Cell Uptake

The murine macrophage cell line RAW264.7 were maintained in Dulbecco´s modified eagle medium (DMEM) supplemented with 10 % FCS, 100 U/mL penicillin, 100 mg/mL streptomycin and 2 mM glutamine (all from Invitrogen, Germany). For the cell uptake experiments, cells were seeded at a density of 150 000 cells/well in 24 well plates. 3 mm

plasma-sterilized sapphire discs (M. Wohlwend GmbH, Sennwald, Switzerland) covered with a 20 nm carbon layer before usage were added in the well plate. HeLa cells (obtained from ATCC® CCL-2™) were cultured in Dulbecco Modified Eagle Medium (DMEM, Gibco, USA) supplemented with 10% fetal bovine serum (FBS), 100 U mL^{-1} penicillin, 100 mg mL^{-1} streptomycin and 2 mM glutamine (all Thermo Fisher, Germany). At 80-90% confluency, cells were split. For cell uptake analysis, cells were detached with 2.5% trypsin (Gibco, Germany) and seeded out in 24-well plates (100 000 cells/well) in cell culture medium with 10% FBS. After overnight incubation, the cells were incubated in fresh serum-free medium for 2 h, before the nanocarriers dispersions were added at a concentration of 300 µg/mL to the cells.

For flow cytometry experiments, adherent cells were washed with PBS and detached from the culture vessel with 2.5 % trypsin (Gibco, Germany) and measurements were performed on a CyFlow ML cytometer (Partec, Germany) with a 488 nm laser for excitation of BODIPY and a 527 nm band pass filter for emission detection. Data analysis was performed using FCS Express V4 software (DeNovo Software, USA) selecting the cells with a FSC/SSC plot, thereby excluding cell debris. The gated events were analyzed by the fluorescent signal (FL1) expressed as median fluorescence intensity (MFI).

To Section 2.3: Intracellular Protein Corona and Cellular Uptake of Protein Nanocarriers

13. Intracellular Protein Corona

Murine DC2.4 dendritic cells (Merck) were cultured in IMDM supplemented with 1% penicillin and streptomycin (100 mg/mL), 5% FBS, and 1% 2-Mercaptoethanol at 37 °C and 5% CO_2 humidity. The cells were checked under the microscope and when reaching a confluence ≥ 80% cells were split. The cells were detached from the dish with 2 mM EDTA in cold PBS, followed suspension and washing in FBS-containing medium. Cell viability was checked with trypan blue and the live count as measured by an automated cell counter (TC10, BioRad). For the preparation of the intracellular protein corona, $3*10^6$ cells per well were seeded in FBS-containing cell culture medium in a 6-well plate and incubated overnight at 37 °C and 5% CO_2. Then, cells were washed with PBS and PNCs (250 µg/mL, in cell culture medium) were added to three wells for each sample ($9*10^6$ cells total) and incubated for 2 h or 24 h. Afterwards, the cells were washed with PBS and detached with PBS containing 2 mM EDTA. The cell suspension of three wells were pooled and subsequently collected by centrifugation (300*g*, 5 min). The cells were re-suspended in 1 mL ice-cold PBS containing Halt™ protease and phosphatase inhibitor and 50 µM EDTA (both Thermo Fisher). The cells were lysed in volumes

of 500 µL by ultracentrifugation with a Q800R3 sonicator (QSonica, U.S.A.). The lysis by ultrasonication was performed for 7 min with an amplitude of 70% pulsing every 30 s at constant 4 °C. After the lysis, PNCs were magnetically isolated for 10 minutes from the cellular debris and washed with ice-cold PBS containing Halt™ protease and phosphatase inhibitor and 50 µM EDTA. The PNCs were additionally washed two more times to remove unbound protein by using centrifugation (10000*g*, 10 min, 4 °C). The adsorbed proteins were removed from the PNCs surface by treating them with 2% SDS with 62.5 mM Tris*HCl at 95 °C for 5 min and using centrifugation (10000*g*, 10 min, 4 °C). The protein-containing supernatant was analyzed by SDS-PAGE, Pierce-Assay and liquid chromatography-mass spectrometry (LC-MS).

14. Flow Cytometry

Cells were selected on a FSC/SSC scatter plot, thereby excluding cell debris population, and evaluated by the fluorescent signal expressed as the median fluorescence intensity (MFI), or as the percentage of gated events or cells. The nanocarriers were detected by the red fluorescence in the RL1 channel with an excitation laser of 638 nm and a 679/14 nm band pass emission filter. Cell viability was performed using Live/Dead fixable Zombie Agua (Biolegend) and the VL2 channel with an excitation laser of 405 nm and a 512/25 nm band pass emission filter. For the secondary antibody test, the fluorescent of the FITC label was detected using the BL1 channel with an excitation laser of 488 nm and a 530/530 nm band pass emission filter.

15. Confocal Laser Scanning Microscopy (cLSM)

Intracellular uptake and internalization of PNCs was studied with confocal laser scanning microscopy (cLSM) experiments. PNCs (75 µg/mL) were incubated with cells at 37 °C and 5% CO_2 for 48 h. CLSM were performed on a LSM SP5 STED Leica Laser Scanning Confocal Microscope (Leica, Germany), composed of an inverse fluorescence microscope DMI 6000 CS equipped with a multi-laser combination using a HCA PL APO CS2 63 x 1.2 water objective. Cy5-Oligo-loaded PNCs were excited with an argon laser (20 mW; λ = 633 nm), detected at 650-670 nm (pseudocolored yellow) and the cell membranes were stained with CellMask Green™ (Thermo Fisher, 1:1000 dilution) using a laser excitation at 514 nm, detected at 525 nm - 550 nm (pseudocolored pink). The cell nucleus were stained with NucBlue ™ (ThermoFisher) and excited with a laser at 360 nm and detected at 460 nm.

To Section 3: Modification of Protein Nanocarriers

16. Functionalization of Protein Nanocarriers with Polyethylene Glycol

For a stock solution, polyethylene glycol was dissolved in dimethylsulfoxide (20 mg/mL). A dispersion of protein nanocarriers was diluted in PBS to 2 mg/mL and PEG-solution was added in different ratios. The dispersion was stirred overnight at 25 °C and purified by washing through a centrifuge filter (MWCO 10 kDa, 1500*g*, 30 min). The concentration of the dispersion was quantified by fluorescence. The unfunctionalized PNCs in a defined concentration act as a standard and the fluorescence of Cy5 measured at 649/679 nm.

17. Functionalization and Characterization of Protein Nanocarriers with Antibodies

For the antibody-modification of protein nanocarriers, the PNCs were functionalized with DBCO groups. A dispersion of PNCs (2 mg/mL) in PBS was reacted with different ratios of DBCO-PEG_4-NHS (Stock solution 10 mg/mL in DMSO) over night at room temperature. The mixture was washed through a centrifuge filter (MWCO 10 kDa, 1500*g*, 30 min) and the amount of PNCs quantified by fluorescence calibration. The amount of DBCO was quantified with Anthracene Assay according to literature.[277] Briefly, Anthracene azide was dissolved in DMSO (Stock solution 2 mg/mL). The PNCs-DBCO dispersion was diluted in water (1 mg/mL) and the anthracene azide solution added in a ratio of 5:1 DBCO. The reaction was stirred for 2 h at room temperature and the amount of reacted azide measured by the increase of fluorescence. Afterwards, the PNCs-DBCO was prepared for antibody-functionalization by diluting in PBS to 1 mg/mL. Antibodies were prepared according to Brueckner *et. al*.[256] For the antibody conjugation (Purified anti-mouse CD11c antibody or purified Armenian hamster IgG Isotype Ctrl antibody, both from Biolegends.com), PNCs-DBCO was incubated with azide-modified antibodies at room temperature overnight. Then, the modified PNCs were washed with PBS by magnetic decantation and resuspended in PBS. To test if antibodies were bound to the PNCs, the dispersion was incubated with a secondary FITC-labeled anti-hamster antibody and analyzed by flow cytometry. Naked and PNCs-DBCO acted as a negative control.

18. *In Vitro* Cell Uptake

Murine DC2.4 dendritic cells (Merck) were cultured in IMDM supplemented with 1% Penicillin, 5% FBS, streptomycin (100 mg/mL), and 1% 2-Mercaptoethanol at 37 °C and 5% CO_2 humidity. Murine MutuDC1940 cells (Applied Biological Materials, abm) were cultivated in IMDM supplemented with 1% Penicillin, 10% FBS, streptomycin (100 mg/mL), and 1% 2-Mercaptoethanol at 37 °C and 5% CO_2 humidity. Both cell lines were checked under the

microscope and when reaching a confluence ≥ 80% cells were split. The DC2.4 cells were detached from the dish with 2 mM EDTA (AppliChem) in cold PBS at 4 °C, while the MutuDC1940 cells were detached with 5 mM EDTA, 20 mM HEPES (Sigma) in warm PBS at 37 °C. Cell viability was checked with trypan blue and the live count was measured by an automated cell counter (TC10, BioRad). For the cell uptake experiments, cells ($1.5*10^5$ cells per mL) were seeded in FBS-containing cell culture medium in a 24-well plate and incubated overnight at 37 °C and 5% CO_2. At the next day, the medium of the cells was exchanged for 30 – 90 min to medium without FBS (same procedure for medium containing FBS). In the meantime, PNC samples were prepared in medium with and without FBS with a sample concentration of 75 µg/mL. PNCs were then incubated with the cells for 2 h. Afterwards, the cells were washed with PBS and detached with PBS containing 2 mM EDTA or 5 mM EDTA, 20 mM HEPES at 4 °C or 37 °C. The cells were collected by centrifugation (300*g*, 5 min), re-suspended in PBS, and analyzed by flow cytometry using the Attune™ NxT (Thermo Fisher Scientific).

19. Blocking Experiments

Before the OVA nanocapsule uptake, the cells of interest were first incubated with a mouse Fc block (Purified Anti-Mouse CD16/CD32, BD Pharmingen, clone 2.4G2). This blocking was performed to exclude an unspecific Fc-mediated uptake of antibody-modified OVA nanocapsules. For the experiment, the Fc block was added with a concentration of 2.5 µg/mL in 0.25 mL IMDM medium to the 24-well plate with 150000 cells per well at 37 °C for 15 min. Following the incubation, the Fc block was removed and the OVA sample incubation was performed as stated above (18. *In vitro* cell uptake).

VI. List of Abbreviations

ABTS	2,2'-azino-bis(3-ethylbenzothiazoline-6-sulphonic acid)
AIBN	2,2’-azobisisobutyronitrile
APC	antigen-presenting cell
approx.	approximately
BCA	bicinchoninic acid
BMDC	bone marrow-derived dendritic cell
BSA	Bovine serum albumin
BTA	Biomacromolecular therapeutic agent
CD	Cluster of differentiation
CD spectroscopy	circular dichroism spectroscpy
CDM	N,N′- bis(methacryloyl)-L-cystine
CH	cyclohexane
cLSM	confocal laser scanning microscopy
CMPVA	Carboxymethylated polyvinyl alcohol
CT	Computed tomography
CTAB	Cetyltrimethylammoniumbromid
CuAAC	Copper-catalyzed alzide-alkyne cycloaddition
DBCO	dibenzocyclooctine
DC	dendritic cell
DCR	derived count rate
DC-SIGN	dendritic cell-specific intercellular adhesion molecule-3-grabbin non-integrin
DEGM	2-(2-Methoxyethoxy)ethyl methacrylate
d_h	hydrodynamic diameters
diABZI	diamidobenzimidazole compound
DLS	dynamic light scattering
DMAP	*p*-dimethylaminobenzaldehyde
DMEM	Dulbecco´s modified eagle medium
DMF	dimethylformamid
DMSO	dimethylsulfoxide
DNA	Desoxynucleic acid
Dox	Doxorubicine
DTT	dithiothreitol
EDTA	ethylenediaminetetraacetic acid
EDX	Energy dispersive X-ray spectroscopy
EE	encapsulation efficiency

EtOAc	Ethylacetat
Eq.	Equivalents
ex	experimental
FACS	fluorescence activated cell sorting
FBS	fetal bovine serum
FCS	fluorescence correlation spectroscopy
FDA	Food and Drug Administration
FITC	fluorescein isothiocyanate
5-HA	5-hexynoic acid
HA	Hyaluronic acid
HDDP	hexanediol dipropiolate
HDDP-SS	hexanediol dipropiolate-disulfide
HES	Hydroxyethyl starch
HLB	hydrophilic-lipophilic balance
HPLC	High-pressure liquid chromatography
HRP	horse radish peroxidase
HRP-N_3	Azide-functionalized HRP
HSA	human serum albumin
HSA-N_3	Azide-functionalized HSA
^{3}HTdR	radioactive [Methyl-3H] thymidine
ICP	Intracellular protein corona
ICP-OES	inductively coupled plasma atomic optical emission spectroscopy
IEDDA	inverse-electron-demand diels-alder reaction
IgG	Interglobulin-G
IL	interleukin
IMDM	Iscove's Modified Dulbecco's Medium
INF	interferon
INP	Inorganic nanoparticles
IR	infrared
kDa	kilodalton
LAL	limulus amebocyte lysate
LC-MS	liquid chromatography-mass spectrometry
LMW	Low molecular weight
LPS	lipopolysaccharide
Lut	Lutensol
Lys	endolysosomes
NCs	nanocarriers

NOD	nucleotide-binding oligomerization domain-containing protein
MALDI-ToF	matrix-assisted laser desorption ionization time-of-flight
MDP	muramyl dipeptide
MeCN	Acetonitril
MFI	Mean fluorescence intensity
mgHES	hydroxyethylstarch coated magnetite nanoparticles
MHC	major histocompatibility complex
mPNCs	Magnetic protein nanocarriers
M_w	Molecular weight
MWCO	Molecular weight cut-off
n	Stoichiometric ratio
NanoDSF	nano differential scanning fluorimetry
NHS	*N*-hydroxysuccinimid
NLR	NOD-like receptor
NMR	Nuclear magnetic resonance
NP	nanoparticle
OVA	ovalbumin
OVA-N_3	Azide-functionalized ovalbumin
OVA-NCs	Ovalbumin nanocarriers
OT	Ovalbumin peptide-specific transgenic
O/W	Oil-in-water emulsion
PACA	Polyalkyl cyanoacrylate
PAMP	pathogen-associated molecular patterns
PBS	Phosphate-buffered saline
PDI	polydispersity index
P(E/B-*b*-EO)	poly((ethylene/butylene)-*block*-(ethylene oxide))
PEG	polyethylene glycol
PEGD	poly (ethylenegylcol) diacrylate
PEG-NHS	polyethyleneglycol-*N*-hydroxysuccinimid ester
PGPR	polyglycerol-polyricinoleate
PLA	polylactic acid
PLGA	polylactic-co-glycolic acid
PNCs	protein nanocarriers
Poly(I:C)	polyinosinic-polycytidylic acid
POx	poly(2-oxazoline)
PPEs	polyphophoester
PRR	pattern recognition receptor

PS	polystyrene
PTFE	polytetrafluoethylene
p-TsOH	*para*-toluenesulfonic acid
PTX	Paclitaxel
PVA	Polyvinyl alcohol
QD	Quantum dots
RNA	Ribonucleic acid
R848	Resiquimod
RAFT	reversible addition fragmentation transfer
SDE	simple double emulsification
SDS	sodium dodecyl sulfate
SDS-PAGE	sodium dodecyl sulfate polyacrylamide gel electrophoresis
SEM	Scanning electron microscopy
SpAAC	strain-promoted azide-alkyne cycloaddition
SPION	superparamagnetic iron oxide nanoparticles
STING	Stimulator of interferon genes
t	time
TCR	T cell receptors
T_m	Melting temperature
TAD	1,2,4-triazoline-3,5-dione
TCA	trichloro acetic acid
TDI	1,4-toluene diisocyanate
TEM	transmission electron microscopy
TET	tetrazole-ene cycloaddition
TMAOH	Tetramethylammonium hydroxide
TNF	Tumo necrosis factor
TFA	trifluoro acetic acid
TLR	toll-like receptors
Trp	Tryptophan
US	ultrasonication
UV	ultraviolet
W/O	Water-in-oil inverse emulsion
W/O/W	Water-in-oil-in-water double emulsion
ZNCs	Zwitterionic nanocapsules

VII. References

1. Pashenkov, M. V.; Murugina, N. E.; Budikhina, A. S.; Pinegin, B. V., Synergistic interactions between NOD receptors and TLRs: Mechanisms and clinical implications. *Journal of leukocyte biology* **2019,** *105* (4), 669-680.
2. Indoria, S.; Singh, V.; Hsieh, M.-F., Recent advances in theranostic polymeric nanoparticles for cancer treatment: A review. *International journal of pharmaceutics* **2020,** *582*, 119314.
3. Zarrintaj, P.; Mostafapoor, F.; Milan, P. B.; Saeb, M. R., Theranostic platforms proposed for cancerous stem cells: a review. *Current stem cell research & therapy* **2019,** *14* (2), 137-145.
4. Devaraj, N. K., The future of bioorthogonal chemistry. *ACS central science* **2018,** *4* (8), 952-959.
5. Hoelder, S.; Clarke, P. A.; Workman, P., Discovery of small molecule cancer drugs: successes, challenges and opportunities. *Molecular oncology* **2012,** *6* (2), 155-176.
6. Ma, Y.-S.; Liu, J.-B.; Yang, X.-L.; Xin, R.; Shi, Y.; Zhang, D.-D.; Wang, H.-M.; Wang, P.-Y.; Lin, Q.-L.; Li, W., Basic approaches, challenges and opportunities for the discovery of small molecule anti-tumor drugs. *American Journal of Cancer Research* **2021,** *11* (6), 2386.
7. Hillaireau, H.; Couvreur, P., Nanocarriers' entry into the cell: relevance to drug delivery. *Cellular and molecular life sciences* **2009,** *66* (17), 2873-2896.
8. Amidi, M.; Mastrobattista, E.; Jiskoot, W.; Hennink, W. E., Chitosan-based delivery systems for protein therapeutics and antigens. *Advanced drug delivery reviews* **2010,** *62* (1), 59-82.
9. Leader, B.; Baca, Q. J.; Golan, D. E., Protein therapeutics: a summary and pharmacological classification. *Nature reviews Drug discovery* **2008,** *7* (1), 21-39.
10. Wang, F.; Zuroske, T.; Watts, J. K., RNA therapeutics on the rise. *Nat Rev Drug Discov* **2020,** *19* (7), 441-442.
11. Patil, S. D.; Rhodes, D. G.; Burgess, D. J., DNA-based therapeutics and DNA delivery systems: a comprehensive review. *The AAPS journal* **2005,** *7* (1), E61-E77.
12. Machtakova, M.; Thérien-Aubin, H.; Landfester, K., Polymer nano-systems for the encapsulation and delivery of active biomacromolecular therapeutic agents. *Chemical Society Reviews* **2021**.
13. Machtakova, M.; Wirsching, S.; Gehring, S.; Landfester, K.; Thérien-Aubin, H., Controlling the semi-permeability of protein nanocapsules influences the cellular response to macromolecular payloads. *Journal of Materials Chemistry B* **2021,** *9* (40), 8389-8398.
14. Israelachvili, J. N., *Intermolecular and surface forces*. Academic press: 2015.
15. Lum, K.; Chandler, D.; Weeks, J. D., Hydrophobicity at small and large length scales. ACS Publications: 1999.
16. Loureiro, A.; G Azoia, N.; C Gomes, A.; Cavaco-Paulo, A., Albumin-based nanodevices as drug carriers. *Current pharmaceutical design* **2016,** *22* (10), 1371-1390.
17. Jain, A.; Singh, S. K.; Arya, S. K.; Kundu, S. C.; Kapoor, S., Protein Nanoparticles: Promising Platforms for Drug Delivery Applications. *ACS Biomaterials Science & Engineering* **2018,** *4* (12), 3939-3961.
18. Kang, B. Carbohydrate nanocarriers in biomedical application : construction and surface modification. Dissertation, Johannes Gutenberg-Universität Mainz, 2017.
19. Elzoghby, A. O.; Samy, W. M.; Elgindy, N. A., Protein-based nanocarriers as promising drug and gene delivery systems. *Journal of controlled release* **2012,** *161* (1), 38-49.

20. Weber, C.; Coester, C.; Kreuter, J.; Langer, K., Desolvation process and surface characterisation of protein nanoparticles. *International journal of pharmaceutics* **2000,** *194* (1), 91-102.
21. Migneault, I.; Dartiguenave, C.; Bertrand, M. J.; Waldron, K. C., Glutaraldehyde: behavior in aqueous solution, reaction with proteins, and application to enzyme crosslinking. *Biotechniques* **2004,** *37* (5), 790-802.
22. Nicolas, J.; Mura, S.; Brambilla, D.; Mackiewicz, N.; Couvreur, P., Design, functionalization strategies and biomedical applications of targeted biodegradable/biocompatible polymer-based nanocarriers for drug delivery. *Chemical Society Reviews* **2013,** *42* (3), 1147-1235.
23. Gong, G.; Xu, Y.; Zhou, Y.; Meng, Z.; Ren, G.; Zhao, Y.; Zhang, X.; Wu, J.; Hu, Y., Molecular switch for the assembly of lipophilic drug incorporated plasma protein nanoparticles and in vivo image. *Biomacromolecules* **2012,** *13* (1), 23-28.
24. Gong, J.; Huo, M.; Zhou, J.; Zhang, Y.; Peng, X.; Yu, D.; Zhang, H.; Li, J., Synthesis, characterization, drug-loading capacity and safety of novel octyl modified serum albumin micelles. *International journal of pharmaceutics* **2009,** *376* (1-2), 161-168.
25. Paál, K.; Müller, J.; Hegedûs, L., High affinity binding of paclitaxel to human serum albumin. *European journal of biochemistry* **2001,** *268* (7), 2187-2191.
26. Zhao, S.; Wang, W.; Huang, Y.; Fu, Y.; Cheng, Y., Paclitaxel loaded human serum albumin nanoparticles stabilized with intermolecular disulfide bonds. *MedChemComm* **2014,** *5* (11), 1658-1663.
27. Paal, K.; Shkarupin, A.; Beckford, L., Paclitaxel binding to human serum albumin—automated docking studies. *Bioorganic & medicinal chemistry* **2007,** *15* (3), 1323-1329.
28. Jacob, J.; Haponiuk, J. T.; Thomas, S.; Gopi, S., Biopolymer based nanomaterials in drug delivery systems: A review. *Materials Today Chemistry* **2018,** *9*, 43-55.
29. Mora-Huertas, C. E.; Garrigues, O.; Fessi, H.; Elaissari, A., Nanocapsules prepared via nanoprecipitation and emulsification–diffusion methods: Comparative study. *European Journal of Pharmaceutics and Biopharmaceutics* **2012,** *80* (1), 235-239.
30. Kumari, A.; Yadav, S. K.; Yadav, S. C., Biodegradable polymeric nanoparticles based drug delivery systems. *Colloids and surfaces B: biointerfaces* **2010,** *75* (1), 1-18.
31. Leo, E.; Brina, B.; Forni, F.; Vandelli, M. A., In vitro evaluation of PLA nanoparticles containing a lipophilic drug in water-soluble or insoluble form. *International journal of pharmaceutics* **2004,** *278* (1), 133-141.
32. Casalini, T.; Rossi, F.; Castrovinci, A.; Perale, G., A perspective on polylactic acid-based polymers use for nanoparticles synthesis and applications. *Frontiers in bioengineering and biotechnology* **2019,** *7*, 259.
33. Mundargi, R. C.; Babu, V. R.; Rangaswamy, V.; Patel, P.; Aminabhavi, T. M., Nano/micro technologies for delivering macromolecular therapeutics using poly (D, L-lactide-co-glycolide) and its derivatives. *Journal of Controlled Release* **2008,** *125* (3), 193-209.
34. Wang, J. J.; Zeng, Z. W.; Xiao, R. Z.; Xie, T.; Zhou, G. L.; Zhan, X. R.; Wang, S. L., Recent advances of chitosan nanoparticles as drug carriers. *International journal of nanomedicine* **2011,** *6*, 765.
35. Hasnain, M. S.; Nayak, A. K.; Kurakula, M.; Hoda, M. N., Alginate nanoparticles in drug delivery. In *Alginates in Drug Delivery*, Elsevier: 2020; pp 129-152.
36. Hathout, R. M.; Metwally, A. A., Gelatin nanoparticles. In *Pharmaceutical Nanotechnology*, Springer: 2019; pp 71-78.
37. Verma, D.; Gulati, N.; Kaul, S.; Mukherjee, S.; Nagaich, U., Protein based nanostructures for drug delivery. *Journal of pharmaceutics* **2018,** *2018*.
38. Biswas, S., Polymeric micelles as drug-delivery systems in cancer: challenges and opportunities. Future Medicine: 2021.

39. Lu, Y.; Park, K., Polymeric micelles and alternative nanonized delivery vehicles for poorly soluble drugs. *International journal of pharmaceutics* **2013,** *453* (1), 198-214.
40. Hussain, Z.; Khan, S.; Imran, M.; Sohail, M.; Shah, S. W. A.; de Matas, M., PEGylation: a promising strategy to overcome challenges to cancer-targeted nanomedicines: a review of challenges to clinical transition and promising resolution. *Drug delivery and translational research* **2019,** *9* (3), 721-734.
41. Viegas, T. X.; Bentley, M. D.; Harris, J. M.; Fang, Z.; Yoon, K.; Dizman, B.; Weimer, R.; Mero, A.; Pasut, G.; Veronese, F. M., Polyoxazoline: chemistry, properties, and applications in drug delivery. *Bioconjugate chemistry* **2011,** *22* (5), 976-986.
42. Almeida, A.; Araújo, M.; Novoa-Carballal, R.; Andrade, F.; Gonçalves, H.; Reis, R. L.; Lúcio, M.; Schwartz Jr, S.; Sarmento, B., Novel amphiphilic chitosan micelles as carriers for hydrophobic anticancer drugs. *Materials Science and Engineering: C* **2020,** *112*, 110920.
43. Lin, B.; Su, H.; Jin, R.; Li, D.; Wu, C.; Jiang, X.; Xia, C.; Gong, Q.; Song, B.; Ai, H., Multifunctional dextran micelles as drug delivery carriers and magnetic resonance imaging probes. *Science Bulletin* **2015,** *60* (14), 1272-1280.
44. Hu, Y.; Jiang, Z.; Chen, R.; Wu, W.; Jiang, X., Degradation and degradation-induced re-assembly of PVP-PCL micelles. *Biomacromolecules* **2010,** *11* (2), 481-488.
45. Yoo, H. S.; Park, T. G., Biodegradable polymeric micelles composed of doxorubicin conjugated PLGA–PEG block copolymer. *Journal of controlled Release* **2001,** *70* (1-2), 63-70.
46. Liu, L.; Venkatraman, S. S.; Yang, Y. Y.; Guo, K.; Lu, J.; He, B.; Moochhala, S.; Kan, L., Polymeric micelles anchored with TAT for delivery of antibiotics across the blood–brain barrier. *Peptide Science* **2008,** *90* (5), 617-623.
47. Dai, Y.; Chen, X.; Zhang, X., Recent Developments in the Area of Click-Crosslinked Nanocarriers for Drug Delivery. *Macromolecular rapid communications* **2019,** *40* (3), 1800541.
48. Liu, Y.; Chen, F.; Zhang, K.; Wang, Q.; Chen, Y.; Luo, X., pH-Responsive reversibly cross-linked micelles by phenol–yne click via curcumin as a drug delivery system in cancer chemotherapy. *Journal of Materials Chemistry B* **2019,** *7* (24), 3884-3893.
49. Landfester, K.; Weiss, C. K., Encapsulation by Miniemulsion Polymerization. In *Modern Techniques for Nano- and Microreactors/-reactions*, 2010; pp 1-49.
50. Landfester, K., Miniemulsion polymerization and the structure of polymer and hybrid nanoparticles. *Angewandte Chemie International Edition* **2009,** *48* (25), 4488-4507.
51. Pavel, F. M., Microemulsion polymerization. *Journal of dispersion science and technology* **2004,** *25* (1), 1-16.
52. Huang, C.-Y.; Chen, C.-M.; Lee, Y.-D., Synthesis of high loading and encapsulation efficient paclitaxel-loaded poly (n-butyl cyanoacrylate) nanoparticles via miniemulsion. *International journal of pharmaceutics* **2007,** *338* (1-2), 267-275.
53. Asgari, S.; Saberi, A. H.; McClements, D. J.; Lin, M., Microemulsions as nanoreactors for synthesis of biopolymer nanoparticles. *Trends in Food Science & Technology* **2019,** *86*, 118-130.
54. Piradashvili, K.; Alexandrino, E. M.; Wurm, F. R.; Landfester, K., Reactions and Polymerizations at the Liquid–Liquid Interface. *Chemical Reviews* **2016,** *116* (4), 2141-2169.
55. Reddy, M. M.; Boominathan, T.; Anand, A. V.; Panicker, R. R.; Kaushal, V.; Das, A.; Jain, N.; Vighnesh, I. S.; Desikan, R.; Vijayakrishna, K., Novel Biocompatible Hydrogels via Click Chemistry. In *Nano Hydrogels*, Springer: 2021; pp 281-304.
56. Heller, D. A.; Levi, Y.; Pelet, J. M.; Doloff, J. C.; Wallas, J.; Pratt, G. W.; Jiang, S.; Sahay, G.; Schroeder, A.; Schroeder, J. E., Modular 'Click-in-Emulsion'Bone-Targeted Nanogels. *Advanced Materials* **2013,** *25* (10), 1449-1454.

57. Bui, Q. T.; Jeon, Y. S.; Kim, J.; Kim, J.-H., Stabilized polymeric nanoparticle from amphiphilic mPEG-b-polyaspartamides containing 'click'functional groups. *International Journal of Polymeric Materials and Polymeric Biomaterials* **2017,** *66* (15), 798-804.
58. González de Torre, I.; Quintanilla, L.; Pinedo-Martín, G.; Alonso, M.; Rodríguez-Cabello, J. C., Nanogel formation from dilute solutions of clickable elastin-like recombinamers and its dependence on temperature: two fractal gelation modes. *ACS applied materials & interfaces* **2014,** *6* (16), 14509-14515.
59. Le, C.; Cao, X.; Tu, T.; Gal, Y.; Lim, K., Facile approach to prepare pH and redox-responsive nanogels via Diels-Alder click reaction. *Express Polymer Letters* **2018,** *12* (8), 688-698.
60. Sletten, E. M.; Bertozzi, C. R., Bioorthogonal chemistry: fishing for selectivity in a sea of functionality. *Angew Chem Int Ed Engl* **2009,** *48* (38), 6974-98.
61. Smeenk, M. L.; Agramunt, J.; Bonger, K. M., Recent developments in bioorthogonal chemistry and the orthogonality within. *Current Opinion in Chemical Biology* **2021,** *60*, 79-88.
62. Zou, J.; Yu, Y.; Yu, L.; Li, Y.; Chen, C. K.; Cheng, C., Well-defined drug-conjugated biodegradable nanoparticles by azide–alkyne click crosslinking in miniemulsion. *Journal of Polymer Science Part A: Polymer Chemistry* **2012,** *50* (1), 142-148.
63. McClements, D. J., Encapsulation, protection, and release of hydrophilic active components: Potential and limitations of colloidal delivery systems. *Advances in colloid and interface science* **2015,** *219*, 27-53.
64. Lammers, T.; Kiessling, F.; Hennink, W. E.; Storm, G., Drug targeting to tumors: principles, pitfalls and (pre-) clinical progress. *J Control Release* **2012,** *161* (2), 175-87.
65. Fathi, M.; Donsi, F.; McClements, D. J., Protein-based delivery systems for the nanoencapsulation of food ingredients. *Comprehensive reviews in food science and food safety* **2018,** *17* (4), 920-936.
66. Large, D. E.; Abdelmessih, R. G.; Fink, E.; Auguste, D. T., Liposome composition in drug delivery design, synthesis, characterization, and clinical application. *Advanced Drug Delivery Reviews* **2021**, 113851.
67. Schwendener, R. A., Liposomes as vaccine delivery systems: a review of the recent advances. *Therapeutic advances in vaccines* **2014,** *2* (6), 159-182.
68. Lingayat, V. J.; Zarekar, N. S.; Shendge, R. S., Solid lipid nanoparticles: a review. *Nanoscience and Nanotechnology Research* **2017,** *2*, 67-72.
69. Gordillo-Galeano, A.; Mora-Huertas, C. E., Solid lipid nanoparticles and nanostructured lipid carriers: A review emphasizing on particle structure and drug release. *European Journal of Pharmaceutics and Biopharmaceutics* **2018,** *133*, 285-308.
70. Hou, X.; Zaks, T.; Langer, R.; Dong, Y., Lipid nanoparticles for mRNA delivery. *Nature Reviews Materials* **2021**, 1-17.
71. Piradashvili, K.; Fichter, M.; Mohr, K.; Gehring, S.; Wurm, F. R.; Landfester, K., Biodegradable protein nanocontainers. *Biomacromolecules* **2015,** *16* (3), 815-821.
72. Baier, G.; Fichter, M.; Kreyes, A.; Klein, K.; Mailander, V.; Gehring, S.; Landfester, K., Glutathione Responsive Hyaluronic Acid Nanocapsules Obtained by Bioorthogonal Interfacial "Click" Reaction. *Biomacromolecules* **2016,** *17* (1), 148-53.
73. Landfester, K.; Mailander, V., Nanocapsules with specific targeting and release properties using miniemulsion polymerization. *Expert Opin Drug Deliv* **2013,** *10* (5), 593-609.
74. Landfester, K., Miniemulsions for Nanoparticle Synthesis. *Top Curr Chem* **2003**, 75-123.
75. Carvalho, B. G.; Vit, F. F.; Carvalho, H. F.; Han, S. W.; Lucimara, G., Recent advances in co-delivery nanosystems for synergistic action in cancer treatment. *Journal of Materials Chemistry B* **2021,** *9* (5), 1208-1237.

76. Landfester, K.; Musyanovych, A.; Mailänder, V., From polymeric particles to multifunctional nanocapsules for biomedical applications using the miniemulsion process. *Journal of Polymer Science Part A: Polymer Chemistry* **2010,** *48* (3), 493-515.
77. Baier, G.; Musyanovych, A.; Dass, M.; Theisinger, S.; Landfester, K., Cross-linked starch capsules containing dsDNA prepared in inverse miniemulsion as "nanoreactors" for polymerase chain reaction. *Biomacromolecules* **2010,** *11* (4), 960-968.
78. Kang, B.; Okwieka, P.; Schottler, S.; Winzen, S.; Langhanki, J.; Mohr, K.; Opatz, T.; Mailander, V.; Landfester, K.; Wurm, F. R., Carbohydrate-Based Nanocarriers Exhibiting Specific Cell Targeting with Minimum Influence from the Protein Corona. *Angew Chem Int Ed Engl* **2015,** *54* (25), 7436-40.
79. Machtakova, M.; Han, S.; Yangazoglu, Y.; Lieberwirth, I.; Thérien-Aubin, H.; Landfester, K., Self-sustaining enzyme nanocapsules perform on-site chemical reactions. *Nanoscale* **2021,** *13* (7), 4051-4059.
80. Fichter, M.; Piradashvili, K.; Pietrzak-Nguyen, A.; Pretsch, L.; Kuhn, G.; Strand, S.; Knuf, M.; Zepp, F.; Wurm, F. R.; Mailänder, V., Polymeric hepatitis C virus non-structural protein 5A nanocapsules induce intrahepatic antigen-specific immune responses. *Biomaterials* **2016,** *108*, 1-12.
81. Paßlick, D.; Piradashvili, K.; Bamberger, D.; Li, M.; Jiang, S.; Strand, D.; Wich, P. R.; Landfester, K.; Bros, M.; Grabbe, S., Delivering all in one: Antigen-nanocapsule loaded with dual adjuvant yields superadditive effects by DC-directed T cell stimulation. *Journal of controlled release* **2018,** *289*, 23-34.
82. Piradashvili, K.; Simon, J.; Paßlick, D.; Höhner, J. R.; Mailänder, V.; Wurm, F. R.; Landfester, K., Fully degradable protein nanocarriers by orthogonal photoclick tetrazole–ene chemistry for the encapsulation and release. *Nanoscale Horizons* **2017,** *2* (5), 297-302.
83. Hüppe, N.; Schunke, J.; Fichter, M.; Mailänder, V.; Wurm, F. R.; Landfester, K., Multicomponent Encapsulation into Fully Degradable Protein Nanocarriers via Interfacial Azide-Alkyne Click Reaction Allows the Co-Delivery of Immunotherapeutics. *Nanoscale Horizons* **2022**.
84. Frey, M.-L.; Simon, J.; Brückner, M.; Mailänder, V.; Morsbach, S.; Landfester, K., Bio-orthogonal triazolinedione (TAD) crosslinked protein nanocapsules affect protein adsorption and cell interaction. *Polymer Chemistry* **2020,** *11* (23), 3821-3830.
85. Alkanawati, M. S.; da Costa Marques, R.; Mailänder, V.; Landfester, K.; Thérien-Aubin, H. l., Polysaccharide-Based pH-Responsive Nanocapsules Prepared with Bio-Orthogonal Chemistry and Their Use as Responsive Delivery Systems. *Biomacromolecules* **2020,** *21* (7), 2764-2771.
86. Sun, Z.; Li, Y.; Zheng, S. Y.; Mao, S.; He, X.; Wang, X.; Yang, J., Zwitterionic Nanocapsules with Salt-and Thermo-Responsiveness for Controlled Encapsulation and Release. *ACS Applied Materials & Interfaces* **2021,** *13* (39), 47090-47099.
87. Craparo, E. F.; Cavallaro, G.; Bondì, M. L.; Giammona, G., Preparation of Polymeric Nanoparticles by Photo-Crosslinking of an Acryloylated Polyaspartamide in w/o Microemulsion. *Macromolecular Chemistry and Physics* **2004,** *205* (14), 1955-1964.
88. Jiang, Y.; Chen, J.; Deng, C.; Suuronen, E. J.; Zhong, Z., Click hydrogels, microgels and nanogels: Emerging platforms for drug delivery and tissue engineering. *Biomaterials* **2014,** *35* (18), 4969-4985.
89. Suhail, M.; Rosenholm, J. M.; Minhas, M. U.; Badshah, S. F.; Naeem, A.; Khan, K. U.; Fahad, M., Nanogels as drug-delivery systems: A comprehensive overview. *Therapeutic delivery* **2019,** *10* (11), 697-717.
90. Chen, J.; Zou, Y.; Deng, C.; Meng, F.; Zhang, J.; Zhong, Z., Multifunctional click hyaluronic acid nanogels for targeted protein delivery and effective cancer treatment in vivo. *Chemistry of Materials* **2016,** *28* (23), 8792-8799.

91. Famili, A.; Rajagopal, K., Bio-orthogonal cross-linking chemistry enables in situ protein encapsulation and provides sustained release from hyaluronic acid based hydrogels. *Molecular pharmaceutics* **2017,** *14* (6), 1961-1968.
92. Sun, H.; Guo, X.; Zeng, S.; Wang, Y.; Hou, J.; Yang, D.; Zhou, S., A multifunctional liposomal nanoplatform co-delivering hydrophobic and hydrophilic doxorubicin for complete eradication of xenografted tumors. *Nanoscale* **2019,** *11* (38), 17759-17772.
93. Su, C.-W.; Chiang, C.-S.; Li, W.-M.; Hu, S.-H.; Chen, S.-Y., Multifunctional nanocarriers for simultaneous encapsulation of hydrophobic and hydrophilic drugs in cancer treatment. *Nanomedicine* **2014,** *9* (10), 1499-1515.
94. Gao, Y.; Tang, M.; Leung, E.; Svirskis, D.; Shelling, A.; Wu, Z., Dual or multiple drug loaded nanoparticles to target breast cancer stem cells. *RSC Advances* **2020,** *10* (32), 19089-19105.
95. Wen, Z.; Liu, F.; Chen, Q.; Xu, Y.; Li, H.; Sun, S., Recent development in biodegradable nanovehicle delivery system-assisted immunotherapy. *Biomaterials science* **2019,** *7* (11), 4414-4443.
96. Van Rooijen, N.; van Nieuwmegen, R., Liposomes in immunology: multilamellar phosphatidylcholine liposomes as a simple, biodegradable and harmless adjuvant without any immunogenic activity of its own. *Immunological communications* **1980,** *9* (3), 243-256.
97. Eloy, J. O.; de Souza, M. C.; Petrilli, R.; Barcellos, J. P. A.; Lee, R. J.; Marchetti, J. M., Liposomes as carriers of hydrophilic small molecule drugs: strategies to enhance encapsulation and delivery. *Colloids and surfaces B: Biointerfaces* **2014,** *123*, 345-363.
98. Briuglia, M.-L.; Rotella, C.; McFarlane, A.; Lamprou, D. A., Influence of cholesterol on liposome stability and on in vitro drug release. *Drug delivery and translational research* **2015,** *5* (3), 231-242.
99. Demel, R.; Kinsky, S.; Kinsky, C.; Van Deenen, L., Effects of temperature and cholesterol on the glucose permeability of liposomes prepared with natural and synthetic lecithins. *Biochimica et Biophysica Acta (BBA)-Biomembranes* **1968,** *150* (4), 655-665.
100. Sułkowski, W.; Pentak, D.; Nowak, K.; Sułkowska, A., The influence of temperature, cholesterol content and pH on liposome stability. *Journal of molecular structure* **2005,** *744*, 737-747.
101. Lee, Y.; Thompson, D., Stimuli-responsive liposomes for drug delivery. *Wiley Interdisciplinary Reviews: Nanomedicine and Nanobiotechnology* **2017,** *9* (5), e1450.
102. Zangabad, P. S.; Mirkiani, S.; Shahsavari, S.; Masoudi, B.; Masroor, M.; Hamed, H.; Jafari, Z.; Taghipour, Y. D.; Hashemi, H.; Karimi, M., Stimulus-responsive liposomes as smart nanoplatforms for drug delivery applications. *Nanotechnology reviews* **2018,** *7* (1), 95-122.
103. Zhang, Y.-f.; Wang, J.-c.; Bian, D.-y.; Zhang, X.; Zhang, Q., Targeted delivery of RGD-modified liposomes encapsulating both combretastatin A-4 and doxorubicin for tumor therapy: in vitro and in vivo studies. *European journal of pharmaceutics and biopharmaceutics* **2010,** *74* (3), 467-473.
104. Rajera, R.; Nagpal, K.; Singh, S. K.; Mishra, D. N., Niosomes: a controlled and novel drug delivery system. *Biological and Pharmaceutical Bulletin* **2011,** *34* (7), 945-953.
105. Lee, J. S.; Feijen, J., Polymersomes for drug delivery: design, formation and characterization. *Journal of controlled release* **2012,** *161* (2), 473-483.
106. Rideau, E.; Dimova, R.; Schwille, P.; Wurm, F. R.; Landfester, K., Liposomes and polymersomes: a comparative review towards cell mimicking. *Chemical society reviews* **2018,** *47* (23), 8572-8610.
107. Houbrechts, M.; da Silva, L. C.; Ethirajan, A.; Landfester, K., Formation of giant polymer vesicles by simple double emulsification using block copolymers as the sole surfactant. *Soft Matter* **2021,** *17* (19), 4942-4948.

108. Klermund, L.; Castiglione, K., Polymersomes as nanoreactors for preparative biocatalytic applications: current challenges and future perspectives. *Bioprocess and biosystems engineering* **2018,** *41* (9), 1233-1246.
109. Da Silva, C.; Camps, M.; Li, T.; Chan, A.; Ossendorp, F.; Cruz, L., Co-delivery of immunomodulators in biodegradable nanoparticles improves therapeutic efficacy of cancer vaccines. *Biomaterials* **2019,** *220*, 119417.
110. Pramod, P.; Takamura, K.; Chaphekar, S.; Balasubramanian, N.; Jayakannan, M., Dextran vesicular carriers for dual encapsulation of hydrophilic and hydrophobic molecules and delivery into cells. *Biomacromolecules* **2012,** *13* (11), 3627-3640.
111. Wohl, B. M.; Engbersen, J. F., Responsive layer-by-layer materials for drug delivery. *Journal of controlled release* **2012,** *158* (1), 2-14.
112. Xu, S.; Shi, J.; Feng, D.; Yang, L.; Cao, S., Hollow hierarchical hydroxyapatite/Au/polyelectrolyte hybrid microparticles for multi-responsive drug delivery. *Journal of Materials Chemistry B* **2014,** *2* (38), 6500-6507.
113. Zhang, X.; Liang, T.; Ma, Q., Layer-by-Layer assembled nano-drug delivery systems for cancer treatment. *Drug Delivery* **2021,** *28* (1), 655-669.
114. Vergara, D.; Bellomo, C.; Zhang, X.; Vergaro, V.; Tinelli, A.; Lorusso, V.; Rinaldi, R.; Lvov, Y. M.; Leporatti, S.; Maffia, M., Lapatinib/Paclitaxel polyelectrolyte nanocapsules for overcoming multidrug resistance in ovarian cancer. *Nanomedicine: Nanotechnology, Biology and Medicine* **2012,** *8* (6), 891-899.
115. Gupta, B.; Ruttala, H. B.; Poudel, B. K.; Pathak, S.; Regmi, S.; Gautam, M.; Poudel, K.; Sung, M. H.; Ou, W.; Jin, S. G., Polyamino acid layer-by-layer (LbL) constructed silica-supported mesoporous titania nanocarriers for stimuli-responsive delivery of microRNA 708 and paclitaxel for combined chemotherapy. *ACS applied materials & interfaces* **2018,** *10* (29), 24392-24405.
116. Huang, J.; Shu, Q.; Wang, L.; Wu, H.; Wang, A. Y.; Mao, H., Layer-by-layer assembled milk protein coated magnetic nanoparticle enabled oral drug delivery with high stability in stomach and enzyme-responsive release in small intestine. *Biomaterials* **2015,** *39*, 105-113.
117. San Juan, A. M. T.; Rodgers, T.; Bedolla, C.; Noriega, F.; Romero, G., Layer by layer surface engineering of poly (lactide-co-glycolide) nanoparticles for plasmid DNA delivery. *Journal of Applied Polymer Science* **2020,** *137* (32), 49377.
118. Shaabani, E.; Sharifiaghdam, M.; De Keersmaecker, H.; De Rycke, R.; De Smedt, S.; Faridi-Majidi, R.; Braeckmans, K.; Fraire, J. C., Layer by layer assembled chitosan-coated gold nanoparticles for enhanced siRNA delivery and silencing. *International journal of molecular sciences* **2021,** *22* (2), 831.
119. Deng, Z. J.; Morton, S. W.; Ben-Akiva, E.; Dreaden, E. C.; Shopsowitz, K. E.; Hammond, P. T., Layer-by-layer nanoparticles for systemic codelivery of an anticancer drug and siRNA for potential triple-negative breast cancer treatment. *ACS nano* **2013,** *7* (11), 9571-9584.
120. Chen, X.; McClements, D. J.; Wang, J.; Zou, L.; Deng, S.; Liu, W.; Yan, C.; Zhu, Y.; Cheng, C.; Liu, C., Coencapsulation of (−)-Epigallocatechin-3-gallate and quercetin in particle-stabilized W/O/W emulsion gels: Controlled release and bioaccessibility. *Journal of agricultural and food chemistry* **2018,** *66* (14), 3691-3699.
121. Piñón-Segundo, E.; G Nava-Arzaluz, M.; Lechuga-Ballesteros, D., Pharmaceutical polymeric nanoparticles prepared by the double emulsion-solvent evaporation technique. *Recent patents on drug delivery & formulation* **2012,** *6* (3), 224-235.
122. Farhadian, N.; Malaekeh-Nikouei, B.; Maghsoud, Z., Co-encapsulation of tamoxifen citrate and quercetin using 2HP-β-cyclodextrin: a response surface experimental design. *RSC advances* **2016,** *6* (112), 111517-111525.

123. Bazylińska, U., Rationally designed double emulsion process for co-encapsulation of hybrid cargo in stealth nanocarriers. *Colloids and Surfaces A: Physicochemical and Engineering Aspects* **2017,** *532*, 476-482.
124. Mezzenga, R.; Folmer, B. M.; Hughes, E., Design of double emulsions by osmotic pressure tailoring. *Langmuir* **2004,** *20* (9), 3574-3582.
125. Mun, S.; Choi, Y.; Rho, S. J.; Kang, C. G.; Park, C. H.; Kim, Y. R., Preparation and characterization of water/oil/water emulsions stabilized by polyglycerol polyricinoleate and whey protein isolate. *Journal of food science* **2010,** *75* (2), E116-E125.
126. Xiao, J.; Lu, X.; Huang, Q., Double emulsion derived from kafirin nanoparticles stabilized Pickering emulsion: Fabrication, microstructure, stability and in vitro digestion profile. *Food Hydrocolloids* **2017,** *62*, 230-238.
127. Lee, Y.; Lee, D.; Park, E.; Jang, S.-y.; Cheon, S. Y.; Han, S.; Koo, H., Rhamnolipid-coated W/O/W double emulsion nanoparticles for efficient delivery of doxorubicin/erlotinib and combination chemotherapy. *Journal of nanobiotechnology* **2021,** *19* (1), 1-13.
128. Bazylińska, U.; Kulbacka, J.; Chodaczek, G., Nanoemulsion structural design in co-encapsulation of hybrid multifunctional agents: influence of the smart PLGA polymers on the nanosystem-enhanced delivery and electro-photodynamic treatment. *Pharmaceutics* **2019,** *11* (8), 405.
129. Buhecha, M. D.; Lansley, A. B.; Somavarapu, S.; Pannala, A. S., Development and characterization of PLA nanoparticles for pulmonary drug delivery: Co-encapsulation of theophylline and budesonide, a hydrophilic and lipophilic drug. *Journal of Drug Delivery Science and Technology* **2019,** *53*, 101128.
130. Torres-Martínez, A.; Angulo-Pachón, C. s. A.; Galindo, F.; Miravet, J. F., Liposome-enveloped molecular nanogels. *Langmuir* **2019,** *35* (41), 13375-13381.
131. Homyak, C. C.; Fernandez, A.; Touve, M. A.; Zhao, B.; Anson, F.; Hardy, J. A.; Vachet, R. W.; Gianneschi, N. C.; Ross, J. L.; Thayumanavan, S., Lipogels for encapsulation of hydrophilic proteins and hydrophobic small molecules. *Biomacromolecules* **2018,** *19* (1), 132-140.
132. Saleem, Q.; Liu, B.; Gradinaru, C. C.; Macdonald, P. M., Lipogels: Single-lipid-bilayer-enclosed hydrogel spheres. *Biomacromolecules* **2011,** *12* (6), 2364-2374.
133. Liong, M.; Lu, J.; Kovochich, M.; Xia, T.; Ruehm, S. G.; Nel, A. E.; Tamanoi, F.; Zink, J. I., Multifunctional inorganic nanoparticles for imaging, targeting, and drug delivery. *ACS nano* **2008,** *2* (5), 889-896.
134. Dreaden, E. C.; Alkilany, A. M.; Huang, X.; Murphy, C. J.; El-Sayed, M. A., The golden age: gold nanoparticles for biomedicine. *Chemical Society Reviews* **2012,** *41* (7), 2740-2779.
135. Wu, W.; He, Q.; Jiang, C., Magnetic iron oxide nanoparticles: synthesis and surface functionalization strategies. *Nanoscale research letters* **2008,** *3* (11), 397-415.
136. Ruman, U.; Fakurazi, S.; Masarudin, M. J.; Hussein, M. Z., Nanocarrier-based therapeutics and theranostics drug delivery systems for next generation of liver cancer nanodrug modalities. *International journal of nanomedicine* **2020,** *15*, 1437.
137. Bao, G.; Mitragotri, S.; Tong, S., Multifunctional nanoparticles for drug delivery and molecular imaging. *Annual review of biomedical engineering* **2013,** *15*, 253-282.
138. Wang, Q.; Bao, Y.; Ahire, J.; Chao, Y., Co-encapsulation of biodegradable nanoparticles with silicon quantum dots and quercetin for monitored delivery. *Advanced healthcare materials* **2013,** *2* (3), 459-466.
139. Hu, S.-H.; Chen, S.-Y.; Gao, X., Multifunctional nanocapsules for simultaneous encapsulation of hydrophilic and hydrophobic compounds and on-demand release. *ACS nano* **2012,** *6* (3), 2558-2565.

140. Hu, S. H.; Liao, B. J.; Chiang, C. S.; Chen, P. J.; Chen, I. W.; Chen, S. Y., Core-shell nanocapsules stabilized by single-component polymer and nanoparticles for magneto-chemotherapy/hyperthermia with multiple drugs. *Advanced materials* **2012,** *24* (27), 3627-3632.
141. Luque-Michel, E.; Sebastian, V.; Larrea, A.; Marquina, C.; Blanco-Prieto, M. J., Co-encapsulation of superparamagnetic nanoparticles and doxorubicin in PLGA nanocarriers: Development, characterization and in vitro antitumor efficacy in glioma cells. *European Journal of Pharmaceutics and Biopharmaceutics* **2019,** *145*, 65-75.
142. Fan, X.; Yang, J.; Loh, X. J.; Li, Z., Polymeric Janus Nanoparticles: Recent Advances in Synthetic Strategies, Materials Properties, and Applications. *Macromol Rapid Commun* **2018**, e1800203.
143. Lim, Y. G. J.; Poh, K. C. W.; Loo, S. C. J., Hybrid Janus microparticles achieving selective encapsulation for theranostic applications via a facile solvent emulsion method. *Macromolecular rapid communications* **2019,** *40* (7), 1800801.
144. Pichichero, M. E., Challenges in vaccination of neonates, infants and young children. *Vaccine* **2014,** *32* (31), 3886-3894.
145. Aspinall, R.; Del Giudice, G.; Effros, R. B.; Grubeck-Loebenstein, B.; Sambhara, S., Challenges for vaccination in the elderly. *Immunity & Ageing* **2007,** *4* (1), 1-9.
146. van der Burg, S. H.; Arens, R.; Ossendorp, F.; van Hall, T.; Melief, C. J., Vaccines for established cancer: overcoming the challenges posed by immune evasion. *Nature Reviews Cancer* **2016,** *16* (4), 219-233.
147. Valastyan, S.; Weinberg, R. A., Tumor metastasis: molecular insights and evolving paradigms. *Cell* **2011,** *147* (2), 275-292.
148. Veiseh, O.; Kievit, F. M.; Ellenbogen, R. G.; Zhang, M., Cancer cell invasion: treatment and monitoring opportunities in nanomedicine. *Advanced drug delivery reviews* **2011,** *63* (8), 582-596.
149. Warger, T.; Osterloh, P.; Rechtsteiner, G.; Fassbender, M.; Heib, V.; Schmid, B.; Schmitt, E.; Schild, H.; Radsak, M. P., Synergistic activation of dendritic cells by combined Toll-like receptor ligation induces superior CTL responses in vivo. *Blood* **2006,** *108* (2), 544-550.
150. Roelofs, M.; Joosten, L.; Abdollahi-Roodsaz, S.; Van Lieshout, A.; Sprong, T.; Van Den Hoogen, F.; Van Den Berg, W.; Radstake, T., The expression of toll-like receptors 3 and 7 in rheumatoid arthritis synovium is increased and costimulation of toll-like receptors 3, 4, and 7/8 results in synergistic cytokine production by dendritic cells. *Arthritis & Rheumatism: Official Journal of the American College of Rheumatology* **2005,** *52* (8), 2313-2322.
151. Tukhvatulin, A. I.; Dzharullaeva, A. S.; Tukhvatulina, N. M.; Shcheblyakov, D. V.; Shmarov, M. M.; Dolzhikova, I. V.; Stanhope-Baker, P.; Naroditsky, B. S.; Gudkov, A. V.; Logunov, D. Y., Powerful complex immunoadjuvant based on synergistic effect of combined TLR4 and NOD2 activation significantly enhances magnitude of humoral and cellular adaptive immune responses. *PLoS One* **2016,** *11* (5), e0155650.
152. Kolb, H. C.; Finn, M.; Sharpless, K. B., Click chemistry: diverse chemical function from a few good reactions. *Angewandte Chemie International Edition* **2001,** *40* (11), 2004-2021.
153. Moses, J. E.; Moorhouse, A. D., The growing applications of click chemistry. *Chemical Society Reviews* **2007,** *36* (8), 1249-1262.
154. Gaetke, L. M.; Chow, C. K., Copper toxicity, oxidative stress, and antioxidant nutrients. *Toxicology* **2003,** *189* (1-2), 147-163.
155. Siebert, J. M.; Baier, G.; Musyanovych, A.; Landfester, K., Towards copper-free nanocapsules obtained by orthogonal interfacial "click" polymerization in miniemulsion. *Chem Commun (Camb)* **2012,** *48* (44), 5470-2.

156. Tarhini, M.; Greige-Gerges, H.; Elaissari, A., Protein-based nanoparticles: From preparation to encapsulation of active molecules. *International journal of pharmaceutics* **2017,** *522* (1-2), 172-197.
157. Neek, M.; Kim, T. I.; Wang, S.-W., Protein-based nanoparticles in cancer vaccine development. *Nanomedicine: Nanotechnology, Biology and Medicine* **2019,** *15* (1), 164-174.
158. Goddard-Borger, E. D.; Stick, R. V., An efficient, inexpensive, and shelf-stable diazotransfer reagent: imidazole-1-sulfonyl azide hydrochloride. *Organic letters* **2007,** *9* (19), 3797-3800.
159. Fischer, N.; Goddard-Borger, E. D.; Greiner, R.; Klapotke, T. M.; Skelton, B. W.; Stierstorfer, J., Sensitivities of some imidazole-1-sulfonyl azide salts. *J Org Chem* **2012,** *77* (4), 1760-4.
160. Schoffelen, S.; van Eldijk, M. B.; Rooijakkers, B.; Raijmakers, R.; Heck, A. J.; van Hest, J. C., Metal-free and pH-controlled introduction of azides in proteins. *Chemical Science* **2011,** *2* (4), 701-705.
161. Thomas, A.; Schlaad, H.; Smarsly, B.; Antonietti, M., Replication of lyotropic block copolymer mesophases into porous silica by nanocasting: Learning about finer details of polymer self-assembly. *Langmuir* **2003,** *19* (10), 4455-4459.
162. Piradashvili, K.; Fichter, M.; Mohr, K.; Gehring, S.; Wurm, F. R.; Landfester, K., Biodegradable protein nanocontainers. *Biomacromolecules* **2015,** *16* (3), 815-21.
163. Administration, U. S. F. a. D. GRN No. 270 Polyglycerol polyricinoleic acid. https://www.cfsanappsexternal.fda.gov/scripts/fdcc/index.cfm?set=GRASNotices&id=270.
164. Sweeney, P. J.; Walker, J. M., Proteinase K (EC 3.4. 21.14). In *Enzymes of molecular biology*, Springer: 1993; pp 305-311.
165. Gardner, A.; Ruffell, B., Dendritic cells and cancer immunity. *Trends in immunology* **2016,** *37* (12), 855-865.
166. Ni, K.; O'neill, H., The role of dendritic cells in T cell activation. *Immunology and cell biology* **1997,** *75* (3), 223-230.
167. Couzin-Frankel, J., Cancer immunotherapy. American Association for the Advancement of Science: 2013.
168. Bergmann-Leitner, E. S.; Leitner, W. W., Adjuvants in the driver's seat: how magnitude, type, fine specificity and longevity of immune responses are driven by distinct classes of immune potentiators. *Vaccines* **2014,** *2* (2), 252-296.
169. Reed, S. G.; Orr, M. T.; Fox, C. B., Key roles of adjuvants in modern vaccines. *Nature medicine* **2013,** *19* (12), 1597-1608.
170. Guy, B., The perfect mix: recent progress in adjuvant research. *Nature Reviews Microbiology* **2007,** *5* (7), 396-397.
171. Jurk, M.; Heil, F.; Vollmer, J.; Schetter, C.; Krieg, A. M.; Wagner, H.; Lipford, G.; Bauer, S., Human TLR7 or TLR8 independently confer responsiveness to the antiviral compound R-848. *Nature immunology* **2002,** *3* (6), 499-499.
172. Girardin, S. E.; Boneca, I. G.; Viala, J.; Chamaillard, M.; Labigne, A.; Thomas, G.; Philpott, D. J.; Sansonetti, P. J., Nod2 is a general sensor of peptidoglycan through muramyl dipeptide (MDP) detection. *Journal of Biological Chemistry* **2003,** *278* (11), 8869-8872.
173. Alexopoulou, L.; Holt, A. C.; Medzhitov, R.; Flavell, R. A., Recognition of double-stranded RNA and activation of NF-κB by Toll-like receptor 3. *Nature* **2001,** *413* (6857), 732-738.
174. Mason, A. F.; Thordarson, P., Polymersomes as protocellular constructs. *Journal of Polymer Science Part A: Polymer Chemistry* **2017,** *55* (23), 3817-3825.
175. Discher, D. E.; Ahmed, F., Polymersomes. *Annu. Rev. Biomed. Eng.* **2006,** *8*, 323-341.

176. Nicholson, L. B., The immune system. *Essays in biochemistry* **2016,** *60* (3), 275-301.
177. Parham, P., *The immune system*. Garland Science: 2014.
178. Kurtz, J., Memory in the innate and adaptive immune systems. *Microbes and Infection* **2004,** *6* (15), 1410-1417.
179. Sun, J. C.; Ugolini, S.; Vivier, E., Immunological memory within the innate immune system. *The EMBO journal* **2014,** *33* (12), 1295-1303.
180. Weng, N.-p., Aging of the immune system: how much can the adaptive immune system adapt? *Immunity* **2006,** *24* (5), 495-499.
181. Morita, C. T.; Mariuzza, R. A.; Brenner, M. B. In *Antigen recognition by human γδ T cells: pattern recognition by the adaptive immune system*, Springer seminars in immunopathology, Springer: 2000; pp 191-217.
182. Han, B. W.; Herrin, B. R.; Cooper, M. D.; Wilson, I. A., Antigen recognition by variable lymphocyte receptors. *Science* **2008,** *321* (5897), 1834-1837.
183. Bloom, D. E.; Canning, D.; Weston, M., The value of vaccination. In *Fighting the Diseases of Poverty*, Routledge: 2017; pp 214-238.
184. Plotkin, S., History of vaccination. *Proceedings of the National Academy of Sciences* **2014,** *111* (34), 12283-12287.
185. Pollard, A. J.; Bijker, E. M., A guide to vaccinology: from basic principles to new developments. *Nature Reviews Immunology* **2021,** *21* (2), 83-100.
186. Greenwood, B., The contribution of vaccination to global health: past, present and future. *Philosophical Transactions of the Royal Society B: Biological Sciences* **2014,** *369* (1645), 20130433.
187. Organization, W. H., WHO report on cancer: setting priorities, investing wisely and providing care for all. **2020**.
188. Wodarz, A.; Näthke, I., Cell polarity in development and cancer. *Nature cell biology* **2007,** *9* (9), 1016-1024.
189. Luczak, M. W.; Jagodziński, P. P., The role of DNA methylation in cancer development. *Folia histochemica et cytobiologica* **2006,** *44* (3), 143-154.
190. Lu, H.; Ouyang, W.; Huang, C., Inflammation, a key event in cancer development. *Molecular cancer research* **2006,** *4* (4), 221-233.
191. Chabner, B. A.; Roberts, T. G., Chemotherapy and the war on cancer. *Nature Reviews Cancer* **2005,** *5* (1), 65-72.
192. Galmarini, D.; Galmarini, C. M.; Galmarini, F. C., Cancer chemotherapy: a critical analysis of its 60 years of history. *Critical reviews in oncology/hematology* **2012,** *84* (2), 181-199.
193. Restifo, N. P.; Dudley, M. E.; Rosenberg, S. A., Adoptive immunotherapy for cancer: harnessing the T cell response. *Nature Reviews Immunology* **2012,** *12* (4), 269-281.
194. Gattinoni, L.; Powell, D. J.; Rosenberg, S. A.; Restifo, N. P., Adoptive immunotherapy for cancer: building on success. *Nature Reviews Immunology* **2006,** *6* (5), 383-393.
195. de Jong, E. C.; Smits, H. H.; Kapsenberg, M. L. In *Dendritic cell-mediated T cell polarization*, Springer seminars in immunopathology, Springer: 2005; pp 289-307.
196. Liu, K.; Nussenzweig, M. C., Origin and development of dendritic cells. *Immunological reviews* **2010,** *234* (1), 45-54.
197. Théry, C.; Amigorena, S., The cell biology of antigen presentation in dendritic cells. *Current opinion in immunology* **2001,** *13* (1), 45-51.
198. Guermonprez, P.; Valladeau, J.; Zitvogel, L.; Théry, C.; Amigorena, S., Antigen presentation and T cell stimulation by dendritic cells. *Annual review of immunology* **2002,** *20* (1), 621-667.
199. Savina, A.; Amigorena, S., Phagocytosis and antigen presentation in dendritic cells. *Immunological reviews* **2007,** *219* (1), 143-156.

200. van der Bruggen, P.; Van den Eynde, B. J., Processing and presentation of tumor antigens and vaccination strategies. *Current opinion in immunology* **2006,** *18* (1), 98-104.
201. Offringa, R.; van der Burg, S. H.; Ossendorp, F.; Toes, R. E.; Melief, C. J., Design and evaluation of antigen-specific vaccination strategies against cancer. *Current opinion in immunology* **2000,** *12* (5), 576-582.
202. Azuma, I.; Seya, T., Development of immunoadjuvants for immunotherapy of cancer. *International immunopharmacology* **2001,** *1* (7), 1249-1259.
203. McKee, A. S.; Munks, M. W.; Marrack, P., How do adjuvants work? Important considerations for new generation adjuvants. *Immunity* **2007,** *27* (5), 687-690.
204. Coffman, R. L.; Sher, A.; Seder, R. A., Vaccine adjuvants: putting innate immunity to work. *Immunity* **2010,** *33* (4), 492-503.
205. Takeuchi, O.; Akira, S., Pattern recognition receptors and inflammation. *Cell* **2010,** *140* (6), 805-820.
206. Kawai, T.; Akira, S., The role of pattern-recognition receptors in innate immunity: update on Toll-like receptors. *Nature immunology* **2010,** *11* (5), 373-384.
207. Iwasaki, A.; Medzhitov, R., Toll-like receptor control of the adaptive immune responses. *Nature immunology* **2004,** *5* (10), 987-995.
208. Kawasaki, T.; Kawai, T., Toll-like receptor signaling pathways. *Frontiers in immunology* **2014,** *5*, 461.
209. Proell, M.; Riedl, S. J.; Fritz, J. H.; Rojas, A. M.; Schwarzenbacher, R., The Nod-like receptor (NLR) family: a tale of similarities and differences. *PloS one* **2008,** *3* (4), e2119.
210. Jensen, S.; Thomsen, A. R., Sensing of RNA viruses: a review of innate immune receptors involved in recognizing RNA virus invasion. *Journal of virology* **2012,** *86* (6), 2900-2910.
211. Seya, T.; Shime, H.; Ebihara, T.; Oshiumi, H.; Matsumoto, M., Pattern recognition receptors of innate immunity and their application to tumor immunotherapy. *Cancer science* **2010,** *101* (2), 313-320.
212. Schweitzer, A. N.; Borriello, F.; Wong, R.; Abbas, A. K.; Sharpe, A. H., Role of costimulators in T cell differentiation: studies using antigen-presenting cells lacking expression of CD80 or CD86. *The Journal of Immunology* **1997,** *158* (6), 2713-2722.
213. Schwartz, R. H., T cell anergy. *Annual review of immunology* **2003,** *21* (1), 305-334.
214. Beyersdorf, N.; Kerkau, T.; Hünig, T., CD28 co-stimulation in T-cell homeostasis: a recent perspective. *ImmunoTargets and therapy* **2015,** *4*, 111.
215. Scott, P., IL-12: initiation cytokine for cell-mediated immunity. *Science* **1993,** *260* (5107), 496-498.
216. Kapsenberg, M. L., Dendritic-cell control of pathogen-driven T-cell polarization. *Nature Reviews Immunology* **2003,** *3* (12), 984-993.
217. Belardelli, F., Role of interferons and other cytokines in the regulation of the immune response. *Apmis* **1995,** *103* (1-6), 161-179.
218. Steinman, R. M.; Swanson, J., The endocytic activity of dendritic cells. *The Journal of experimental medicine* **1995,** *182* (2), 283-288.
219. Rosales-Mendoza, S.; González-Ortega, O., *Nanovaccines*. Springer: 2019.
220. Paulis, L. E.; Mandal, S.; Kreutz, M.; Figdor, C. G., Dendritic cell-based nanovaccines for cancer immunotherapy. *Current opinion in immunology* **2013,** *25* (3), 389-395.
221. Zhu, G.; Zhang, F.; Ni, Q.; Niu, G.; Chen, X., Efficient nanovaccine delivery in cancer immunotherapy. *ACS nano* **2017,** *11* (3), 2387-2392.
222. Zhang, Y.; Lin, S.; Wang, X. Y.; Zhu, G., Nanovaccines for cancer immunotherapy. *Wiley Interdisciplinary Reviews: Nanomedicine and Nanobiotechnology* **2019,** *11* (5), e1559.
223. Garg, T.; K Goyal, A., Liposomes: targeted and controlled delivery system. *Drug delivery letters* **2014,** *4* (1), 62-71.

224. Gregory, A. E.; Williamson, D.; Titball, R., Vaccine delivery using nanoparticles. *Frontiers in cellular and infection microbiology* **2013,** *3*, 13.
225. Pavot, V.; Berthet, M.; Rességuier, J.; Legaz, S.; Handké, N.; Gilbert, S. C.; Paul, S.; Verrier, B., Poly (lactic acid) and poly (lactic-co-glycolic acid) particles as versatile carrier platforms for vaccine delivery. *Nanomedicine* **2014,** *9* (17), 2703-2718.
226. Hamdy, S.; Haddadi, A.; Hung, R. W.; Lavasanifar, A., Targeting dendritic cells with nano-particulate PLGA cancer vaccine formulations. *Advanced drug delivery reviews* **2011,** *63* (10-11), 943-955.
227. Koseki, T.; Kitabatake, N.; Doi, E., Irreversible thermal denaturation and formation of linear aggregates of ovalbumin. *Food Hydrocolloids* **1989,** *3* (2), 123-134.
228. Niccoli, M.; Castronuovo, G., The conformational stability of ovalbumin and lysozyme in the aqueous solutions of various cosolvents. *Journal of Thermal Analysis and Calorimetry* **2016,** *123* (3), 2149-2156.
229. Mebius, R. E.; Kraal, G., Structure and function of the spleen. *Nature reviews immunology* **2005,** *5* (8), 606-616.
230. Ramanjulu, J. M.; Pesiridis, G. S.; Yang, J.; Concha, N.; Singhaus, R.; Zhang, S.-Y.; Tran, J.-L.; Moore, P.; Lehmann, S.; Eberl, H. C., Design of amidobenzimidazole STING receptor agonists with systemic activity. *Nature* **2018,** *564* (7736), 439-443.
231. Wu, J. J.; Zhao, L.; Hu, H. G.; Li, W. H.; Li, Y. M., Agonists and inhibitors of the STING pathway: Potential agents for immunotherapy. *Medicinal research reviews* **2020,** *40* (3), 1117-1141.
232. Palucka, K.; Banchereau, J., Cancer immunotherapy via dendritic cells. *Nature Reviews Cancer* **2012,** *12* (4), 265-277.
233. Miele, E.; Spinelli, G. P.; Miele, E.; Tomao, F.; Tomao, S., Albumin-bound formulation of paclitaxel (Abraxane® ABI-007) in the treatment of breast cancer. *International journal of nanomedicine* **2009,** *4*, 99.
234. Mohammadian, M.; Waly, M. I.; Moghadam, M.; Emam-Djomeh, Z.; Salami, M.; Moosavi-Movahedi, A. A., Nanostructured food proteins as efficient systems for the encapsulation of bioactive compounds. *Food Science and Human Wellness* **2020,** *9* (3), 199-213.
235. Jahanban-Esfahlan, A.; Dastmalchi, S.; Davaran, S., A simple improved desolvation method for the rapid preparation of albumin nanoparticles. *International journal of biological macromolecules* **2016,** *91*, 703-709.
236. Wilson, B.; Ambika, T.; Patel, R. D. K.; Jenita, J. L.; Priyadarshini, S., Nanoparticles based on albumin: preparation, characterization and the use for 5-flurouracil delivery. *International journal of biological macromolecules* **2012,** *51* (5), 874-878.
237. Ziegler, G. R.; Foegeding, E. A., The gelation of proteins. In *Advances in food and nutrition research*, Elsevier: 1990; Vol. 34, pp 203-298.
238. Malafaya, P. B.; Silva, G. A.; Reis, R. L., Natural–origin polymers as carriers and scaffolds for biomolecules and cell delivery in tissue engineering applications. *Advanced drug delivery reviews* **2007,** *59* (4-5), 207-233.
239. Leo, E.; Vandelli, M. A.; Cameroni, R.; Forni, F., Doxorubicin-loaded gelatin nanoparticles stabilized by glutaraldehyde: involvement of the drug in the cross-linking process. *International journal of Pharmaceutics* **1997,** *155* (1), 75-82.
240. Liang, H. C.; Chang, W. H.; Lin, K. J.; Sung, H. W., Genipin-crosslinked gelatin microspheres as a drug carrier for intramuscular administration: In vitro and in vivo studies. *Journal of Biomedical Materials Research Part A: An Official Journal of The Society for Biomaterials, The Japanese Society for Biomaterials, and The Australian Society for Biomaterials and the Korean Society for Biomaterials* **2003,** *65* (2), 271-282.
241. Tanford, C., Protein denaturation. *Advances in protein chemistry* **1968,** *23*, 121-282.

242. McKenzie, H.; Ralston, G. B., The denaturation of proteins: two state? reversible or irreversible? *Experientia* **1971,** *27* (6), 617-624.
243. Becktel, W. J.; Schellman, J. A., Protein stability curves. *Biopolymers: Original Research on Biomolecules* **1987,** *26* (11), 1859-1877.
244. Khmelnitsky, Y. L.; Belova, A. B.; Levashov, A. V.; Mozhaev, V. V., Relationship between surface hydrophilicity of a protein and its stability against denaturation by organic solvents. *FEBS letters* **1991,** *284* (2), 267-269.
245. Cowan, D., Thermophilic proteins: stability and function in aqueous and organic solvents. *Comparative Biochemistry and Physiology Part A: Physiology* **1997,** *118* (3), 429-438.
246. Griebenow, K.; Klibanov, A. M., On protein denaturation in aqueous− organic mixtures but not in pure organic solvents. *Journal of the American Chemical Society* **1996,** *118* (47), 11695-11700.
247. Hong, K.; Park, S., Polyurea microcapsules with different structures: Preparation and properties. *Journal of applied polymer science* **2000,** *78* (4), 894-898.
248. Han, H.; Li, S.; Zhu, X.; Jiang, X.; Kong, X. Z., One step preparation of porous polyurea by reaction of toluene diisocyanate with water and its characterization. *RSC advances* **2014,** *4* (63), 33520-33529.
249. Heit, A.; Schmitz, F.; Haas, T.; Busch, D. H.; Wagner, H., Antigen co-encapsulated with adjuvants efficiently drive protective T cell immunity. *European journal of immunology* **2007,** *37* (8), 2063-2074.
250. Klippstein, R.; Pozo, D., Nanotechnology-based manipulation of dendritic cells for enhanced immunotherapy strategies. *Nanomedicine: Nanotechnology, Biology and Medicine* **2010,** *6* (4), 523-529.
251. M Cardoso, M.; N Peca, I.; CA Roque, A., Antibody-conjugated nanoparticles for therapeutic applications. *Current medicinal chemistry* **2012,** *19* (19), 3103-3127.
252. Simon, J.; Fichter, M.; Kuhn, G.; Brückner, M.; Kappel, C.; Schunke, J.; Grabbe, S.; Landfester, K.; Mailänder, V., Achieving dendritic cell subset-specific targeting in vivo by site-directed conjugation of targeting antibodies to nanocarriers. *bioRxiv* **2021**.
253. Krumb, M.; Frey, M.-L.; Langhanki, J.; Forster, R.; Kowalczyk, D.; Mailänder, V.; Landfester, K.; Opatz, T., Multivalency Beats Complexity: A Study on the Cell Uptake of Carbohydrate Functionalized Nanocarriers to Dendritic Cells. *Cells* **2020,** *9* (9), 2087.
254. Wagener, K.; Bros, M.; Krumb, M.; Langhanki, J.; Pektor, S.; Worm, M.; Schinnerer, M.; Montermann, E.; Miederer, M.; Frey, H., Targeting of immune cells with trimannosylated liposomes. *Advanced Therapeutics* **2020,** *3* (6), 1900185.
255. Anarjan, F. S., Active targeting drug delivery nanocarriers: Ligands. *Nano-Structures & Nano-Objects* **2019,** *19*, 100370.
256. Brückner, M.; Simon, J.; Landfester, K.; Mailänder, V., The conjugation strategy affects antibody orientation and targeting properties of nanocarriers. *Nanoscale* **2021,** *13* (21), 9816-9824.
257. Haute, D. V.; Berlin, J. M., Challenges in realizing selectivity for nanoparticle biodistribution and clearance: lessons from gold nanoparticles. *Therapeutic delivery* **2017,** *8* (9), 763-774.
258. Venditto, V. J.; Szoka Jr, F. C., Cancer nanomedicines: so many papers and so few drugs! *Advanced drug delivery reviews* **2013,** *65* (1), 80-88.
259. Bros, M.; Nuhn, L.; Simon, J.; Moll, L.; Mailänder, V.; Landfester, K.; Grabbe, S., The protein corona as a confounding variable of nanoparticle-mediated targeted vaccine delivery. *Frontiers in immunology* **2018,** *9*, 1760.
260. Tenzer, S.; Docter, D.; Kuharev, J.; Musyanovych, A.; Fetz, V.; Hecht, R.; Schlenk, F.; Fischer, D.; Kiouptsi, K.; Reinhardt, C., Rapid formation of plasma protein corona critically affects nanoparticle pathophysiology. *Nature nanotechnology* **2013,** *8* (10), 772-781.

261. Ritz, S.; Schottler, S.; Kotman, N.; Baier, G.; Musyanovych, A.; Kuharev, J.; Landfester, K.; Schild, H.; Jahn, O.; Tenzer, S.; Mailander, V., Protein corona of nanoparticles: distinct proteins regulate the cellular uptake. *Biomacromolecules* **2015,** *16* (4), 1311-21.
262. Kokkinopoulou, M.; Simon, J.; Landfester, K.; Mailänder, V.; Lieberwirth, I., Visualization of the protein corona: towards a biomolecular understanding of nanoparticle-cell-interactions. *Nanoscale* **2017,** *9* (25), 8858-8870.
263. Simon, J.; Wolf, T.; Klein, K.; Landfester, K.; Wurm, F. R.; Mailander, V., Hydrophilicity Regulates the Stealth Properties of Polyphosphoester-Coated Nanocarriers. *Angew Chem Int Ed Engl* **2018,** *57* (19), 5548-5553.
264. Bleher, S.; Buck, J.; Muhl, C.; Sieber, S.; Barnert, S.; Witzigmann, D.; Huwyler, J.; Barz, M.; Süss, R., Poly (Sarcosine) Surface Modification Imparts Stealth-Like Properties to Liposomes. *Small* **2019,** *15* (50), 1904716.
265. Schottler, S.; Becker, G.; Winzen, S.; Steinbach, T.; Mohr, K.; Landfester, K.; Mailander, V.; Wurm, F. R., Protein adsorption is required for stealth effect of poly(ethylene glycol)- and poly(phosphoester)-coated nanocarriers. *Nat Nanotechnol* **2016,** *11* (4), 372-7.
266. Qin, M.; Zhang, J.; Li, M.; Yang, D.; Liu, D.; Song, S.; Fu, J.; Zhang, H.; Dai, W.; Wang, X., Proteomic analysis of intracellular protein corona of nanoparticles elucidates nano-trafficking network and nano-bio interactions. *Theranostics* **2020,** *10* (3), 1213.
267. Wang, C.; Chen, B.; He, M.; Hu, B., Composition of Intracellular Protein Corona around Nanoparticles during Internalization. *ACS nano* **2021,** *15* (2), 3108-3122.
268. Hofmann, D.; Tenzer, S.; Bannwarth, M. B.; Messerschmidt, C.; Glaser, S.-F.; Schild, H. r.; Landfester, K.; Mailänder, V., Mass spectrometry and imaging analysis of nanoparticle-containing vesicles provide a mechanistic insight into cellular trafficking. *Acs Nano* **2014,** *8* (10), 10077-10088.
269. Bannwarth, M. B.; Kazer, S. W.; Ulrich, S.; Glasser, G.; Crespy, D.; Landfester, K., Well-Defined Nanofibers with Tunable Morphology from Spherical Colloidal Building Blocks. *Angewandte Chemie International Edition* **2013,** *52* (38), 10107-10111.
270. Gilbert, D., Fate of TDI and MDI in air, soil, and water. *Journal of cellular plastics* **1988,** *24* (2), 178-192.
271. Matsuo, H.; Somiya, M.; Iijima, M.; Arakawa, T.; Kuroda, S. i., CD11c-specific bio-nanocapsule enhances vaccine immunogenicity by targeting immune cells. *Journal of nanobiotechnology* **2018,** *16* (1), 1-12.
272. Kurts, C., CD11c: not merely a murine DC marker, but also a useful vaccination target. *European journal of immunology* **2008,** *38* (8), 2072-2075.
273. Schottler, S.; Landfester, K.; Mailander, V., Controlling the Stealth Effect of Nanocarriers through Understanding the Protein Corona. *Angew Chem Int Ed Engl* **2016,** *55* (31), 8806-15.
274. Li, M.; Jiang, S.; Simon, J.; Paßlick, D.; Frey, M.-L.; Wagner, M.; Mailänder, V.; Crespy, D.; Landfester, K., Brush Conformation of Polyethylene Glycol Determines the Stealth Effect of Nanocarriers in the Low Protein Adsorption Regime. *Nano letters* **2021,** *21* (4), 1591-1598.
275. Pelosi, C.; Tinè, M. R.; Wurm, F. R., Main-chain water-soluble polyphosphoesters: Multi-functional polymers as degradable PEG-alternatives for biomedical applications. *Eur. Polym. J* **2020,** *141* (110079.10), 1016.
276. Macri, C.; Dumont, C.; Johnston, A. P.; Mintern, J. D., Targeting dendritic cells: a promising strategy to improve vaccine effectiveness. *Clinical & translational immunology* **2016,** *5* (3), e66.

277. Baier, G.; Siebert, J. M.; Landfester, K.; Musyanovych, A., Surface Click Reactions on Polymeric Nanocapsules for Versatile Functionalization. *Macromolecules* **2012,** *45* (8), 3419-3427.
278. Didierlaurent, A. M.; Collignon, C.; Bourguignon, P.; Wouters, S.; Fierens, K.; Fochesato, M.; Dendouga, N.; Langlet, C.; Malissen, B.; Lambrecht, B. N., Enhancement of adaptive immunity by the human vaccine adjuvant AS01 depends on activated dendritic cells. *The Journal of Immunology* **2014,** *193* (4), 1920-1930.
279. Silva, J. C.; Gorenstein, M. V.; Li, G.-Z.; Vissers, J. P.; Geromanos, S. J., Absolute Quantification of Proteins by LCMSE: A Virtue of Parallel ms Acquisition* S. *Molecular & Cellular Proteomics* **2006,** *5* (1), 144-156.